

Biomolecule interactions at the interface of the aqueous silica surface

Stefan Rauwolf

Vollständiger Abdruck der von der TUM School of Engineering and Design der Technischen Universität München zur Erlangung eines
Doktors der Ingenieurwissenschaften (Dr.-Ing.)
genehmigten Dissertation.

Vorsitz: Prof. Dr.-Ing. Andreas Kremling

Prüfer*innen der Dissertation:

1. Prof. Dr. rer. nat. Sonja Berensmeier
2. Prof. Giorgio Carta, Ph.D., University of Virginia

Die Dissertation wurde am 21.04.2022 bei der Technischen Universität München eingereicht und durch die TUM School of Engineering and Design am 24.07.2022 angenommen.

“If you try and take a cat apart to see how it works, the first thing you have on your hands is a nonworking cat.”

Douglas Adams

Acknowledgments

First and foremost, I would like to thank my supervisor Professor Sonja Berensmeier for the trust you have placed in me and for giving me the necessary freedom to work on the project. I always felt that I was challenged and encouraged and that I received support when I needed it. I could not have wished for a better supervisor. Many thanks for this!

Thank you, Professor Giorgio Carta, for your expertise and your immediate willingness to be my examiner. It is an honor for me.

A special thanks goes to my mentor Dr. Sebastian Schwaminger for all the fruitful discussions and crazy ideas. You always had time to listen and encouraged me to follow new ideas. Thank you for all the support, teaching, and becoming a friend along the way.

I would like to express my gratitude to the whole project team. I had a great time with Alexander Zanker working in the lab and discussing new ideas for the project. Furthermore, I would like to thank our project partner Dr. Saientan Bag from the KIT for the great work on the simulation part of the project and the great discussions during all our meetings. Our joined work makes me proud. I also like to thank Professor Wolfgang Wenzel from the KIT who always gave great advice and ideas.

My further thanks go to Professor Ana Cristina Dias-Cabral for hosting me in your lab and introducing me to the Flow-Microcalorimetry during my stay in Covilhã. I really enjoyed the time in your lab and learned a lot from you during all our discussions. In this context, I also want to thank Rodrigo Rouqueiro for introducing me to the daily life at another university and enduring the long days in the lab with me.

I would also like to thank Professor Börje Sellergren for hosting me at Malmö University and showing me the world of Molecularly Imprinted Polymers. Special thanks to Thomas Janssens and Anil Incel for helping me with organizing the research stay. I would also like to thank all the other PhD students and PostDocs from Malmö University for the great time during my stay. I really enjoyed it.

In addition, I would like to thank all my colleagues from STT, SBT, and BioVT for the great time. Thank you Tatjana Trunzer and Lea Martin for sharing an office with me and the always more or less productive conversations, it could not have been better. For similar reasons I would like to thank Dr. Paula Fraga Garcia, Dr. Ljubomir Grozdev, Yasmin Kaveh Baghbaderani, Eva Krolitzki, Michael Schobesberger, Gregor Essert, Lucía Abarca-Cabrera, Chiara Turrina, Leonie Wittmann, Marko Tesanovic, and Karina Hobmeier. Thank you, Stefan Darchinger, for keeping the lab running. A special thanks to Susanne Kuchenbaur for all the administrative work. You all made this time unforgettable for me!

Likewise, I would like to thank my students Sussi Wang, Anna Fürst, Yannik Widmaier, Deike Dinter, Veronika Huber, Tobias Steegmüller und Nadja Sommer. You have contributed to the success of this work with your hours in the lab and your joy of discussion. I enjoyed supervising every single one of you!

Thank you, Tim Gerster, for being my partner in crime since the very first semester and a big thank you to all my friends who accompanied me over the years. I could not ask for better friends!

Finally, I would like to thank my parents, my brothers, and my girlfriend Melanie and her family for their patience and everlasting support. Without you, none of this would have been possible. Thank you for always being there for me!

Abstract

In the production of therapeutic antibodies and recombinant proteins the downstream process is still responsible for most of the production costs, supporting the development of innovative methods. Silica in the form of silica gel is the most common material used in the history of liquid chromatography. The main advantages of silica gel are high solvolytic and mechanical stability, porous structure, and high specific surface area thus offering a new, inexpensive, and scalable method to improve one of the major tools of the downstream process: preparative chromatography. Despite its widespread use, the interactions of biomolecules such as amino acids and DNA taking place at the aqueous-silica interface are still not fully understood. With the use of chromatographic zonal elution and flow microcalorimetry experiments combined with molecular dynamics simulation this work sheds light on the interaction of the 20 amino acids in different buffer systems revealing lysine and arginine as strong silica binders. Selected capped L-alanine and L-arginine were used to reveal the individual contribution of backbone and functional charged groups of the amino acids. Experiments and simulations indicated that electrostatic interactions dominate the interaction of amino acids with silica. The mechanism is not classical ion exchange but ion-pairing, indicated by the flow microcalorimetry profile, which shows no desorption before the adsorption event. Based on the results from amino acid interactions the rational designed (RH)₄ peptide tag was chosen to purify fusion proteins with a bare silica chromatographic column with over 90% purity and recovery in one run. Additionally, simulation and batch adsorption experiments helped to explain dsDNA adsorption in the presence of different salts and amino acids. Adsorption of DNA to silica is dominated by the concentration and valency of positively charged ions in the solution highlighted by a cooperative adsorption model. The higher the concentration and valency, the higher the adsorbed amount of DNA. The results demonstrate the importance of different charges on biomolecules as well as different charged ions in the surrounding environment for the complex biomolecule-silica interaction in aqueous solutions. These findings could also be applicable to other inorganic-biomolecule interactions in medicine and biotechnology to help understand the complex interactions between biomolecules and inorganic surfaces. The designed peptide-tag combined with the purification process allows bare silica to be exploited in preparative chromatography for downstream bioprocessing. This method is not only restricted to large scale but also for everyday laboratory use.

Kurzzusammenfassung

Bei der Herstellung von therapeutischen Antikörpern und rekombinanten Proteinen ist die Aufreinigung immer noch für den größten Teil der Produktionskosten verantwortlich. Dies fördert die Entwicklung innovativer Methoden. Silicagel ist das am häufigsten verwendete Material in der Geschichte der Flüssigkeitschromatographie. Die Hauptvorteile von Silicagel sind die hohe solvolytische und mechanische Stabilität, die poröse Struktur und die hohe spezifische Oberfläche. Dadurch bietet es eine neue, kostengünstige und skalierbare Methode zur Verbesserung eines der wichtigsten Werkzeuge der Proteinreinigung: die präparative Chromatographie. Trotz ihrer weiten Verbreitung sind die Wechselwirkungen von Biomolekülen wie Aminosäuren und DNA, die an der Grenzfläche zwischen Wasser und Silicagel stattfinden, noch immer nicht vollständig verstanden. Durch chromatographische Elutions- und Durchflussmikrokalorimetrieexperimente in Verbindung mit Molekulardynamiksimulationen wird in dieser Arbeit die Wechselwirkung der 20 Aminosäuren in verschiedenen Puffersystemen beleuchtet, wobei Lysin und Arginin als starke Bindungspartner identifiziert wurden. Ausgewählte Derivate von L-Alanine und L-Arginine wurden verwendet, um den individuellen Beitrag des Rückgrats und der funktionellen, geladenen Gruppen der Aminosäuren zu ermitteln. Experimente und Simulationen zeigten, dass elektrostatische Wechselwirkungen die Interaktion von Aminosäuren mit Silica dominieren. Bei dem Mechanismus handelt es sich nicht um einen klassischen Ionenaustausch, sondern um eine Ionenpaarung, da das Profil der Durchflussmikrokalorimetrie keine Desorption vor dem Adsorptionereignis zeigt. Auf der Grundlage der Ergebnisse der Aminosäure-Interaktionen wurde der rational entworfene (RH)4-Peptid-Tag ausgewählt, um Fusionsproteine mit einer reinen Silicagel-Chromatographiesäule mit über 90 % Reinheit und Wiederfindung in einem Durchlauf zu reinigen. Zusätzlich halfen Simulationen und Batch-Adsorptionsexperimente die Adsorption von dsDNA in Gegenwart verschiedener Salze und Aminosäuren zu erklären. Die Adsorption von DNA an Siliziumdioxid wird von der Konzentration und der Wertigkeit der positiv geladenen Ionen in der Lösung bestimmt. Dies wird durch ein kooperatives Adsorptionsmodell verdeutlicht. Je höher die Konzentration und die Wertigkeit, desto größer ist die adsorbierte DNA-Menge. Die Ergebnisse zeigen, wie wichtig unterschiedliche Ladungen von Biomolekülen sowie unterschiedlich geladene Ionen in der Umgebung für die komplexe Wechselwirkung zwischen Biomolekülen und Silicagel in wässrigen Lösungen sind. Diese Ergebnisse können auch auf andere Wechselwirkungen zwischen anorganischen Biomolekülen in der Medizin und Biotechnologie angewendet werden und zum Verständnis der komplexen Wechselwirkungen zwischen Biomolekülen und anorganischen Oberflächen beitragen. Der

untersuchte Peptid-Tag in Verbindung mit dem Reinigungsverfahren ermöglicht die Nutzung von reinem Siliziumdioxid in der präparativen Chromatographie für die Proteinreinigung. Diese Methode ist nicht nur auf den Großmaßstab beschränkt, sondern kann auch im Laboralltag eingesetzt werden.

Table of content

Table of content.....	I
Abbreviations	III
Symbols.....	IV
Greek symbols.....	VI
1 Introduction	1
1.1 Silica.....	2
1.1.1 Properties and manufacturing process.....	3
1.1.2 Applications	8
1.1.3 Silica in chromatography	10
1.2 Biomolecule-silica interactions	13
1.2.1 General definition of adsorption	13
1.2.2 Amino acids.....	16
1.2.3 Peptides and proteins.....	19
1.2.4 Nucleic acids	21
1.3 Chromatography.....	24
1.3.1 Performance parameters.....	25
1.3.2 Chromatography for characterization.....	28
1.3.3 Applications in protein purification	30
2 Motivation	34
3 Publications	35
3.1 Buffer influence on the amino acid silica interaction	35
3.2 Insights on alanine and arginine binding to silica with atomic resolution.....	46
3.3 Purification of a peptide tagged protein via an affinity chromatographic process with underivatized silica.....	54
3.4 DNA binding to the silica: Cooperative adsorption in action	64
4 Discussion	72

5	Conclusion and Outlook.....	82
6	References	85
7	Appendix	i
7.1	Supporting Information	i
7.1.1	Buffer influence on the amino acid silica interaction	i
7.1.2	Insights on alanine and arginine binding to silica with atomic resolution	xiii
7.2	List of publications.....	xxix
7.3	Permissions.....	xxx
7.3.1	Buffer influence on the amino acid silica interaction	xxx
7.3.2	Insights on alanine and arginine binding to silica with atomic resolution	xxx
7.3.3	Purification of a peptide tagged protein via an affinity chromatographic process with underivatized silica.....	xxx
7.3.4	DNA binding to the silica: Cooperative adsorption in action	xxx

Abbreviations

AC	affinity chromatography
AEX	anion exchange chromatography
BET	Brunauer-Emmett-Teller
BIC	biospecific interaction chromatography
DBC	dynamic binding capacity
DNA	deoxyribonucleic acid
EBC	equilibrium binding capacity
FMC	flow microcalorimetry
GC	gas chromatography
GST	glutathione S-transferase
HETP	height equivalent to a theoretical plate
HIC	hydrophobic interaction chromatography
HILIC	hydrophilic interaction liquid chromatography
HPLC	high-performance liquid chromatography
IC	inverse chromatography
IEX	ion-exchange chromatography
IMAC	immobilized metal ion affinity chromatography
IR	infrared spectroscopy
ITC	isothermal titration calorimetry
LC	liquid chromatography
MBP	maltose-binding protein
MD	molecular dynamics
MNP	magnetic iron oxide nanoparticles
MST	microscale thermophoresis

NMR	magnetic resonance spectroscopy
NPC	normal phase chromatography
PZC	point of zero charge
QCM	quartz crystal microbalance
RNA	ribonucleic acid
R-P	Redlich-Peterson isotherm model
RPC	reversed phase chromatography.
RP-HPLC	reversed phase high-performance liquid chromatography
SBP	solid binding peptide
SEC	size exclusion chromatography
SFC	supercritical fluid chromatography
SPR	surface plasmon resonance spectroscopy
TEOS	tetraethoxysilane
TEV	Tobacco Etch Virus
UHPLC	ultra-high performance liquid chromatography
UPLC	ultra-performance liquid chromatography
ZE	zonal elution chromatography

Symbols

a	distance left between peak curve and t middle of the peak [L / s]
a_{RP}	Redlich-Peterson constant [mg^{-1}]
A	Eddy diffusion
A_s	asymmetry factor

b	distance right between peak curve and t middle of the peak [L / s]
B	longitudinal diffusion
c	concentration [g L ⁻¹ / mol L ⁻¹]
C	mass transfer
c _{eq}	equilibrium concentration [g L ⁻¹ / mol L ⁻¹]
D ₀	molecular diffusivity [m ² s ⁻¹]
d _p	particle size [m]
g _{RP}	Redlich-Peterson exponent
H	HETP [m]
h	reduced HETP
h _{0.1}	10% peak height [AU]
h _{0.5}	half peak high [AU]
H _K	Henry coefficient
K	equilibrium constant
K _D	Langmuir sorption coefficient [L g ⁻¹]
K _F	Freundlich sorption coefficient [L g ⁻¹]
K _{RP}	Redlich-Peterson sorption coefficient [L g ⁻¹]
K _S	Sips sorption coefficient [L g ⁻¹]
L	column length [m]
m _L	total moles of binding sites for the solute in the column [mol]
n _{1...n_n}	total moles of binding sites for the solute in the column [mol]
n _F	Freundlich exponent
n _S	Sips constant [L mg ⁻¹]
N	plate number
q	load [g g ⁻¹]

q_{\max}	maximum load [g g^{-1}]
R	universal gas constant ($8.3144598 \text{ J mol}^{-1} \text{ K}^{-1}$)
r_f	retention factor
T	temperature [$^{\circ}\text{C}$]
t_0	retention time of tracer [s]
t_{\max}	elution time of the peak maximum [s]
t_r	retention time of substance [s]
v	linear flow velocity [cm h^{-1}]
v'	reduced velocity [cm h^{-1}]
V_M	volume mobile phase [L]
V_m	void volume [L]
V_S	volume stationary phase [L]
$w_{0.1}$	peak width at 10% peak height [L / s]
$w_{0.5}$	peak width at half peak height [L / s]
ΔG^0	Gibbs free energy [$\text{kg m}^2 \text{ s}^{-2}$]
ΔH	enthalpy change [$\text{kg m}^2 \text{ s}^{-2}$]
ΔS	entropy change [$\text{kg m}^2 \text{ s}^{-2} \text{ K}^{-1}$]

Greek symbols

ε	extra-particle porosity
ε_p	intra-particle porosity
ε_t	total porosity
Φ	phase ratio

1 Introduction

Silica is an unknown hero in the history of humankind, and the scientific tale of silica has many chapters. Silica was there when life began around 3.5 billion years ago as a key player. Disguised as stone tools, silica contributed to the evolution of humankind to create and understand technology, mathematics, and other complex systems, which finally led to whom we are today. Silica is omnipresent in our world, and you probably cannot live a day without encountering silica directly or something that was made with its help. The importance of interactions at the silica-water-interface thus already rose with the origin of life and is what keeps us alive today.^{1,2} Every drop of water you drink was filtered through silica at some point, and many of the drugs taken against deadly diseases are produced with the help of modified silica in the form of stationary chromatographic phases.³ However, silica has hardly been used in its pure form for bioproduct processing, despite its high binding affinity towards proteins and DNA.⁴ Instead, silica is usually used as a carrier material due to its high chemical and mechanical stability. Therefore, the surface must first be functionalized, which leads to a reduced binding capacity of the material, increased material costs, and, at the same time, the functional ligands tend to be unstable.⁵ In connection with the growing demand for high-quality bioproducts, the demand for alternative, low-cost purification processes rises. Consequently, the question arises on how biomolecules interact at the aqueous silica surface and whether it is possible to use earth-abundant materials such as silica in combination with solid-binding peptide tags for cost-efficient purification of recombinant fusion proteins.

After critically reviewing the existing literature on silica, chromatography, and silica-biomolecule interactions Section 3.1 shows the scientific new results on the interaction between all 20 amino acids individually with silica in the context of buffer effects. A deeper understanding of the interaction process and the underlying mechanism improves the understanding of protein-silica interactions. Hence, in Section 3.2, differently capped amino acids are studied to identify the contribution of the individual functional groups of the amino acids on the interaction. After identifying silica binding amino acids, a suitable peptide tag is further validated and tested in Section 3.3. The implementation of a model for amino acid-silica interactions led to the investigation of DNA binding to silica in Section 3.4.

You are about to find out how and why biomolecules interact with inorganic oxide surfaces such as silica and how we can make use of this knowledge for protein and DNA purification. Starting with the smallest building blocks, the amino acids, up to the purification of a protein using a newly designed peptide tag.

1.1 Silica

Silica is the combination of the two most abundant elements in the Earth's crust. Oxygen and silicon make up 46.6% and 27.7% of the Earth's crust (Figure 1.1), respectively.^{6,7} This abundance manifest in the wide variety of silica and silicate materials resulting in the ubiquity of silica. Silicone is also the eighth most common element in the universe, originating from the stellar evolution of massive stars. The nuclear fusion reaction forms large amounts of magnesium, silicon, and oxygen, and after exploding as a supernova, the newly formed elements are discharged into deep space, accumulating on rocky planets, like Earth.⁸

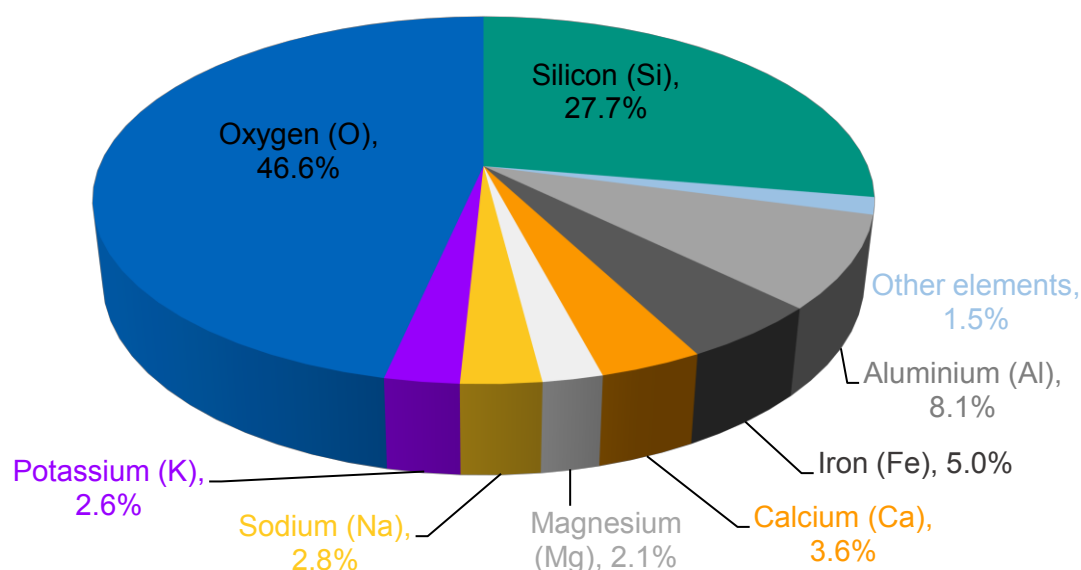


Figure 1.1 The elite eight of the Earth's crust.

Generally, silica takes the form of a triangular pyramid, or rather, a tetrahedron, where four oxygen atoms corner the silicon atom (Figure 1.2 A).^{1,4,9-12} This tetrahedron form exists for two reasons. First, silicon has four bonds to fill, and second, the four oxygen binding partners repel each other due to their charge.^{1,11} The silica tetrahedron is not just a stable pyramid. The four oxygen atoms leave the silica tetrahedron incomplete because every oxygen itself needs to engage two bonds. One solution for this issue is the assembly of multiple silica tetrahedra resulting in each oxygen atom being shared by two silicon atoms (Figure 1.2 B). In this bigger, more complex silica there are, on average, two oxygen atoms per one silicon atom, also known as silicon dioxide (SiO_2).^{1,10,13} Nevertheless, how much silica tetrahedra assemble, there will always be unsaturated oxygen atoms at the periphery. In the presence of water, hydrogen atoms substitute as second partner resulting in terminal hydroxyl (OH) groups (Figure 1.2 C and D).^{1,11-13}

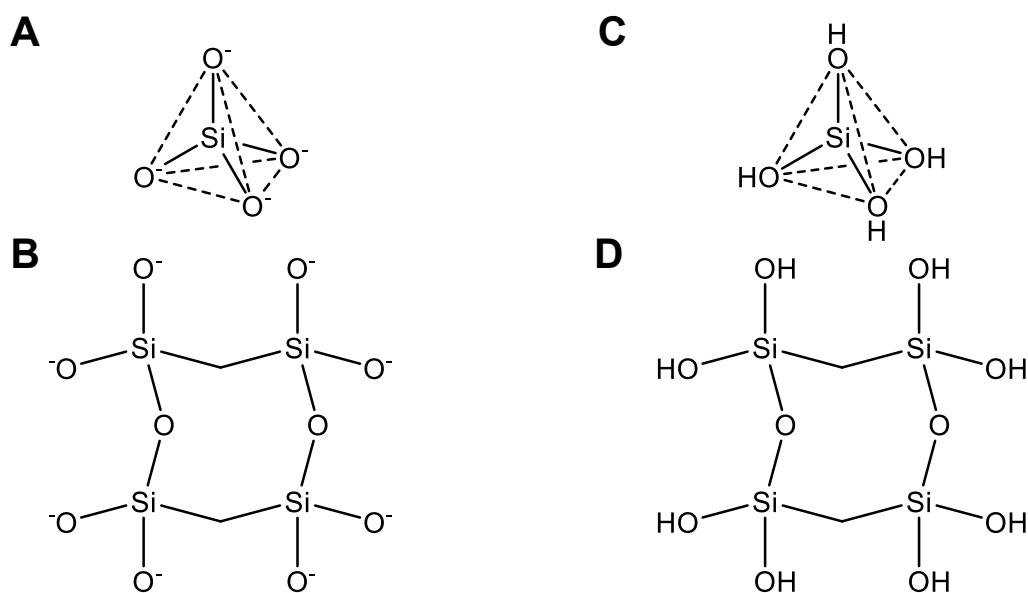


Figure 1.2: The forms of silica: (A) The silica tetrahedron. (B) Silica tetrahedra. (C) Silica acid. (D) Silica tetrahedra with hydrogen atoms saturating the peripheral oxygen atoms (OH). The solid lines indicate bonds between atoms; the dashed lines outline the tetrahedral shape.

Depending on its origin, silica is present in different crystalline and amorphous allotropic forms. In nature, silica is usually found as quartz, the only polymorph stable at Earth's surface, which makes up about 12-14 wt% of the Earth's crust mass, second after feldspar.³ Quartz is also the primary component of most sands. However, SiO₂ is also important in biology in the form of silica biomineralization, also known as biosilicification, a process by which organisms incorporate silica into their skeletal structure.¹⁴⁻¹⁷ Eukaryotes like diatoms, radiolarians, and siliceous sponges use this process to enhance their structural integrity, and some higher plants such as rice and horsetail use biosilicification to reduce biotic and abiotic stress. Biosilicification in prokaryotes is less well studied and just recently has been recognized.¹⁴ It is yet unclear if and how silica is vital for animals, but due to omnipresence of silica, animals are constantly ingesting silica.¹ The wide range of applications attributable to the intrinsic properties of silica has led to increasing attention and research on biosilicification in the context of the constant call for sustainability to conserve natural resources.^{15,16}

1.1.1 Properties and manufacturing process

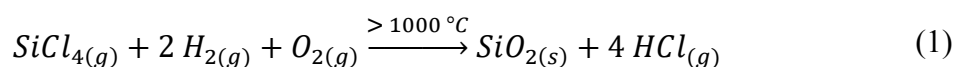
The intrinsic properties of silica originate from the strong Si-O bond and the three-dimensional connectivity of the tetrahedra.^{1,3,11,12,18} The four sp³ orbitals of silicon overlap with the 2p orbitals of the four oxygen atoms coordinating around the silicon to form strong σ bonds.³ The mean bond length of Si-O in the tetrahedra is 0.162 nm, which is responsible for the high bond

strength. Due to the high bond strength, silica has a high melting point of ~ 2000 °C and a high hardness of 1103 – 1260 kg mm⁻² (Vickers hardness test).^{3,19} Therefore, silica is also almost stable towards thermal expansion or high-pressure compression, reacting with rotating or tilting of the tetrahedra.³ Silica is practically chemically inert to acids, except for hydrofluoric acid, but prone to being dissolved in alkali solutions.^{11,12} Furthermore, silica has insulating properties regarding heat and electricity.³ Crystalline silica such as quartz responds to applied mechanical stress with electric polarization resulting in an electric current. This so-called direct piezoelectric effect was discovered in 1880 by Pierre and Jacques Curie.^{1,3} The process is also reversible: An applied electric field changes the shape of the quartz crystal, and an alternating field even causes crystals to vibrate. Other properties of silica such as particle size, porosity, pore size, surface area, or surface chemistry depend on the origin of the used material and the manufacturing process.^{3,11,12,20}

As silica can be crystalline or amorphous and thus is used for different applications, various manufacturing processes exist. Crystalline silica in the form of natural quartz is usually gained by quarrying followed by further processing to uniform and clean the quartz grains from impurities. Impurities can be accessory minerals such as feldspar, iron oxides, titanium oxides, but also ions incorporated in the crystal structure such as iron, aluminum, potassium, calcium, and sodium.^{3,21} To get rid of these impurities various cleaning processes are used including, amongst others: washing, crushing, grinding, sieving, magnetic separation, chemical treatment, and color sorting. Amorphous silica in nature is found as diatomite, which refers to sedimented, fossilized remains of single-celled diatoms.^{3,22} Diatomite exhibits low density, high porosity, and low thermal conductivity. Diatoms are algae that use unique proteins for the biosilicification of silicic acid monomers from the surrounding water to enhance their membrane with silica, called a frustule.²³ Diatomite deposits are found worldwide and are mined in open-cast mines. The most crucial part of mining diatoms is to keep the structural integrity of the porous diatom skeleton intact to retain the high porosity. Drying or calcination removes impurities such as water and organic substances. A homogeneous particle-size distribution is achieved by grinding or calcination.³

While natural silica is widely available in different forms, they are often difficult to process and clean for applications relying on pure, uniform silica particles. Therefore, the implementation of different synthetic processes allowed the generation of uniform silica with reproducible properties.²⁰ The different processes generate different types of silica regarding shape, size, porosity, and surface groups: colloidal silica, pyrogenic silica, silica gel, precipitated silica, and

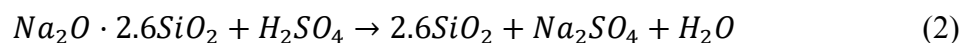
mesoporous silica nanoparticles. The three most important methods to obtain the different silicas are high-temperature flame decomposition, reverse microemulsion, and sol-gel synthesis.^{20,24} While the first method is conducted in an anhydrous vapor phase (gaseous route), the other two are performed in liquid environments (liquid route). The gaseous route leads to pyrogenic silica, also known as fumed silica, and can be performed via flame hydrolysis, electric arc, or plasma methods.²⁴ However, flame hydrolysis is the only method viable on an industrial scale. For flame hydrolysis, silicon tetrachloride (SiCl_4) is the standard raw material, which is vaporized in dry air and hydrogen flame at over 1000 °C. The reaction proceeds via Equation 1:



Silica produced this way is spherical, nonporous, and has a particle size between 7-40 nm.²⁵ These primary particles agglomerate through partial sintering and high-temperature fusion into larger, mesoporous silica aggregates. The pyrogenic silica has a high specific surface area of 50-400 m² g⁻¹, measured by the Brunauer-Emmett-Teller (BET) method.^{20,25} The properties of this silica can be controlled by the concentration of reactants, flame temperature, and residence time in the flame.²⁵ Additives can be used to alter the surface properties of the silica to get mixed metal oxides, hydrophilic silica, or hydrophobic silica.³ The flame hydrolysis results in high purity silica with only metallic element contaminants in trace concentration and low silanol surface density (2.5-3.5 SiOH nm⁻²).^{3,12} However, due to the high energy needed for the reaction, they are also more expensive than silica produced via one of the liquid routes.

Liquid synthesis routes for silica use supersaturation resulting in the polymerization of silicic acid ($\text{Si}(\text{OH})_4$).^{20,26} The condensation polymerization occurs at neutral pH and can form gel networks (silica-gel) or individual particles (precipitated silica). In general, gels form in acidic conditions due to little or no surface charge leading to flocculation of silica particles. Alkaline conditions stabilize individual particles through a high surface charge, which can grow under Oswald ripening.¹² In contrast to the gaseous route, silica derived from the liquid route has a higher silanol surface density (5-6 SiOH nm⁻²).³ The two most commonly used methods for liquid synthesis are microemulsion and sol-gel synthesis.²⁷ For the microemulsion synthesis, a water-in-oil microemulsion is used, also often referred to as reverse microemulsion. Silica nucleation and growth happen in the water phase. Hence, the form of the droplets controls the shape and size of the particles. The microemulsion environment inhibits cross-particle polymerization enabling this method to generate much smaller particles than the other liquid

methods.²⁸ In the early stages, this method generated silica particles of 1-10 μm . After optimization, the technique generated silica nanoparticles of around 20 nm and up to 10 μm with narrow size distributions.²⁰ The microemulsion synthesis is generally performed in alkaline environments. However, through the addition of fluoride, the process also works in acidic conditions.²⁹ Microemulsion synthesis also allows the synthesis of core-shell particles with silica as shell or core.³⁰⁻³² The sol-gel process is based on the polymerization of monomers into a colloidal solution (sol), followed by gelation into an integrated network (gel). Dependent on the particular process, the formation of distinct particles or a polymer network is possible.^{3,12} Methods of the sol-gel process include precipitating, the Stöber method, and biomimetic synthesis. The precipitating method is the most important synthetic methods and holds the highest market value.^{3,20,33} The synthesis is based on neutralizing soluble silicate with acid generating oversaturation of the silicic acid leading to polymerization and precipitation out of solution through neutralization.^{11,12,20} Commercially, it is generally produced from sodium silicate neutralized with sulfuric acid per Equation 2:



If the pH is adjusted and hold at a value between pH 8-10, discrete spherical primary particles of 2-20 nm form. These particles intergrow into three-dimensional aggregates forming larger agglomerates in the final stage. If the pH is shifted further into the acidic region, silica-gel forms. Properties of the precipitated silica and silica gel are controlled mainly by pH, temperature, stirring rate, and reactant concentration.²⁰ Precipitated silica offers a BET surface area of 25-800 $\text{m}^2 \text{g}^{-1}$ and silica gel 300-1000 $\text{m}^2 \text{g}^{-1}$.³ The Stöber method is another sol-gel process named after its inventor Werner Stöber, who reported this method first in 1968.³⁴ Silica particles synthesis via this method is easy to control and generally generates spherical, monodisperse, nano- to micrometer size particles and is the most applied method regarding the manufacturing of silica nanoparticles.^{20,35,36} The synthesis is based on the hydrolysis and condensation polymerization of alkoxy silanes, generally tetraethoxysilane (TEOS). Therefore, TEOS is added into a water-alcohol solution in the presence of ammonia as an alkaline catalyst. This way, particles of 50 nm to 2 μm can be obtained based on the reaction conditions.^{34,36} Over the years, the Stöber method was thoroughly investigated on the influence of the reaction conditions on particle properties. Modified Stöber synthesis allows the production of mesoporous silica nanoparticles and aerogels.^{37,38} Last but not least, humankind once more used nature as a role model, even to produce silica particles. Biomimetic synthesis summarizes sol-gel methods based and inspired by biosilicification of diatoms and siliceous sponges.²⁰ To date,

only a few silaffin peptides, mostly from diatoms and silicate in proteins from siliceous sponges, are known to accomplish this task. The most investigated silaffin peptides are silaffin-1A₁, silaffin-1A₂, silaffin-1B, and the R5 variant, which all derive from the sil1 protein of the diatom *Cylindrotheca fusiformis*.^{39,40} These native silica precipitating peptides work at mild reaction conditions and promise superior control over the process to generate, besides the typically spherical particles, structures like thin sheets⁴¹, nanotubes,⁴² and nanorods.⁴³ While not being used commercially yet, biomimetic synthesis is a promising technique for silica manufacturing due to the low energy consumption and mild reaction conditions.²⁰

While properties such as shape, size, porosity, and specific surface area are essential traits to silica, the surface and, more specific the surface groups on the silica surface are the critical property regarding interactions between silica and other molecules.^{11,12} Generally, two functional groups can be found at the silica surface: siloxane links (Si-O-Si) and silanol groups (Si-OH).¹² The siloxanes originate from the silica bulk structure and are labeled as Q⁴ by NMR Qⁿ terminology, where *n* indicates the number of bridging oxygens.³ Silanol groups form in the presence of water, and as can be seen in Figure 1.3, different silanol groups exist on the silica surface. *Isolated* silanols (Q³) are single Si-OH groups that are more than 0.33 nm from neighboring silanols, thus unable to form mutual hydrogen bonds. If two silanol groups are less than 0.33 nm away, they can establish hydrogen bonds forming *vicinal* or *interacting* silanols. Two OH groups linked to the same silicon (Q²) form a silanediol called *geminal* silanols.^{11,12} Siloxanes are hydrophobic, while silanol groups are responsible for the hydrophilic character of silica.³ The surface chemistry thus depends on the distribution of the siloxane, silanol, and ionic siloxide groups. Siloxide groups arise from silanol groups through deprotonation at pH > 2-3, equivalent to the point of zero charge (PZC) of the respective silica.^{18,44}

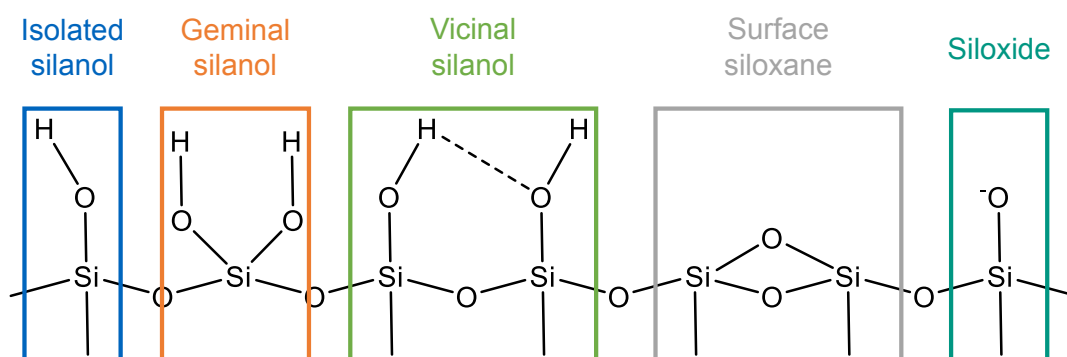


Figure 1.3: Illustration of the surface groups occurring at the silica surface. Siloxide groups are deprotonated silanol groups (isolated, geminal, and vicinal) that appear and accumulate in aqueous environments with increasing pH.

The siloxanes constitute around 23-30% of the functional surface groups. A significant part of the silanol surface groups consists of isolated and vicinal silanols with 60-65%. From this, isolated silanols make up 6-19%. The geminal silanols constitute around 10-12% of the total silanols on the surface.¹³ The ratio of the surface groups shifts with increasing temperature to only siloxanes at >1000 °C. The surface silanol can also be divided into two populations of acidity. The more acidic population represents around 15-20% of total silanols with a $pK_a \sim 4.5$, and the less acidic population has a $pK_a \sim 8.5$.^{4,45} In contact with water, these silanols deprotonate and produce a negative charge on the surface. The surface charge density increases with pH. A thermally unprocessed, fully hydroxylated silica surface contains about 4.7 SiOH nm^{-2} .^{3,18,44} At a pH ~ 7.5 , 4% to 21% are deprotonated, strongly dependent on the synthesis method and ionic strength in solution.⁴⁴ The reported amount of siloxide groups per nm^2 at pH 7.5 and ionic strength of 0.1 M range between 0.21 and 1.0.⁴⁶⁻⁵² The broad range of results highlights the sensitivity of the silica surface to synthesis conditions and the importance of controlling the properties of silica for its various applications.

1.1.2 Applications

Silica plays a vital role in everyday life. Depending on its form and origin, silica is used in a wide field of applications. Raw crystalline quartz material mainly goes into the construction and glass industry. It is also used to produce high-quality glasses with exceptional optical properties for optical applications as lenses, prisms, and quartz glass. For the purification and softening of drinking water, quartz pebbles and sand are the primary filter materials. Grinding and milling processes use quartz sand and powder due to their hardness. Quartz is also essential as raw material to produce precursors for other silica reactions such as silicic acid, waterglass, and elemental silicon.³

Due to the natural high surface area, natural amorphous silica from diatoms primarily finds application as a filtration agent.³ Filtration of beer, wine, juices, swimming pool water, solvents for chemical cleaning, wastewater, varnishes, and paints are performed with special filters from diatoms. Insulating material often consists of diatomite due to the high volume of trapped air in the porous structure. Another important use of diatom silica is as an absorption agent for gases, in cat litter, and drying agents. As a fine scourer material, it finds applications in car polisher, toothpaste, and other polishing products. As catalytic support, it secures the handling of dangerous goods such as pyrotechnics and matches.^{3,53}

Synthetic silica finds its applications based on the synthesis route. Precipitated silica has the highest production scale regarding synthetic silicas and has the benefit of tailor-made synthesis. Among many applications, the oldest and most important use is reinforcing elastomer products: Shoe soles, tires compounds, cable sheathing, and technical rubber articles. The addition of silica improves the rubber's tensile strength, tear strength, hardness, and abrasion resistance. Additionally, a major application of the precipitated silica is as a carrier. The high adsorptivity and flowability enables the production of powders containing up to 70% liquid, which is essential, for example, in the animal feed industry for feed additives or as a carrier of insecticides.^{3,20}

Pyrogenic silica from flame hydrolysis has a very high purity (>99.8 wt% SiO₂) and low moisture content, making it ideal as reinforcing filler in rubbers or as an electrical insulator. As a thickening agent for liquid systems such as printing ink, paints, and resins, pyrogenic silica finds another important application in adjusting the rheological properties of liquids. Similarly, pyrogenic silica controls the rheological properties of liquid systems as an anti-settling agent in filler- or pigment-containing liquids or as a dispersant in solid-containing liquid systems.^{3,20,25}

Silica also found its way into nanotechnology, and mesoporous silica nanoparticles find wide applications in today's society. The most typical representatives of this class are MCM41 and SBA15. Mesoporous silica nanoparticles are mainly used in research towards medicine for drug delivery and biosensor technologies. Their huge surface area with small particle size allows vast amounts of drug substances to be transported into cells with only a few particles. Similarly, the particles can be filled with fluorescent dyes, transporting the dye into target cells due to surface functionalizations.⁵⁴⁻⁵⁶

Last but not least, silica gel is a widely used variant of silica. It offers high surface areas and a porous structure, which makes it predestined as an adsorbent. Its main and also first use was as a desiccant. In World War I, it was used for adsorption of vapor and gases in gas masks and later in World War II to keep penicillin dry. Today, we meet it as little bags to protect especially electronic devices from moisture damage during transportation. However, silica gel also finds its applications in high technological applications. In the form of aerogels, dried silica gels with intact porous structure, the low dielectric constant of silica is being exploited. Silica gel is also used to purify nucleic acids and is the most used stationary phase material in chromatography.^{3,20,24,57}

In listing the major applications of the various types of silica, it should be noted that this was only a glimpse and the applications for silica are far greater considering silica to be easily modified. The silanol groups give rise to the possibility of surface functionalization, especially by silanization, to obtain surfaces with physicochemical desirable properties for even more specialized applications.^{58,59} The need for these different types of silica is why the different methods of manufacturing described earlier are all still relevant and used.

1.1.3 Silica in chromatography

As mentioned above, silica in the form of silica gel is the most used material for stationary phases in chromatography.^{24,60,61} The extensive use of silica for chromatography has different reasons. One natural advantage of silica for chromatography is the natural chemical stability against solvents and acids, as well as the mechanical strength due to the high hardness, increasing the longevity of the material and enabling working at high pressures in column chromatography, especially high-performance liquid chromatography (HPLC). Another advantage of silica is the possibility to generate various forms of silica gel regarding particle shape, particle size, and pore size depending on the manufacturing process as described in Section 1.1.1. Monodisperse, spherical particles allow homogenous packing of columns resulting in more efficient separation and are commonly synthesized by the Stöber method.⁶¹ The pore size of the silica particles controls the retention of analytes due to the resulting usable surface area.⁶⁰ The pores contain the majority of the surface area of the particles, which means that the surface area is inverse proportional to the pore size. These properties result in high reproducibility, rapid mass transfer, and good capacity, which are highly desired in chromatography. Last but not least, silicas' potential to be easily modified by silanization enables it as initial material for bonded stationary phases. Therefore, different chemical groups are introduced to obtain desired physiochemical properties such as a hydrophobic surface through the introduction of organic groups such as octyl (C8) or octadecyl (C18) resulting in so-called reverse phase chromatography (RPC). Bare silica is used for normal phase chromatography (NPC) or hydrophilic interaction liquid chromatography (HILIC). However, RP-HPLC with modified silica as stationary phase is still the most frequently used analytical chromatography method today.^{24,60,61}

Historically, before 2000, the industry used fully porous spherical silica particles with 5–10 μm particle size and organic groups bonded to the surface in HPLC columns for most applications.⁶⁰ Over several decades different optimization strategies were followed to increase efficiency. The

major action was reducing the average particle size to sub-2 μm particles. Due to the drawback of higher backpressure the Waters Corp. (Milford, MA, USA) presented the first equipment enabling the work with these small particles in 2004, named ultra-performance liquid chromatography (UPLC), which later generally got accepted as ultra-high performance liquid chromatography (UHPLC).⁶⁰ To tackle the drawback of high backpressure core-shell particles were first developed by Kirkland, becoming commercially available from Agilent Technologies in 2001 under the trademark Poroshell 300 with particle sizes of 5 μm .⁶² The particles consist of a solid core and an overlying porous shell as illustrated in Figure 1.4, which acts as the actual separation layer. This setup shortens the diffusion paths of the analytes in the stationary phase and reduces the dead volume of the entire column. Advanced Materials Technology was the first to supply smaller particles with 2.7 μm under the trademark Halo, followed by Ascentis Express from Sigma-Aldrich, and Kinetex and Aeris from Phenomenex.⁶³ Today, all big brands provide these kinds of silica core-shell particles under different trademarks.

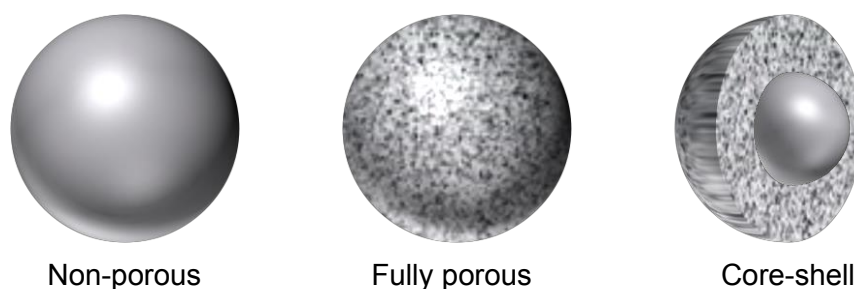


Figure 1.4: Illustration of different chromatographic silica particle types.

Besides the particle size, the silica itself was optimized concurrently due to the main problem of peak broadening of basic compounds in RP-HPLC: the silanol groups. Before the year 2000, silica often had a high metal content, which increased the acidity of free silanol groups on the surface and thus the interaction with basic compounds. This silica is commonly referred to as Type A silica. To solve this problem, many manufacturers used a mineral acid wash before the bonding step to eliminate the metal impurities. Today silica stationary phases are prepared from highly pure silica, such as TEOS, which has low metal concentrations and is referred to as Type B silica. However, RP silica from Type B silica still exhibits residual silanols of $\sim 50\%$ on the surface. The derivatization is inefficient because of the steric hindrance of the bulky, long alkyl chains linked to the surface.^{24,60,61}

A first approach to reduce the number of free silanol groups on the surface was the introduction of organosilanes into the structure resulting in hybrid silica particles resulting in hybrid silicas as shown in Figure 1.5. The first-generation hybrid silica was a combination of TEOS with

methyltriethoxysilane (XTerra) from 1999. In 2004 Waters introduced the second-generation hybrid silicas using TEOS with bis(triethoxysilyl)ethane (XBridge). Hybrid silica materials achieve silanol coverages of $\sim 2.5 \mu\text{mol m}^{-2}$, which is at least $1.5 \mu\text{mol m}^{-2}$ less than conventional silica supports. Furthermore, the material can sustain pH values up to 12.⁶¹

A new type of silica for HPLC stationary phase is the hydride silica, developed by Joseph Pesek at the San Jose State University, USA.⁶⁴⁻⁶⁷ This type of silica is based on Type B silica, where silica hydrides (Si-H) replace the free silanols otherwise present on the surface (Figure 1.5), consequently named Type C silica. Type C silica is marketed today by the company MicroSolv™ Technology Corporation. The advantage of this silica is the negligible amount of free silanols on the surface, as $\sim 95\%$ of silanols are converted to silica hydrides.^{60,61} Type C silica is a promising new material, which has yet to reach the utility, breadth, and importance of Type B silica mainly due to the limited number of suppliers and the unavailability as core-shell or sub- $2 \mu\text{m}$ material.⁶⁰

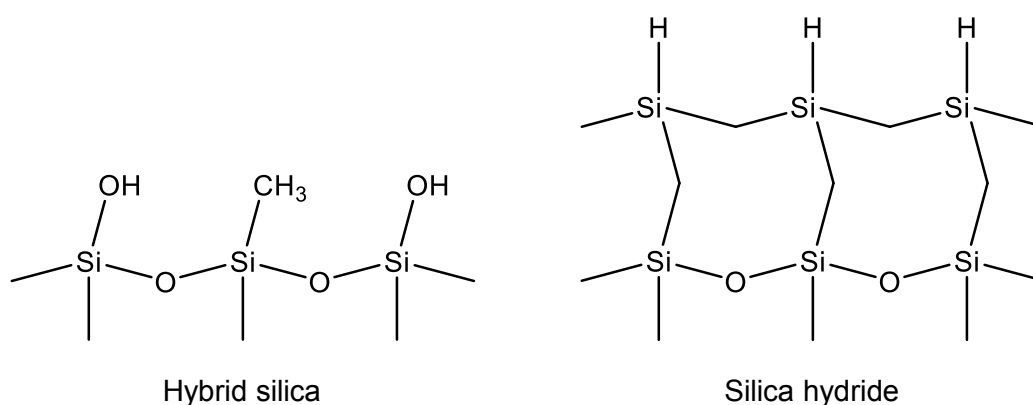


Figure 1.5: Chemical structure of hybrid and hydride silica

An alternative to particle technology as a packing material is the use of monoliths. Monoliths were commercialized under the trademark Chromolith by Merck, Germany. Unlike conventionally filled columns, monolithic columns do not consist of particles but a single piece of high-purity monolithic silica gel. Chromatographic efficiency is achieved through the dual pore structure. Macropores create a flow channel through the column with an average diameter of $2 \mu\text{m}$ allowing rapid flow at reduced backpressure. The mesopores within the porous structure create a very large surface area for adsorption and thus separation.^{24,61}

1.2 Biomolecule-silica interactions

Studying interactions between biomolecules and silica is of great interest from many points of view. As already outlined in Section 1.1, silica is ubiquitous. It was there when life began on Earth, and it is used in all kinds of products of our daily life. Interactions between a solid inorganic surface such as silica and biomolecules depend on the detailed structure and the composition of both surface and biomolecule. The silica surface provides siloxane bridges and silanol groups, enabling hydrophobic, hydrophilic, and electrostatic interactions. Biomolecules are organic molecules such as peptides, proteins, or nucleic acids, consisting of different base materials, enabling various interaction types. Which interactions there can occur between silica and biomolecules leading to adsorption are discussed in the following.

1.2.1 General definition of adsorption

Adsorption describes the increase in the concentration of a substance at the gas-solid or liquid-solid interface, mediated by surface forces. The adsorbed film is called adsorbate, the respective surface adsorbent. Generally, adsorption is divided into chemisorption or physisorption. Chemisorption occurs due to the formation of covalent bonds by sharing or transferring electrons. Physisorption is based on weaker interactions such as electrostatic interactions, hydrogen bonds, or van der Waals interactions.^{68,69}

Usually, isotherms describe the adsorption of gases and solutes to a surface. Isotherms describe the equilibrium state of the adsorbate on the adsorbent at a constant temperature and can provide information about the mechanism of the adsorption. The simplest adsorption isotherm model is Henry's isotherm model. The linear model can be used under the assumption of adsorbed molecules being secluded from each other, unable to interact, and all the spaces on the adsorbent are energetically equal. However, the linear model is limited to low concentrations of solute. In order to describe the adsorption of molecules to solid surfaces, multiple isotherm models have been formulated. The most commonly applied isotherm model is the Langmuir isotherm as shown in Equation 3, where q represents the load, q_{max} the maximal possible load, and c_{eq} the equilibrium concentration of the adsorptive.⁷⁰ K_D is the sorption coefficient, or dissociation constant, which need to be determined along q_{max} to obtain the isotherms.^{68,69,71}

$$q = \frac{q_{max} * c_{eq}}{K_D + c_{eq}} \quad (3)$$

The Langmuir isotherm works under four distinct assumptions: (1) monolayer adsorption; (2) adsorption sites are homogeneous distributed; (3) constant adsorption energy; (4) negligible

interaction between adsorbate molecules. The dissociation constant is linked to the Gibbs free energy via:

$$\Delta G^0 = RT \ln K_D \quad (4)$$

with the gas constant R and the temperature T .

Langmuir already acknowledged the diversity of different surfaces and adsorbate species manifesting in different physical adsorption mechanisms. Therefore, he classified six simple adsorption mechanisms displayed in Figure 1.6: (A) single-site Langmuir adsorption, where the surface hosts only identical adsorption sites for a single host molecule; (B) multisite Langmuir adsorption, where more than one adsorption site is available, each independently fitting for a its own host molecule; (C) generalized Langmuir adsorption, where the surface consists of an intractable amount of different binding sites; (D) cooperative Langmuir adsorption, where binding sites are identical but different host molecules can adsorb on the same site; (E) dissociative Langmuir adsorption, where adsorption is a 2-fold process accompanied by molecular dissociation; (F) multilayer Langmuir adsorption, where binding sites are identical and independent but molecules are permitted to adsorb above each other.^{70,72} For case 6 Langmuir had no explicit adsorption isotherm formulated. However, here the well-known Brunauer-Emmett-Teller (BET) model is considered as special Langmuir model.^{69,73} The BET model has the same assumptions applied for the Langmuir isotherm and additionally assumes binding energies for adsorption in all layers to be equivalent to the first layer. The BET model is most widely used to calculate the specific surface area of nonporous and porous materials.⁷²

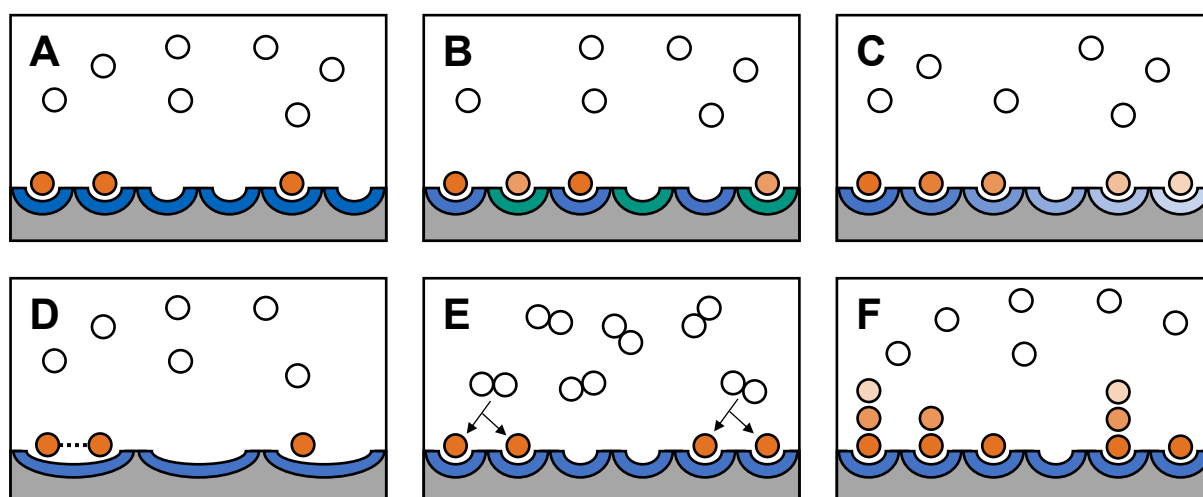


Figure 1.6: The six adsorption classifications proposed by Langmuir: (A) single-site adsorption, (B) multi-site adsorption, (C) generalized adsorption, (D) cooperative adsorption, (E) dissociative adsorption, (F) multilayer adsorption. White circles illustrate the gas/liquid molecules, the orange shaded circles different types of adsorbed molecules, the blue shaded and green half arches different adsorption sites.

The second most used isotherm model is the Freundlich model, especially for nonlinear adsorption phenomena. In contrast to the Langmuir model, the Freundlich model (Equation 5, with the Freundlich constant K_F and exponent n_F) is regarded an empirical equation without physical meaning.⁷⁴

$$q = K_F * c_{eq}^{\frac{1}{n_F}} \quad (5)$$

The Freundlich isotherm is not restricted to monolayer formation and is often applied for multi-layer adsorption on heterogenous surfaces.^{69,74} The Freundlich isotherm is only applicable for low pressure and fails at high pressure. For $n_F = 1$ the Freundlich models reduces to the linear model.⁶⁹

To overcome some of the drawbacks of the Langmuir and Freundlich model hybrid models of the two were created. The two most notable and used are the Sips and the Redlich-Peterson (R-P) three-parameter isotherm models.^{69,74} The Sips model is a combination of the Langmuir and Freundlich isotherm model and applicable for monolayer adsorption in homogenous and heterogenous systems. The Sips isotherm model is presented through:

$$q = q_{max} \frac{K_S * c_{eq}^{n_S}}{1 + K_S * c_{eq}^{n_S}} \quad (6)$$

with K_S and n_S being the Sips constants. The Sips model becomes the Langmuir model for $n_S = 1$ and the Freundlich model for low adsorbate concentration. Similarly, to the Freundlich model, the Sips model does not satisfy Henry's law for low adsorbate concentrations. The R-P isotherm model can also be used for heterogenous and homogeneous systems and is represented through:

$$q = \frac{K_{RP} * c_{eq}}{1 + a_{RP} * c_{eq}^{g_{RP}}} \quad (7)$$

with K_{RP} and a_{RP} being constants and g_{RP} being the exponent ($0 \leq g_{RP} \leq 1$). For $g = 1$ the R-P model reduces to the Langmuir model, when $g = 0$ or c_{eq} gets very low, it reduces to the linear model. Additionally, if c_{eq} approaches infinite, it reduces to the Freundlich model. In theory both, the Sips and R-P isotherm model, provide better predictions for the equilibrium, because they use three parameters. However, they are also more complicated regarding linear regression, which makes it difficult to solve the Sips and R-P model.⁷⁴

As already stated, the Langmuir and Freundlich model are the most commonly applied models, especially for metal ions, dyes, pharmaceuticals, and other organic pollutants. The main reasons

therefore is the simplicity of the models due to linear regression, which is complicated for other isotherm models.⁷⁴

The dissociation constant and maximum load are usually determined with supernatant analysis. However, there are other methods to determine the dissociation constant such as isothermal titration calorimetry (ITC), microscale thermophoresis (MST), surface plasmon resonance spectroscopy (SPR), or quartz crystal microbalance (QCM). Getting detailed information about the binding mechanism is generally performed by spectroscopic methods such as infrared spectroscopy (IR), Raman spectroscopy, or magnetic resonance spectroscopy (NMR).⁷⁵

1.2.2 Amino acids

Amino acids are organic molecules embodying an amino, carboxyl, and a functional side chain group. There are 20 canonical amino acids, each with a specific side chain responsible for their individual properties (see Figure 1.7). While amino acids can be present in L or D configuration, only the L variants are used in nature to build proteins. In solution, amino acids undergo rapid deprotonation when changing the pH from low to high.⁷⁶ Especially the interaction with silica is of great interest in various research fields such as medicine, engineering, chromatography, biotechnology, and even for the search of the origin of life.^{2,4,24,77-80}

Of all the amino acids, glycine and alanine are the most studied, as they have the simplest structure with only the backbone amino and carboxyl group and are present in a zwitterionic state in solution. Zwitterionic amino acids can adsorb to the neutral silica surface through hydrogen bonds between the amino and carboxyl group of the amino acid and the silanol groups on the silica surface.⁸¹⁻⁸⁴ However, NMR measurements and molecular dynamic (MD) simulation revealed that direct adsorption is prevented in the presence of water molecules, and the water molecules bridge adsorption.⁸⁵⁻⁹⁰ While adsorption can occur in both the gas and liquid phases, the hygroscopic properties of silica lead to water adsorption, making liquid phase adsorption studies more reasonable. Additionally, water is ubiquitous in biological media. It needs to be considered in the adsorption process as the hydration conditions influence the interaction up to a single water molecule being able to remove a bound amino acid from the silica surface.⁸⁵ While a neutral silica surface is only present below the point of zero charge (PZC) of silica, which is, depending on the production method, around pH 2-3, in the presence of water, another effect has to be counted in: the silica surface charge. If the pH rises above the PZC, deprotonation of the silanol groups on the silica surface occurs, leading to the formation

of negative charges. These negatively charged groups can serve as binding partners for electrostatic interactions with charged amino acids such as arginine, lysine, histidine, glutamic acid, and aspartic acid. As far as glutamic and aspartic acid is concerned, adsorption only happens due to so-called ‘surface-induced precipitation’, meaning the precipitation of a mineral exclusively on an adsorbent’s surface under undersaturated bulk solution conditions.^{4,91} In contrast, studies on the adsorption of basic amino acids showed adsorption to the negatively charged silica surface in dependence of pH and ionic strength of the solution through electrostatic interactions.⁹²⁻⁹⁴ However, while the PZC of silica is around pH 2-3, sufficient ionization of the silica surface is observed for $\text{pH} > 5$, and the concentration of bound amino acids increases with pH until deprotonation of the amino acid side chains occurs. The reason for this behavior is the increasing degree of ionization on the silica surface with pH and thus the increasing number of binding sites.^{95,96} Churchill et al. investigated the influence of the PZC and the IEP of amino acids on the adsorption of different quartz surfaces.⁹⁷ They found that the further the IEP and PZC differ, the more of the respective amino acid adsorbed to the quartz surfaces. At pH values above the PZC of silica but below the IEP of the amino acid, the surface of the quartz and amino acid are oppositely charged. A few individual studies also dealt with the adsorption of nonpolar amino acids indicating hydrophobic interactions to play a role to some extent.⁹⁸⁻¹⁰⁰

A few systematic studies compared the adsorption of different amino acids in solution experimentally.^{93,95,98,101-104} The conclusion drawn is that most amino acids do not interact with the silica surface in aqueous systems because the amino acids are present in their zwitterionic form, where the attraction of NH_3^+ and repulsion of COO^- groups by the silanol groups balance each other.⁹⁵ Only amino acids with additional positively charged groups can interact electrostatically with the negatively charged silanols on the silica surface, which highly depends on pH and ionic charge.^{92,95,105} So, while in theory, electrostatic, hydrophobic, and hydrogen bond interactions can occur, with higher pH the influence of hydrogen bonds and hydrophobic interactions diminish due to the increasing electrostatic interactions.

As can be seen from the various studies on this complex topic, the underlying mechanism of amino acids adsorption to silica is not fully understood yet. Investigating the interactions of amino acids helps to understand the interactions of more complex molecules such as peptides and proteins.

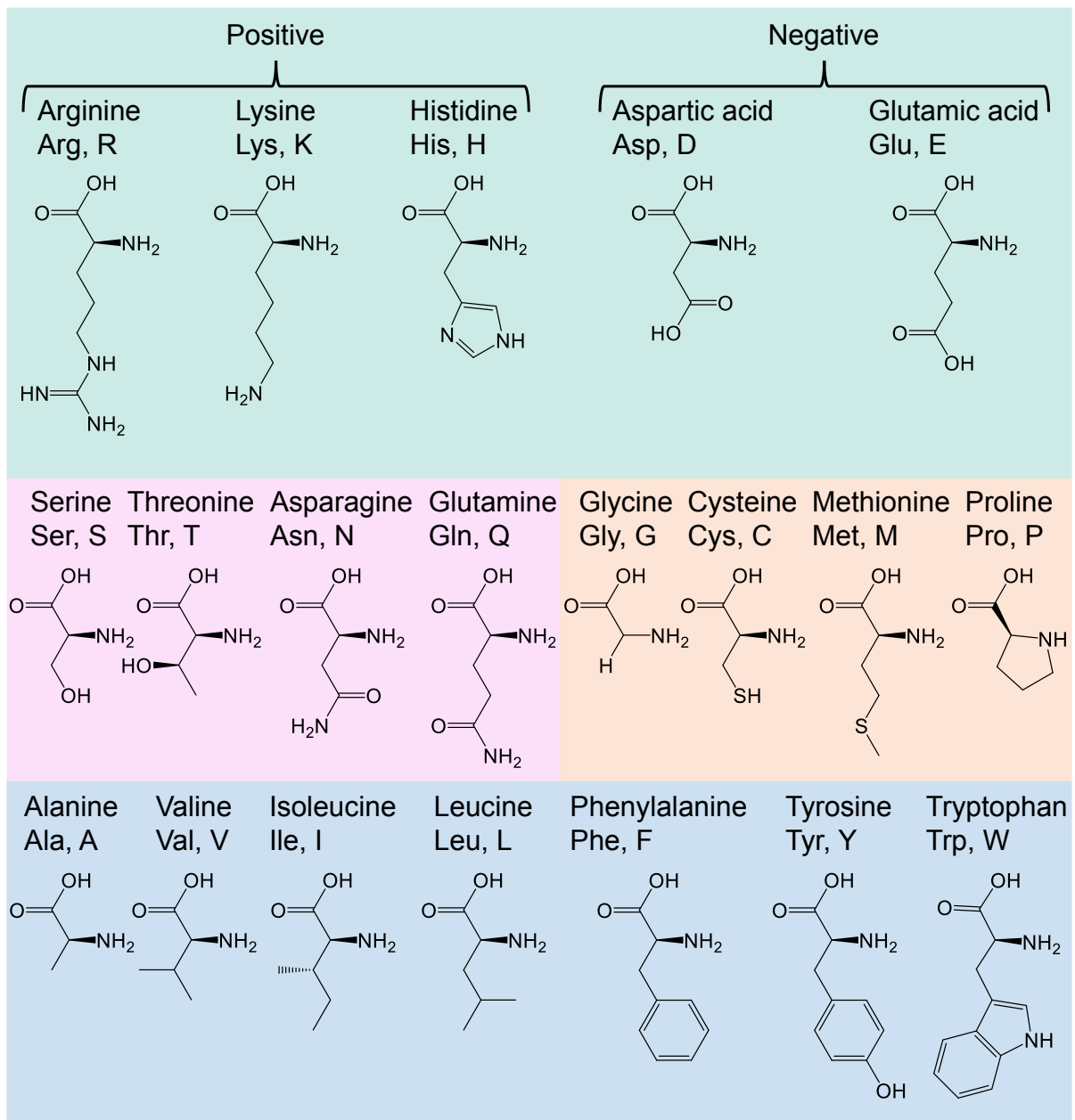
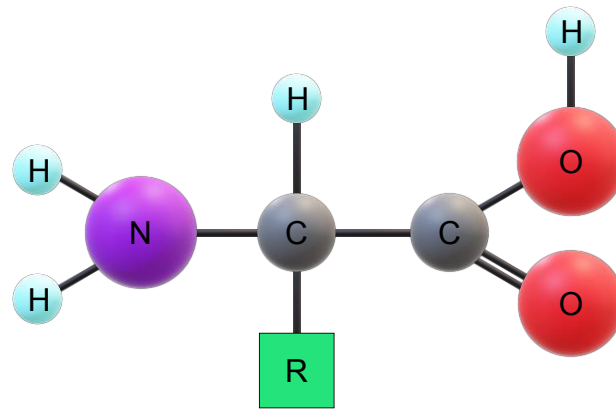


Figure 1.7: Top: General structure of amino acids. C = Carbon, N = Nitrogen, H = Hydrogen, O = Oxygen. Bottom: Structure of the 20 canonical amino acids divided by general properties with 3-letter and 1-letter code. Green = charged side chains, Pink = polar side chains, Orange = special cases, Blue = hydrophobic side chains

1.2.3 Peptides and proteins

Peptides are natural polymers formed by the condensation of an amino group of one amino acid with the carboxyl group of another amino acid leading to the formation of a peptide bond. A peptide with more than 50 amino acids is generally known as a protein, which is usually arranged in a three-dimensional, biologically functional structure. The sequence and distribution of the amino acids, or more precisely of the functional side chains of the amino acids, define the peptides' or proteins' chemical properties.

With increasing length and, therefore, functional groups, the prediction and analysis of peptide and protein adsorption processes become more complex. However, peptides show, in general, a similar trend to amino acid adsorption. In the study of Patwardhan et al., seven different dodecapeptides were investigated on their adsorption behavior on different aqueous silica nanoparticles, which exhibit different silanol surface densities due to the synthesis methods.⁴⁴ It was shown that peptides with more basic residues adsorbed stronger to silica. Additionally, the adsorption was stronger on silica surfaces with a larger density of negatively charged siloxide groups. This behavior is supported by the finding that cationic peptides are adsorbed at a low initial concentration while noncationic peptides showed no to weak interaction with silica, demonstrating that electrostatic interactions are the dominant force. However, noncationic peptides adsorbed after they overcame a certain initial peptide concentration threshold value. The authors explained the adsorption through hydrogen bonding due to the peptides containing polar amino acids such as serine, threonine, and tyrosine. At the same time, however, it was observed that the loading of the silica surface with peptide cations reaches saturation, while an increase in the adsorption amount continued to be measured for polar peptides with increasing concentration. Consequently, adsorption via electrostatic interactions reaches a saturation region as soon as the deprotonated silanol groups are occupied. Since only the silanol groups serve as binding partners, monolayer adsorption occurs. Binding based on hydrogen bonding, on the other hand, leads to the formation of a multilayer, since after saturation of the silica surface, the already adsorbed peptides can continue to serve as binding partners. In conjunction with hydrophobic regions within the silica structures, hydrophobic interactions can also continue to play a role in peptide adsorption, analogous to the observations for the adsorption of amino acids. The same group of authors investigated the experimentally found behaviors using simulation and concluded ion pairing via electrostatic interactions as the main interaction force. Hydrogen bonding, hydrophobic interactions, and conformational effects diminish with increasing pH and only play a role at lower pH.^{44,106} A similar conclusion was drawn by Maity et al., who did an alanine scan on a short peptide (QPASSRY) with single

molecule force spectroscopy by atomic force microscopy and molecular simulations.¹⁰⁷ The alanine scan revealed the crucial role of the arginine residue and, even more interesting, the influence of the proline, which increased the adhesion of the peptide towards the surface due to conformational stiffness. Another well-studied example is the work by Jonsson and co-workers, who showed that synthesized peptides with basic amino acid residues placed particularly at positions, where they will be positioned at the same site of an α -helical structure, will change their structure from linear to α -helical upon adsorption.^{108,109}

While peptides' interaction with silica generally seems to follow the trend seen for amino acids, proteins exhibit a far more complex three-dimensional structure. As structural properties already influence the adsorption of small peptides, thermodynamic and kinetic factors get crucial when looking into the adsorption of proteins on inorganic surfaces such as silica.⁷⁸ However, the adsorption affinity continues to be dominated by electrostatic interactions while hydrogen bonds and hydrophobic interactions play a minor role.^{110–115} The amino acid content of the proteins in combination with the pH value thus strongly influences interaction. It was observed that proteins with high tertiary structural flexibility adsorb faster, but they get displaced by proteins with higher affinity in the long term. The rigidity of proteins is determined by intramolecular interactions such as disulfide or salt bridges. Proteins with a flexible structure are able to adapt to the shape of the adsorption surface and establish a larger contact area, and as a consequence, a greater number of interactions is formed between the protein and the surface.^{116,117} However, due to adsorption, there is a loss of native folding and thus, in the worst case, a loss of protein activity. Experiments showed that the conversion of α -helices to β -folds could be observed as a result of adsorption.¹¹⁸ The extent to which adsorption leads to unfolding is determined by the material's surface properties, protein stability, protein concentration, pH, and ionic strength. Protein stability can be influenced to a certain extent by genetic engineering. The surface structure can be adapted to a certain extent by modifying the manufacturing process but basically remains unchanged. Thus, in addition to protein flexibility, the adsorption mechanism primarily determines the extent of denaturation. For example, adsorption based on hydrophobic interactions usually leads to a stronger denaturation than adsorption based on electrostatic interactions or hydrogen bonds since the hydrophobic core is located in the shielded center of the protein.^{119–121}

In the last couple of years, silica binding tags have moved into focus to overcome these drawbacks. Finding solid binding peptides (SBPs) is achieved by various methods. The most popular being phage display.^{44,107,122–126} Another method is using peptides or proteins from

nature as blueprints.^{39,127–132} A related method to the prior is a bioinformatic approach, where known silica-binding peptides are classified, and an optimized peptide sequence is generated.^{133,134} In some studies, specially designed peptides are used to investigate specific properties such as three-dimensional structures.^{135–139}

Two groups have mainly done considerable work on silica binding tags for protein purification and immobilization. Kuroda and co-workers were the first to investigate this specific topic with the 273 amino acid large ribosomal protein L2 from *E. coli*, titled the ‘Si-Tag’.¹⁴⁰ While showing promising results for immobilization and purification of different proteins in regards to purity (87/90%) and recovery (84/92%), the size of the tag had considerable influence on the enzyme partner.^{132,140–143} Consequently, they switched to the CotB1 protein (171 amino acids) from *B. cereus* using only the C-terminal 14 amino acid region (CotB1p) for affinity purification achieving 95% purity and 85% recovery.¹³¹ They further optimized CotB1p regarding the length down to only seven amino acids (SB7: RQSSRGR), achieving ~90% purity and recovery of 75-90%.¹⁴⁴ An alanine scan with the SB7 peptide revealed the necessity of the arginine groups in the peptide for interaction with silica.¹⁴⁴ In a further search for silica binding peptides, Abdelhamid identified the Colp1 (20 amino acids), Salp1 (15 amino acids), EctP1 (19 amino acids), and Sil3K/Sil3R (12 amino acids) peptides, which he derived from natural marine proteins.^{145–147} Baneyx and co-workers are the second group of people working on silica binding tags. However, they focus exclusively on the Car9 (DSARGFKKPGKR) peptide, identified initially as a carbon binder.^{125,148} They achieved purities of over 90% at a low recovery of around 63% but optimized the method in 96-well plate format for high-throughput experiments.^{149,150} They also distinguished the arginine and lysine residues as main driver for adsorption by testing alanine and glutamine modified Car9 variants.¹⁵¹ Additionally, they identified a cooperated binding mechanism for Car9 experimentally and simulative.^{151,152} Both groups filed a patent for their tag system.^{153,154}

1.2.4 Nucleic acids

Nucleic acids are large biomolecules composed of nucleotides, which are essential for all forms of life. The nucleotides are built by a sugar (ribose or deoxyribose), a phosphate group, and a nitrogenous base (adenine, cytosine, guanine, thymine, and uracil). They chain together to form ribonucleic acid (RNA) or deoxyribonucleic acid (DNA). Since we know how nucleic acids are built and how to modify them, nucleic acid separation has become an increasingly important tool.¹⁵⁵ While at the beginning purification of nucleic acids was time-consuming and required

toxic reagents, with the development of solid-phase extraction techniques, commercial purification kits can be purchased today for easy and fast nucleic acid purification.^{155–157} Vogelstein and Gillespie pioneered in 1979 with an approach for the extraction of DNA from a biological sample with the use of a silica matrix.¹⁵⁸ Since then, silica has developed into the standard material for the purification of nucleic acids.^{155,159} Methods with silica matrices are easy to perform, reproducible, and deliver high-purity nucleic acids, the disadvantages are the one-time usage, and small DNA fragments cannot be recovered due to strong binding.¹⁵⁵ Glass particles as a powder in the stationary chromatography phase or as microbeads have been developed as a simple, sensitive, and reproducible method for nucleic acid extraction. However, the right equipment is needed for the extraction, and the method exhibits a comparatively high cost. Natural diatomaceous earth is also used for nucleic acid purification. However, this method is not routinely used due to the high costs.¹⁵⁵ Concurrently, different setups for the extraction were developed. The most notable are spin columns filled with silica or ion exchange material, which operate under specific buffer conditions. The column-based method is very fast and reproducible, and the main drawback is the need for a small centrifuge. Magnetic beads are an alternative to the column method because they eliminate the centrifugation steps. The magnetic beads are functionalized with different surface groups such as amino groups or silica.¹⁶⁰ The magnetic beads allow an equipment-free process with high potential for automation.^{155,161}

While silica seems to be the choice for nucleic acid extraction due to the easy handling, low toxicity, cost, and detailed knowledge about fabrication, a fundamental question arises. DNA and RNA are polyanions, and silica also bears negative charges on the surface when $\text{pH} > \text{PZC}$. So how do nucleic acids actually interact with silica? Different and also varying driving forces have been attributed to DNA adsorption to silica. In general, the nucleic acid extraction methods use chaotropic salts such as guanidinium thiocyanate or sodium perchlorate. The salt is added to overcome the long-ranged electrostatic repulsion, which neutralizes the negative charge of the DNA and silica, establishing a cation-bridge.^{162–165} Elution afterward is achieved at high pH and low ionic strength. Other methods control the pH to alter the negative charge on silica to achieve adsorption or functionalize the silica surface with positively charged groups.^{166–168} In recent studies, Vandeventer et al. showed DNA adsorption to silica using amino acid buffers.^{169,170} There are also investigators claiming hydrogen bonding of uncoiled nucleotides and the surface of silica.^{171,172} Alternatively, the adsorption is attributed to an entropy shift with dehydration of DNA and the silica surface, followed by hydrogen bonding is the dominant effect.¹⁶⁷ The entropy also plays a role when attributing the adsorption of DNA to silica to

hydrophobic effects.^{173,174} It is also known that single-stranded DNA binds more strongly to silica than double-stranded DNA, which has been attributed to the higher flexibility of single-stranded DNA, hydrophobic interactions through free unpaired bases, and lower charge density and thus charge repulsion.¹⁷⁵ Nucleic acid adsorption to silica depends on various conditions such as pH, ionic strength, electrolyte type and valency, and conformation of the nucleic acid (linear, plasmid, supercoiled, single-stranded, double-stranded).^{160,165,167,169,171,175-179}

1.3 Chromatography

Chromatography is a physical separation process for substances in which separation is based on the differential distribution between a stationary and mobile phase. Credits for discovering the technique generally go to the Russian-Italian botanist Mikhail Tsvet, who used the term ‘chromatography’ first in his publication in 1906 working on chlorophyll. The name chromatography derives from the Greek words for ‘color’ (*chroma*) and ‘to write’, (*graphein*) inheriting its first use for separating plant pigments. However, Tsvet’s method was not immediately recognized as key to many separation problems. It took another roughly 40 years until Archer J. P. Martin and Richard L. M. Synge revived the method by developing partition chromatography, for which they received the Nobel Prize in Chemistry in 1952. Today chromatography is manifold and an essential unit-operations in chemical and biotechnical processes.^{180–182}

Chromatography is generally defined as a process in which a fluid phase (mobile phase), carrying a mixture of components, flows through a fixed bed (stationary phase). The two phases are immiscible and can have different physical states by which different chromatographic techniques are distinguished. While the stationary phase can be a liquid or a solid, chromatographic nomenclature is mostly done by the physical state of the mobile phase. In gas chromatography (GC), an inert gas is used as mobile phase. In supercritical fluid chromatography (SFC), the mobile phase is a dense gas above its critical temperature and pressure, and in liquid chromatography (LC), a liquid of low viscosity is used as the mobile phase. Regarding the stationary phase, the nomenclature refers more to the bed shape and distinguishes in planar (two dimensional) and column (three dimensional) chromatography.^{180–182} In the scope of this thesis, the focus lies on liquid column chromatography.

Chromatographic processes offer unprecedented versatility due to the many different separation mechanisms. The size of molecules is exploited in size exclusion chromatography (SEC) by diffusion of molecules within the porous stationary phase; no direct interactions play a role in the separation. Polarity is used in normal-phase (NPC) and reversed-phase (RPC) chromatography. In NPC, the stationary phase is more hydrophilic than the mobile phase, while in RPC, the stationary phase is more hydrophobic than the mobile phase, and molecules are separated through different strengths of interaction with the stationary phase. Hydrophobic interaction chromatography (HIC) uses the same principle as RPC but in a non-denaturing environment due to the absence of organic solvents. High concentrations of salt mediate the interactions. Ion-exchange chromatography (IEX) exploits positive and negative charges on

molecules by a reversible interchange of ions, positive or negative, between the stationary and mobile phases. In affinity chromatography (AC) highly specific macromolecular binding is used for the interaction of a target molecule with the counterpart on the stationary phase. The most prominent representatives for affinity chromatography are immobilized metal ion affinity chromatography (IMAC) and biospecific interaction chromatography (BIC), such as biotin-streptavidin or antibody-antigen interactions. The overall purpose of the process also divides the nomenclature for chromatography. The detailed analysis of a mixture or substance is called analytical chromatography, where the so-called high-performance liquid chromatography (HPLC) predominately is used. In HPLC, the operating pressure is significantly higher as in traditional LC, allowing smaller particles for higher separation efficiency. In analytical chromatography, small volumes and low concentrations can be characterized. If the purpose of the chromatography is the isolation and purification of a substance, it is called preparative chromatography, which can be scaled from small-scale laboratory with only a few milliliters up to commercial production of several hundred liters.^{180–182}

1.3.1 Performance parameters

Like every process, the separation success in chromatography depends on several process parameters.^{180–185} One of the most important parameters to describe the efficiency of a chromatographic column is the height equivalent to a theoretical plate (HETP), H . The HETP is a hypothetical zone, in which the two chromatographic phases are in an equilibrium, and corresponds to the plate number, N , via the column length, L , shown in Equation 8:

$$H = \frac{L}{N} \quad (8)$$

In an ideal column $H \rightarrow 0$ or correspondingly $N \rightarrow \infty$. The HETP depends on the material and the linear flow velocity, v . The dependence of the HETP on the flow rate, is described by the van Deemter equation, which considers physical, kinetic, and thermodynamic properties:

$$HETP = A + \frac{B}{v} + C * v \quad (9)$$

with A being the Eddy-diffusion resulting from different channeling through the column, B describing the dispersion resulting from longitudinal diffusion, and C representing the mass transfer between mobile and stationary phase. A schematic diagram of the van Deemter equation is shown in Figure 1.8.

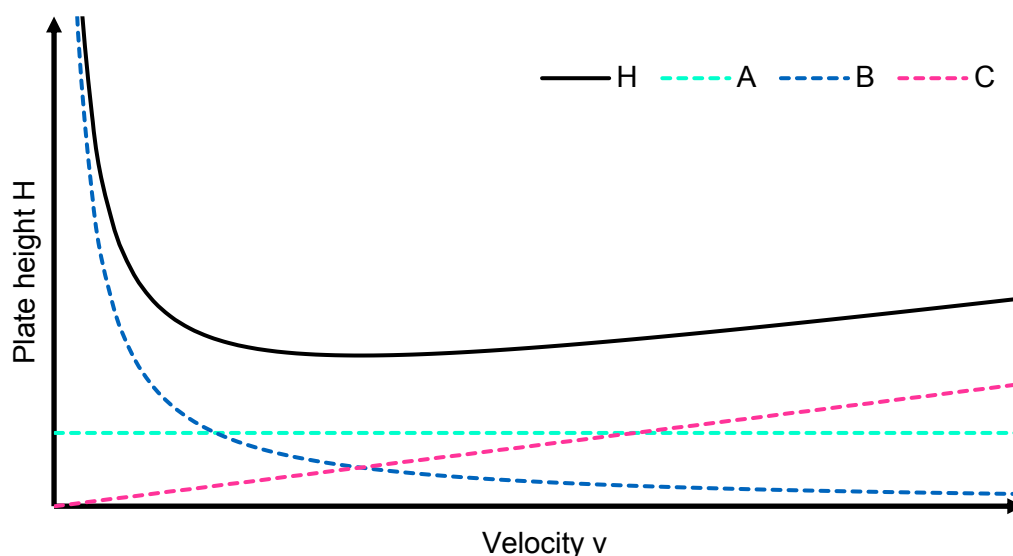


Figure 1.8: Schematic illustration of the van Deemter equation showing the dependence of the plate height H from the flow rate v . A illustrates the effect of the Eddy-diffusion, B the longitudinal diffusion, and C the mass transfer.

The HETP can be determined experimentally with a pulse injection of a tracer substance. If the resulting peak is nearly symmetrical, H can be determined by:

$$H = \frac{L}{5.54} \left(\frac{w_{0.5}}{t_{max}} \right)^2 \quad (10)$$

where $w_{0.5}$ is the peak width at half peak height, and t_{max} is the elution time of the peak maximum as shown in Figure 1.9. The symmetry of the peak is important for calculating the HETP and is also a parameter for chromatographic efficiency. The asymmetry factor, A_s , shows how close the peak shape is to a Gaussian function and is calculated by:

$$A_s = \frac{b}{a} \quad (11)$$

with a and b being the peak width at 10% height as defined according to Figure 1.9. An ideal peak exhibits an $A_s = 1$. An $A_s > 1$ displays a tailing peak and an $A_s < 1$ displays a fronting peak. Generally, in chromatography $0.8 < A_s < 1.8$ is desirable.

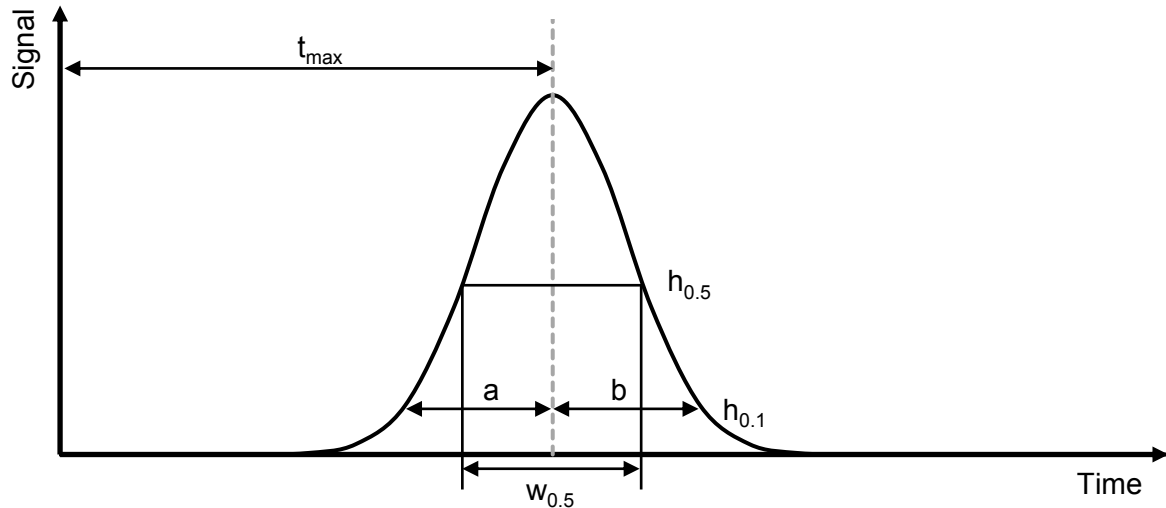


Figure 1.9: Illustration of a chromatographic peak with the parameters used for calculation of HETP and asymmetry factor. t_{max} is the elution time of the peak maximum, $w_{0.5}$ is the peak width at half peak height $h_{0.5}$, a and b are the distances between the peak curve and the middle of the peak at 10% peak high $h_{0.1}$.

To compare different stationary phases with different particle sizes, d_p , with each other, the reduced HETP, h , is used, which is determined by:

$$h = \frac{H}{d_p} \quad (12)$$

The reduced HETP is generally a function of the reduced velocity, v' :

$$v' = \frac{v d_p}{D_0} \quad (13)$$

with D_0 being the solute molecular diffusivity in the mobile phase.

Another critical parameter in chromatographic separation is the retention factor, r_f , of a substance and is calculated by:

$$r_f = \frac{t_R - t_0}{t_0} \quad (14)$$

where t_R is the retention time of the substance and t_0 is the retention time of a non-interacting tracer. The tracer should be around the same size as the compared substance to assure the same fluid dynamical behavior in the column.

As the binding events in the column mediate retention in chromatography, the retention factor can be converted into the Henry adsorption coefficient, H_K , by

$$H_K = \frac{r_f}{\Phi} \quad (15)$$

with the phase ratio Φ being calculated by:

$$\Phi = \frac{1 - \varepsilon_t}{\varepsilon_t} \quad (16)$$

where ε_t is the total porosity of the column.

Generally, there are three relevant porosities when using porous particles in the column: the total porosity ε_t , the intra-particle porosity ε_p and the extra-particle porosity ε . The total porosity is related to the intra-particle and extra-particle porosity by:

$$\varepsilon_t = \varepsilon + (1 - \varepsilon)\varepsilon_p \quad (17)$$

The total porosity can be determined by a tracer small enough to access all pores of the particles. The extra-particle porosity can be determined by a tracer, which is unable to access the pores.

The Henry coefficient refers to the linear equilibrium constant between the solid and liquid phase in chromatography. Therefore, it can be used as equilibrium constant K in the van't Hoff equation giving information about the difference in free energy of adsorption by:

$$\ln r_f = \ln K + \ln \frac{V_S}{V_M} = -\frac{\Delta G^0}{RT} + \ln \frac{V_S}{V_M} \quad (18)$$

where ΔG^0 is the free energy of adsorption. The phase ratio between the stationary and mobile phase is calculated with V_S and V_M , respectively. R is the gas constant, and T the temperature.^{180–182}

In both analytical and preparative chromatography of proteins, the process parameters play a crucial role for the efficiency and need to be monitored and optimized.

1.3.2 Chromatography for characterization

Various techniques enable the characterization of surface properties and interactions between surface functional groups with molecules such as Raman spectroscopy, X-ray diffraction, contact angle measurements, IR, NMR, QCM, NMR, MST, and others.^{186,187} However, these methods are limited regarding observing surrounding environmental influences. Furthermore, the methods for determining interactions are based on batch sorption experiments, which cannot track weak adsorption due to small deviations between the initial and equilibrium concentration.¹⁸⁷ Batch experiments also have the drawback of long equilibration times, large amounts of needed sorbent, and low automation potential. Column chromatography provides an alternative, complementary method to overcome these drawbacks. In chromatography, the retention factor relies on the interaction between the probe molecule and the stationary phase and increases with stronger interaction following the equation:

$$r_f = \frac{(K_{A1}n_1 + \dots + K_{An}n_n)m_L}{V_m} \quad (19)$$

The retention depends on the total moles of binding sites for the solute in the column, m_L , the association equilibrium constants for the solute at each binding site, K_{A1} to K_{An} , and the relative mole fraction for each type of binding site in the column, n_1 to n_n , and the void volume, V_m .¹⁸⁸ Equation 19 highlights that retention is a function of the solute's binding strength for the column, the total amount of binding sites present, and the relative distribution of these sites. Thus, the retention factor is equivalent to the probe molecule's interaction strength with the stationary phase's surface groups and can be acquired by measuring different probe molecule retentions under various experimental conditions – the retention changes due to the influence of solute-solvent, solute-stationary phase, and solvent-stationary phase interactions. Changes to the retention factor can be addressed to various physico-chemical properties of the investigated material or probe molecules. This connection is used in chromatographic methods such as inverse chromatography (IC) or zonal elution chromatography (ZE). Both methods rely on determining the retention time of a small fraction of a simple probe molecule under varying conditions in the chromatographic environment such as the probe molecule chemistry, size, and concentration but also column temperature, mobile phase compositions, and flowrate.^{188–192}

IC is a method originally used in gas chromatography to study stationary phase materials' surface and bulk properties, which can also be applied for liquid chromatography. In this method, the change in retention time depending on the probe molecule properties is measured and addressed to material properties and is thus considered a material characterization method. IC has been successfully used to determine the surface energies of hydrophobic stationary phases,^{190,193} the activity of residual silanol groups in RP-HPLC,¹⁹¹ and solute adsorption isotherms.^{192,194} In contrast, ZE is a method originating from affinity chromatography to characterize the interaction between the probe molecule, a competing agent, and the immobilized binding agent. It is thus considered a method for determining the kinetics of biological systems and measuring the rate constants of these processes.^{188–190,192,193,195–197}

The interaction between a material and a probe molecule also depends on the change of the Gibbs free energy of adsorption ΔG_{ads} . The free energy change, in turn, depends on the adsorption's enthalpy change, ΔH_{ads} . Adsorption can be both exothermic, indicated by a temperature increase, or endothermic, indicated by a temperature decrease. Attractive forces between a surface and an adsorbed molecule or between molecules are attributed to exothermic adsorption events. In contrast, endothermic events are attributed to conformation or orientation

changes, such as hydrophobic protein adsorption, or solvent release from the surface, making the adsorption entropy-driven. This thermodynamic relationship can be written as:

$$\Delta G_{ads} = \Delta H_{ads} - T\Delta S \quad (20)$$

with ΔS representing the entropy change in the system. The enthalpy change in the system can be measured by calorimetric methods such as the commonly used isothermal titration calorimetry (ITC). However, ITC is a batch experiment and cannot account for the dynamic effects of chromatographic processes. Therefore, flow microcalorimetry (FMC) has been developed to measure the heat change *on-line* and *in-situ* for a better understanding of chromatography processes, simulating a packed-bed chromatographic system at a micro-scale. Additionally, FMC can reveal the subprocesses involved in the interaction between molecules and surfaces.^{198–200} FMC has been successfully used to describe the kinetics of the adsorption and desorption process of biomolecules such as amino acids,^{201,202} proteins,^{199–204} and DNA.²⁰⁵

FMC is able to reveal the complexity of interactions between biomolecules and adsorbent. For example, the crystallinity of an adsorbent (calcium hydroxyapatite) significantly influences the affinity of protein adsorption: higher crystallinity leads to higher protein affinity.²⁰⁶ In ion-exchange processes with proteins an initial endothermic peak, corresponding to an entropic change, accompanies the exothermic electrostatic interactions due to the release of water from the surface and conformational changes of the protein upon adsorption.²⁰⁷ In a recent study, FMC revealed the binding between monoclonal antibodies and *m*-aminophenylboronate is not only affinity-based, as described for decades, but has electrostatic character as well and must therefore be understood as multimodal interaction.¹⁹⁹ These studies highlight how FMC can contribute to understanding adsorption processes.

1.3.3 Applications in protein purification

Proteins are large and complex amphipathic molecules made up of amino acids with a delicate three-dimensional structure that exposes hydrophobic, hydrophilic, polar, apolar, and charged regions to the environment, allowing them to interact with different materials. These properties are used in one of the most important unit operations in the downstream processing of proteins: chromatography. Among the various modes in chromatography, especially SEC, HIC, IEX, and AC, are used to separate proteins out of complex mixtures. Different aspects such as temperature, pH, buffer species, and ionic strength must be considered when controlling the

complex protein adsorption process. However, the chemistry and physical structure of the stationary phase is as important for the adsorption process.^{180–182}

In SEC separation is achieved by different migration of solutes through the column due to the steric exclusion of larger molecules from the porous network of the chromatographic stationary phase. Thus, SEC is the only chromatographic method in the list not using direct interactions between the stationary phase and the proteins for separation. Proteins of different sizes can enter the porous particles to a different degree and elute at different times, with larger molecules eluting earlier than smaller molecules. In comparison to other chromatographic methods, the selectivity and productivity in SEC are generally not very high, because of that, SEC is mainly used as a final step for changing the buffer or refolding the proteins. Another common use of SEC is for the estimation of the molecular weight of proteins or protein complexes.^{180–182,208}

In HIC, the stationary phase is functionalized with hydrophobic ligands. The interaction of the proteins is promoted by salt, and elution is triggered by reducing the salt concentration in the mobile phase with the least hydrophobic protein eluting first. High concentrations of salt (>1 M) are necessary for the hydrophobic interaction, with the most popular salt being ammonium sulfate, which makes HIC an ideal follow up for protein precipitation methods or IEX.^{180–182,209,210}

In IEX, electrostatic interactions are the dominant binding mechanism. Proteins expose different charges on their surface dependent on the content of acidic and basic amino acids. The overall charge of the protein depends on the pH in the solution. The pH at which a protein carries no electrical net charge, is called the isoelectric point (IEP). At $\text{pH} > \text{IEP}$, the protein has a negative net charge; at $\text{pH} < \text{IEP}$, a positive net charge. The interaction occurs reversibly to an oppositely charged group on the surface of the stationary phase. Elution is triggered by increasing the salt concentration in the mobile phase leading to elution by displacement. The stronger the electrostatic interaction, the higher salt concentration is needed to elute a protein. IEX resins are classified into cation-exchangers (negatively charged) and anion-exchangers (positively charged). Another way IEX resins are categorized is into weak and strong ion-exchangers. As the name may suggest, the distinction does not reflect the protein binding strength but the stability of the protonation behavior of the surface groups to pH changes. Weak ion-exchangers change their charge with pH, while strong ion-exchangers keep their charge over a wide range of pH, generally at least from pH 2 to 10. IEX is a common technique in protein purification because of the versatility due to the availability of different stationary

phases and buffer systems. Additionally, IEX provides high binding capacities and preserves the biological activity of proteins.^{180–182,211,212}

To achieve the high purities needed in the production of therapeutic proteins such as antibodies, AC is unavoidable. While in SEC, HIC, and IEX, the intrinsic properties of the target protein limit the selectivity of the methods, AC uses highly specific macromolecular binding to separate a target protein from complex mixtures. Examples from nature for these interactions are antibody-antigen, enzyme-substrate, or ligand-receptor.^{196,213} In AC, one of the two partners is immobilized on the surface of the chromatographic material and is known as ‘affinity ligand’. Elution in AC is achieved either non-specific by changing pH, ionic strength, or the composition of the mobile phase, or biospecific by a competing agent.²¹³ One of the most commonly used AC technique is Protein A affinity chromatography, the gold standard for purifying monoclonal antibodies.²¹⁴ However, the affinity mechanism is limited to the individual binding partners and with the rise of proteomics and the growing need for recombinant proteins, another affinity purification technique has been established: a polypeptide fusion partner, termed ‘affinity tag’.^{215–217}

Affinity tags are unique amino acid sequences, initially designed for protein purification only. Today, they are considered an essential tool in multiple methods such as western blotting, flow cytometry, microarrays, mass spectrometry, lab-on-a-chip, and protein localization studies.²¹⁸ The tag can be a whole protein, a protein domain, or a small peptide chain and attach to a wide range of substrates, including carbohydrates, biomolecules, metal chelators, or antibodies. Affinity tags are generally classified by their location and interference. Commonly the tags are attached to the N- or C-terminus of a recombinant protein, but there are also so-called internal tags, which are added within the coding sequence of a protein.^{219,220} Regarding their biochemistry, affinity tags are classified as interfering or non-interfering, which refers to whether they influence the protein of interest’s biochemical properties. Non-interfering tags generally exhibit a short sequence of amino acids such as the His-tag (6 histidines) or the FLAG-tag (DYKDDDDK) and are not needed to be removed after purification. However, these tags can have some beneficial effects on the properties and efficacy of recombinant proteins and improve the production quality and yield of the expression system. They can also facilitate proper folding of the protein of interest, prevent proteolysis, improve functional properties, or increase solubility.^{218,221} Interfering affinity tag sequences such as the maltose-binding protein (MBP, 396 amino acids) or glutathione S-transferase (GST, 211 amino acids) have long sequences and interfere with the structure and function of the main protein and thus must be

removed after purification. The interference often includes alternations in the biological activity, decreased protein yield, toxicity, protein aggregation, improper structural flexibility, or misfolding.^{218,220,222} Removing the tag can sometimes resolve the undesirable effects of the tags via a specific protease system such as the TEV protease (Tobacco Etch Virus). The success of tag-based purification depends on the right tag choice. The most critical choices include easy removal, single-step purification, minimal influence on structure and function, versatility (transferability to different kinds of proteins), and accessibility (freedom of the tag from the protein to be able to interact).^{220,223} However, protein type, nature of the expression system, and consecutive applications are also critical factors. While large tags may be disadvantageous at first glance, they are often needed and used in bacterial expression systems such as *E. coli* due to only 25% to 50% of the prepared proteins being soluble.²²⁴ The most commonly used tag system is the His-tag, which forms coordinated bonds with cations such as Ni²⁺, Cu²⁺, Zn²⁺, and Co²⁺, a method also known as IMAC.^{5,221,222} The His-tag has low interference with the protein function and is well studied. The most significant drawbacks are possible dimerization of the target protein, competitive adsorption of histidine-rich proteins, and toxic metal ion leaching. While each individual affinity tag has its pros and cons, there is no perfect system. Therefore, tandem tag systems have been developed. Tandem tags consist of two or even more affinity tags, often separated by a protease cleavage site, either on the C- or N-terminus or on both. With the use of tandem tags, the advantages of different tag systems can be used simultaneously, such as higher solubility (MBP) combined with a high specific interaction (His-tag). Tandem tags are recommended when preparing high purity recombinant proteins for crystallization or protein interaction studies.²²⁰ Affinity tags have improved the downstream processing of recombinant proteins. However, whether using natural interactions or affinity tags, the major drawback of affinity tags is the functionalization of the affinity ligands onto the chromatographic material, which is highly cost-intensive.^{5,225} Therefore, the interest in solid-binding peptides (SBPs) has grown in recent years. SBPs exhibit the purification of proteins with non-functionalized materials such as polymers, metal oxides, carbon-based materials, or silica.²²⁵

2 Motivation

The downstream processing of biomolecules is still an ambitious task to tackle in all kinds of biotechnological processes. Especially for therapeutic proteins, the downstream process alone can account for up to 80% of the total production costs. Also, in research labs worldwide, the need for easy purification methods of biomolecules such as recombinant proteins or DNA is essential.

Chromatography methods, such as ion-exchange or affinity chromatography, are usually the key unit operation for purifying biomolecules. For affinity chromatography, short peptide sequences such as the His-tag or FLAG-tag are exploited as highly specific affinity tags. However, there is no rose without a thorn. The affinity tags need the specific counterpart, the ligand, functionalized to the surface of the stationary phase. The manufacturing of these materials is cost-intensive, and the functionalization can be chemically unstable. Because of that, solid-binding peptides, which bind to a surface without ligand functionalization, became intriguing.

In this context, silica is a diamond in the rough. While it has been used as a backbone for stationary phases in chromatography since the beginning, it never made it as bare material. Furthermore, despite its frequent use, the interactions with biomolecules are still not fully understood and a reason for silica being used only as backbone material.

It is time to grind this diamond to its full beauty. Therefore, this work aims to unravel biomolecule interaction and the underlying mechanism behind the interaction with silica and develop, in a rational way, a peptide tag with a high affinity towards bare silica to give rise to new, cost-efficient separation processes. Hence, this dissertation sheds light on interactions between biomolecules and silica for past and future applications.

3 Publications

3.1 Buffer influence on the amino acid silica interaction

Interactions between silica and biomolecules at the solid-liquid interface are highly complex phenomena. The interactions are the foundation of many applications and even of the origin of life itself. This investigation offers insights into the adsorption behavior of all 20 amino acids on silica. The focus of this study lies on the influence of different buffer systems (TRIS and MOPS) on the adsorption of the basic amino acids lysine and arginine. The interactions are investigated by chromatographic zonal elution (ZE) experiments and molecular dynamics (MD) simulations. The work presents data on the Henry coefficient and calculated binding affinities of all 20 amino acids. Furthermore, calculations on the interactions between buffer molecules and between amino acids and buffer molecules complement the model. At last, the interaction of arginine and lysine with silica in the presence of the different buffers is presented experimentally and simulatively.

Lysine and arginine were identified as strong binders on silica from chromatographic experiments and MD simulation. Simulating the binding affinity between buffer molecules and silica revealed positive TRIS ions and neutral MOPS ions to be competitive with arginine and lysine and need to be considered in the adsorption process. Furthermore, the interaction of arginine and lysine with negatively charged MOPS ions is substantial and can interfere with the adsorption process. Finally, when comparing the interaction of arginine and lysine with different buffer species by varying the pH of the solution, the effect of the buffer can be observed. While for TRIS, a steady increase in affinity is observed, for MOPS buffer, the affinity decreases below the IEP and increases above the IEP of MOPS buffer. Hence, the investigation emphasizes using arginine and lysine as silica binders and taking the effect of buffer into account when working in biological environments.

The substantial contribution of the doctoral candidate was the conception and the design of the experimental part of the study after critical reviewing existing literature. The doctoral candidate was one of the two leading equal authors and carried out all experimental works including data analysis and processing as well as discussing the simulative data.

Buffer Influence on the Amino Acid Silica Interaction

Saïentan Bag⁺,^[a] Stefan Rauwolf⁺,^[b] Mikhail Suyetin,^[a] Sebastian P. Schwaminger,^[b] Wolfgang Wenzel,^{*[a]} and Sonja Berensmeier^{*[b]}

Protein-surface interactions are exploited in various processes in life sciences and biotechnology. Many of such processes are performed in presence of a buffer system, which is generally believed to have an influence on the protein-surface interaction but is rarely investigated systematically. Combining experimental and theoretical methodologies, we herein demonstrate the strong influence of the buffer type on protein-surface interactions. Using state of the art chromatographic experiments, we measure the interaction between individual amino acids and silica, as a reference to understand protein-surface interactions. Among all the 20 proteinogenic amino acids studied, we found that arginine (R) and lysine (K) bind most strongly to silica, a finding

validated by free energy calculations. We further measured the binding of R and K at different pH in presence of two different buffers, MOPS (3-(*N*-morpholino)propanesulfonic acid) and TRIS (tris(hydroxymethyl)aminomethane), and find dramatically different behavior. In presence of TRIS, the binding affinity of R/K increases with pH, whereas we observe an opposite trend for MOPS. These results can be understood using a multiscale modelling framework combining molecular dynamics simulation and Langmuir adsorption model. The modelling approach helps to optimize buffer conditions in various fields like biosensors, drug delivery or bio separation engineering prior to the experiment.

1. Introduction

Protein and peptide-surface interactions at the solid-liquid interface play an important role in various research fields like medicine,^[1,2] engineering^[3] and biotechnology.^[4] These interactions depend on the detailed structure and the composition of both surface and protein. However, it is difficult to characterize these interactions for small peptides or individual amino acids (AAs). There have been a number of studies that investigated such interactions for metal, metal oxide, polymer or silica surfaces both experimentally and theoretically,^[5–7] but trends for peptides have been difficult to derive due to complexities of the composition of the system.^[8] The latter comprises not only the peptide and the surface but also the solvent, which often contains a buffer to stabilize the pH of the system. The fact that buffer ions can compete with the peptide/ protein in binding to the surface is well known and investigated,^[9–20] but to the best of our

knowledge this has never been done for single amino acids especially for silica. A rational understanding of peptide or protein interactions with surfaces would benefit greatly from data on the interactions of individual amino acids. Calculations of such interactions are often complicated by the lack of adequate models that describe the surface and its interactions with the amino acids. For this reason, we study here silica surface, which is widely used in various applications and for which a pH dependent model has been recently developed.^[21] In an earlier work, Rimola et al.^[22] tried to quantify the adsorption affinity of 15 AAs on silica by calculating the adsorption energy using ab INITIO ONIOM2 within a cluster approach. A heuristic entropy correction was made to obtain the adsorption free energy from the adsorption energy.

There are many different ways to study the interaction between amino acids and surfaces like silica, such as spectroscopic methods or controlled bind and release experiments, which have been already discussed in depth in several reviews.^[5–7] Most studies focus on glycine and alanine, which are the most simple structured molecules having both, an amino and a carboxy functional^[23–28] group. Only few comparative studies between different amino acids, pH and ion strength exist.^[29–34] Most of the AAs do not interact with the silica surface in aqueous systems because they are present in their zwitterionic form in which the attraction of NH³⁺ and repulsion of COO⁻ groups by the silanol groups balance each other.^[32] Only AAs with additional charged groups, e.g. arginine, lysine and histidine can interact electrostatically with the negatively charged silanols on the silica surface.^[32,35] These interactions are highly pH dependent. A significant interaction can be observed at pH > 5 which can be explained through appearance and accumulation of negatively charged groups on the silica surface^[32] at pH > 5.

[a] Dr. S. Bag,⁺ Dr. M. Suyetin, Prof. W. Wenzel
 Institute of Nanotechnology (INT)
 Karlsruhe Institute of Technology (KIT)
 Karlsruhe, Germany
 E-mail: wolfgang.wenzel@kit.edu

[b] S. Rauwolf,⁺ Dr. S. P. Schwaminger, Prof. S. Berensmeier
 Bioseparation Engineering Group
 Department of Mechanical Engineering
 Technical University of Munich (TUM)
 Garching, Germany
 E-mail: s.berensmeier@tum.de

[†] These authors contributed equally to this work

Supporting information for this article is available on the WWW under <https://doi.org/10.1002/cphc.202000572>

© 2020 The Authors. Published by Wiley-VCH GmbH. This is an open access article under the terms of the Creative Commons Attribution License, which permits use, distribution and reproduction in any medium, provided the original work is properly cited.

The electrostatic interaction can lead to the formation of outer-sphere complexes, where positively charged amino acids coordinate to the silica surface.^[32] There are also studies indicating that hydrogen bonding between silanols and the functional groups of the amino acids has a huge influence on amino acid adsorption at very high pH (pH > 10).^[28] The third contribution to adsorption of amino acids are hydrophobic interactions with the Si–O–Si surface groups of silica as shown for phenylalanine or benzene as aromatic molecules.^[33,36] But with higher pH the influence of hydrogen bonds and hydrophobic interactions diminish due to the increasing electrostatic interactions.^[37]

Chromatography, which usually exploits the different interaction strengths of various components in a mixture with a surface is widely used for analytical purposes and for the purification of biopharmaceuticals.^[38] Although in high-performance affinity chromatography, zonal elution is one of the most common formats to study biomolecular interactions, it is yet rarely used for interaction studies of amino acids with silica. Zonal elution is performed by injecting a small volume of analyte onto a column under isocratic conditions and by monitoring the elution time. The elution time of the target is directly related to the target's interaction strength with the resin. These experiments are performed with different conditions, which lead to detailed information about the nature of interactions. Conditions that can be altered are pH, ionic strength, temperature, composition of the mobile phase.^[39–41] Basiuk and coworkers were the first to use chromatographic retention data to obtain free adsorption energies for single AAs on silica in water.^[29–31] Here we extend this work to determine the strength of the interactions under different conditions by measuring the time an analyte needs to pass through the column in relation to a non-binding analyte.^[42–44] In order to understand the binding behavior of peptides and proteins, the natural AAs serve as a useful reference to improve the understanding of the protein and peptide-surface interactions with the stationary phase.^[6,45] As the use of buffer is essential in biotechnology the AA-surface interaction should also be investigated in presence of the buffer.^[38] However, a detailed understanding

of the buffer influence is required to make results transferable between systems. In this paper, we demonstrate the strong influence of buffers on AA interaction with silica combining experimental and theoretical methodologies. We perform the column chromatography zonal elution experiment to determine the Henry coefficient, which is a descriptor for the propensity of binding events between solid and liquid phase in chromatography.^[46] The interaction of all the 20 AAs with the silica solid phase were investigated in presence of different buffers. We also formulated a multiscale modelling framework combining molecular dynamics (MD) simulation and different flavors of Langmuir model to understand the amino-acid adsorption in presence of different buffers. MD simulation was performed to evaluate the energetic parameters of the adsorption of a single molecule which is further used in mechanistically different Langmuir models to predict adsorption behavior of thermodynamically large numbers of adsorbate molecules in different physical conditions.

2. Results and Discussion

2.1. Amino Acid Binding in Aqueous Solution

We first measured the interactions between AAs and silica solid phase in a chromatographic system in aqueous buffered solution (Figure 1a). The retention factor k_r of the amino acids is measured (see Experimental Section) in relation to a non-binding analyte (in this case Uracil) and converted into the Henry adsorption coefficient H (see Table S6 in Supporting Information). In chromatography, retention factor of 1 means a slight interaction with the column. A retention factor of 20 means strong interactions because the analyte is spending a lot of time interacting with the resin. Retention factors > 20 are problematic because this means extreme long run times and poor sensitivity due to peak broadening.^[47] The Henry coefficient is directly related to the retention factor only multiplied by the phase ratio of the column [see Equation (1)] for better comparison of different packing. As the phase ratio

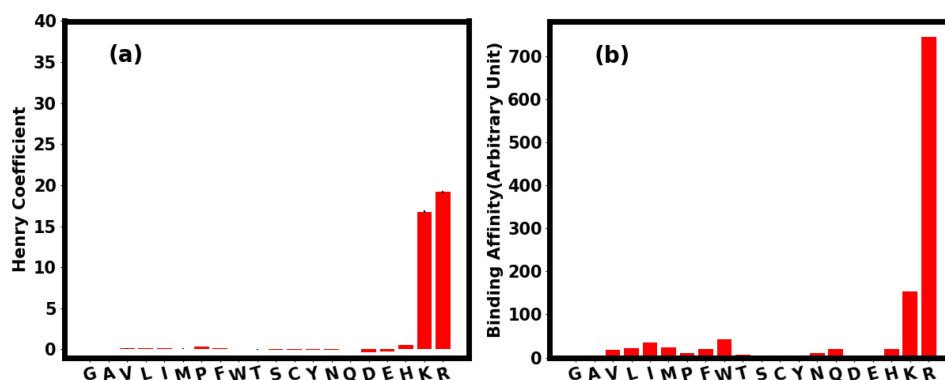


Figure 1. a) Henry coefficient for the binding of AAs to silica in 10 mM TRIS pH 8 as measured [see Equation (1)] using the chromatography experiment. b) Binding affinity of the AAs in water calculated using umbrella sampling simulation [see Equation (2)]. The positive charged AAs, R and K bind strongly to silica as found in both experiment and simulation.

of the columns is between 0.7 and 0.9 the values can also be applied for the Henry coefficient. The Henry coefficient (H) is the linear equilibrium constant between solid and liquid phase in chromatography and can thus be used as the equilibrium constant K in the van't Hoff equation which gives information about the difference in free energy of adsorption.^[30]

$$\ln k_i = \ln K + \ln \frac{V_s}{V_m} = \frac{-\Delta G^0}{RT} + \ln \frac{V_s}{V_m} \quad (1)$$

Here ΔG^0 is the free energy of adsorption. V_s and V_m are the phase ratio between the volumes of the stationary phase and mobile phase of the chromatographic system respectively. R is the gas constant and T the temperature. The Henry coefficient was measured for all 20 AAs as shown in Figure 1a below. The binding free energy of all 20 AAs with the silica were evaluated using Umbrella Sampling (US) simulation and the binding affinity (K_{calc}) was calculated by integrating the free energy curve as follows^[48]

$$K_{calc} = C \int_0^{cutoff} dz \exp(-\beta W_{calc}(z)) \quad (2)$$

Here $W_{calc}(z)$ is the calculated free energy of binding for an AA to silica as a function of distance (z) to the silica surface (see Experimental Section). *cutoff* is the distance up to which an AA is interacting with silica. A quantitative comparison of the calculated binding affinities and the experimental Henry coefficient is not possible because the constant C in Equation (2) cannot be determined. However, irrespective of this constant, the calculated binding affinity (K_{calc}/C) is proportional to the measured Henry coefficient (see Figure 1). The numerical values of the calculated free energy minima and the binding affinities of all the AAs are tabulated in Table S1 of the Supporting Information. As we observe from the Figure 1, the positively charged AAs arginine (R) and lysine (K) are the strongest binding AAs as revealed in both simulation and the experiment. These findings are in line with other experiments^[5-7,32] that indicate that the basic amino acids interact with silica at higher pH the most and the other AAs show low to no interaction at these conditions. The driving force for interaction of AAs with silica are the additional basic groups in R and K^[32] which provide strong electrostatic interactions with silica at high pH.^[37] It is important to note that in Figure 1 the experimental results are from the 10 mM TRIS pH 8 run and the simulation is in water. This is due to the problem, that in plain water the basic amino acids show high adsorption and thus no measurable retention time. This effect is mainly due to the competitive effect of TRIS on the AA adsorption and will be discussed in greater detail in the section below.

2.2. Influence of the Buffer

In the chromatography experiments, we used two different buffers: TRIS and MOPS. Depending on the pH of the solution, these buffers will have different protonation states as shown in Figure 2(a) below. TRIS has two protonation states with net charge $+1e$ (TRIS^{positive}) and 0 (TRIS^{neutral}), while the protonation state of MOPS have net charge 0 (MOPS^{neutral}) and $-1e$ (MOPS^{negative}). It has been previously reported that the buffer interacts with different oxide surfaces of titanium.^[11] Due to their charge the buffer species will also interact with silica and the AA, leading to competing interactions.^[11,49] Therefore, we evaluated the free energy of adsorption of the different buffer species to silica and also quantified the interaction between the buffer species and AAs. The binding affinity of the buffer species and the two strongly binding AAs (R and K) are shown in Figure 2b below. The corresponding free energy profile for the binding affinities are shown in Figure S1 and the Henry coefficient conversion for the experimental data in table S7 of the Supporting Information. As we observe from Figure 2b, the binding affinity of buffer species MOPS^{neutral} and TRIS^{positive} are quite comparable with amino acids K and R. Therefore, the buffer binding affinity cannot be ignored to determine the overall binding capacity of the AA in presence of the buffer. It's worth mentioning that although we have considered different protonation state of the buffer, we have only assumed the positively charged (protonated) species of R and K. However, this assumption is justified since the pKa values for corresponding amino group of R and K are 12.10 and 10.67 which is far above the pH range studied in this article. We further quantified the interaction between the amino acids (K and R) and the buffer species by calculating the interaction energy between them (see Experimental Section).

We can see from the Figure 2c, that the interaction energy is largest between R and MOPS^{negative} species. All other interaction energies are quite similar to the R–R dimer interaction. In case of K (Figure 2d) also, the strongest interaction was found to be between K and MOPS^{negative}. The interaction energy at a specific distance between the two molecules are tabulated in Table S3 and S4 of the Supporting Information.

2.3. Binding of R and K to Silica in Presence of TRIS Buffer

Henry coefficient for the interaction of R and K were measured in presence of TRIS buffer for the pH range of 7.2 to 8.5. The binding affinity of both R and K increases with pH in presence of TRIS buffer. This effect is expected due to the increasing negative charge of silica surface with increasing pH.^[32,50] Nevertheless, TRIS buffer has a strong impact on the binding of AA because we were not able to gain Henry coefficients in plain water due to strong interactions of K and R with the silica surface. This can be explained by the higher ionic strength of the solution through the buffer and thus a competitive absorption of TRIS and the AA.^[50] Although

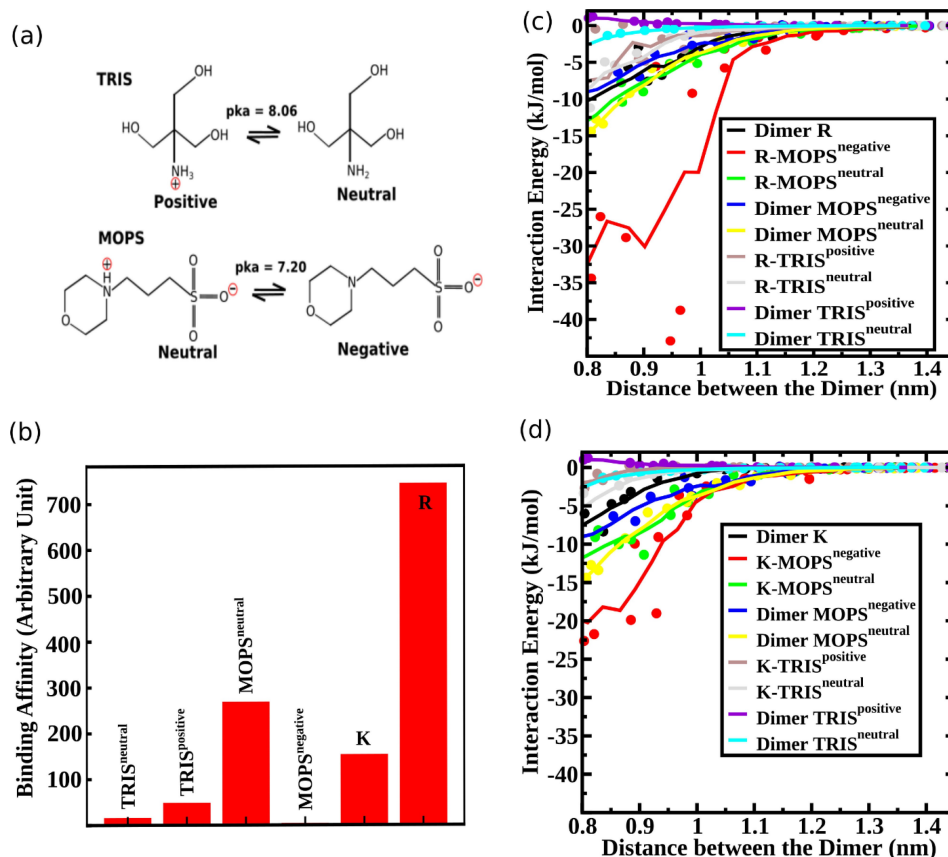


Figure 2. a) Molecular model of different protonation state of MOPS and TRIS buffer at different pH. TRIS has two protonation states with net charge +1e (TRIS^{positive}) and 0 (TRIS^{neutral}), while the protonation state of MOPS have net charge 0 (MOPS^{neutral}) and -1e (MOPS^{negative}). b) Binding affinities of the different buffer species to the silica. The binding affinities of K and R are also plotted for comparison. c) Interaction energy between the AA, R and different buffer species as a function of distance between them. d) Interaction energy between the AA, K and different buffer species as a function of distance between them. The interaction energy between the buffer species are plotted in both (c) and (d) for comparison. In both cases, there is a strong attraction between the R/K and the MOPS^{negative} species. (c-d) The concentric circles in the figures indicate the actual calculated values while the solid lines are the running average over these data.

higher pH leads to higher surface charge of silica the increase of the Henry coefficient is not comparable to adsorption experiments in the same pH range showing a more linear like increase.^[33,50]

To understand this pH dependent interaction of R and K in presence of buffer, we set-up a multiscale modelling framework for adsorption. The multiscale modelling consists of calculations of energetic parameters of binding from the MD simulation (see Experimental Section) and further use of these parameters in two mechanistically different multicomponent Langmuir adsorption models. The models provide the fraction of R/K bound to silica which is again proportional to the measured Henry coefficient. Depending on the interaction strength between the AA and the buffer species in an adsorbed state, we invoke one of the two different kinds of Langmuir models^[51] as shown schematically in Figure 4 below. As the name suggests, in the non-cooperative model (Figure 4a) the interaction between the adsorbates (A and B) are neglected while the cooperative model (Figure 4b) is formulated assuming an interaction between the adsorbates. The black semicircles are the

adsorption sites (silica in our case) which can either accommodate one (non-cooperative model) or two (cooperative model) adsorbates (A and B). In an equilibrium situation, the adsorptive molecules continuously adsorb and desorb (see Supporting Information). The type of multicomponent cooperative adsorption model we consider here was first derived by Moreau et al.^[52] and therefore also known as the Moreau model in the literature. Although, Langmuir model was originally developed to study adsorption from the gas phase, the model is much more general and appears in variety of other physical situations (e.g. ligand binding to protein) described by a simple combination reaction where loss of mass action is valid in equilibrium.^[51] Therefore, use of Langmuir model to describe adsorption in Liquid-Solid interface is fully justified. Esposito et al.^[53] fitted their experimental adsorption isotherm with this kind of multicomponent Langmuir model to study the bio-separation of metal ions. The pH dependence of the isotherms was captured in the ratio of the different protonated and unprotonated metal ions. Xiao et al.^[54] measured the adsorption isotherm of several organic acids and bases on graphite and fitted the

isotherm with the multicomponent Langmuir model. The pH dependence was captured by the protonation and deprotonation of the organic acid and bases similar to the work by Esposito et al.^[53]

Since, there is no strong interaction between different molecular species (see Figure 2c,d) and Table S3 and S4 in the supporting information) in presence of TRIS buffer, we will invoke the non-cooperative (Figure 4a) competitive Langmuir model to understand the pH dependent binding as described in the Experimental Section in detail. We calculate the fraction of bound AA for different pH (Figure 3c,d) and found qualitatively same behavior with the experiment. The increase of binding fraction of K/R with the pH can be simply understood as follows. When the pH of the solution is low (< 8), there will be more TRIS^{positive} species in the solution than the TRIS^{neutral} (see Figure 2a). Therefore, the effect is simply a competitive effect between TRIS and the AA for the negatively charged silica surface. With the increase in pH, the TRIS^{positive} species will deprotonate giving rise to more TRIS^{neutral} species. Therefore, as pH increases, K/R has to compete with TRIS^{neutral} for the binding sites while for low pH the competition for the binding sites will be between the K/R and TRIS^{positive} which has a much higher binding affinity (to silica) in comparison to TRIS^{neutral}. As a result, the binding fraction of K/R increases significantly when the pH is higher than the pKa of the TRIS buffer.

2.4. Binding of R and K to Silica in Presence of MOPS Buffer

Retention factors for the binding of R and K were again measured in presence of MOPS buffer for the pH range of 6 to 7.6 and converted in Henry coefficient (see table S8 of Supporting Information). As shown in Figure 5a,b below, for a pH range 6 to 7.2 the interaction of both the AAs slowly decreases and at a pH of 7.6 we see a sudden increase in interaction. Previous experiments always indicated higher adsorption capacities with increasing pH.^[32,33,50] To understand the experimental binding behavior, we again use our multiscale modelling framework as described in the previous section. Since the deprotonated species of the MOPS buffer (MOPS^{negative}) has a net attractive interaction (see Figure 2c,d) with the R/K species, the binding will be described by the cooperative Langmuir adsorption model (also known as Moreau model^[52]) rather than by the non-cooperative one (see Figure 4b). Gritti et al.^[55] measured the adsorption isotherm of various alcohol with porous silica and fitted the isotherm with non-cooperative and cooperative Langmuir model (also known as Moreau model) depending on whether the alcohol solution is buffered or not. Neither the interaction between the solid phase and the buffer nor the interaction between the buffer and the alcohol was considered in their models. Figure 5a,b show the experimentally measured Henry coefficients for K/R, while Figure 5c,d shows the calculated fraction of bound K/R (see Experimental Section). We observe a good qualitative match between the experiment and the modelling for this scenario.

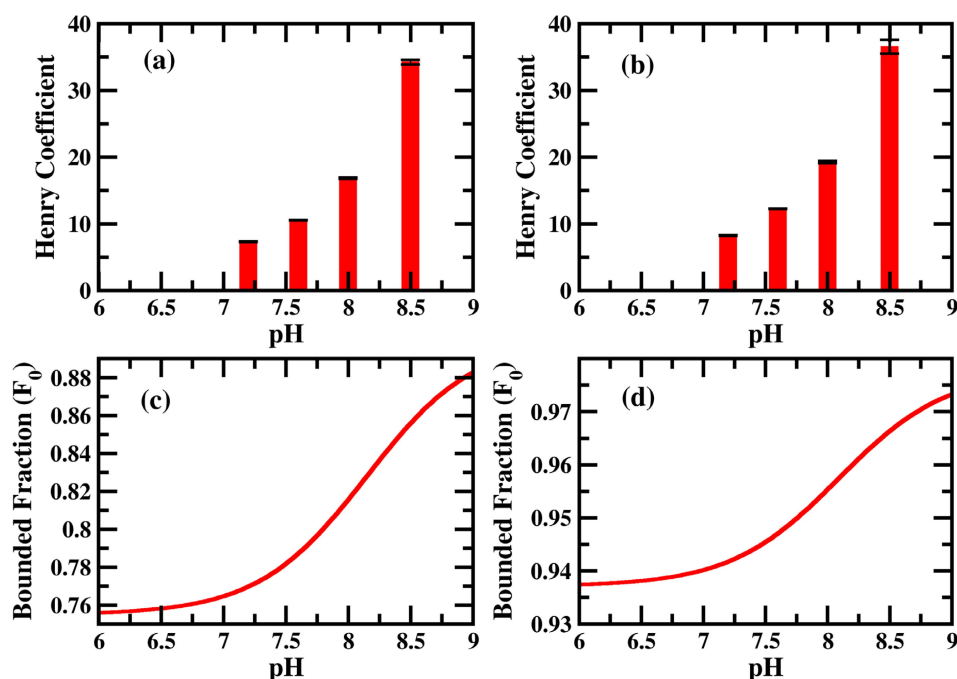


Figure 3. Measured Henry coefficient of K (a) and R (b) as a function of pH in presence of TRIS buffer. pH values are quoted on top of the bars. Fraction of K (c) and R (d) bound to silica as a function of pH as calculated using multiscale modelling. The experimental Henry coefficient and calculated bounded fraction show qualitatively similar behaviors.

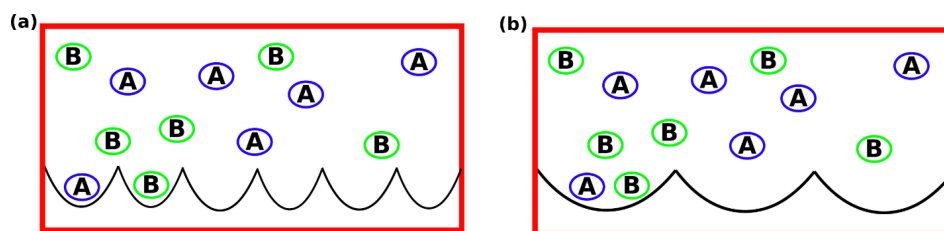


Figure 4. a) Schematic diagram illustrating non-cooperative competitive Langmuir adsorption model of two different species A and B. The black semi circles represent the adsorption sites which can accommodate only one molecule. There is no interaction between A and B. b) Schematic diagram illustrating a cooperative adsorption model of two different species A and B. The black semi circles now represent adsorption sites which can accommodate up to two molecules. There is an interaction between the molecular species when adsorbed in a same adsorption site.

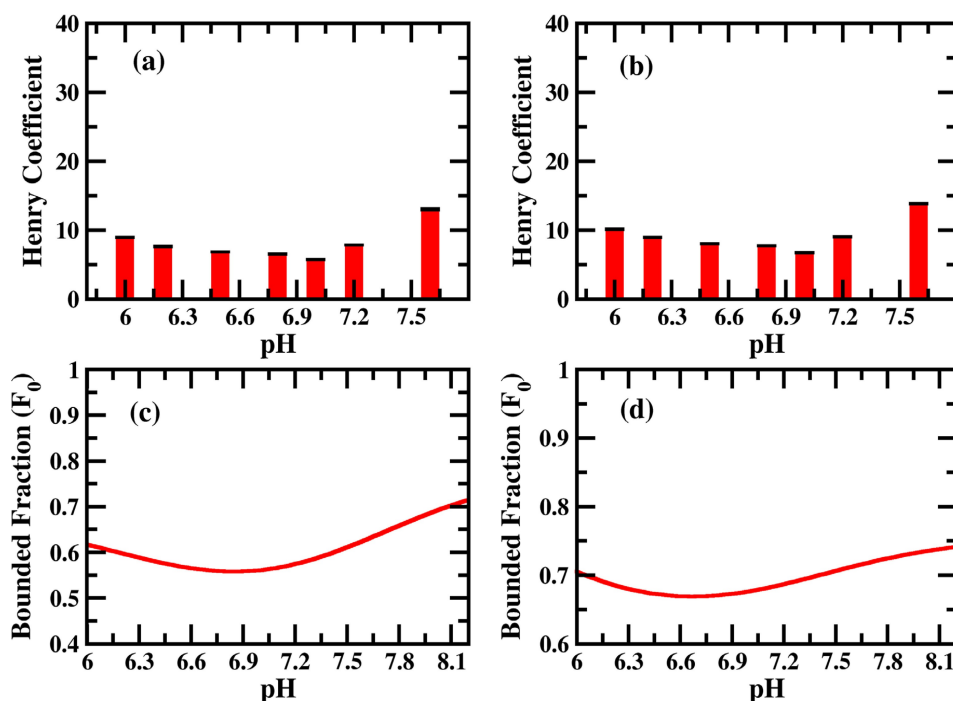


Figure 5. a)/b) Experimentally measured Henry coefficients of K/R as a function of pH in presence of MOPS buffer. pH values are quoted on top of the bars. c)/d) Fraction of K/R bound to silica calculated using multiscale modeling.

The physical origin of the binding behavior of K/R with respect to pH can be understood as follows. Since MOPS buffer has a pKa of 7.2, for low pH (<7.2), the solution in the chromatographic column will be populated by MOPS^{neutral} species, while for high pH (>7.2) most of the MOPS^{neutral} species will be deprotonated and as a result there will be more MOPS^{negative} species in the solution (see Figure 2a). If there is no interaction between the K/R and MOPS, for low pH, K/R has to compete with MOPS^{neutral} while for high pH, it has to compete with MOPS^{negative} species for silica binding sites. Since MOPS^{neutral} has a much higher binding affinity than the MOPS^{negative}, the K/R binding fraction will increase with increasing pH. However, the situation is different when there is a moderate attraction between K/R and MOPS^{negative}. Since MOPS^{negative} has a pretty low binding affinity, it cannot compete with K/R for binding sites on its own. However, due to the strong attraction of the K/R with MOPS^{negative}, when a

K/R binds to silica, it sometimes accompanies a MOPS^{negative} with it and as a result the binding sites are occupied by MOPS^{negative} also. Therefore, the overall binding of K/R decreases with increasing concentration of MOPS^{negative} and seems to be more relevant than the increasing negative charge of the silica surface with increasing pH. However, as the pH increases further, the concentration of MOPS^{negative} increases together with the negative surface charge of the silica.^[32] K/R cannot interact with additional MOPS^{negative} molecules to form complexes. Due to a decrease in MOPS^{neutral} concentration and increased negative charge on the surface more silica binding sites are available for K/R, resulting in an increased overall binding in the end.

3. Conclusions

To summarize, we have measured the binding affinity of all 20 AAs with silica using zonal elution chromatography. We could show the capability of chromatography for studying interactions between single AAs and silica surfaces under different conditions in aqueous systems. Furthermore, chromatography has the advantage of real time monitoring and the possibility to have an automated high throughput system, which leads to a lot of data points with little effort. Among the 20 AAs, the positively charged AAs R and K were found to have highest affinity towards silica, which was validated by calculation of binding free energy using US simulation. The binding behavior of R and K was further studied in presence of different buffers and was found to be strongly dependent on the choice of buffer which is never accounted in biotechnology experiments. When TRIS was used as buffer the binding affinity of R/K increases with pH (7.3 to 8.5) while in case of MOPS the affinity first decreases with pH (6.0 to 7.0) and with further increase of pH (> 7) the affinity again goes up. In addition, with its conventional role, the buffer can be used to tune the AA-silica interaction increasing the efficiency of AA separation, by a significant amount. We also present a multiscale modelling framework to understand the binding of AA in presence of buffer. The multiscale modelling consists of calculations of energetic parameters of binding from the MD simulation and further use of these parameters in mechanistically different multi-component Langmuir models. In a very recent work, similar multiscale modelling approach involving MD simulation and the non-cooperative Langmuir model was adopted by Angelis et al.^[56] to predict the adsorption of surfactant to the alumina. In this work, we extend the Langmuir model to account for multiple interacting species which is relevant in variety of physical situations including ours. The multiscale-modeling framework can be used to screen the suitable buffer prior to the experiment, which is often expensive, and time consuming to perform. Our model helps to predict the relative interactions strength between different components in a bio molecular mixture (AA, peptides, proteins etc.) appears in variety of physical situations like chromatographic purification. We hope to extend the cooperative adsorption model in the future to describe the incorporation of peptides and proteins in mesoporous silica materials as well.

Experimental Section

Adsorbent and AAs: The silica used for the experiments was Silica Gel 60 from AppliChem, Germany. The porous silica had a particle size of 40 to 60 μm . The pore diameter was 55 to 65 \AA and the pore volume 0.7 to 0.8 mL g^{-1} . The surface area was given with 450 to 550 $\text{m}^2 \text{g}^{-1}$. TRIS was purchased from VWR, Germany. MOPS was purchased from Carl Roth, Germany. All AAs were purchased as L-stereoisomer. Most AAs were purchased in research grade from SERVA, Germany. Arginine, histidine and proline (Cellpure $\geq 98\%$) were purchased from Carl Roth, Germany. Cysteine, lysine and phenylalanine were purchased with a purity $\geq 98\%$ from Sigma-Aldrich, Germany. For the column,

column blank kit (Supelco) with L \times ID 25 $\text{cm} \times 4.6 \text{ mm}$ from Sigma-Aldrich was purchased and shortened to a length of 3.3 cm resulting in a volume of 0.55 mL . The buffers were prepared in DI water. The AAs were also prepared in DI water with concentrations between 1 and 50 mM (see Table S5 of the Supporting Information). All buffers were degassed and filtered through a 0.2 μm cellulose-acetate-filter from Labsolute, Germany. The AAs were also filtered with 0.2 μm cellulose-acetate syringe filters from Macherey-Nagel, Germany.

Henry coefficients: The chromatographic column was operated on an Agilent 1100 HPLC system with an UV/Vis detector. AAs were measured at 210 nm , aromatic AAs at 280 nm additionally. The flow rate was $\sim 12 \text{ cm min}^{-1}$ for every run and the injection volume for every AA was 20 μL . Every AA was measured at least three times per experiment in random sequences. The Henry coefficients H was determined with $H = k'/\phi$. Where k' is the retention factor of the AA and ϕ is the phase ratio of the column. The retention factor is calculated as $k' = (t_{\text{r}} - t_0)/t_0$. Here t_{r} stands for the retention time of the AA and t_0 for the retention time of a non-interacting tracer in this case 1 g L^{-1} uracil. The phase ratio of the column is calculated with $\phi = (1 - \epsilon^t)/\epsilon^t$. Here ϵ^t is the total porosity of the column calculated with the flow rate $\dot{V} = 2 \text{ mL min}^{-1}$: $\epsilon^t = (t_0 \dot{V})/V_{\text{column}}$.

The Langmuir adsorption model for two different non-interacting adsorbates (non-cooperative Langmuir model): Consider two adsorbates A and B (See Figure 4a) with binding affinity K'_A and K'_B with the adsorbent having a total Γ number of adsorption sites. The average number of A molecule bound (N_A) is given by^[51]

$$\langle N_A \rangle / \Gamma = F_A = \frac{K'_A \theta_A}{1 + \theta_A K'_A + \theta_B K'_B} \quad (3)$$

See the Supporting Information for more details.

The Langmuir adsorption model for two different interacting adsorbates (cooperative Langmuir model): Consider two adsorbates A and B with binding affinity K'_A and K'_B with the adsorbent having a total Γ number of adsorption sites (see Figure 4b). U_{AA} is the interaction energy between two A molecules when both of these two are adsorbed on a single adsorption site. U_{BB} is the corresponding interaction energy for the B molecules and U_{AB} is the interaction energy between A and B in case the adsorption site is occupied by one A and one B molecule respectively. In equilibrium, the average number of A molecule bound (N_A) is given by^[51,52]

$$\langle N_A \rangle / \Gamma = F_A = \frac{2K'_A \theta_A + 2\theta_A^2 K'^2_A e^{-\beta U_{AA}} + 2\theta_A K'_A \theta_B K'_B e^{-\beta U_{AB}}}{1 + 2\theta_A K'_A + \theta_A^2 K'^2_A e^{-\beta U_{AA}} + 2\theta_B K'_B + \theta_B^2 K'^2_B e^{-\beta U_{BB}} + 2\theta_A K'_A \theta_B K'_B e^{-\beta U_{AB}}} \quad (4)$$

The complete derivation of Equation (4) above is presented in the Supporting Information.

Binding affinity of the AAs and the buffers to the silica surface: To estimate the binding affinity of the different molecular species with the silica surface we calculate the potential of mean force (PMF) (between the molecule and silica) of binding using umbrella sampling (US) simulation. The atomistic model (Figure 6a,b) of the porous silica surface for the MD simulation was chosen from the database provided by Emami et al.^[21] From the database we chose a Q^3 silica surface model (33.6 $\text{\AA} \times 34.9 \text{\AA}$)

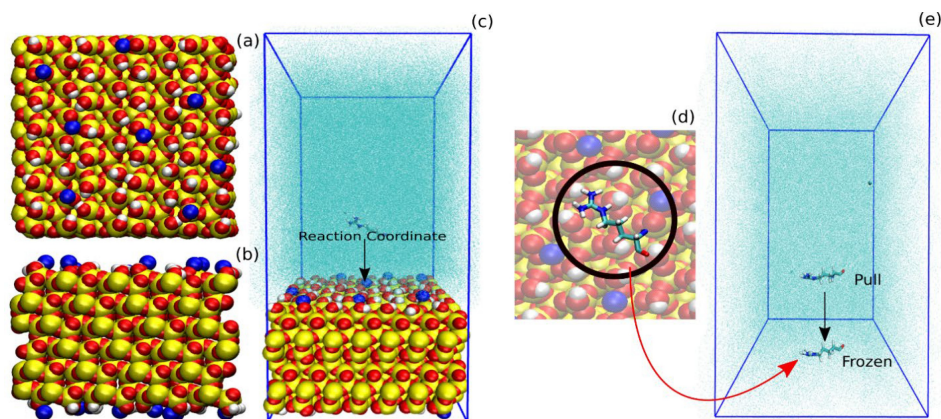


Figure 6. Atomistic model of the silica used in the MD simulation: a) Top and b) side view. Silicon atoms are represented in yellow, oxygen atoms in red and hydrogens in white. Na^+ ions are shown in blue. c) Snapshot of the initial system prepared for MD simulation with silica in the end and the AA in the middle of the simulation box. The surrounding water medium is not shown in full atomistic details but as collection of cyan dots ("solvent" representation in VMD^[63]) for clarity. The free energy of binding was computed as a function of distance between the AA and Silica (Reaction Coordinate). d) Equilibrated snapshot of the AA adsorbed on silica. e) Initial snapshot of a system prepared to calculate the interaction energy between the adsorbed AA and another molecule. The AA was kept frozen to its adsorbed geometry while another molecule is pulled towards it and the interaction energy is measured.

containing 4.7 silanol groups per nm^2 of the surface of which 14% are deprotonated corresponding to a pH of 7.4. The model for the AAs were built using Ambertools^[57] program. A simulation box with the silica in one end and AA in the middle was prepared. The full system was then solvated in TIP3P water^[58] (Figure 6c). A sufficient number of Na^+ and Cl^- counter ions were added to achieve overall charge neutrality of the system. The force field for the silica surface were taken from Emami et al.^[21] while AMBER99SB-ILDN^[59] force field was used for AAs including the solvents. The system (~10,000 atoms) was first energy minimized and then MD simulation in isothermal ensemble (NVT) was performed to equilibrate the system. The silica surface was kept frozen during the simulation and periodic boundary condition was imposed in all three directions. The x- and y-dimensions of the box were kept equal to the x- and y-dimensions of the silica surface, and the atoms located at the edge of the silica patch were connected through bonds via the periodic boundary condition to avoid boundary effects. A series of short NVT simulations with varying z dimension of the box were performed thereafter to achieve the correct density of the water in the bulk. We used Nose-Hoover thermostat^[60] to maintain the system temperature at 300 K. The system with correct water density was further used for US simulations. All the simulations were performed using GROMACS^[61] simulation package. We further proceed to calculate PMF of AA with the silica surface using US simulation with the distance between the silica surface and the center of mass of the AA as reaction coordinate (Figure 6c). To generate the configuration for US run, the AA was pulled towards the silica surface and the overall system is equilibrated again when the AA is adsorbed on top of the silica surface. The AA is then pulled off from the silica surface and the system configuration is saved at a regular distance (between the AA and the silica surface) interval for the umbrella sampling run. We used a spring constant of 1000 $\text{kJ mol}^{-1} \text{nm}^{-2}$ and the pull rate 0.01 nm/ps for the pulling simulations. The umbrella sampling simulation were further performed with these configurations with the strength of the umbrella potential 1000 $\text{kJ mol}^{-1} \text{nm}^{-2}$. Each umbrella sampling windows were first equilibrated for 4 ns and then from another 10 ns run we save the histograms for PMF generation. The PMF curves were calculated using the Weighted Histogram Analysis Method (WHAM)^[62] also implemented in GROMACS. The obtained histograms and the PMF profile for a

specific case are shown in Figure S5 of the Supporting Information. In this article, we use the term free energy profile as alternative to the PMF profile both having same meaning.

Interaction energy between R/K and the buffer species: To measure the interaction energy of R/K with another R/K or the different buffer species, we chose the equilibrated geometry of R/K as it adsorbed on the silica (Figure 6d). The R/K was kept frozen in that geometry while other molecule (another R/K or buffer species) was pulled towards it (Figure 6e) and the interaction energy was measured. The interaction energy between different buffer-species was also measured the same way.

The multiscale modelling (binding of K/R in presence of TRIS): There are 3 different molecular species present in the chromatography column in this case: K/R and two buffer species $\text{TRIS}^{\text{neutral}}$ and $\text{TRIS}^{\text{positive}}$ (see Figure 2a). The concentration of K/R in the chromatographic column is X_0 and the concentration of the $\text{TRIS}^{\text{neutral}}$ and $\text{TRIS}^{\text{positive}}$ buffer species are X_1 and X_2 . If the total concentration of the buffer species is C_B and pka is the buffer pKa value, then

$$X_1 + X_2 = C_B \text{ and } X_1/X_2 = 10^{ph-pka} \quad (5)$$

For a given value of C_B , Equation (5) can be solved for X_1 and X_2 at a particular pH.

According to Equation (3), the total fraction of R/K bound F_0 is given by,

$$F_0 = \left(\frac{X_0 K_0}{1 + X_0 K_0 + X_1 K_1 + X_2 K_2} \right) \quad (6)$$

Here K_0 , K_1 and K_2 are the binding affinity for AA, $\text{TRIS}^{\text{neutral}}$ and $\text{TRIS}^{\text{positive}}$ respectively. Please note that the binding affinities in Equation (6) and the ones calculated in the simulation (Equation 2) are not quantitatively same but proportional to each other. The use of the binding affinity from the simulation in the Equation (6) is still justified, if one is not looking for quantitative prediction but the qualitative behavior. In all our calculation, the

concentration of both buffer (C_B) and AA (X_0) was assumed to be 1 (arbitrary unit).

The multiscale modelling (binding of K/R in presence of MOPS): As before, there are 3 different molecular species present in the chromatography column: K/R and two buffer species MOPS^{neutral} and MOPS^{negative} (see Figure 2a). The concentration of K/R in the chromatographic column is X_0 and the concentration of the MOPS^{negative} and MOPS^{neutral} buffer species are X_1 and X_2 . We can write equation similar to Equation (5) as

$$X_1 + X_2 = C_B \text{ and } X_1/X_2 = 10^{ph-pka} \quad (7)$$

Now, the total fraction of K/R bound to silica is given by

$$F_0 = 1/2(F_{01} + F_{02}) \quad (8)$$

Here, F_{01} is the fraction of K/R bound to silica due to cooperative adsorption between K/R and MOPS^{negative}. F_{02} is the corresponding fraction when K/R and MOPS^{neutral} are considered. According to Equation (4), we can write

$$F_{01} = \frac{2X_0K_0 + 2X_0^2K_0^2\exp(-\beta U_{00}) + X_0K_0X_1K_1\exp(-\beta U_{01})}{1 + 2X_0K_0 + X_0^2K_0^2\exp(-\beta U_{00}) + 2X_1K_1 + X_1^2K_1^2\exp(-\beta U_{11}) + X_0K_0X_1K_1\exp(-\beta U_{01})} \quad (9)$$

$$F_{02} = \frac{2X_0K_0 + 2X_0^2K_0^2\exp(-\beta U_{00}) + X_0K_0X_2K_2\exp(-\beta U_{02})}{1 + 2X_0K_0 + X_0^2K_0^2\exp(-\beta U_{00}) + 2X_2K_2 + X_2^2K_2^2\exp(-\beta U_{22}) + X_0K_0X_2K_2\exp(-\beta U_{02})} \quad (10)$$

The parameter U 's are the interaction between different species and K 's are the binding affinity. Among the different intermolecular interaction energies in Equations (9) and (10), only the interaction energy between the R/K and MOPS^{negative} (U_{01}) is significant (see Figure 2c,d). Therefore we keep all other intermolecular interaction energies (U_{00} , U_{02} , U_{11} , U_{22}) zero except U_{01} . In case of binding of R we use a value of U_{01} to be -20 kJ/mol while in case of K the value is -12 kJ/mol (see Table S3 and S4 of the Supporting Information) and get the binding behavior as shown in Figure 5c,d. In all our calculation, the concentration of both buffer (C_B) and AA (X_0) was assumed to be 1 (arbitrary unit). Please note that the interaction energies are calculated at a distance of 8 Å between the species (see Table S3 and S4 of the Supporting Information) which may not be the case in reality. Therefore, we calculate the binding fraction of R/K with pH for different value of U_{01} . We observe (see Figure S6 of Supporting Information) that in case of R, an attractive interaction (between the R and MOPS^{negative}) of magnitude > 11 kJ/mol is required to qualitatively reproduce the experimental behavior while in case of K the respective interaction energy is 7 kJ/mol. It is evident from the Figure 2c,d (and Tables S3 and S4 of the Supporting Information) that R and MOPS^{negative} have higher attractive interaction than K and MOPS^{negative}.

Acknowledgements

The authors would like to express their gratitude for the financial support of this work by the Federal Ministry of Education and

Research (Grant No. 031A173A, 031A173B). Open access funding enabled and organized by Projekt DEAL.

Conflict of Interest

The authors declare no conflict of interest.

Keywords: amino acids · buffer · chromatography · multiscale modelling of adsorption · silica

- [1] S. Ferraris, S. Spriano, *Mater. Sci. Eng. C* **2016**, *61*, 965–978.
- [2] B. Kasemo, *Surf. Sci.* **2002**, *500*, 656–677.
- [3] R. A. Hartvig, M. Van De Weert, J. Østergaard, L. Jorgensen, H. Jensen, *Langmuir* **2011**, *27*, 2634–2643.
- [4] M. Rabe, D. Verdes, S. Seeger, *Adv. Colloid Interface Sci.* **2011**, *162*, 87–106.
- [5] A. Rimola, D. Costa, M. Sodupe, J.-F. Lambert, P. Ugliengo, *Chem. Rev.* **2013**, *113*, 4216–4313.
- [6] D. Costa, L. Savio, C.-M. Pradier, *J. Phys. Chem. B* **2016**, *120*, 7039–7052.
- [7] J.-F. Lambert, *Origins Life Evol. Biospheres.* **2008**, *38*, 211–242.
- [8] S. Schwaminger, S. A. Blank-Shim, M. Borkowska-Panek, P. Anand, P. Fraga-García, K. Fink, W. Wenzel, S. Berensmeier, *Eng. Life Sci.* **2018**, *18*, 84–100.
- [9] F. Cugia, S. Sedda, F. Pitzalis, D. F. Parsons, M. Monduzzi, A. Salis, *RSC Adv.* **2016**, *6*, 94617–94621.
- [10] T. Wei, S. Kaewtathip, K. Shing, *J. Phys. Chem. C.* **2009**, *113*, 2053–2062.
- [11] S. Loreto, B. Cuypers, J. Brokken, S. Van Doorslaer, K. De Wael, V. Meynen, *Phys. Chem. Chem. Phys.* **2017**, *19*, 13503–13514.
- [12] T. J. Zbacnik, R. E. Holcomb, D. S. Katayama, B. M. Murphy, R. W. Payne, R. C. Coccaro, G. J. Evans, J. E. Matsuura, C. S. Henry, M. C. Manning, *J. Pharm. Sci.* **2017**, *106*, 713–733.
- [13] A. C. Rodrigo, E. Laurini, V. M. Vieira, S. Pricl, D. K. Smith, *Chem. Commun.* **2017**, *53*, 11580–11583.
- [14] A. Salis, M. Monduzzi, *Curr. Opin. Colloid Interface Sci.* **2016**, *23*, 1–9.
- [15] C. W. Chan, D. K. Smith, *Supramol. Chem.* **2017**, *29*, 688–695.
- [16] S. Brudar, B. Hribar-Lee, *Biomolecules.* **2019**, *9*, 65.
- [17] E. Olewnik-Kruszkowska, *Polym. Degrad. Stab.* **2016**, *129*, 87–95.
- [18] A. Salis, M. S. Bhattacharyya, M. Monduzzi, *J. Phys. Chem. B* **2010**, *114*, 7996–8001.
- [19] H. G. Manyar, E. Gianotti, Y. Sakamoto, O. Terasaki, S. Coluccia, S. Tumbiolo, *J. Phys. Chem. C.* **2008**, *112*, 18110–18116.
- [20] L. Giussani, G. Tabacchi, E. Gianotti, S. Coluccia, E. Fois, *Philos. Trans. R. Soc., A.* **2012**, *370*, 1463–1477.
- [21] F. S. Emami, V. Puddu, R. J. Berry, V. Varshney, S. V. Patwardhan, C. C. Perry, H. Heinz, *Chem. Mater.* **2014**, *26*, 2647–2658.
- [22] A. Rimola, M. Sodupe, P. Ugliengo, *J. Phys. Chem. C* **2009**, *113*, 5741–5750.
- [23] I. Ben Shir, S. Kababya, T. Amitay-Rosen, Y. S. Balazs, A. Schmidt, *J. Phys. Chem. B* **2010**, *114*, 5989–5996.
- [24] I. Ben Shir, S. Kababya, A. Schmidt, *J. Phys. Chem. C* **2012**, *116*, 9691–9702.
- [25] I. Ben Shir, S. Kababya, A. Schmidt, *J. Phys. Chem. C* **2014**, *118*, 7901–7909.
- [26] T. Amitay-Rosen, S. Kababya, S. Vega, *J. Phys. Chem. B.* **2009**, *113*, 6267–6282.
- [27] L. Stievano, L. Y. Piao, I. Lopes, M. Meng, D. Costa, J.-F. Lambert, *Eur. J. Mineral.* **2007**, *19*, 321–331.
- [28] C. Guo, G. P. Holland, *J. Phys. Chem. C* **2015**, *119*, 25663–25672.
- [29] V. Basiuk, T. Y. Gromovoy, *Amino Acids* **1994**, *7*, 305–309.
- [30] V. A. Basiuk, T. Y. Gromovoy, *Colloids Surf. A* **1996**, *118*, 127–140.
- [31] V. A. Basiuk, T. Y. Gromovoy, *Adsorption* **1996**, *2*, 145–152.
- [32] N. Vlasova, L. Golovkova, *Colloid J.* **2004**, *66*, 657–662.
- [33] Q. Gao, W. Xu, Y. Xu, D. Wu, Y. Sun, F. Deng, W. Shen, *J. Phys. Chem. B* **2008**, *112*, 2261–2267.
- [34] Y. Razvag, V. Gutkin, M. Reches, *Langmuir.* **2013**, *29*, 10102–10109.
- [35] A. J. O'Connor, A. Hokura, J. M. Kislner, S. Shimazu, G. W. Stevens, Y. Komatsu, *Sep. Purif. Technol.* **2006**, *48*, 197–201.
- [36] A. Rimola, B. Civalleri, P. Ugliengo, *Phys. Chem. Chem. Phys.* **2010**, *12*, 6357–6366.

- [37] F. S. Emami, V. Puddu, R. J. Berry, V. Varshney, S. V. Patwardhan, C. C. Perry, H. Heinz, *Chem. Mater.* **2014**, *26*, 5725–5734.
- [38] G. Carta, A. Jungbauer, Protein chromatography: process development and scale-up, John Wiley & Sons, **2010**.
- [39] X. Zheng, Z. Li, S. Beeram, M. Podariu, R. Matsuda, E. L. Pfaumiller, C. J. White II, N. Carter, D. S. Hage, *J. Chromatogr. B* **2014**, *968*, 49–63.
- [40] D. S. Hage, S. A. Tweed, *J. Chromatogr. B: Anal. Technol. Biomed. Life Sci.* **1997**, *699*, 499–525.
- [41] P. Tao, S. Poddar, Z. Sun, D. S. Hage, J. Chen, *Methods.* **2018**, *146*, 3–11.
- [42] P. Doran, *Bioprocess Engineering Principles*, Academic Press, UK, **1995**.
- [43] D. Zopf, S. Ohlson, *Nature* **1990**, *346*, 87–88.
- [44] F. Gritti, Y. Kazakevich, G. Guiochon, *J. Chromatogr. A* **2007**, *1161*, 157–169.
- [45] I. A. Mudunkotuwa, V. H. Grassian, *Langmuir* **2014**, *30*, 8751–8760.
- [46] A. Seidel-Morgenstern, H. Schmidt-Traub, M. Michel, A. Epping, A. Jupke, *Modeling and Model Parameters. Preparative Chromatography*, Second Edition; Wiley-VCH, **2012**, 321–424.
- [47] R. M. Orna, M. W. Dong, *Key concepts of HPLC in pharmaceutical analysis. Separation Science and Technology*, Elsevier: **2005**, Vol. 6, 19–45.
- [48] J. Comer, R. Chen, H. Poblete, A. Vergara-Jaque, J. E. Riviere, *ACS Nano* **2015**, *9*, 11761–11774.
- [49] M. Manzano, M. Vallet-Regí, *Adv. Funct. Mater.* **2020**, *30*, 1902634.
- [50] N. Kitadai, T. Yokoyama, S. Nakashima, *J. Colloid Interface Sci.* **2009**, *329*, 31–37.
- [51] H. Swenson, N. P. Stadie, *Langmuir* **2019**, *35*, 5409–5426.
- [52] M. Moreau, P. Valentin, C. Vidal-Madjar, B. C. Lin, G. Guiochon, *J. Colloid Interface Sci.* **1991**, *141*, 127–136.
- [53] A. Esposito, F. Pagnanelli, F. Veglio, *Chem. Eng. Sci.* **2002**, *57*, 307–313.
- [54] F. Xiao, J. J. Pignatello, *Langmuir* **2014**, *30*, 1994–2001.
- [55] F. Gritti, G. Guiochon, *J. Chromatogr. A.* **2004**, *1028*, 197–210.
- [56] P. De Angelis, A. Cardellini, P. Asinari, *ACS Cent. Sci.* **2019**, *5*, 1804–1812.
- [57] D. Case, T. Darden, T. Cheatham III, C. Simmerling, J. Wang, R. Duke, R. Luo, M. Crowley, R. Walker, W. Zhang, AmberTools, *San Francisco, CA: University of California*, **2008**.
- [58] P. Mark, L. Nilsson, *J. Phys. Chem. A.* **2001**, *105*, 9954–9960.
- [59] K. Lindorff-Larsen, S. Piana, K. Palmo, P. Maragakis, J. L. Klepeis, R. O. Dror, D. E. Shaw, *Proteins Struct. Funct. Bioinf.* **2010**, *78*, 1950–1958.
- [60] D. J. Evans, B. L. Holian, *J. Chem. Phys.* **1985**, *83*, 4069–4074.
- [61] D. Van Der Spoel, E. Lindahl, B. Hess, G. Groenhof, A. E. Mark, H. J. Berendsen, *J. Comput. Chem.* **2005**, *26*, 1701–1718.
- [62] S. Kumar, J. M. Rosenberg, D. Bouzida, R. H. Swendsen, P. A. Kollman, *J. Comput. Chem.* **1992**, *13*, 1011–1021.
- [63] W. Humphrey, A. Dalke, K. Schulten, *J. Mol. Graphics* **1996**, *14*, 33–38.

Manuscript received: July 4, 2020

Revised manuscript received: August 11, 2020

Accepted manuscript online: August 13, 2020

Version of record online: September 23, 2020

3.2 Insights on alanine and arginine binding to silica with atomic resolution

While there is a general understanding of electrostatic interactions dominating the adsorption of amino acids, peptides, and proteins to silica, the nature of the interaction is still not fully understood yet. Here the interaction of the amino acids alanine and arginine with the silica surface is investigated. The focus lies on the contribution of the individual functional groups of the amino acid backbone and basic site group using different capped amino acid variants of alanine and arginine. The interactions are investigated by chromatographic zonal elution (ZE), flow microcalorimetry (FMC), and molecular dynamics (MD) simulation. The work presents data of heat signals from FMC, retention factors from ZE, and calculated affinities from MD simulation. Furthermore, the distances between the individual functional groups of the amino acids and the silica surface are calculated by MD simulation and presented as histograms.

When capping the carboxyl group of alanine, the capped L-alanine ethyl ester and L-alanine-*tert*-butyl ester adsorbed to silica with the positively charged amino group of the backbone. No adsorption was measured for the negatively charged acetyl-L-alanine, and in ZE, a repulsion from the negatively charged silica surface could be measured. For arginine, the affinity generally depends on the total charge of the derivative. The zwitterionic acetyl-L-arginine has little to no affinity to the silica surface, while the double positively charged L-arginine methyl ester has the highest affinity for silica. Interestingly, not only the overall net charge but also the total individual charges influence the affinity. L-arginine with two positive and one negative charge (total net charge of +1) has a lower affinity than acetyl-L-arginine methyl ester with only the free guanidine side group being charged (total net charge of +1). MD simulation confirmed the affinity scale and indicated that adsorption is dominated by the guanidine side chain group of arginine. Experiments with NaCl and sorbitol confirmed that electrostatic interactions drive the adsorption of alanine and arginine, and no hydrogen bonding is involved. The FMC experiments revealed the nature of the interaction of amino acids with silica. While silica is generally seen as a weak ion-exchanger, FMC heat signals suggest otherwise. No ion exchange is happening upon adsorption but ion pairing.

The substantial contribution of the doctoral candidate was the conception and the design of the experimental part of the study after critical reviewing existing literature. The doctoral candidate was the leading author and carried out all experimental works regarding chromatography and the data analysis and processing of all experimental data and discussing the simulative data. The FMC measurements were carried out together with R. Rouqueiro.

Insights on Alanine and Arginine Binding to Silica with Atomic Resolution

Stefan Rauwolf, Saientan Bag, Rodrigo Rouqueiro, Sebastian Patrick Schwaminger, Ana Cristina Dias-Cabral, Sonja Berensmeier,* and Wolfgang Wenzel*



Cite This: *J. Phys. Chem. Lett.* 2021, 12, 9384–9390



Read Online

ACCESS |



Metrics & More

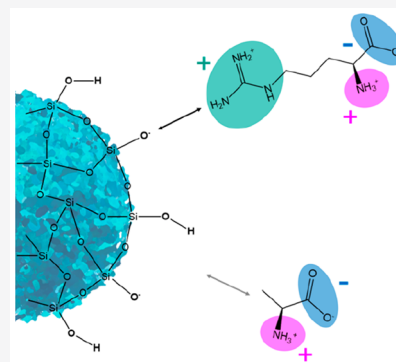


Article Recommendations



Supporting Information

ABSTRACT: Interactions of biomolecules with inorganic oxide surfaces such as silica in aqueous solutions are of profound interest in various research fields, including chemistry, biotechnology, and medicine. While there is a general understanding of the dominating electrostatic interactions, the binding mechanism is still not fully understood. Here, chromatographic zonal elution and flow microcalorimetry experiments were combined with molecular dynamic simulations to describe the interaction of different capped amino acids with the silica surface. We demonstrate that ion pairing is the dominant electrostatic interaction. Surprisingly, the interaction strength is more dependent on the repulsive carboxy group than on the attracting amino group. These findings are essential for conducting experimental and simulative studies on amino acids when transferring the results to biomolecule–surface interactions.



Amino acids (aa) are the building blocks for peptides and proteins, and understanding the mechanism that governs their interaction allows one to control the interactions of aa to different surfaces.^{1–4} Controlling these interactions is essential in several research fields in chemistry, medicine, and biotechnology.^{5–13} Inorganic materials, especially silica, play an important role in fields where the interaction of aa with the surface is important, such as chromatography,¹⁴ biosensors,^{15–17} and drug delivery.^{18–24} Additionally, these interactions play a role in the origin of life, because, in its early stages, peptides were built by condensation of aa on inorganic solid surfaces such as silica.^{25–27} Silica features two types of surface groups responsible for the intrinsic surface properties and the resulting interactions with other molecules: siloxane bridges (Si–O–Si) and silanol groups (Si–OH). Silanol groups deprotonate at pH > 3, leading to a negative charge density on the surface which increases with pH.^{28,29} The silica surface and its features regarding biomolecule interactions have been discussed thoroughly in various reviews.^{30–32}

Due to the broad interest to different scientific fields, experimental and theoretical studies identified electrostatic interactions as the driving force for interaction of silica with aa,^{33–35} peptides,^{36–38} and proteins.^{39–42} However, the influences of the individual groups of aa on these interactions are still not fully understood.^{29,43} The pH influences the charge of molecules and surfaces and, therefore, electrostatic interactions. Amino acids are primarily zwitterionic at ambient conditions due to α -amino and α -carboxy groups' charges.⁴⁴ Only aa such as histidine, lysine, and arginine carry a positive charge. Glutamic acid and aspartic acid bear an overall negative

charge, each. These five aa carry the charge of proteins and thus strongly influence protein interactions.

The aim of this study is to elucidate, with atomic precision, which functional groups of aa contribute to the binding and whether electrostatic interactions are solely or dominantly responsible for binding. To obtain insight about the influence of individual aa groups on their adsorption to the silica surface, the interaction of selected aa and their specific capped variants with silica were analyzed. For the first time, N- and C-capped variations of amino acids are used for experimental interaction studies with silica surfaces. In earlier studies we were able to show that in aqueous systems only basic positively charged amino acids adsorb with silica.^{45,46} Therefore, in this study only the zwitterionic L-alanine (Ala) and the positively charged L-arginine (Arg) are investigated. These model aa were chosen on the basis of their backbone and functional group charge. The respective aa variants with blocked N- and/or C-terminus were acetylated L-alanine (Ac-A), ethylated L-alanine (A-ethyl), *tert*-butylated L-alanine (A-tbutyl), L-arginine (Arg), acetylated L-arginine (Ac-R), methylated L-arginine (R-OMe), and a double-capped L-arginine (Ac-R-OMe).

In the case of Ala when the negative carboxy group is blocked, an overall positive charge due to the remaining amino

Received: July 23, 2021

Accepted: September 17, 2021

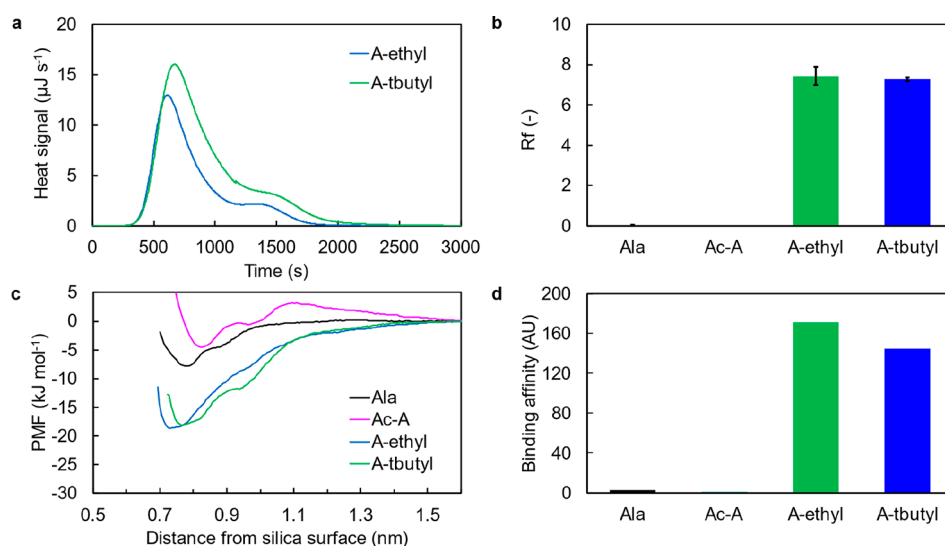


Figure 1. (a) Heat exchange profile of 10 mM *L*-alanine ethyl (A-ethyl) ester and 10 mM *L*-alanine *tert*-butyl ester (A-tbutyl) obtained from FMC experiments. Injection loop, 30 μL ; mobile phase: 1.5 mL h^{-1} H_2O , pH 7.4. (b) Retention factors (R_f) of alanine variants (50 mM) calculated from measured retention time in relation to a nonbinding tracer (1 g L^{-1} uracil) using zonal elution experiments. Injection, 20 μL ; mobile phase, 2 mL min^{-1} of 10 mM TRIS, pH 7.4. Error bars indicate standard deviation resulting from three runs per experiment. (c) PMF profile for the interaction between different capped and noncapped alanines to the silica surface as obtained from umbrella sampling simulation. (d) Binding affinity of different alanine species calculated by integrating (see eq S1) the PMF curves.

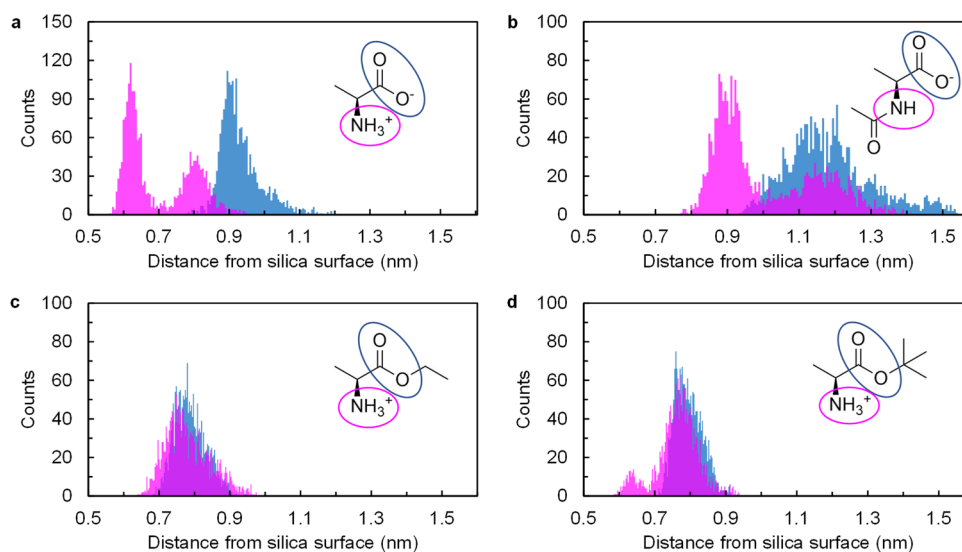


Figure 2. Histograms of the distances of the C- and N-termini of *L*-alanine (a), acetyl-*L*-alanine (b), *L*-alanine ethyl ester (c), and *L*-alanine *tert*-butyl ester (d) from the silica surface when the aa are adsorbed on silica as obtained from the MD simulation. In magenta and blue are the amino and carboxy groups of the backbone, respectively. For more details on the “distances” calculated here, see Figure S4 of the Supporting Information and text therein.

group should be observed resulting in binding to silica. For Arg, depending on the blocked groups, different strengths of interaction are expected.

To facilitate the elucidation of the interaction mechanism between aa and a silica surface, thermodynamic studies by means of flow microcalorimetry (FMC) were used to in situ monitor the enthalpy of the interactions. Compared to other microcalorimetric techniques, FMC can be used to simulate a packed-bed chromatographic system at microscale. FMC can dissect the subprocesses involved in the interaction between molecules and surface and, as a consequence, be used to discriminate between different energy contributions.^{47–49} The FMC used in this study can detect power changes with a

magnitude of 10^{-7} W, resulting in an energy resolution in the order of 10^{-9} J, enabling analysis of very weak interactions.^{47–49} The FMC is ideally complemented with zonal elution chromatography (ZE) to provide fundamental data for molecular dynamic (MD) simulation.⁴⁵ For MD simulation the atomistic model of silica and corresponding force field parameters from a database by Emami et al. was used.²⁸ To investigate the adsorption behavior, the Q3 silica surface model (see Supporting Information Figure S1 and text therein for more details) was chosen. It considers 4.7 silanol groups per nm^2 of surface, of which 14% are deprotonated at a pH of 7.4. For the experiments all aa variants were purchased and designed for simulation (Figure S2 and Figure S3).

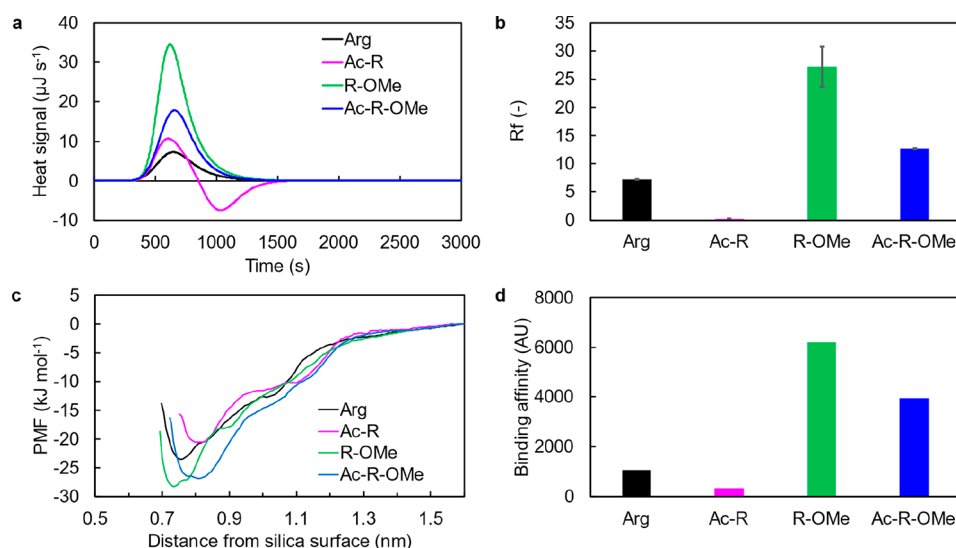


Figure 3. (a) Heat exchange profile of different capped arginine (10 mM) obtained from FMC experiments. Injection loop, 30 μL ; mobile phase, 1.5 mL h^{-1} H_2O , pH 7.4. (b) Retention factors (R_f) of arginine variants (50 mM) calculated from measured retention time in relation to a nonbinding tracer (1 g L^{-1} uracil) using zonal elution experiments. Injection, 20 μL ; mobile phase, 2 mL min^{-1} of 10 mM TRIS, pH 7.4. Error bars indicate standard deviation resulting from three runs per experiment. (c) PMF profile for the interaction between different capped and noncapped arginines (Args) to the silica surface as obtained from umbrella sampling simulation. (d) Binding affinity of different Arg species calculated by integrating (see eq S1) the PMF curves.

Different capped alanines were investigated for the influence of the backbone amino and carboxy group inherited in every aa. For the zwitterionic Ala, there was no detectable heat signal in FMC, suggesting no interaction between alanine and silica. This is supported by ZE experiments in which Ala elutes at the same time as the tracer (Figure 1B, Table S1). This behavior can be explained by the MD data where the distances of the centers of mass of the different alanine side groups from the silica surface were calculated via simulation. For more details on the “distances” calculated here, see Figure S4 of the Supporting Information and text therein. For noncapped Ala, the amino group can be near the surface, while the carboxy group is pendent (Figure 2A). Two peaks for the amino group at 0.6 and 0.8 nm indicate different conformations. The amino group of Ala can interact via electrostatic interactions or H-bonds with the water on the surface.⁵⁰ Solid-state NMR investigation suggests that the interaction of L-alanine with hydrated silica most likely happens with water (mobile phase) molecules on the surface, resulting in washing out of the silica in a dynamic setup.⁵⁰ Ben Shir et al. found an N–Si distance of 0.4–0.42 nm for L-alanine and glycine on silica and declared it as direct binding as no molecule such as water would fit between the molecules.^{51–53} The potentials of mean force (PMF, Figure 1C) profiles were calculated by umbrella sampling (US). By integrating the PMF profiles, the binding affinity was calculated showing no binding affinity (Figure 1D).

For the Ac-A derivative FMC also showed a small exothermic peak, which can be associated with salt effects on the silica surface due to pH adjustment (Figure S5). Therefore, silica and Ac-A do not interact. The MD data support the assumption of no binding: the integration of the PMF profiles showed no binding affinity for Ac-A with silica (Figure 1C,D). In the case of Ac-A, the amino group is blocked, and the aa bears a total net charge of -1 . As can be seen in the histogram, both groups are far from the surface with very broad distributions, indicating no relevance for the adsorption to silica (Figure 2B). However, ZE experiments indicate electro-

static repulsion of Ac-A from the silica surface. The negative charge of the aa results in faster run times through the column than the tracer solution. This observation points out the mitigating effect of the negatively charged carboxy group on the interaction of aa and silica (Table S1).

For both carboxy-capped derivatives A-ethyl and A-butyl only exothermic peaks with net heats of -6.2 ± 0.21 and -8.9 ± 0.31 mJ, respectively, were observed in the FMC (Figure 1A, Table S2), indicating adsorption to silica, as the occurrence of interactions of an exothermal nature contributes majorly to the adsorptive process enthalpy.⁴⁹ The interaction event is supported by the ZE experiments, which show a retention factor of >7 (Figure 1B, Table S1). In chromatography, a retention factor of 1 means a slight interaction with the column. A retention factor of 20 means strong interactions because the analyte is spending a lot of time interacting with the resin. Retention factors > 20 are problematic because it means extremely long run times and poor sensitivity due to peak broadening.⁵⁴ The retention can be explained by the overall net charge of $+1$ for both aa. Integration of the PMF profiles from simulation further validated the interaction (Figure 1C,D). A second exothermic peak for A-ethyl with 1.0 ± 0.32 mJ and for A-butyl with 0.78 ± 0.29 mJ overlapping the binding peak indicates the rearrangement of both aa derivatives following the binding process. The signal is aligned at a time beyond aa pulse residence time at the FMC cell (around 480 s after heat signal start), compatible with the establishment of a favorable arrangement of the adsorbed aa at the surface. The energy for this rearrangement would be given by the decrease of enthalpy from the first to the second observed exothermic event.⁴⁹ This behavior can be explained by steric hindrance by the capping groups (Figure S6 and Figure S7). However, this hindrance does not affect the retention time in chromatography significantly and therefore has only a little to no effect on the interaction between aa and silica.

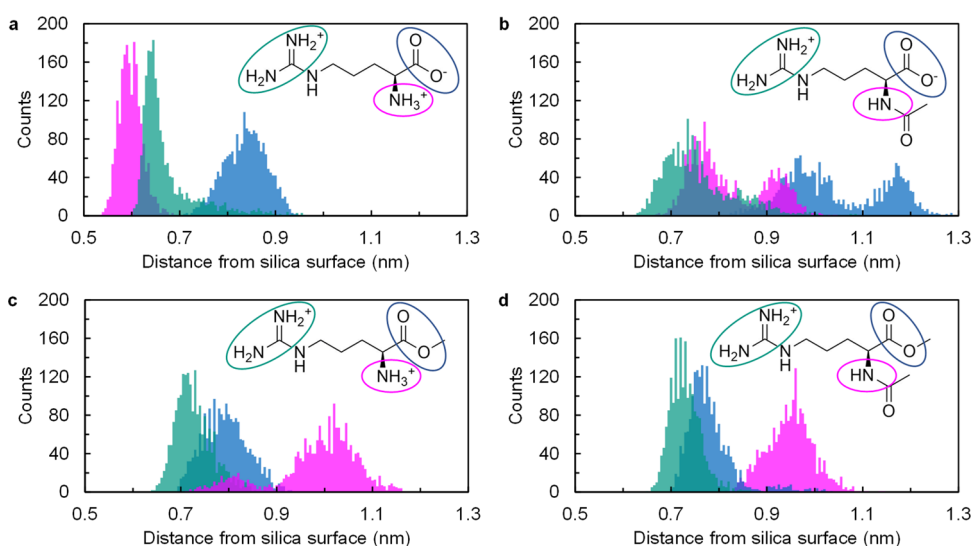


Figure 4. Histograms of the distances of the C- and N-termini of *L*-arginine (a), acetyl-*L*-arginine (b), *L*-arginine methyl ester (c), and acetyl-*L*-arginine methyl ester (d) from the silica surface when the aa are adsorbed on silica as obtained from the MD simulation. In magenta and blue are the amino and carboxy groups of the backbone, respectively. In turquoise is the guanidine side group. For more details on the “distances” calculated here, see Figure S4 of the Supporting Information and text therein.

The most interesting effect the FMC shows is the missing of an initial endothermic peak. According to literature, the FMC profile characteristic for ion exchange involves a first endothermic peak related to the desolvation entropic process overlapped with an exothermic peak related to the electrostatic interaction itself. The missing of the endothermic peak indicates a reduced contribution from desolvation subprocess to adsorption, essential to an ion-exchange binding mechanism, and suggests ion pairing as a possible mechanism.³⁶

MD simulations indicate a contribution of the methylated carboxy group as well as the amino group to the interaction with silica surfaces. The interaction contribution is indicated by two superimposed histograms at around 0.75–0.80 nm (Figure 2C,D). Furthermore, ZE experiments with 200 mM sorbitol as H-bond competitor and 1 M NaCl revealed the electrostatic nature of the binding. While there was no influence on the retention using sorbitol, NaCl negated the interaction of A-ethyl and A-*t*-butyl (Figure S8). Snapshots of the simulations illustrate the spatial location of the different alanine derivatives to silica (Figure S9). Both the simulation and ZE experiments show the same trend for binding affinities: A-ethyl \sim A-*t*-butyl > Ala > Ac-A.

FMC and ZE experiments combined with MD simulation elucidated the influence of the aa C- and N-termini on the interaction of Ala. Given these findings, Arg with a strongly positive guanidinium side group was investigated for the additional interaction effects of the functional side group in combination with the backbone groups.^{35,36,55}

In FMC the tendency R-OMe > Ac-R-OMe > Arg > Ac-R for binding enthalpy was observed (Table S3). The same trend was found in ZE experiments and MD simulation in terms of affinity (Figure 3). Considering that electrostatic interactions are the dominating forces for interaction, the charges of the aa can explain the trend. R-OMe bears a net charge of +2 and has the highest affinity. As shown for Ala, the amino group of the backbone can interact with the surface in addition to the guanidine side chain. The net heats of the single exothermic event for the binding of Arg and R-OMe are -2.81 ± 0.08 and -10.31 ± 0.92 mJ (Figure 3B, Table S3), respectively. Both

the ZE experiments with $R_{f, \text{R-OMe}} = 27 \pm 3.3$ being four times that of $R_{f, \text{Arg}} = 7.25 \pm 0.06$ and integration of PMF profiles from simulation support the findings of the FMC. In the case of noncapped Arg, MD shows both positively charged amino and guanidine groups are at distances of 0.60 and 0.65 nm, respectively, from the silica surface during adsorption, whereas the negatively charged carboxy group is pendent (Figure 4A). MD indicates direct binding of the guanidine group to the surface.^{51–53} For R-OMe, when the carboxy group is capped, all three functional groups can be near the surface (Figure 4C and Figure S10). The positive amino and guanidine groups can interact at distances of 0.8 and 0.7 nm from the surface, respectively, while the capped carboxy group could interact through H-bonds between the carbonyl group (C=O) and surface silanol groups.^{35,37,38}

In contrast, when the amino group is capped and the zwitterionic Ac-R is used, ZE experiments indicate a low affinity; a significantly lower R_f of 0.29 ± 0.00 was measured compared to Arg (Figure 3B, Table S4). Ac-R has an overall neutral charge due to its zwitterionic state and low affinity comparable to Ala, and other zwitterionic aa are expected.^{45,55,56} Low affinity is supported by the FMC signal; the exothermic event (binding) with -5.0 ± 0.14 mJ and the endothermic event (more consistent with elution) with 4.3 ± 0.20 mJ are about the same size, resulting in a net heat of -0.74 ± 0.09 mJ (Table S3 and Figure S11). Further proof can be found in the MD simulations. For Ac-R the broad peaks and the greater distances of all groups to the surface indicate very loose binding. The histogram for Ac-R indicates that the adsorption is mainly mediated by the guanidine side group of the Ac-R and the negative carboxy group is pendent (Figure 4B). This result is clear evidence for the interaction of amino acids with silica through amine groups. The fact that in FMC for Ac-R binding and elution could be observed with a negative total neat heat and the R_f is still somewhat higher than for the comparable zwitterionic Ala indicates the interaction of the guanidine group with silica is stronger than the α -amino group of the aa backbone with silica. These observations demonstrate again the influence of the negatively charged carboxy group on

the adsorption of basic aa. The results for the doubly capped Ac-R-OMe confirmed this influence. The derivative shows in FMC a higher interaction heat of -5.9 ± 0.36 mJ compared to that of the noncapped Arg, despite having the same net charge of +1. Due to the missing negative charge on the carboxy group the doubly capped aa experiences no repulsion from the surface, resulting in stronger interaction. However, it also shows a lower binding enthalpy than R-OMe, because it lacks the additional positively charged amino group. The same trend is found in ZE experiments. This effect can be explained by MD, where the side chain guanidine (0.7 nm) and the carbonyl group (0.8 nm) are near the surface, while the capped amino group is pendent (Figure 4D and Figure S10); only the guanidine group is interacting with silica, while the carboxy group cannot mitigate the interaction due to the capping group. More detailed analysis concluding the closest distance of the different functional groups (of uncapped and capped Arg) from the silica surface are presented in the Supporting Information (see Figure S10 and text therein).

The thermogram profiles for arginine derivatives (Figure 3A) show considerable differences compared to alanine (Figure 1A). No second exothermic peak is observed for the first, indicating the absence of rearrangements during interaction. This reinforces the idea of arginine multipoint attachment to silica surface through positively charged amino and guanidine groups, which is not so prone to rearrangement processes.

Competitive ZE experiments with sorbitol and NaCl with arginine derivatives (Figure S8) showed the same trend as that for alanine, indicating that only electrostatic interactions play a role for binding. The positively charged groups are attracted, while negatively charged groups are repelled, from the negatively charged silica surface. This indicates electrostatic interactions mediate the adsorption between positively charged amino and guanidine groups with deprotonated silanol groups on the surface.^{36,38,55,57} Snapshots of the simulations illustrate the binding of arginine to silica (Figure S12).

Besides the influence of the functional groups on binding of amino acids to silica the FMC suggests the same mechanism for binding of the Arg derivatives as for Ala. The results indicate again that the binding mechanism is not accompanied by an ion exchange. Since the aa thermograms miss the initial endothermic peak, the binding mechanism probably follows the principle of ion pairing between positively charged amino and guanidine groups with siloxide groups (SiO^-) as already theorized for peptides.³⁶

In summary, this study shows how flow microcalorimetry experiments combined with chromatographic zonal elution experiments and molecular dynamic simulation can reveal the specific influence of different functional groups on the binding affinity of aa to silica in aqueous environments. Investigating different capped Ala and Arg showed the overall charge dominating the strength of interaction with silica and exposed the influence of the negatively charged carboxy group due to repulsion from the negatively charged silica surface. Furthermore, this is the first study which experimentally proves that aa binding on silica does not follow ion exchange but an ion-pairing mechanisms. These results help to improve models and to further understand the binding behaviors for amino acid, peptide, and protein adsorption not only to silica but also other oxide surfaces. These findings can be applied in various research fields, ranging from purification of biomolecules to drug delivery systems.

■ ASSOCIATED CONTENT

Supporting Information

The Supporting Information is available free of charge at <https://pubs.acs.org/doi/10.1021/acs.jpcllett.1c02398>.

Computational and experimental methods; tables of retention times from zonal elution and heat signal area from FMC; FMC heat exchange profiles and snapshots from simulation (PDF)

■ AUTHOR INFORMATION

Corresponding Authors

Sonja Berensmeier – Department Mechanical Engineering, Bioseparation Engineering Group, Technical University of Munich, 85748 Garching, Germany; orcid.org/0000-0002-4943-848X; Email: s.berensmeier@tum.de

Wolfgang Wenzel – Institute for Nanotechnology, Karlsruhe Institute of Technology, 76344 Eggenstein-Leopoldshafen, Germany; orcid.org/0000-0001-9487-4689; Email: wolfgang.wenzel@kit.edu

Authors

Stefan Rauwolf – Department Mechanical Engineering, Bioseparation Engineering Group, Technical University of Munich, 85748 Garching, Germany; orcid.org/0000-0002-0756-2749

Saïentan Bag – Institute for Nanotechnology, Karlsruhe Institute of Technology, 76344 Eggenstein-Leopoldshafen, Germany; orcid.org/0000-0003-1000-7719

Rodrigo Rouqueiro – Department of Chemistry, CICS-UBI Health Science Research Center, University Beira Interior, 6200-506 Covilhã, Portugal

Sebastian Patrick Schwaminger – Department Mechanical Engineering, Bioseparation Engineering Group, Technical University of Munich, 85748 Garching, Germany; Present Address: Department of Chemical Engineering, Massachusetts Institute of Technology, 77 Massachusetts Ave., Cambridge, MA 02139, USA; orcid.org/0000-0002-8627-0807

Ana Cristina Dias-Cabral – Department of Chemistry, CICS-UBI Health Science Research Center, University Beira Interior, 6200-506 Covilhã, Portugal; orcid.org/0000-0002-2759-7762

Complete contact information is available at:

<https://pubs.acs.org/doi/10.1021/acs.jpcllett.1c02398>

Author Contributions

S.R. and Sa.B. contributed equally to this work. S.R. and R.R. performed the experiments. Sa.B. performed the simulation. S.R., S.P.S., Sa.B., and A.C.D.-C. contributed to the design and preparation of the experimental and simulative setup. A.C.D.-C., S.P.S., W.W., and So.B. contributed to discussion and interpretation of the results. A.C.D.-C., W.W., and So.B. supervised the project. S.R. and Sa.B. wrote the manuscript with input from all coauthors.

Notes

The authors declare no competing financial interest.

■ ACKNOWLEDGMENTS

We express our gratitude for the financial support of this work by the Federal Ministry of Education and Research (Grant No. 031A173A+B and supported by TUM International Graduate School of Science and Engineering (IGSSE)). CICS-UBI also

acknowledges FCT (Foundation for Science and Technology) for funding through the Research Contract No. UIDB/00709/2020.

ABBREVIATIONS

Ac-A	acetylated L-alanine
Ac-R	acetylated L-arginine
Ac-R-OMe	acetyl L-arginine methyl ester
A-ethyl	ethylated L-alanine
Ala	L-alanine
Arg	L-arginine
A-tbutyl	tert-butylated L-alanine
FF	force field
FMC	flow microcalorimetry
MD	molecular dynamics
PMF	potential mean force
R-OMe	methylated L-arginine
ZE	zonal elution.

REFERENCES

- (1) Sheldon, R. A.; van Pelt, S. Enzyme immobilisation in biocatalysis: Why, what and how. *Chem. Soc. Rev.* **2013**, *42*, 6223–6235.
- (2) Costa, D.; Savio, L.; Pradier, C.-M. Adsorption of amino acids and peptides on metal and oxide surfaces in water environment: A synthetic and prospective review. *J. Phys. Chem. B* **2016**, *120*, 7039–7052.
- (3) Das, P.; Reches, M. Review insights into the interactions of amino acids and peptides with inorganic materials using single molecule force spectroscopy. *Biopolymers* **2015**, *104*, 480–494.
- (4) Kang, J. H.; McCusker, L. B.; Deem, M. W.; Baerlocher, C.; Davis, M. E. Further investigations of racemic and chiral molecular sieves of the STW topology. *Chem. Mater.* **2021**, *33*, 1752–1759.
- (5) Henderson, C. J.; Pumford, E.; Seevaratnam, D. J.; Daly, R.; Hall, E. A. H. Gene to diagnostic: Self immobilizing protein for silica microparticle biosensor, modelled with sarcosine oxidase. *Biomaterials* **2019**, *193*, 58–70.
- (6) Govrin, R.; Schlesinger, I.; Tcherner, S.; Sivan, U. Regulation of surface charge by biological osmolytes. *J. Am. Chem. Soc.* **2017**, *139*, 15013–15021.
- (7) Yuan, P.; Mao, X.; Wu, X.; Liew, S. S.; Li, L.; Yao, S. Q. Mitochondria-targeting, intracellular delivery of native proteins using biodegradable silica nanoparticles. *Angew. Chem., Int. Ed.* **2019**, *58*, 7657–7661.
- (8) Pyles, H.; Zhang, S.; De Yoreo, J. J.; Baker, D. Controlling protein assembly on inorganic crystals through designed protein interfaces. *Nature* **2019**, *571*, 251–256.
- (9) El-Shetehy, M.; Moradi, A.; Maceroni, M.; Reinhardt, D.; Petri-Fink, A.; Rothen-Rutishauser, B.; Mauch, F.; Schwab, F. Silica nanoparticles enhance disease resistance in Arabidopsis plants. *Nat. Nanotechnol.* **2021**, *16*, 344–353.
- (10) Matange, K.; Tuck, J. M.; Keung, A. J. DNA stability: a central design consideration for DNA data storage systems. *Nat. Commun.* **2021**, *12*, 1358.
- (11) Benmerzoug, S.; Rose, S.; Bounab, B.; Gosset, D.; Duneau, L.; Chenuet, P.; Mollet, L.; Le Bert, M.; Lambers, C.; Geleff, S.; Roth, M.; Fauconnier, L.; Sedda, D.; Carvalho, C.; Perche, O.; Laurenceau, D.; Ryffel, B.; Apetoh, L.; Kiziltunc, A.; Uslu, H.; Albez, F. S.; Akgun, M.; Togbe, D.; Quesniaux, V. F. J. STING-dependent sensing of self-DNA drives silica-induced lung inflammation. *Nat. Commun.* **2018**, *9*, 5226.
- (12) Nguyen, M.-K.; Nguyen, V. H.; Natarajan, A. K.; Huang, Y.; Ryssy, J.; Shen, B.; Kuzyk, A. Ultrathin silica coating of DNA origami nanostructures. *Chem. Mater.* **2020**, *32*, 6657–6665.
- (13) Lee, J. Y.; Kim, M. K.; Nguyen, T. L.; Kim, J. Hollow Mesoporous Silica Nanoparticles with Extra-Large Mesopores for Enhanced Cancer Vaccine. *ACS Appl. Mater. Interfaces* **2020**, *12*, 34658–34666.
- (14) González-García, T.; Margola, T.; Silvagni, A.; Mancin, F.; Rastrelli, F. Chromatographic NMR spectroscopy with hollow silica spheres. *Angew. Chem., Int. Ed.* **2016**, *55*, 2733–2737.
- (15) Yang, X.; Qiu, P.; Yang, J.; Fan, Y.; Wang, L.; Jiang, W.; Cheng, X.; Deng, Y.; Luo, W. Mesoporous materials-based electrochemical biosensors from enzymatic to nonenzymatic. *Small* **2021**, *17*, No. 1904022.
- (16) Su, Q.; Xu, P.; Zhou, L.; Wu, F.; Dong, A.; Wan, Y.; Qian, W. Real-Time and Label-Free Monitoring of Biomolecular Interactions within Complex Biological Media Using a Silica Colloidal Crystal Film. *ACS Appl. Mater. Interfaces* **2020**, *12*, 35950–35957.
- (17) Yuan, P.; Mao, X.; Liew, S. S.; Wu, S.; Huang, Y.; Li, L.; Yao, S. Q. Versatile multiplex endogenous RNA detection with simultaneous signal normalization using mesoporous silica nanoquenchers. *ACS Appl. Mater. Interfaces* **2020**, *12*, 57695–57709.
- (18) Hofmann, C.; Duerkop, A.; Baumann, A. J. Nanocontainers for analytical applications. *Angew. Chem., Int. Ed.* **2019**, *58*, 12840–12860.
- (19) Xuan, M.; Shao, J.; Zhao, J.; Li, Q.; Dai, L.; Li, J. Magnetic mesoporous silica nanoparticles cloaked by red blood cell membranes: Applications in cancer therapy. *Angew. Chem., Int. Ed.* **2018**, *57*, 6049–6053.
- (20) Yang, G.; Liu, Y.; Wang, H.; Wilson, R.; Hui, Y.; Yu, L.; Wibowo, D.; Zhang, C.; Whittaker, A. K.; Middelberg, A. P. J.; Zhao, C.-X. Bioinspired core-shell nanoparticles for hydrophobic drug delivery. *Angew. Chem., Int. Ed.* **2019**, *58*, 14357–14364.
- (21) Yuan, P.; Zhang, H.; Qian, L.; Mao, X.; Du, S.; Yu, C.; Peng, B.; Yao, S. Q. Intracellular delivery of functional native antibodies under hypoxic conditions by using a biodegradable silica nanoquencher. *Angew. Chem., Int. Ed.* **2017**, *56*, 12481–12485.
- (22) Hong, X.; Zhong, X.; Du, G.; Hou, Y.; Zhang, Y.; Zhang, Z.; Gong, T.; Zhang, L.; Sun, X. The pore size of mesoporous silica nanoparticles regulates their antigen delivery efficiency. *Sci. Adv.* **2020**, *6*, No. eaaz4462.
- (23) Yan, M.; Xie, L.; Tang, J.; Liang, K.; Mei, Y.; Kong, B. Recent advances in heterosilica-based micro/nanomotors: designs, biomedical applications, and future perspectives. *Chem. Mater.* **2021**, *33*, 3022–3046.
- (24) Juneja, R.; Vadarevu, H.; Halman, J.; Tarannum, M.; Rackley, L.; Dobbs, J.; Marquez, J.; Chandler, M.; Afonin, K.; Vivero-Escoto, J. L. Combination of Nucleic Acid and Mesoporous Silica Nanoparticles: Optimization and Therapeutic Performance In Vitro. *ACS Appl. Mater. Interfaces* **2020**, *12*, 38873–38886.
- (25) Erastova, V.; Degiacomi, M. T.; Fraser, D. G.; Greenwell, H. C. Mineral surface chemistry control for origin of prebiotic peptides. *Nat. Commun.* **2017**, *8*, 2033.
- (26) Navrotsky, A.; Hervig, R.; Lyons, J.; Seo, D.-K.; Shock, E.; Voskanyan, A. Cooperative formation of porous silica and peptides on the prebiotic Earth. *Proc. Natl. Acad. Sci. U. S. A.* **2021**, *118*, e2021117118.
- (27) Guo, W.; Kinghorn, A. B.; Zhang, Y.; Li, Q.; Poonam, A. D.; Tanner, J. A.; Shum, H. C. Non-associative phase separation in an evaporating droplet as a model for prebiotic compartmentalization. *Nat. Commun.* **2021**, *12*, 3194.
- (28) Emami, F. S.; Puddu, V.; Berry, R. J.; Varshney, V.; Patwardhan, S. V.; Perry, C. C.; Heinz, H. Force field and a surface model database for silica to simulate interfacial properties in atomic resolution. *Chem. Mater.* **2014**, *26*, 2647–2658.
- (29) Buszewska-Forajta, M.; Markuszewski, M. J.; Kalisz, R. Free silanols and ionic liquids as their suppressors in liquid chromatography. *J. Chromatogr. A* **2018**, *1559*, 17–43.
- (30) Rimola, A.; Costa, D.; Sodupe, M.; Lambert, J.-F.; Ugliengo, P. Silica surface features and their role in the adsorption of biomolecules: computational modeling and experiments. *Chem. Rev.* **2013**, *113*, 4216–4313.

- (31) Lambert, J.-F. Adsorption and polymerization of amino acids on mineral surfaces: a review. *Origins Life Evol. Biospheres* **2008**, *38*, 211–242.
- (32) Fenoglio, I.; Fubini, B.; Ghibaudi, E. M.; Turci, F. Multiple aspects of the interaction of biomacromolecules with inorganic surfaces. *Adv. Drug Delivery Rev.* **2011**, *63*, 1186–1209.
- (33) Holinga, G. J.; York, R. L.; Onorato, R. M.; Thompson, C. M.; Webb, N. E.; Yoon, A. P.; Somorjai, G. A. An SFG study of interfacial amino acids at the hydrophilic SiO₂ and hydrophobic deuterated polystyrene surfaces. *J. Am. Chem. Soc.* **2011**, *133*, 6243–6253.
- (34) Razvag, Y.; Gutkin, V.; Reches, M. Probing the interaction of individual amino acids with inorganic surfaces using atomic force spectroscopy. *Langmuir* **2013**, *29*, 10102–10109.
- (35) Rimola, A.; Sodupe, M.; Ugliengo, P. Affinity scale for the interaction of amino acids with silica surfaces. *J. Phys. Chem. C* **2009**, *113*, 5741–5750.
- (36) Patwardhan, S. V.; Emami, F. S.; Berry, R. J.; Jones, S. E.; Naik, R. R.; Deschaume, O.; Heinz, H.; Perry, C. C. Chemistry of aqueous silica nanoparticle surfaces and the mechanism of selective peptide adsorption. *J. Am. Chem. Soc.* **2012**, *134*, 6244–6256.
- (37) Emami, F. S.; Puddu, V.; Berry, R. J.; Varshney, V.; Patwardhan, S. V.; Perry, C. C.; Heinz, H. Prediction of specific biomolecule adsorption on silica surfaces as a function of pH and particle size. *Chem. Mater.* **2014**, *26*, 5725–5734.
- (38) Maity, S.; Zanuy, D.; Razvag, Y.; Das, P.; Alemán, C.; Reches, M. Elucidating the mechanism of interaction between peptides and inorganic surfaces. *Phys. Chem. Chem. Phys.* **2015**, *17*, 15305–15315.
- (39) Hoehne, M.; Samuel, F.; Dong, A.; Wurth, C.; Mahler, H.-C.; Carpenter, J. F.; Randolph, T. W. Adsorption of monoclonal antibodies to glass microparticles. *J. Pharm. Sci.* **2011**, *100*, 123–132.
- (40) Tarasevich, Y. I.; Monakhova, L. I. Interaction between globular proteins and silica surface. *Colloid J.* **2002**, *64*, 482–487.
- (41) Turci, F.; Ghibaudi, E.; Colonna, M.; Boscolo, B.; Fenoglio, I.; Fubini, B. An integrated approach to the study of the interaction between proteins and nanoparticles. *Langmuir* **2010**, *26*, 8336–8346.
- (42) Mohammad-Beigi, H.; Hayashi, Y.; Zeuthen, C. M.; Eskandari, H.; Scavenius, C.; Juul-Madsen, K.; Vorup-Jensen, T.; Enghild, J. J.; Sutherland, D. S. Mapping and identification of soft corona proteins at nanoparticles and their impact on cellular association. *Nat. Commun.* **2020**, *11*, 4535.
- (43) Puddu, V.; Perry, C. C. Peptide adsorption on silica nanoparticles: evidence of hydrophobic interactions. *ACS Nano* **2012**, *6*, 6356–6363.
- (44) Nelson, D. L.; Cox, M. M. *Lehninger principles of biochemistry*, 6th ed.; W. H. Freeman: New York, 2013.
- (45) Bag, S.; Rauwolf, S.; Suyetin, M.; Schwaminger, S. P.; Wenzel, W.; Berensmeier, S. Buffer influence on the amino acid silica interaction. *ChemPhysChem* **2020**, *21*, 2347–2356.
- (46) Bag, S.; Rauwolf, S.; Schwaminger, S. P.; Wenzel, W.; Berensmeier, S. DNA binding to the silica: Cooperative adsorption in action. *Langmuir* **2021**, *37*, 5902–5908.
- (47) Rosa, S. A.S.L.; da Silva, C. L.; Aires-Barros, M. R.; Dias-Cabral, A. C.; Azevedo, A. M. Thermodynamics of the adsorption of monoclonal antibodies in phenylboronate chromatography: Affinity versus multimodal interactions. *J. Chromatogr. A* **2018**, *1569*, 118–127.
- (48) Silva, G. L.; Marques, F. S.; Thrash, M. E.; Dias-Cabral, A. C. Enthalpy contributions to adsorption of highly charged lysozyme onto a cation-exchanger under linear and overloaded conditions. *J. Chromatogr. A* **2014**, *1352*, 46–54.
- (49) Da Silva, G. F. L.; Plewka, J.; Tscheließnig, R.; Lichtenegger, H.; Jungbauer, A.; Dias-Cabral, A. C. M. Antibody Binding Heterogeneity of Protein A Resins. *Biotechnol. J.* **2019**, *14*, No. 1800632.
- (50) Guo, C.; Holland, G. P. Alanine adsorption and thermal condensation at the interface of fumed silica nanoparticles: A solid-state NMR investigation. *J. Phys. Chem. C* **2015**, *119*, 25663–25672.
- (51) Ben Shir, I.; Kababya, S.; Amitay-Rosen, T.; Balazs, Y. S.; Schmidt, A. Molecular level characterization of the inorganic-bioorganic interface by solid state NMR: alanine on a silica surface, a case study. *J. Phys. Chem. B* **2010**, *114*, 5989–5996.
- (52) Ben Shir, I.; Kababya, S.; Schmidt, A. Binding specificity of amino acids to amorphous silica surfaces: Solid-state NMR of glycine on SBA-15. *J. Phys. Chem. C* **2012**, *116*, 9691–9702.
- (53) Ben Shir, I.; Kababya, S.; Schmidt, A. Molecular details of amorphous silica surfaces determine binding specificity to small amino acids. *J. Phys. Chem. C* **2014**, *118*, 7901–7909.
- (54) Orna, R. M.; Dong, M. W. Key concepts of HPLC in pharmaceutical analysis. In *Handbook of Pharmaceutical Analysis by HPLC*; Elsevier, 2005; Vol. 6, pp 19–45. DOI: 10.1016/S0149-6395(05)80046-7.
- (55) Vlasova, N. N.; Golovkova, L. P. The adsorption of amino acids on the surface of highly dispersed silica. *Colloid J.* **2004**, *66*, 657–662.
- (56) Basiuk, V. A.; Gromovoy, T. Y. Free energies of amino acid adsorption on silica in neutral aqueous medium as estimated from high-performance liquid-chromatographic retention data. *Amino Acids* **1994**, *7*, 305–309.
- (57) Gao, Q.; Xu, W.; Xu, Y.; Wu, D.; Sun, Y.; Deng, F.; Shen, W. Amino acid adsorption on mesoporous materials: influence of types of amino acids, modification of mesoporous materials, and solution conditions. *J. Phys. Chem. B* **2008**, *112*, 2261–2267.

3.3 Purification of a peptide tagged protein via an affinity chromatographic process with underivatized silica

Underivatized silica is an abundant and inexpensive material with outstanding performance, especially in analytical chromatographic processes due to its high mechanical strength, column efficiency, and easy manufacturing. Despite these positive attributes to silica, it has yet to find its place in protein purification. In this study, the octapeptide (RH)₄ (RHRHRHRH) is investigated as a silica binding tag for high-purity protein purification chromatography of eGFP on bare silica. The focus lies on the proof-of-concept using the newly designed tag to purify the fusion protein GFP-(RH)₄ from lysate. Besides the proof of the (RH)₄ tag being responsible for protein binding, the work presents data on equilibrium and dynamic binding capacities, an upscaling attempt, and a comparison of the process in different buffers.

(RH)₄ is a silica binding peptide and able to bind fused proteins on silica in a chromatographic process. For the operating buffer and flow conditions, the equilibrium binding capacity of the fusion protein GFP-(RH)₄ on silica was determined at 450 mg g⁻¹ and the dynamic binding capacity at around 3 mg mL⁻¹. In the one-step purification from the clarified lysate, the process achieved a purity of 93% at 94% recovery. Further studies revealed that overloading the column leads to purities of over 95% at the cost of recovery due to affinity displacement. Upscaling the process confirmed the findings as on the partially loaded column with only around 80% purity, more lysate proteins were found in the eluate. Experiments with different buffers indicated a robust process applicable under various conditions.

The substantial contribution of the doctoral candidate was the conception and the design of the study after critical reviewing existing literature. The doctoral candidate was the leading author and carried out the experiments together with T. Steegmüller, as well as the data analysis and processing.

RESEARCH ARTICLE

Purification of a peptide tagged protein via an affinity chromatographic process with underivatized silica

Stefan Rauwolf  | Tobias Steegmüller | Sebastian Patrick Schwaminger  |
Sonja Berensmeier 

Department of Mechanical Engineering,
Technical University of Munich, Munich,
Germany (Email: s.rauwolf@tum.de)

Correspondence

Sonja Berensmeier, Department of
Mechanical Engineering, Bioseparation
Engineering Group, Boltzmannstraße 15,
85748 Garching, Germany.
Email: s.berensmeier@tum.de

Stefan Rauwolf and Tobias Steegmüller
contributed equally to this work.

Funding information

Federal Ministry of Education and
Research, Grant/Award Number:
031A173A+B

Abstract

Silica is widely used for chromatography resins due to its high mechanical strength, column efficiency, easy manufacturing (i.e. controlled size and porosity), and low-cost. Despite these positive attributes to silica, it is currently used as a backbone for chromatographic resins in biotechnological downstream processing. The aim of this study is to show how the octapeptide (RH)4 can be used as peptide tag for high-purity protein purification on bare silica. The tag possesses a high affinity to deprotonated silanol groups because the tag's arginine groups interact with the surface via an ion pairing mechanism. A chromatographic workflow to purify GFP fused with (RH)4 could be implemented. Purities were determined by SDS-PAGE and RP-HPLC. The equilibrium binding capacity of the fusion protein GFP-(RH)4 on silica is 450 mg/g and the dynamic binding capacity around 3 mg/mL. One-step purification from clarified lysate achieved a purity of 93% and a recovery of 94%. Overloading the column enhances the purity to >95%. Static experiments with different buffers showed variability of the method making the system independent from buffer choice. Our designed peptide tag allows bare silica to be utilized in preparative chromatography for downstream bioprocessing; thus, providing a cost saving factor regarding expensive surface functionalization. Underivatized silica in combination with our (RH)4 peptide tag allows the purification of proteins, in all scales, without relying on complex resins.

KEYWORDS

affinity chromatography, amino acids, peptide tag, protein purification, silica

Abbreviations: BC, big column; CV, column volume; DBC, dynamic binding capacity; EBC, equilibrium binding capacity; Egfp, enhanced green fluorescent protein; PB, phosphate buffer; SC, small column

This is an open access article under the terms of the [Creative Commons Attribution](https://creativecommons.org/licenses/by/4.0/) License, which permits use, distribution and reproduction in any medium, provided the original work is properly cited.

© 2021 The Authors. *Engineering in Life Sciences* published by Wiley-VCH GmbH

1 | INTRODUCTION

Downstream processing is currently the costliest aspect during protein purifications [1]. Especially the biotechnological production of pharmaceuticals (e.g. antibodies,

enzymes), with necessary purities of more than 99%, require several processing steps [1, 2]. A frequent choice of method is the chromatographic separation of molecules. The chromatographic separation can be based upon several interactions [3]. Affinity chromatography, as one of the most selective separation methods, seems to be inevitable when trying to achieve maximum purities of the product [2]. Affinity chromatography relies on specific binding between two ligands [4]. Therefore, peptide tag systems such as Strep-tag, poly(His)-tag, Maltose-binding protein, and so on. are often used to achieve a strong chemical interaction to the functionalized stationary phase [5–7]. The benefit of a tag system is the ability to bind the target protein specifically, through molecular engineering; therefore, achieving high purities after a single step. However, in most tag systems the stationary phase needs to be functionalized to fit the properties of desired chemical interaction [5, 7]. Functionalizations of the resin are often unstable and reduce the overall number of available binding sites. Reduced capacity and limited lifetime are reflected in the process costs [5].

Silica, an abundant resource on earth, is inexpensive and the most used material in liquid chromatography (LC), especially in reversed phase, normal phase, and hydrophilic LC [8–10]. It offers low counter pressure and the silanol groups on the surface can be easily functionalized with various surface modifications [10]. The silanol groups, negatively charged at pH >2–3, can undergo electrostatic interactions which are not favored in conservative silica applications [10–12]. However, there are only a few studies on protein purification on underivatized silica [13, 14]. Recent developments suggest that peptide tags enable the purification of proteins with bare silica, putting silica resins back in the focus for protein purification research [15–21].

In aqueous systems silica interacts mainly with the basic amino acids lysine and arginine via electrostatic interactions [22–24]. This was also shown by our group in a previous study for different buffer systems [25]. These findings led to the idea to use one of our peptide tags, which have been originally designed for bare magnetic nanoparticles: (RH)4 [26]. The (RH)4-tag is a short peptide, consisting of four consecutive arginine-histidine groups with a total of eight amino acids and can be used for immobilized metal affinity chromatography (IMAC) as well [26]. For this study, previous work on silica related tags was considered. However, these works have been done in static binding systems such as a batch method, involved larger peptide tags and were applied on a smaller scale [15–20, 27–29]. In this study the (RH)4-tag system was implemented for protein purification in a conventional chromatographic workflow. The process shows to be applicable on a larger scale and due to its small size of eight amino acids, the

PRACTICAL APPLICATION

Underivatized silica is an abundant and cheap material with outstanding performance especially in analytical chromatographic processes and has yet to find its place in protein purification. Chromatography is one of the most important unit operations in protein purification scenarios. There is a need for new, affordable, and innovative methods in downstream processing of proteins. Our rationally designed (RH)4 peptide tag in combination with underivatized silica as a stationary phase, allows an easy and inexpensive affinity purification process of fusion proteins. In laboratory scale runs, the fully dynamical process is automated from equilibration over loading, elution, and column washing and completed within 1–2 h depending on the amount of lysate. Purities of >95% are achieved in a single step with a recovery of about 94%. In regards to column packing, Silica is easy to handle, thus, allowing proving this method useful for beginner to advanced chromatographers with potential for up-scaling.

influence on the POIs biological activity and structure are minimized [30].

A functional process using underivatized silica would be inexpensive and easily applicable for many proteins. This study demonstrates the capture of a target protein (i.e. eGFP), with the designed (RH)4 tag system, on an underivatized silica matrix. eGFP was used as model protein since its fluorescence at 488 nm makes it easy to detect [31]. The protein could be captured, and a fully dynamic chromatographic workflow was developed. With a single step chromatography ~90–95% pure GFP-(RH)4 is recovered. Silica in its nature has a huge specific surface area, e. g. the Davisil 643 used in this study has 300 m²/g. Therefore, by using it as a stationary phase, a high binding capacity could be observed. Effectiveness of the (RH)4 tag chromatographic workflow is shown in its high purities after only one-step. Thus, an application-ready process could be developed for purification of (RH)4-tagged proteins on bare silica resins.

2 | MATERIALS AND METHODS

2.1 | Materials

All solvents and chemicals were of analytical grade. Buffers used for preparative and analytical

chromatography were filtered ($0.2\ \mu\text{m}\ \varnothing$) and degassed. The cloning of the GFP-(RH)4 variant was published earlier by our group [26, 32]. The *E. coli* strain BL21DE was used and incubated at 37°C in baffled flasks, at 150 rpm until an OD600 of 0.7 was achieved. After induction with 1 mM IPTG, the protein expression was carried out at 16°C at 150 rpm. For chromatographic experiments a $10 \times 100\ \text{mm}$ Omnifit column (Kinesis, Germany) filled with Davisil 643 (Sigma, Germany) was used. The bed volume was set to 1.5 mL if not stated otherwise. The column was connected to an ÄKTApurifier (GE Healthcare, Germany).

2.2 | Characterization of tag-silica interaction

For binding experiments GFP-(RH)4 was purified via IMAC as reported previously [26]. To achieve the cleavage, a 1:100 w/w ratio of a 1000 U TEV-protease to protein were mixed. The mixture was placed in a 32 mm wide dialysis tube (Thermo Fisher Scientific Inc, USA, MWCO 10000). After the tube was locked it was incubated overnight in 2 L of a 50 mM Tris buffer (pH 8.0). Both intact GFP-(RH)4 and a TEV-cleaved GFP-(RH)4 were injected into a silica column using 50 mM Tris pH 8.0.

For the dynamic binding capacity (DBC) a concentration (c_p) of 1 mg/mL GFP-(RH)4 was first measured via the systems bypass, to gather the max reference absorbance. The GFP-(RH)4 was then directed through a silica column with a column volume (CV) of 1.5 mL until a breakthrough curve could be observed. The DBC, at 10% of the obtained max mAU value, was then calculated with equation 1.

$$DBC_{10} = \frac{c_p * Q * t_{10}}{CV} \quad (1)$$

With Q being the volumetric flowrate and t_{10} the time passed until the 10% breakthrough curve occurred.

For the static equilibrium binding capacity (EBC), 1 g/L silica particles were supplemented with set dilutions of GFP-(RH)4 (3, 2, 1.5, 1, 0.75, 0.5, 0.2, 0.1 g/L; purity >95%). A supernatant analysis via UV/vis and as an orthogonal analysis a particle-BCA were performed to assess the total amount of protein bound to the silica particles and calculate the static binding capacity, as well as the K_d .

Therefore, the collected pellets were washed three times with buffer. After washing, the samples were transferred to a filter 96-well plate on top of a regular 96-well plate. The assembled plates were centrifuged at $3000 \times g$ for 10 min to remove remaining liquid. The BCA assay was then carried out with the Pierce BCA protein assay kit (Thermo Fisher Scientific Inc., USA). After incubation, the stacked

plates were centrifuged at $3000 \times g$ for 30 min until the BCA reagent passed through the filter into the 96-well plate below. The absorbance at 562 nm was measured via an Infinite M200 microplate reader (Tecan Deutschland, Germany). All samples were analyzed in analytical and technical triplicates

2.3 | Chromatographic purification of fusion protein

Cell pellets were resuspended in 50 mM Tris-HCl pH 8.0 and supplemented with protease inhibitor (Roche, Switzerland), EDTA (Carl Roth, Germany) and DNase I (AppliChem, Germany). Cell lysis was performed via French press (Julabo GmbH, Germany) at 1.8 kbar. The lysate was centrifuged at 20,000 rpm for 50 min at 4°C to collect the soluble proteins of interest and hold on ice during the whole process. The column was equilibrated for four CV with 50 mM Tris-HCl, 5% Glycerol, pH 8.0 at a flowrate of 1 mL/min. The equilibration step was followed by loading of the cleared lysate onto the column. Once the lysate was loaded on the column, it was washed with four CV equilibration buffer. As soon as the UV signal for 280 nm decreased back to the baseline, the elution process was started. For elution 50 mM Tris-HCl buffer was supplemented with 0.5 M L-lysine, pH 8.0.

2.4 | Buffer experiments

For the buffer experiments three different buffer system were prepared, 50 mM MOPS pH 8.0, 50 mM Phosphate pH 8.0, and 50 mM Tris pH 8.0. All samples were prepared in technical triplicates. 0.1 g of silica were added to 1 mL of the respective buffer and supplemented with 1 mL of the respective cleared lysate. The mixture was incubated overnight at 16°C at 1200 rpm. After incubation, the tubes were centrifuged at $16,000 \times g$ for 5 min and the supernatant was removed. The washing step was repeated twice. After washing, 0.5 M L-lysine dissolved in the respective buffer system was added to the tubes. The mixture was incubated for 1 h at 16°C . After incubation, the tubes were centrifuged, and the supernatant was collected and analyzed via BCA and HPLC.

2.5 | Protein analysis

The concentration and purity were determined by UV/Vis, SDS-PAGE, and RP-HPLC.

The amount of protein in solution was determined via UV/Vis spectroscopy and the measured values were

transformed via Beer-Lambert law (Equation 2).

$$A_{489} = \epsilon * d * c \quad (2)$$

With A being the measured absorbance value at 489 nm, the extinction coefficient of eGFP at $\epsilon_{489\text{nm}} = 56,000 \text{ M}^{-1} \text{ cm}^{-1}$ [31], d the path length, and c the molar concentration.

For SDS-PAGE the samples were mixed with a SDS loading buffer (containing 10 mM DTT), heated for 5 min at 95°C, and loaded onto a 12% polyacrylamide gel unless stated otherwise. The gel was scanned with the high-resolution scanner Amersham Typhoon NIR Plus (GE Healthcare Europe GmbH, Germany), and the densitometric analysis was performed with its analysis software Image Quant TL.

For RP-HPLC analysis 8 μL of approximately 0.5 g/L protein sample was loaded onto a C4 column (Aeris, 3.6 μm , Wipacore, 150 \times 2.1 mm). The samples were analyzed three times and the following buffers were used: buffer A - ddH₂O with 20 mM TFA; buffer B - 100% acetonitrile with 20 mM TFA. The gradient ran from 40% to 60% B in ten CV followed by three CV at 100% B and an equilibration step of five CV at 40% B. For evaluation, all peaks at 233 nm were integrated and the purity was calculated using the ratio of the eGFP peak to the total protein peak area subtracting the buffer peaks from the total peak area.

3 | RESULTS AND DISCUSSION

3.1 | Characterization of the tag-silica interaction

For a short octapeptide such as (RH)4 it is crucial for the tag to be separated from the protein and able to interact with the silica surface, without forcing the protein to the surface of the highly negative charged silica. This is achieved by inclusion of a short linker sequence (SSG) between protein and tag as well as a protease restriction site (TEV protease) as indicated in Figure 1A. The online deep learning protein structure prediction service Robetta provided by the Baker Lab at the University of Washington was used, to get a preliminary understanding of the general structure of the fusion protein (see Figure 1B) [33, 34]. For better understandability, the eGFP is marked in green, the linker + TEV site in pink, and the (RH)4-tag in yellow and blue for arginine and histidine, respectively. The structure prediction shows that the peptide tag is super exposed from the protein and thus has no steric hindrance for binding.

The design of the tag allows for it to be positively charged while the overall protein remains negatively charged at

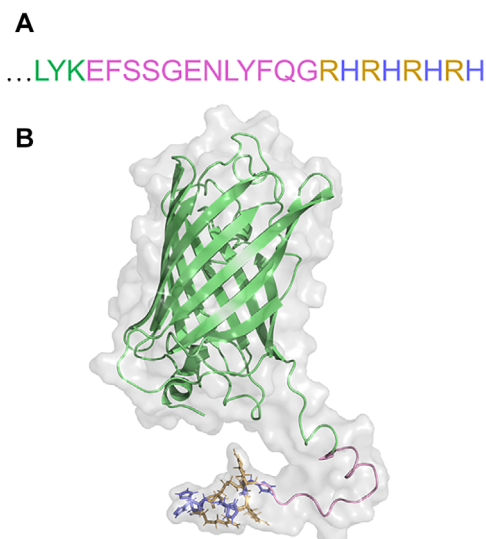


FIGURE 1 (A) Sequence of the C-terminal attachment of (RH)4 to GFP and (B) 3-dimensional structure of GFP-(RH)4 via Robetta simulation. The GFP sequence (green) ends with Leu-Tyr-Lys followed by an SSG-linker, a TEV-protease site (pink) and ends with the arginine (yellow)-histidine (blue) tag

alkaline pH. At acidic pH, the whole protein will be positively charged, since GFP-(RH)4 shows a theoretical pI of 6.11 (ExPASy); thus, binding to the negatively charged silica matrix, alongside many other proteins [13, 35–37]. Therefore, a basic pH is preferable since the protein will be repelled by the negative silanol groups, whereas the positively charged tag is still able to bind to the stationary phase. Keeping the stability of the protein and silica in mind, a pH of 8.0 was chosen to satisfy these parameters. A pH between 7.5 and 8.5 was also used by other groups for silica binding peptides such as Car9 or the Si-Tag [15, 17, 29].

To proof experimentally that the (RH)4 peptide is responsible for the binding, intact GFP-(RH)4 and TEV protease cleaved GFP-(RH)4 were compared for their binding ability under the same conditions. As shown in Figure 2 the intact GFP-(RH)4 bound to the column and did not elute until L-lysine was added. As displayed in Figure 2 elution took around five CV to start indicating potential in optimizing the elution step by testing different lysine concentrations or other eluting agents such as arginine [27]. The cleaved eGFP did not bind to the silica stationary phase and started eluting after 1 CV indicating that the (RH)4 is responsible for protein binding.

For elution L-lysine was chosen because, as previously stated, NaCl is not suitable to achieve good elution and amino acids such as lysine and arginine showed a preferable result [19, 28, 29, 38]. Using these amino acids has the additional advantage of stabilizing eluted proteins [39, 40]. Eluting with salts such as NaCl and MgCl₂ (1 M) was not

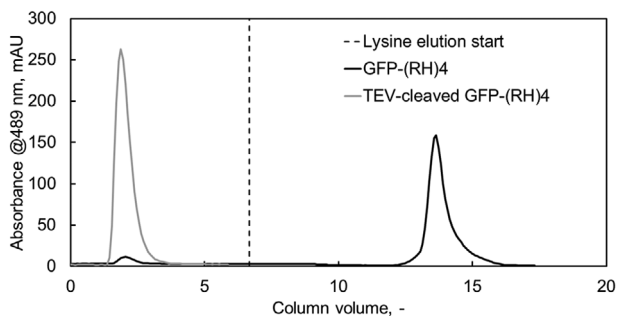


FIGURE 2 Chromatogram of GFP-(RH)4 (black) and TEV-cleaved GFP-(RH)4 (grey) with 50 mM Tris pH 8.0 as running buffer. TEV-cleaved GFP-(RH)4 eluted after roughly one column volume indicating no binding to the silica stationary phase. The intact GFP-(RH)4 eluted only after switching to the eluting buffer (dashed black line) supplemented with 0.5 M L-lysine

possible and seems to be bothersome even at high concentrations (1–5 M) [15, 17, 41]. Lysine's and arginine's competitive elution effects work at moderate concentrations of around 0.5 M but were also reported to elute at lower concentration (0.1 M) [20]. Concluding previous studies on amino acids [22, 25], peptides [42], and protein interactions with silica [14, 43], electrostatic interactions play the main role in binding. In case of (RH)4 the four positively charged arginine groups in the tag interact with the negatively charged silanol groups on the silica surface. Although, silica showed to be a weak ion exchanger [35], the resistance to salt elution in our study would suggest otherwise. In classical ion exchange chromatography NaCl gradients up to 400 mM trigger protein elution and regeneration of columns is performed with 1 M NaCl [44]. Elution of the Arg-tag, consisting of five to six arginine residues, was also shown to be possible with the classical setup [6, 45]. Considering the resistance of different silica binding peptides to salt elution from bare silica, the binding mechanism does not seem to be a classical ion exchange, but rather ion pairing. This binding mechanism was already suggested in a previous study where binding of cationic peptides to silica showed no change in the distribution of Na^+ ions in solution and binding occurred even at low initial peptide concentration thresholds. [42].

The (RH)4-tag with its eight amino acids is a short peptide-tag capable of enhancing the thermostability of fused proteins and due to its rational design allows binding to multiple surfaces such as silica, magnetic nanoparticles and immobilized metal ions in IMAC [26]. IMAC is still one of the most used chromatographic techniques for protein purification [7, 46], making the (RH)4-tag an affinity tag for two chromatographic systems.

3.2 | Binding capacities of silica

Purification of a protein with a silica affinity tag was previously optimized for GFP regarding silica type, buffers, and pH [20, 29, 41]. Therefore, Davisil 643 silica particles were chosen and Tris buffer at pH 8.0. The silica particles possess a narrow size distribution of 35–70 μm enabling homogenous packing in the column and promises good chromatographic resolution. Since Davisil 643 is a porous silica with a large specific surface area of 300 m^2/g , pores of 15 nm diameter, and a pore volume of 1.15 cm^3/g (given by manufacturer), a high binding capacity for relatively small proteins such as eGFP is expected and an important property for chromatographic materials. It should be noted, that for larger proteins such as antibodies a silica with larger pores could be more suitable due to pore-diffusion issues [47]. The equilibrium binding capacity (EBC, Figure 3A) and the dynamic binding capacity (DBC_{10} , Figure 3B) for GFP-(RH)4 on silica were determined in this study. The resulting adsorption isotherm of EBC experiments can be described by the Langmuir model with a dissociation constant $K_D = 0.02 \text{ g/L}$ (0.7 μM) and maximum load $q_{\text{max}} = 450 \text{ mg/g}$. The K_D is in the same order of magnitude as for our magnetic nanoparticles [26], and also comparable to the equivalent small Car9 peptide [15]. The maximum load is higher or in the same order of magnitude as other protein loadings on silica [35, 48, 49].

In contrast to the EBC, which shows the maximum load of a protein to a material, the dynamic binding capacity (DBC_{10}) takes the chromatographic process parameters into account. Thus, the DBC_{10} yields the binding capacity under operating conditions. The DBC_{10} for the 1.5 mL column was performed at 1 mL/min and a protein concentration of $c_P = 1 \text{ g/L}$. The dead volume of 1.6 mL was previously determined and includes the column and wires. With the breakthrough curve (Figure 3B) the DBC_{10} calculates to $\sim 3 \text{ mg/mL}$, and is comparable to other affinity tag systems [5, 15]. However, due to silica's nature of high surface area and lack of functionalizations, a higher capacity even under operating conditions is expected. Improvements on the binding capacity may be achieved by varying the process parameters such as pH or ionic strength of the buffers.

3.3 | Purification process from clarified lysate

For the purification process the chromatographic column was set to a CV of 1.5 mL and operated at 1 mL/min. Five hundred microliter lysate were injected via a sample loading loop. With these parameters, a purity of 90–93% by HPLC and SDS-PAGE evaluation (see Figure 4) with

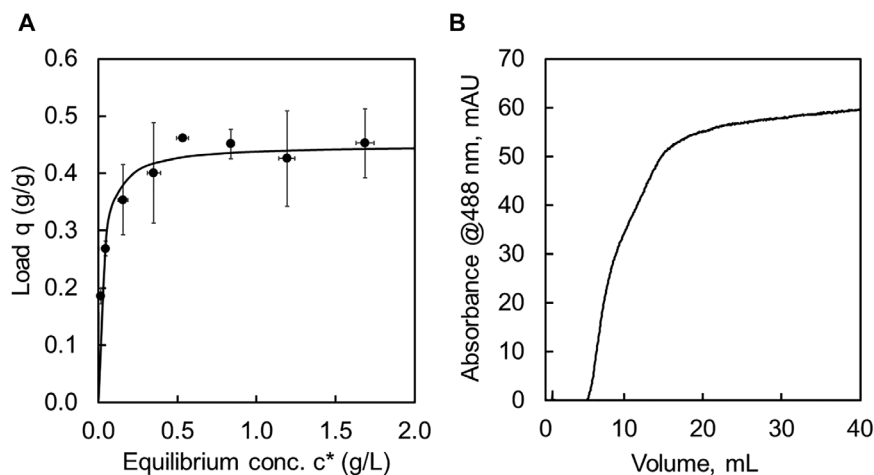


FIGURE 3 (A) Equilibrium binding capacity (EBC) at 50 mM Tris pH 8.0 and 1 g/L silica. Adsorption isotherm after Langmuir model. (B) Breakthrough curve of dynamic binding capacity (DBC₁₀) for 1 g/L GFP-(RH)4 with 50 mM Tris pH 8.0 on silica with a flowrate of 1 mL/min (column volume 1.5 mL)

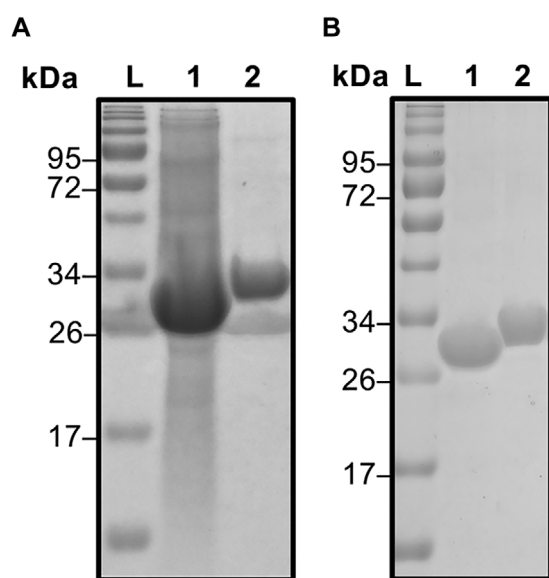


FIGURE 4 (A) SDS-PAGE of GFP-(RH)4 purification out of lysate with lysate (1) and elution fraction (2). (B) SDS-PAGE of TEV-protease digestion of GFP-(RH)4 with digested GFP-(RH)4 (1) and an intact GFP-(RH)4 (2). Protein standard ladder (L) for comparison in both gels

a recovery of about 94% has been achieved. The protein purity is comparable to purities gained with other peptide tags such as SB7 and Car9 [27, 29]. However, the recovery in our system is higher compared to both systems with ~65% and 75–90%, respectively. Loss of protein occurs due to tag degradation and during the ultrafiltration process. Considering that GFP-(RH)4 is already overexpressed and abundant (SDS-PAGE ~60%) in the lysate the selective binding of (RH)4 enables a one-step purification of fusion proteins out of lysates in a classical chromatographic workflow. Previous studies on silica binding tags either bound in static systems or in very small scaled spin columns with 600 μ L working volume [15, 19, 20, 29]. In this study a fully work-

ing chromatographic workflow was implemented, which allows real time monitoring of the loading, washing, and elution step. The degradation of the tag can be a result due to its super exposed nature or problems in the sequence which can lead to degradation by proteases [15, 50]. A degradation of the tag (26 kDa eGFP, 29 kDa GFP-(RH)4) could be possible and would explain the additional band which can be seen in Figure 3A in the lysate (lane 2) and the purified fraction (lane 3). This was confirmed by a TEV-protease digestion of GFP-(RH)4 which was compared to an untagged eGFP standard (Figure 4B). Subsequently, EDTA and 5% glycerol were used, as additional additives to support the protein's stability [51]. Impurities in the process are caused by non-specific binding of proteins [14, 29]. The main contaminant around 43 kDa most likely seems to be an RNA-binding protein with natural high affinity to silica [29, 52].

3.4 | Up-scaling and optimization of process parameters

The potential of process-up-scaling was investigated. Therefore, a XK16 column was prepared (GE Healthcare, Germany) with a column volume of 75 mL. The column was loaded with 50 mL lysate (with a eGFP concentration of 2 g/L). The column, which was only partially loaded, (indicated by a green color change of the stationary phase) showed a purity of >80% after elution, also indicated by multiple protein bands in the SDS-PAGE (Figure 5A, lane 2). An explanation for the reduced purity could be that many binding sites were left open for other lysate proteins to bind to silica, due to only partially loading the column. However, it was possible to up-scale the process (i.e. for preparative capture steps), regarding polishing there is potential for optimization. Theoretically, the specific binding of the (RH)4-tag should be stronger than unspecific

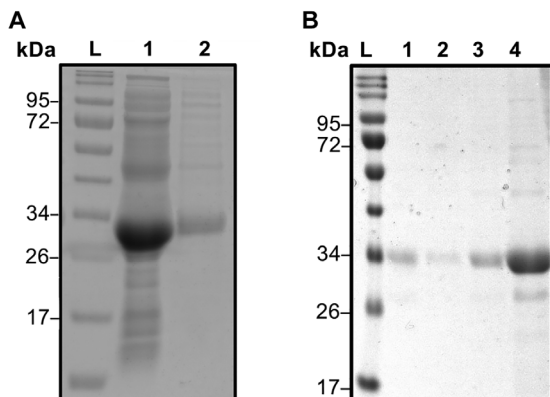


FIGURE 5 (A) SDS-PAGE with lysate (1) and elution fraction (2) of XK16 column with a column volume of 75 mL. The column was loaded with 50 mL lysate. (B) SDS-PAGE analysis of elution fractions from different columns and injection volumes. A 1 mL column with injections of 50 μ L (1) and 500 μ L (2) and a 2 mL column with injections of 50 μ L (3) and 500 μ L (4) of 2 g/L GFP-(RH)4. Protein standard ladder (L) for comparison in both gels

binding of other proteins. Therefore, different volumes (50 and 500 μ L) of the same lysate were loaded on a small column with a column volume of 1 mL (SC) and a bigger column (BC) with a volume of 2 mL. The size of the column and the amount of protein loaded consequently impacted the purity. For the small column with a CV of 1 mL even 50 μ L of the lysate were enough to have to achieve a purity >95% (Figure 5B, lane 1+2). The BC with a CV of 2 mL showed a purity of roughly 92% when injecting 500 μ L lysate (Figure 5B, lane 3). The BC showed a purity over 95% upon overloading with the lysate (Figure 5B, lane 4) indicating that the competitive effect of the (RH)4-tag enhances purity. The competitive effect of the target protein could not occur on the XK16 column; thus, resulting in a lower purity indicating the importance of the equilibrium on the column. These results show the limitation and application potential of the chromatographic method and also the silica-peptide system itself: Overloading the silica, to get high purities, lead to loss in protein recovery; high protein recovery leads to decrease in purity. However, the loss in protein recovery for high purity can be minimized due to real-time measurement of eGFP at 488 nm. For other proteins this is more challenging as they do not have a unique absorption wavelength and the amount of lysate for loading must be calculated.

3.5 | Influence of the buffer system on the process

As previously shown, the buffer can greatly influence the interaction of biomolecules with silica [25]. Until now,

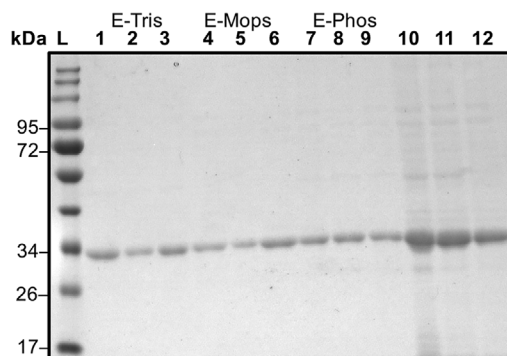


FIGURE 6 SDS-PAGE of elution fractions from static buffer experiments of 50 mM Tris (E-Tris: 1–3), MOPS (E-MOPS: 4–6), and phosphate (E-Phos: 7–9) at pH 8.0. Lysate in respective buffers for illustration (10–12). Protein standard ladder (L) for comparison

studies on silica affine peptide tags used mainly Tris buffer for the binding and purification process. However, due to the binding mechanism other buffer system should work as well. Consequently, the influence of different buffer systems on the purification system was investigated. Three buffers were chosen which can buffer in the region of pH 8.0: Tris (bearing a positive charge), phosphate (PB, bearing a negative charge), and MOPS (bearing a positive and a negative charge). Figure 6 suggests that the GFP-(RH)4 purity is not influenced by the buffer species and therefore buffer charge. Purities >90% were achieved for every buffer in the static system (Figure 6).

In classic ion exchange the buffer system impacts the process due to electrostatic interactions between charged buffer species and stationary phase [53]. However, buffer charge seems not to significantly influence our process, providing further evidence for the binding mechanism not being ion exchange but a more affinity like ion pairing mechanism which allows the (RH)4-tag system to be used with a variety of buffer systems.

4 | CONCLUDING REMARKS

Chromatographic processes remain the most important unit operation for achieving high purities in protein purification. For this purpose, Underivatized silica in combination with the (RH)4-tag is a promising method. A conventional chromatographic process for the purification of GFP-(RH)4 was implemented, with resulting purities of >90% and a recovery of >94%. The process can be easily up-scaled, considering that the column needs to be loaded completely with the protein of interest. The enhancing effect of overloading the column and improving the purity of the protein of interest to >95% could be shown. Our system proved to be independent from the buffer species,

leading to a more flexible use of this method. This process is immensely versatile, in that it can be both up- and downscaled for industrial or laboratory use; respectively enabling a widespread use for high-purity (RH)₄ tagged proteins among a wide range of buffer systems. The most promising application of this system would be as capture or polishing step in combination with another chromatographic system such as IMAC or ion exchange chromatography, which both are frequently used in protein chromatography. We are currently investigating the up-scaling and the transferability of the (RH)₄ tag system to other proteins and enzymes, which are not as overexpressed and abundant in the lysate as eGFP, for purification and immobilization.

ACKNOWLEDGMENTS

The authors thank Dr. Silvia Blank-Shim, Yasmin Kaveh-Baghbaderani, and Alexander Zanker for the cloned eGFP variants and any help in microbiological questions. Moreover, the authors are especially grateful for the financial support of the Federal Ministry of Education and Research (Grant number 031A173A+B), and the support by TUM International Graduate School of Science and Engineering (IGSSE), which made this research possible.

Open access funding enabled and organized by Projekt DEAL.

CONFLICT OF INTEREST


The authors have declared no conflicts of interest.


DATA AVAILABILITY STATEMENT

The data that support the findings of this study are available from the corresponding author upon reasonable request.

ORCID

Stefan Rauwolf  <https://orcid.org/0000-0002-0756-2749>

Sebastian Patrick Schwaminger  <https://orcid.org/0000-0002-8627-0807>

Sonja Berensmeier  <https://orcid.org/0000-0002-4943-848X>

REFERENCES

- Harrison, R. G., Todd, P., Rudge, S. R., Petrides, D. P. *Bioseparations science and engineering. Topics in chemical engineering: a series of textbooks and monographs*, 2nd Ed., Oxford University Press, New York, NY 2015.
- Arora, S., Saxena, V., Ayyar, B. V. Affinity chromatography: a versatile technique for antibody purification. *Methods* 2017, 116, 84-94.
- Carta, G., Jungbauer, A. *Protein chromatography: Process development and scale-up*, 1st Ed., Wiley-VCH, Weinheim op. 2010 (imp. 2011).
- Hage, D. S. Liquid chromatography | affinity chromatography, in: *Encyclopedia of Analytical Science*, Elsevier, 2005, 190-197.
- Lichty, J. J., Malecki, J. L., Agnew, H. D., Michelson-Horowitz, D. J., et al. Comparison of affinity tags for protein purification. *Protein Expression Purif.* 2005, 41, 98-105.
- Terpe, K. Overview of tag protein fusions: from molecular and biochemical fundamentals to commercial systems. *Appl. Microbiol. Biotechnol.* 2003, 60, 523-533.
- Kimple, M. E., Brill, A. L., Pasker, R. L. Overview of affinity tags for protein purification. *Curr. Protoc. Protein Sci.* 2013, 73, 9.9.1-9.9.23.
- Skoczylas, M., Krzemińska, K., Bocian, S., Buszewski, B. Silica gel and its derivatization for liquid chromatography, in: Meyers, R. A. (Ed.), *Encyclopedia of Analytical Chemistry*, John Wiley & Sons, Ltd, Chichester, UK 2006, 1-39.
- Borges, E. M. Silica, hybrid silica, hydride silica and non-silica stationary phases for liquid chromatography. *J. Chromatogr. Sci.* 2015, 53, 580-597.
- Buszewska-Forajta, M., Markuszewski, M. J., Kalisz, R. Free silanols and ionic liquids as their suppressors in liquid chromatography. *J. Chromatogr. A* 2018, 1559, 17-43.
- Rimola, A., Costa, D., Sodupe, M., Lambert, J.-F., et al. Silica surface features and their role in the adsorption of biomolecules: computational modeling and experiments. *Chem. Rev* 2013, 113, 4216-4313.
- Emami, F. S., Puddu, V., Berry, R. J., Varshney, V. et al. Force field and a surface model database for silica to simulate interfacial properties in atomic resolution. *Chem. Mater.* 2014, 26, 2647-2658.
- Reifsnnyder, D. H., Olson, C. V., Etcheverry, T., Prashad, H. et al. Purification of insulin-like growth factor-I and related proteins using underivatized silica. *J. Chromatogr. A* 1996, 753, 73-80.
- Ghose, S., McNerney, T. M., Hubbard, B. Preparative protein purification on underivatized silica. *Biotechnol. Bioeng.* 2004, 87, 413-423.
- Coyle, B. L., Baneyx, F. A cleavable silica-binding affinity tag for rapid and inexpensive protein purification. *Biotechnol. Bioeng.* 2014, 111, 2019-2026.
- Ikeda, T., Hata, Y., Ninomiya, K.-I., Ikura, Y., et al. Oriented immobilization of antibodies on a silicon wafer using Si-tagged protein A. *Anal. Biochem.* 2009, 385, 132-137.
- Ikeda, T., Ninomiya, K.-I., Hirota, R., Kuroda, A. Single-step affinity purification of recombinant proteins using the silica-binding Si-tag as a fusion partner. *Protein Expression Purif.* 2010, 71, 91-95.
- Bolivar, J. M., Nidetzky, B. Positively charged mini-protein Zbasic2 as a highly efficient silica binding module: opportunities for enzyme immobilization on unmodified silica supports. *Langmuir* 2012, 28, 10040-10049.
- Abdelhamid, M. A. A., Motomura, K., Ikeda, T., Ishida, T., et al. Affinity purification of recombinant proteins using a novel silica-binding peptide as a fusion tag. *Appl. Microbiol. Biotechnol.* 2014, 98, 5677-5684.
- Xu, M., Bailey, M. J., Look, J., Baneyx, F. Affinity purification of Car9-tagged proteins on silica-derivatized spin columns and 96-well plates. *Protein Expression Purif.* 2020, 170, 105608.
- Wang, M., Qi, W., Xu, H., Yu, H., et al. Affinity-binding immobilization of D-amino acid oxidase on mesoporous silica by a

- silica-specific peptide. *J. Ind. Microbiol. Biotechnol.* 2019, 46, 1461-1467.
22. Vlasova, N. N., Golovkova, L. P. The adsorption of amino acids on the surface of highly dispersed silica. *Colloid J.* 2004, 66, 657-662.
 23. Rimola, A., Sodupe, M., Ugliengo, P. Affinity scale for the interaction of amino acids with silica surfaces. *J. Phys. Chem. C* 2009, 113, 5741-5750.
 24. O'Connor, A. J., Hokura, A., Kisler, J. M., Shimazu, S., et al. Amino acid adsorption onto mesoporous silica molecular sieves. *Sep. Purif. Technol.* 2006, 48, 197-201.
 25. Bag, S., Rauwolf, S., Suyetin, M., Schwaminger, S. P., et al. Buffer influence on the amino acid silica interaction. *ChemPhysChem* 2020, 21, 2347-2356.
 26. Zanker, A. A., Ahmad, N., Son, T. H., Schwaminger, S. P., et al. Selective ene-reductase immobilization to magnetic nanoparticles through a novel affinity tag. *Biotechnol. J.* 2020, e2000366.
 27. Abdelhamid, M. A. A., Ikeda, T., Motomura, K., Tanaka, T., et al. Application of volcanic ash particles for protein affinity purification with a minimized silica-binding tag. *J. Biosci. Bioeng.* 2016, 122, 633-638.
 28. Taniguchi, K., Nomura, K., Hata, Y., Nishimura, T., et al. The Si-tag for immobilizing proteins on a silica surface. *Biotechnol. Bioeng.* 2007, 96, 1023-1029.
 29. Soto-Rodríguez, J., Coyle, B. L., Samuelson, A., Aravagiri, K., et al. Affinity purification of Car9-tagged proteins on silica matrices: optimization of a rapid and inexpensive protein purification technology. *Protein Expression Purif.* 2017, 135, 70-77.
 30. Zhao, X., Li, G., Liang, S. Several affinity tags commonly used in chromatographic purification. *J. Anal. Methods Chem.* 2013, 2013, 581093.
 31. Vámosi, G., Mücke, N., Müller, G., Krieger, J. W., et al. EGFP oligomers as natural fluorescence and hydrodynamic standards. *Sci. Rep.* 2016, 6, 33022.
 32. Kaveh-Baghbaderani, Y., Blank-Shim, S. A., Koch, T., Berensmeier, S. Selective release of overexpressed recombinant proteins from *E. coli* cells facilitates one-step chromatographic purification of peptide-tagged green fluorescent protein variants. *Protein Expression Purif.* 2018, 152, 155-160.
 33. Yang, J., Anishchenko, I., Park, H., Peng, Z., et al. Improved protein structure prediction using predicted interresidue orientations. *Proc. Natl. Acad. Sci. U. S. A.* 2020, 117, 1496-1503.
 34. Kim, D. E., Chivian, D., Baker, D. Protein structure prediction and analysis using the Robetta server. *Nucleic Acids Res.* 2004, 32, W526-31.
 35. Meissner, J., Prause, A., Bharti, B., Findenegg, G. H. Characterization of protein adsorption onto silica nanoparticles: influence of pH and ionic strength. *Colloid Polym. Sci.* 2015, 293, 3381-3391.
 36. Parkes, M., Myant, C., Cann, P. M., Wong, J. S. The effect of buffer solution choice on protein adsorption and lubrication. *Tribol. Int.* 2014, 72, 108-117.
 37. van der Veen, M., Norde, W., Stuart, M. C. Electrostatic interactions in protein adsorption probed by comparing lysozyme and succinylated lysozyme. *Colloids Surf., B* 2004, 35, 33-40.
 38. Abdelhamid, M. A. A., Yeo, K. B., Ki, M.-R., Pack, S. P. Self-encapsulation and controlled release of recombinant proteins using novel silica-forming peptides as fusion linkers. *Int. J. Biol. Macromol.* 2019, 125, 1175-1183.
 39. Arakawa, T., Tsumoto, K., Kita, Y., Chang, B., et al. Biotechnology applications of amino acids in protein purification and formulations. *Amino acids* 2007, 33, 587-605.
 40. Tsumoto, K., Umetsu, M., Kumagai, I., Ejima, D., et al. Role of arginine in protein refolding, solubilization, and purification. *Biotechnol. Prog.* 2004, 20, 1301-1308.
 41. Kim, J. K., Abdelhamid, M. A. A., Pack, S. P. Direct immobilization and recovery of recombinant proteins from cell lysates by using EctPI-peptide as a short fusion tag for silica and titania supports. *Int. J. Biol. Macromol.* 2019, 135, 969-977.
 42. Patwardhan, S. V., Emami, F. S., Berry, R. J., Jones, S. E., et al. Chemistry of aqueous silica nanoparticle surfaces and the mechanism of selective peptide adsorption. *J. Am. Chem. Soc.* 2012, 134, 6244-6256.
 43. Hellner, B., Alamdari, S., Pyles, H., Zhang, S., et al. Sequence-structure-binding relationships reveal adhesion behavior of the Car9 solid-binding peptide: an integrated experimental and simulation study. *J. Am. Chem. Soc.* 2020, 142, 2355-2363.
 44. Jungbauer, A., Hahn, R. Chapter 22 Ion-Exchange Chromatography, in: *Guide to Protein Purification*, 2nd Edition. *Methods in Enzymology*, Elsevier, 2009, 349-371.
 45. Sassenfeld, H. M., Brewer, S. J. A polypeptide fusion designed for the purification of recombinant proteins. *Nat. Biotechnol.* 1984, 2, 76-81.
 46. Kosobokova, E. N., Skrypnik, K. A., Kosorukov, V. S. Overview of fusion tags for recombinant proteins. *Biochemistry* 2016, 81, 187-200.
 47. Lenhoff, A. M. Ion-exchange chromatography of proteins: the inside story. *Materials Today: Proceedings* 2016, 3, 3559-3567.
 48. Desch, R. J., Kim, J., Thiel, S. W. Interactions between biomolecules and an iron-silica surface. *Microporous Mesoporous Mater.* 2014, 187, 29-39.
 49. Cugia, F., Sedda, S., Pitzalis, F., Parsons, D. F., et al. Are specific buffer effects the new frontier of Hofmeister phenomena? Insights from lysozyme adsorption on ordered mesoporous silica. *RSC Adv.* 2016, 6, 94617-94621.
 50. Bräuer, M., Zich, M. T., Önder, K., Müller, N. The influence of commonly used tags on structural propensities and internal dynamics of peptides. *Monatsh Chem* 2019, 150, 913-925.
 51. Vagenende, V., Yap, M. G. S., Trout, B. L. Mechanisms of protein stabilization and prevention of protein aggregation by glycerol. *Biochemistry* 2009, 48, 11084-11096.
 52. Klein, G., Mathé, C., Biola-Clier, M., Devineau, S., et al. RNA-binding proteins are a major target of silica nanoparticles in cell extracts. *Nanotoxicology* 2016, 10, 1555-1564.
 53. Schmidt-Traub, H., Schulte, M. Seidel-Morgenstern, A. (Eds.), *Preparative Chromatography*, Wiley-VCH, Weinheim, Germany 2020.

How to cite this article: Rauwolf S, Steegmüller T, Schwaminger SP, Berensmeier S. Purification of a peptide tagged protein via an affinity chromatographic process with underivatized silica. *Eng Life Sci.* 2021;1-9.

<https://doi.org/10.1002/elsc.202100019>

3.4 DNA binding to the silica: Cooperative adsorption in action

The adsorption and desorption of nucleic acids to a solid surface is ubiquitous in various research areas since we know how nucleic acids are built and how to modify them. Therefore, the separation of nucleic acids gains more and more importance. Today commercial purification kits exist for easy and fast nucleic acid purification through solid-phase extraction techniques, where silica is usually used as adsorbate. Despite the widespread use, it is still not well understood how the negatively charged deoxyribonucleic acid (DNA) adsorbs to the negatively charged silica surface in an aqueous solution. In this study, the influence of different salt on the interaction of salmon DNA is investigated. The focus lies on how the salts mediated DNA binding as binding agents. The work presents data on the cooperative Langmuir adsorption model from molecular dynamics simulation and results from bulk-depletion experiments with different salts and amino acids.

The cooperative Langmuir model was able to capture the DNA binding to silica and identified the salts as binding agents. Only positively charged salts and amino acids can mediate the DNA adsorption on the negatively charged silica surface, forming a complex. Bulk-depletion experiments also revealed higher amounts of DNA bound to silica when ions with a higher oxidation state are present. Therefore, magnesium ions lead to higher amounts of bound DNA than potassium, sodium, or arginine.

The substantial contribution of the doctoral candidate was the conception and the design of the experimental part of the study after critical reviewing existing literature. The doctoral candidate was one of the two leading equal authors and carried out all experimental works and the data analysis and processing of all experimental data and discussing the simulative data.

DNA Binding to the Silica: Cooperative Adsorption in Action

Saiantan Bag,[#] Stefan Rauwolf,[#] Sebastian P. Schwaminger, Wolfgang Wenzel,^{*} and Sonja Berensmeier^{*}Cite This: *Langmuir* 2021, 37, 5902–5908

Read Online

ACCESS |

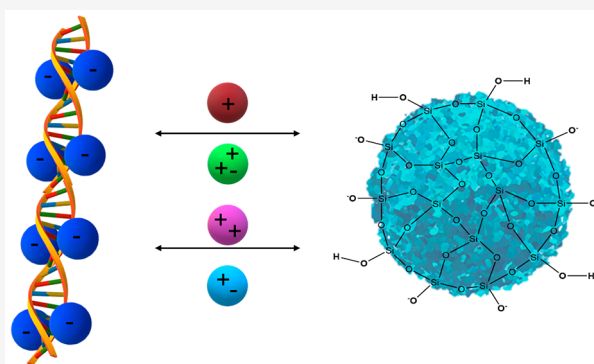


Metrics & More



Article Recommendations

ABSTRACT: The adsorption and desorption of nucleic acid to a solid surface is ubiquitous in various research areas like pharmaceuticals, nanotechnology, molecular biology, and molecular electronics. In spite of this widespread importance, it is still not well understood how the negatively charged deoxyribonucleic acid (DNA) binds to the negatively charged silica surface in an aqueous solution. In this article, we study the adsorption of DNA to the silica surface using both modeling and experiments and shed light on the complicated binding (DNA to silica) process. The binding agent mediated DNA adsorption was elegantly captured by cooperative Langmuir model. Bulk-depletion experiments were performed to conclude the necessity of a positively charged binding agent for efficient DNA binding, which complements the findings from the model. A profound understanding of DNA binding will help to tune various processes for efficient nucleic acid extraction and purification. However, this work goes beyond the DNA binding and can shed light on other binding agent mediated surface–surface, surface–molecule, molecule–molecule interaction.



I. INTRODUCTION

The adsorption of deoxyribonucleic acid (DNA), the carrier of genetic information, to a solid surface is of immense interest in pharmaceuticals, nanotechnology, medicine, and recently in organic electronics.^{1–4} Especially, in the last years, the purification of plasmids gained increasing scientific attention.⁵ The extraction, separation, and purification of DNA, which nowadays is mostly done by solid-phase extraction (SPE), relies on its adsorption capacity, where silica is primarily used as an adsorbent medium.^{6–9} Silica is an abundant, low cost material that can be easily functionalized for purification processes and represents one of the standard materials for filtration, SPE and column chromatography.^{8,10,11} Multiple approaches exist to investigate the interaction of silica with biomolecules and understand the complexity of silica surface chemistry.^{12–14} The question, which arises, is how can DNA be extracted with silica-based materials? Silica and DNA are both negatively charged over a wide pH range. DNA possesses a negatively charged¹⁵ phosphate backbone, while silica's point of zero charge (PZC) lies in a range of pH 2–3.¹³ At neutral pH, silica possesses¹⁶ around one negative charge per nm². Hence, DNA should not bind to silica due to electrostatic repulsion.

A variety of techniques^{1,17} have been devised in the past to make the DNA binding possible to the silica and even a standard procedure for DNA purification has been established. One of the possible ways in this direction is to alter the negative charge of the silica surface by controlling the pH.¹⁵

Geng et al.¹⁸ used an electrical switch to lower the solution pH facilitating the DNA binding to silica. The silica surface can also be functionalized with different groups to make the silica surface positive to allow DNA binding.^{17,19–21} Forming layers of positive ions also enhances the DNA–silica interaction^{22–24} on the silica surface by building a salt bridge between the silica surface and the DNA backbone.^{25,26} In another approach, the DNA–silica interaction is enhanced by using a high concentration of chaotropic salt^{27,28} in the solution which has the disadvantage of changing the DNA native structure. The usage of other molecular species in the solution together with DNA to tune the DNA–silica interaction has been recently reported in various experiments. Zhai et al.²⁹ studied the adsorption of environmental DNA on mica in the presence of a protein using atomic force microscopy. Vandevanter et al.³⁰ studied the adsorption and elution of DNA from the silica surface, in the presence of an amino acid (AA) buffer. During this experiment, a significant dependence of different AAs on the DNA–silica binding was observed. Both Zhai²⁹ and Vandevanter et al.³⁰ hypothesized the formation of a DNA–AA complex, which shows higher interaction to silica than

Received: February 8, 2021

Revised: April 22, 2021

Published: May 5, 2021



DNA itself. No theoretical understanding of these AA mediated interactions was accomplished. However, theoretical investigation exploring only DNA–silica interaction has been done in the past. Shi et al.³¹ developed a silica model to study the interaction of both single-strand DNA (ssDNA) and double-strand DNA (dsDNA). They calculated the binding free energy and explored different binding modes of ssDNA and dsDNA to silica. Furthermore, no stable binding modes for the dsDNA were found.

Although there were numerous experiments conducted in the past studying the DNA binding to silica, there is no modeling work attempting to understand the binding agent mediated DNA adsorption. It is worth mentioning that there have been numerous modeling attempts^{12,32–35} to understand other small molecule adsorption to various carbon and silica surfaces. The original version of the Langmuir model (noncooperative) has been extensively used^{12,35,36} in the past to understand a variety of adsorption processes. However, the simple noncooperative Langmuir model, which does not consider the interaction between the adsorbates, fails when the adsorption is cooperative in nature.¹² In this paper, we employ the cooperative Langmuir model to understand the DNA binding in different aqueous environments. The influence of different metal ions and amino acids (binding agents) on the interaction was investigated with static bulk depletion experiments to understand the equilibrium binding capacity and affinity of DNA to silica surfaces. We found that DNA binds well to silica in the presence of metal ions and the positively charged amino acid arginine (R), while no binding was observed in deionized water or the noncharged reference amino acid glycine (G). DNA binding was also measured in the presence of two binding agents, where no significant change in binding was observed. The DNA binding both in the presence of one and two binding agents was satisfactorily understood using the cooperative Langmuir model.

We hope this work will significantly impact molecular biology, especially where nucleic acid extraction is one of the more essential processes. Our work, which provides a profound understanding of the binding agent mediated DNA binding, will also be of great interest in the field of high purity

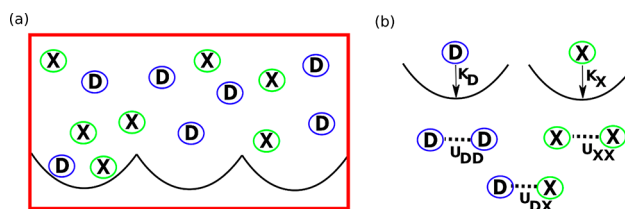


Figure 1. (a) Schematic diagram showing the cooperative Langmuir model. The adsorptive DNA (D) and the binding agents (X) bind and unbind to the silica adsorption sites, shown in black parabolas. (b) The parameters in the cooperative adsorption model are shown schematically.

purification of DNA,^{37,38} plasmids,⁵ gene therapy,^{39–41} and sensor chips.⁴² Furthermore, our approach can improve the understanding of other binding agent mediated surface–surface, surface–molecule, molecule–molecule interactions.

II. RESULTS AND DISCUSSIONS

II.A. DNA Binding to the Silica: One Binding Agent.

II.A.1. Modeling: The Cooperative Langmuir Model with One Binding Agent. DNA can not bind to the silica on its own because of the electrostatic repulsion of its negatively charged backbone with the negatively charged silica surface. Therefore, simple noncooperative Langmuir model cannot explain DNA binding. Hence, we propose the cooperative Langmuir model to understand the DNA binding to silica described as follows. Assuming the binding affinities of the DNA and the binding agent to silica are K_D and K_X respectively. The interaction energy between the two DNAs is U_{DD} , between two binding agents is U_{XX} , between a binding agent and a DNA U_{DX} . Γ is the total number of available silica binding sites as shown as black parabola in Figure 1(a). Each binding site can hold a maximum of two adsorbates. The energetic parameters of the cooperative Langmuir model is shown schematically in Figure 1 (b).

In equilibrium, the average number of DNA bound to silica (N_{DNA}) per unit binding site (F_{DNA}) is given by¹²

$$\langle N_{DNA} \rangle / \Gamma = F_{DNA} = \frac{2K_D\theta_D + 2\theta_D^2K_D^2e^{-\beta U_{DD}} + 2\theta_DK_D\theta_XK_Xe^{-\beta U_{DX}}}{1 + 2\theta_DK_D + \theta_D^2K_D^2e^{-\beta U_{DD}} + 2\theta_XK_X + \theta_X^2K_X^2e^{-\beta U_{XX}} + 2\theta_DK_D\theta_XK_Xe^{-\beta U_{DX}}} \quad (1)$$

Here, θ_D and θ_X are the concentrations of DNA and binding agent, respectively. For a complete derivation of the eq 1, see our earlier work¹² and the Supporting Information therein. The eq 1 above can also be rewritten in terms of the

concentration ratio of the adsorbates $r_\theta = \theta_X/\theta_D$ and their ratio of the binding affinity $r_K = K_X/K_D$. $\beta = 1/k_B T$. Here k_B is the Boltzmann constant and T is the temperature.

$$\begin{aligned} \langle N_{DNA} \rangle / \Gamma &= F_{DNA} \\ &= \frac{2K_D\theta_D + 2\theta_D^2r_K^2e^{-\beta U_{DD}} + 2\theta_DK_Dr_\theta r_K K_D e^{-\beta U_{DX}}}{1 + 2\theta_DK_D + \theta_D^2K_D^2e^{-\beta U_{DD}} + 2r_\theta r_K K_D + r_\theta^2r_K^2K_D^2e^{-\beta U_{XX}} + 2\theta_DK_Dr_\theta r_K K_D e^{-\beta U_{DX}}} \quad (2) \end{aligned}$$

Now, we try to understand the behavior of the DNA binding fraction (F_{DNA}) as we tune different parameters of the eq 2 above. Since it was previously hypothesized³⁰ in the literature that the binding of the DNA with the binding agent initiates the DNA adsorption to silica, we first check how the F_{DNA} depends on the parameter U_{DX} (interaction energy between DNA and the binding agent) and the r_K (the ratio of

adsorption affinity of the binding agent with respect to the DNA adsorption affinity). We compute F_{DNA} as a function of U_{DX} and r_K for different values of the U_{DD} (interaction energy between two DNA's) and U_{XX} (interaction energy between two binding agents).

As evident from the Figure 2 above, for the DNA to bind to the silica, the following conditions need to be satisfied:

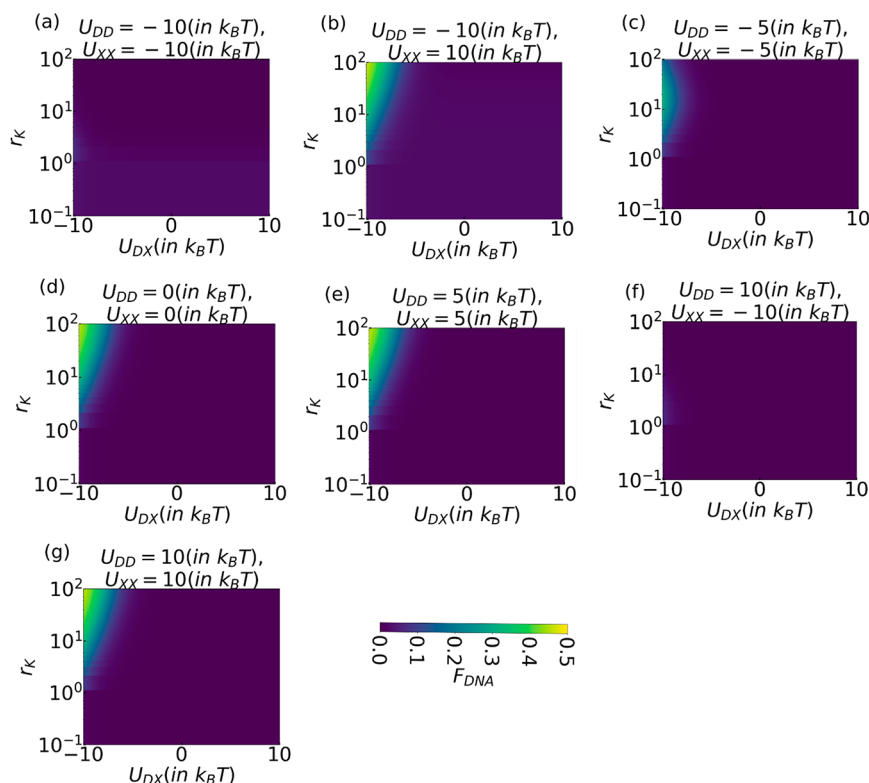


Figure 2. Binding fraction of the DNA (F_{DNA}) as a function of U_{DX} (interaction energy between DNA and the binding agent) and the r_K (the ratio of adsorption affinity of the binding agent with respect to the DNA adsorption affinity) as calculated using the cooperative Langmuir model (see eq 2). Interaction between two DNAs (U_{DD}) and interaction between the binding agents (U_{XX}) are also varied. The temperature (T) was assumed to be at 300 K and the concentration ratio of the binding agents to the DNA (r_θ) was fixed at 5. The color scale used for all the subfigures is shown in the inset.

- 1 The binding agents should have a high adsorption affinity to the silica.
- 2 There has to be an attraction between the DNA and the binding agents.
- 3 There should not be an attraction between two binding agents.

Please note that we have ruled out the possibility of an attraction between two bare DNAs ($U_{DD} < 0$) because of their high negative charge. These three conditions above can be physically understood as follows. Since DNA cannot bind to silica on its own, the attraction between the binding agent and DNA (condition 2) will ensure that the DNA sticks to the binding agent whereas the complex (DNA+binding agent) binds to silica. The binding agents have to bind to silica for this to happen (condition 1). However, if there is an attraction between two binding agents, it is energetically more favorable to form a complex between two binding agents, rather than a DNA-binding agent complex (condition 3). This will decrease the DNAs binding probability to the silica.

It is worth mentioning here that the ranges chosen for the parameter sweep in this work were guided by our earlier works^{12,43} where extensive unbiased and biased molecular dynamics simulation (umbrella sampling simulation) were done to evaluate the parameters. Here because of the complexity of the system, we could not evaluate the exact value of the parameters and therefore a parameter sweep was attempted.

In all the calculations described above, we have fixed the concentration ratio of the binding agents to the DNA (r_θ) as 5.

We now check the effect of this concentration ratio on the DNA binding fraction (F_{DNA}) as shown in Figure 3 below.

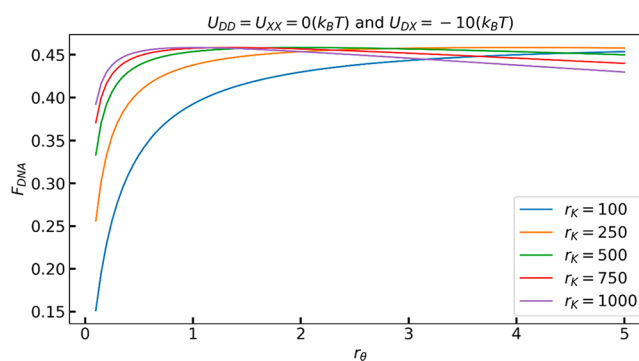


Figure 3. DNA binding fraction as a function of the concentration ratio (r_θ) of the binding agents to the DNA for different values of (r_K) as calculated using the cooperative Langmuir model (see eq 2). We have fixed the interaction between two DNA molecules (U_{DD}) and interaction between the binding agents (U_{XX}) at zero. Interaction energy of $-10 k_B T$ between the DNA and the binding agent (U_{DX}) was assumed.

As mentioned in the previous paragraph DNA cannot bind to silica on its own, and needs a binding agent to form a complex to bind to silica. If the concentration of the binding agent is too low, the binding amount of DNA is also reduced. As one increases the concentration of binding agents, DNA binding also increases because of the formation of the complex (DNA+binding agent).^{25,28} However, when there are many

more binding agents than the DNA, the complex (binding agent + DNA) has to further compete with the free binding agents. Since the complex will have low binding affinity compared to the free binding agent, an increase of free binding agents will reduce the chance of DNA binding to silica.

II.A.2. Experiment: DNA Binding to the Silica in the Presence of One Binding Agent. To validate the findings of the simulation, experiments were conducted where the amount of DNA bound to silica in the presence of different binding agents was measured. As shown in the Figure 4 below, the

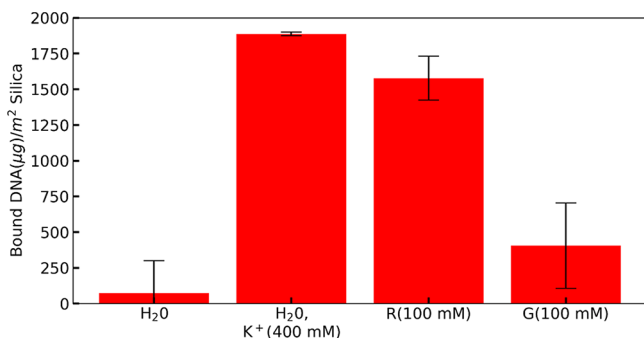


Figure 4. Amount of DNA bound to the silica for different solvation conditions. For the bulk depletion experiments ddH₂O, 400 mM KCl in H₂O (K⁺), 100 mM arginine (R), and 100 mM glycine (G) were set to pH 5. 150 μL of 0.2 g/L of the DNA solution were then added to 250 μg MagPrep. The standard deviations result from three parallel experiments.

DNA does not bind to silica if deionized water (H₂O) or 100 mM glycine (G) is used, whereas binding increases in the presence of 400 mM potassium (K⁺) ions or 100 mM arginine (R) in the solution. These results can be understood using the three main conditions (for the efficient DNA binding) concluded from the cooperative adsorption model (see Section II.A.1). While DNA is negatively charged, K⁺ ions and R (binding agent) are positively charged. K⁺ and R both bind to silica,¹² furthermore, show an attraction to DNA.⁴⁴ Due to the charge screening of negative loadings and the resulting salt bridging of positive charged ions with the silica surface, DNA binds to silica surface.^{45,46} The glycine (G), due to its zwitterionic state binds only weakly to silica and the DNA and therefore, the adsorption of DNA to silica is relatively low. This indicates that the G has, in comparison, only a minor role in DNA binding. In the case of H₂O, none of the above conditions (see Section II.A.1) are satisfied, resulting in no DNA adsorption.

Next, the DNA binding as a function of the concentration of the binding agents (K⁺/R) was measured (Figure 5). As found in our modeling described in the previous section (see Figure 3), the amount of bound DNA increases with the

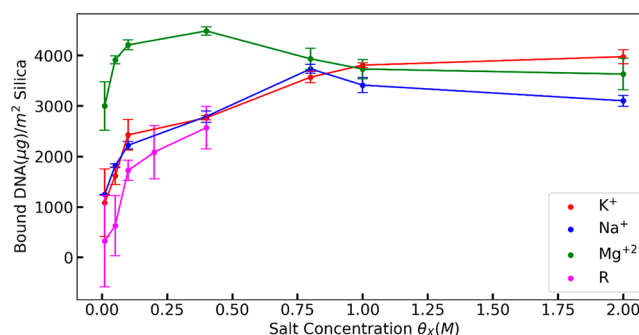


Figure 5. Amount of DNA bound to silica as a function of the concentration of the binding agents. For the bulk depletion experiments KCl, NaCl, MgCl₂, and arginine (R) were diluted in ddH₂O and set to pH 5. 150 μL of 0.2 g/L of the DNA solution were then added to 250 μg MagPrep. The standard deviations result from three parallel experiments.

concentration of the binding agents, as well as the valence of the cations.^{25,28,47,48} It is worth noting (Figure 5) that for a very high (>1.5 M) salt concentration DNA binding slightly decreases, which was also well captured (see Figure 3) in our model.

So far, we have not discussed the effect of DNA length in our calculation. However, the information on the DNA length is encoded in the total number of binding sites Γ (see eqs 1 and 2). The longer DNA will certainly occupy more space on the silica than the shorter DNA. Therefore, for a given total surface area of the silica, there will be a higher number of binding sites (Γ) available for the shorter DNA than the longer ones. Since, we always report the number of DNA bound to silica per unit binding sites (F_{DNA}) (see eqs 1 and 2), all the theoretical predictions are independent of the actual value of Γ . We want to emphasize that the DNA used in all experiments does not have a specific size but ranges from 0.2 to 2 kbp. Hence, the DNA adsorption is independent of the DNA molecule's length.

II.B. DNA Binding to Silica: Two Binding Agents.

II.B.1. The Cooperative Langmuir Model with Two Binding Agents. As already showed above the usage of a binding agent is necessary to bind DNA to silica. In the following section, we ask how the binding of the DNA changes in the presence of two binding agents. In this case, we assume that the DNA takes part in the cooperative adsorption separately with the two binding agents. If, F_{DNA1} is the binding fraction of the DNA which took part in cooperative adsorption with the binding agents X1 and F_{DNA2} is the corresponding fraction in case of the binding agent X2. The total binding fraction is given by¹²

$$F_{\text{DNA}} = 1/2(F_{\text{DNA1}} + F_{\text{DNA2}}) \quad (3)$$

Where F_{DNA1} and F_{DNA2} are given by,

$$F_{\text{DNA1}} = \frac{2K_D\theta_D + 2\theta_D^2K_D^2e^{-\beta U_{DD}} + 2\theta_D K_D r_{\theta_1} \theta_{D'} r_{K_1} K_D e^{-\beta U_{DX1}}}{1 + 2\theta_D K_D + \theta_D^2 K_D^2 e^{-\beta U_{DD}} + 2\theta_D r_{\theta_1} \theta_{D'} r_{K_1} K_D + r_{\theta_1}^2 \theta_{D'}^2 r_{K_1}^2 K_D^2 e^{-\beta U_{X1X1}} + 2\theta_D K_D r_{\theta_1} \theta_{D'} r_{K_1} K_D e^{-\beta U_{DX1}}} \quad (4)$$

$$F_{\text{DNA2}} = \frac{2K_D\theta_D + 2\theta_D^2K_D^2e^{-\beta U_{DD}} + 2\theta_DK_Dr_{\theta 2}\theta_Dr_{K2}K_De^{-\beta U_{DX2}}}{1 + 2\theta_DK_D + \theta_D^2K_D^2e^{-\beta U_{DD}} + 2\theta_Dr_{\theta 2}\theta_Dr_{K2}K_D + r_{\theta 2}^2\theta_D^2r_{K2}^2K_D^2e^{-\beta U_{X2X2}} + 2\theta_DK_Dr_{\theta 2}\theta_Dr_{K2}K_De^{-\beta U_{DX2}}} \quad (5)$$

Here K_{X1} and K_{X2} are the binding affinity (to the silica) of the binding agent $X1$ and $X2$ respectively. θ_{X1} and θ_{X2} are the concentration of the binding agents. $r_{K1} = K_{X1}/K_D$ and $r_{K2} = K_{X2}/K_D$. $r_{\theta 1} = \theta_{X1}/\theta_{X2}$ and $r_{\theta 2} = \theta_{X2}/\theta_D$. $r_{\theta} = r_{\theta 1} + r_{\theta 2}$.

Among the various parameters in eqs 4 and 5, we first decided to tune the most significant ones (see Sections II.A.I and II.A.II) and check their effect on DNA binding as shown in Figure 6. The results presented in Figure 6(a) can be

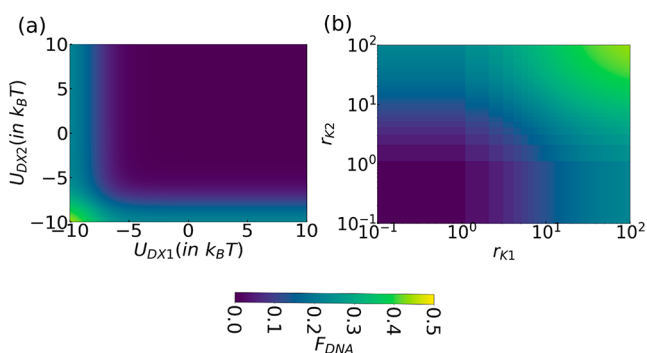


Figure 6. (a) The fraction of DNA bound (F_{DNA}) to silica as we vary the interaction of the DNA to the binding agents (U_{DX1}) and (U_{DX2}). The r_{K1} and r_{K2} were fixed at 100. The U_{DD} , U_{X1X1} , U_{X2X2} were kept at zero. (b) The DNA binding fraction as we tune the adsorption efficiency (r_{K1} and r_{K2}) of the binding agents. U_{DX1} and U_{DX2} were fixed at -10 ($k_B T$). The U_{DD} , U_{X1X1} , U_{X2X2} were kept at zero. The calculations are performed using eqs 3, 4, and 5. The color scale used for all the subfigures is shown in the inset.

understood physically as follows: if there are more than one type of binding agents present, both of the binding agents should be attractive toward DNA to achieve maximum DNA binding, provided the binding agents both favor silica. If one of the binding agents forms a complex with DNA while the other one does not, then the complex (DNA+one of the binding agents) has to compete with the free binding agent. As a result,

the DNA binding will be hindered. In the end, we also check how the DNA binding fraction (Figure 6(b)) depends on the binding affinity of the individual binding agents. If both binding agents like DNA, both binding agents should have high adsorption affinity (compared to DNA) to silica, to maximize DNA binding. If the binding agent favors DNA, it forms a complex with it. However, the complex cannot further bind to silica if the binding agent does not have a high adsorption affinity (to silica). A quick comparison of Figures 2 and 6 reveals that in the best parameter regime (for maximum DNA binding), DNA binding efficiency remains unaltered in the presence of one and two types of binding agents.

II.B.2. Experiment: DNA Binding to Silica in the Presence of Two Binding Agents. Again, to validate the results from the simulation the amount of DNA binding to silica was measured, this time in the presence of two binding agents, R and K. For a particular amount of R (100 mM) in the solution, we change the amount of K^+ ions (0, 200, 400 mM) and measure the binding of DNA. We also kept the K^+ concentration at 400 mM and increased the R concentration to 500 mM. The binding of DNA remained unaffected for all changes, as shown in Figure 7 below. This behavior can be explained from our cooperative model, which infers that the presence of two binding agents does not increase the efficiency of DNA binding. However, the addition of K^+ ions to the G results in the DNA binding to the silica again, comparable to the conditions when only K^+ is in solution (Figure 4), simply because K^+ ions act as binding agents again.⁴⁹ This effect of K^+ ions on the binding behavior of DNA in the presence of glycine further verifies the cooperative model.

III. CONCLUSIONS

To conclude, in this contribution we have provided a profound understanding of adsorption of the negatively charged macromolecule DNA to the negatively charged surface silica using both modeling and experiments. DNA binding to silica is facilitated by a binding agent, which was nicely captured in the

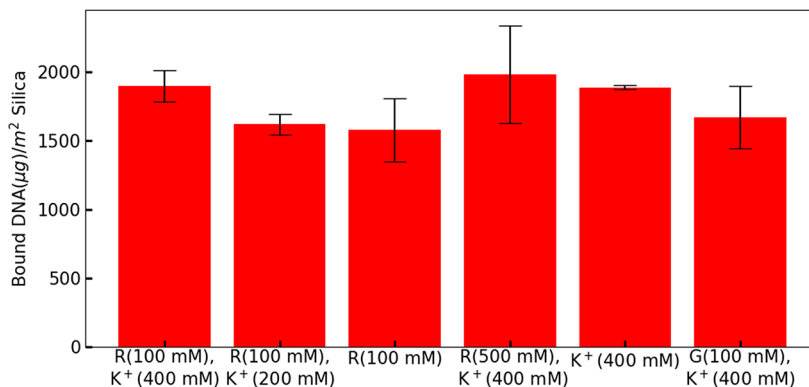


Figure 7. Amount of bound DNA to silica in the presence of both R and different amounts of K^+ ions. The case where the solution contains only 400 mM K^+ ions (without R), a higher R concentration (500 mM) and G with 400 mM K^+ ions are also shown for comparison. For the bulk depletion experiments, KCl (K^+) and arginine (R/G) were diluted in ddH₂O and set to pH 5. 150 μ L of 0.2 g/L of the DNA solution were then added to 250 μ g MagPrep. The standard deviations result from three parallel experiments.

cooperative adsorption model. In order to validate the findings of the models, bulk-depletion experiments were performed and the DNA binding was measured for different chemical environments. We found that a positively charged binding agent (which forms a complex with DNA) needs to be present, for the DNA adsorption to occur, which aligned with the findings of the models. Although only one binding agent is necessary for the DNA binding, the usage of multiple binding agents increases the DNA binding efficiency. The understanding of DNA binding will significantly impact high purity purification of DNA, plasmids, gene therapy, and sensor chips where nucleic acid adsorption–desorption is an extremely important process. Furthermore, our work goes beyond the DNA binding and can shed light on any other binding agent mediated surface–surface, surface–molecule, molecule–molecule binding.

MATERIALS AND METHODS

Experimental Details. *Reagents.* L-arginine (Cellpure $\geq 98\%$) was purchased from Carl Roth, Germany. L-glycine (analytical grade $\geq 98\%$) was purchased from SERVA, Germany. Sodium chloride and magnesium chloride hexahydrate were purchased from Carl Roth, Germany. Potassium chloride was purchased from Sigma-Aldrich, Germany. The MagPrep silica particles used in the experimental part were purchased from Sigma-Aldrich, Germany. For binding experiments, we used Invitrogen UltraPure salmon sperm DNA (double stranded DNA sheared to ≤ 2 kb).

Binding Experiments. All amino acid and salt test solutions (TS) were prepared in their respective concentration in deionized water and adjusted to pH 5 with HCl. For the binding experiment, 250 μg of MapPrep silica particles were added in an Eppendorf tube and washed with 150 μL of TS. The DNA was diluted in TS to 0.2 g/L and 150 μL were added to the tubes and were incubated for 2 h at room temperature with linear agitation at 1000 rpm using the Thermomixer comfort from Eppendorf. The particles were then removed from the solution magnetically, and the concentration of DNA in the supernatant was determined spectrophotometrically at 260 nm with an Infinite M200 Microplate Reader (Tecan Deutschland, Germany).

AUTHOR INFORMATION

Corresponding Authors

Wolfgang Wenzel – Institute of Nanotechnology (INT), Karlsruhe Institute of Technology (KIT), 76344 Eggenstein-Leopoldshafen, Germany; Email: wolfgang.wenzel@kit.edu

Sonja Berensmeier – Bioseparation Engineering Group, Department of Mechanical Engineering, Technical University of Munich (TUM), Munich 85748, Germany; orcid.org/0000-0002-4943-848X; Email: s.berensmeier@tum.de

Authors

Saïantan Bag – Institute of Nanotechnology (INT), Karlsruhe Institute of Technology (KIT), 76344 Eggenstein-Leopoldshafen, Germany; orcid.org/0000-0003-1000-7719

Stefan Rauwolf – Bioseparation Engineering Group, Department of Mechanical Engineering, Technical University of Munich (TUM), Munich 85748, Germany

Sebastian P. Schwaminger – Bioseparation Engineering Group, Department of Mechanical Engineering, Technical University of Munich (TUM), Munich 85748, Germany; orcid.org/0000-0002-8627-0807

Complete contact information is available at:

<https://pubs.acs.org/10.1021/acs.langmuir.1c00381>

Author Contributions

#Sa. B and S. R. contributed equally to the work. So.B. and W.W. conceived the idea and designed the study. Sa.B. performed all the theoretical calculations. S.R. and S.P.S. performed all the experiments. The manuscript was written by Sa.B., S.R., S.P.S., So.B., and W.W.

Notes

The authors declare no competing financial interest.

ACKNOWLEDGMENTS

We express our gratitude for the financial support of this work by the Federal Ministry of Education and Research (Grant No. 031A173A+B).

REFERENCES

- (1) Zhang, Y.; Zhang, Y.; Burke, J. M.; Gleitsman, K.; Friedrich, S. M.; Liu, K. J.; Wang, T. H. A Simple Thermoplastic Substrate Containing Hierarchical Silica Lamellae for High-Molecular-Weight DNA Extraction. *Adv. Mater.* **2016**, *28*, 10630–10636.
- (2) Castillo, R. R.; Baeza, A.; Vallet-Regi, M. Recent applications of the combination of mesoporous silica nanoparticles with nucleic acids: development of bioresponsive devices, carriers and sensors. *Biomater. Sci.* **2017**, *5*, 353–377.
- (3) Michaels, P.; Alam, M. T.; Ciampi, S.; Rouesnel, W.; Parker, S. G.; Choudhury, M. H.; Gooding, J. J. A robust DNA interface on a silicon electrode. *Chem. Commun.* **2014**, *50*, 7878–7880.
- (4) Liu, J.; Wang, B.; Hartono, S. B.; Liu, T.; Kantharidis, P.; Middelberg, A. P.; Lu, G. Q. M.; He, L.; Qiao, S. Z. Magnetic silica spheres with large nanopores for nucleic acid adsorption and cellular uptake. *Biomaterials* **2012**, *33*, 970–978.
- (5) Chiang, C.-L.; Sung, C.-S.; Chen, C.-Y. Application of silica–magnetite nanocomposites to the isolation of ultrapure plasmid DNA from bacterial cells. *J. Magn. Magn. Mater.* **2006**, *305*, 483–490.
- (6) Berensmeier, S. Magnetic particles for the separation and purification of nucleic acids. *Appl. Microbiol. Biotechnol.* **2006**, *73*, 495–504.
- (7) Tan, S. C.; Yip, B. C. DNA, RNA, and protein extraction: the past and the present. *J. Biomed. Biotechnol.* **2009**, *2009*, 1–11.
- (8) Price, C. W.; Leslie, D. C.; Landers, J. P. Nucleic acid extraction techniques and application to the microchip. *Lab Chip* **2009**, *9*, 2484–2494.
- (9) Hawkins, T. L.; O'Connor-Morin, T.; Roy, A.; Santillan, C. DNA purification and isolation using a solid-phase. *Nucleic Acids Res.* **1994**, *22*, 4543.
- (10) Neue, U. D. Silica gel and its derivatization for liquid chromatography. *Encyclopedia of Analytical Chemistry: Applications, Theory and Instrumentation* **2000**, 11450–11472.
- (11) Vogelstein, B.; Gillespie, D. Preparative and analytical purification of DNA from agarose. *Proc. Natl. Acad. Sci. U. S. A.* **1979**, *76*, 615–619.
- (12) Bag, S.; Rauwolf, S.; Suyetin, M.; Schwaminger, S. P.; Wenzel, W.; Berensmeier, S. Buffer Influence on the Amino Acid Silica Interaction. *ChemPhysChem* **2020**, *21*, 2347–2356.
- (13) Rimola, A.; Costa, D.; Sodupe, M.; Lambert, J.-F.; Ugliengo, P. Silica surface features and their role in the adsorption of biomolecules: computational modeling and experiments. *Chem. Rev.* **2013**, *113*, 4216–4313.
- (14) Emami, F. S.; Puddu, V.; Berry, R. J.; Varshney, V.; Patwardhan, S. V.; Perry, C. C.; Heinz, H. Prediction of specific biomolecule adsorption on silica surfaces as a function of pH and particle size. *Chem. Mater.* **2014**, *26*, 5725–5734.
- (15) Melzak, K. A.; Sherwood, C. S.; Turner, R. F.; Haynes, C. A. Driving forces for DNA adsorption to silica in perchlorate solutions. *J. Colloid Interface Sci.* **1996**, *181*, 635–644.
- (16) Emami, F. S.; Puddu, V.; Berry, R. J.; Varshney, V.; Patwardhan, S. V.; Perry, C. C.; Heinz, H. Force field and a surface model database

for silica to simulate interfacial properties in atomic resolution. *Chem. Mater.* **2014**, *26*, 2647–2658.

(17) Liu, L.; Guo, Z.; Huang, Z.; Zhuang, J.; Yang, W. Size-selective separation of DNA fragments by using lysine-functionalized silica particles. *Sci. Rep.* **2016**, *6*, 22029.

(18) Geng, T.; Bao, N.; Gall, O. Z.; Lu, C. Modulating DNA adsorption on silica beads using an electrical switch. *Chem. Commun.* **2009**, 800–802.

(19) Sheng, W.; Wei, W.; Li, J.; Qi, X.; Zuo, G.; Chen, Q.; Pan, X.; Dong, W. Amine-functionalized magnetic mesoporous silica nanoparticles for DNA separation. *Appl. Surf. Sci.* **2016**, *387*, 1116–1124.

(20) Kastania, A. S.; Petrou, P. S.; Loukas, C.-M.; Gogolides, E. Poly-L-histidine coated microfluidic devices for bacterial DNA purification without chaotropic solutions. *Biomed. Microdevices* **2020**, *22*, 1–12.

(21) Choi, H. K.; Chang, J. H.; Ko, I. H.; Lee, J. H.; Jeong, B. Y.; Kim, J. H.; Kim, J. B. Electrostatic interaction effect for human DNA separation with functionalized mesoporous silicas. *J. Solid State Chem.* **2011**, *184*, 805–810.

(22) Deserno, M.; Jiménez-Ángeles, F.; Holm, C.; Lozada-Cassou, M. Overcharging of DNA in the Presence of Salt: Theory and Simulation. *J. Phys. Chem. B* **2001**, *105*, 10983–10991.

(23) Nguyen, T.; Grosberg, A. Y.; Shklovskii, B. Screening of a charged particle by multivalent counterions in salty water: Strong charge inversion. *J. Chem. Phys.* **2000**, *113*, 1110–1125.

(24) Pastré, D.; Piétrement, O.; Fusil, S.; Landousy, F.; Jeusset, J.; David, M.-O.; Hamon, L.; Le Cam, E.; Zozime, A. Adsorption of DNA to mica mediated by divalent counterions: a theoretical and experimental study. *Biophys. J.* **2003**, *85*, 2507–2518.

(25) Nguyen, T. H.; Elimelech, M. Plasmid DNA adsorption on silica: kinetics and conformational changes in monovalent and divalent salts. *Biomacromolecules* **2007**, *8*, 24–32.

(26) Libera, J. A.; Cheng, H.; Olvera de la Cruz, M.; Bedzyk, M. J. Direct observation of cations and polynucleotides explains polyion adsorption to like-charged surfaces. *J. Phys. Chem. B* **2005**, *109*, 23001–23007.

(27) Li, X.; Zhang, J.; Gu, H. Adsorption and desorption behaviors of DNA with magnetic mesoporous silica nanoparticles. *Langmuir* **2011**, *27*, 6099–6106.

(28) Vandeventer, P. E.; Lin, J. S.; Zwang, T. J.; Nadim, A.; Johal, M. S.; Niemz, A. Multiphasic DNA adsorption to silica surfaces under varying buffer, pH, and ionic strength conditions. *J. Phys. Chem. B* **2012**, *116*, 5661–5670.

(29) Zhai, H.; Wang, L.; Putnis, C. V. Molecular-scale investigations reveal noncovalent bonding underlying the adsorption of environmental DNA on mica. *Environ. Sci. Technol.* **2019**, *53*, 11251–11259.

(30) Vandeventer, P. E.; Mejia, J.; Nadim, A.; Johal, M. S.; Niemz, A. DNA adsorption to and elution from silica surfaces: influence of amino acid buffers. *J. Phys. Chem. B* **2013**, *117*, 10742–10749.

(31) Shi, B.; Shin, Y. K.; Hassanali, A. A.; Singer, S. J. DNA binding to the silica surface. *J. Phys. Chem. B* **2015**, *119*, 11030–11040.

(32) Getzen, F. W.; Ward, T. M. A model for the adsorption of weak electrolytes on solids as a function of pH: I. Carboxylic acid-charcoal systems. *J. Colloid Interface Sci.* **1969**, *31*, 441–453.

(33) Swenson, H.; Stadie, N. P. Langmuir's theory of adsorption: A centennial review. *Langmuir* **2019**, *35*, 5409–5426.

(34) Ward, T. M.; Getzen, F. M. Influence of pH on the adsorption of aromatic acids on activated carbon. *Environ. Sci. Technol.* **1970**, *4*, 64–67.

(35) De Angelis, P.; Cardellini, A.; Asinari, P. Exploring the Free Energy Landscape To Predict the Surfactant Adsorption Isotherm at the Nanoparticle–Water Interface. *ACS Cent. Sci.* **2019**, *5*, 1804–1812.

(36) Xiao, F.; Pignatello, J. J. Effect of adsorption nonlinearity on the pH–adsorption profile of ionizable organic compounds. *Langmuir* **2014**, *30*, 1994–2001.

(37) Ferreira, G. N. Chromatographic approaches in the purification of plasmid DNA for therapy and vaccination. *Chem. Eng. Technol.* **2005**, *28*, 1285–1294.

(38) Ali, N.; Rampazzo, R. d. C. P.; Costa, A. D. T.; Krieger, M. A. Current nucleic acid extraction methods and their implications to point-of-care diagnostics. *BioMed Res. Int.* **2017**, *2017*, 1–13.

(39) Carvalho, A. M.; Cordeiro, R. A.; Faneca, H. Silica-Based Gene Delivery Systems: From Design to Therapeutic Applications. *Pharmaceutics* **2020**, *12*, 649.

(40) Zhou, Y.; Quan, G.; Wu, Q.; Zhang, X.; Niu, B.; Wu, B.; Huang, Y.; Pan, X.; Wu, C. Mesoporous silica nanoparticles for drug and gene delivery. *Acta Pharm. Sin. B* **2018**, *8*, 165–177.

(41) Keasberry, N.; Yapp, C.; Idris, A. Mesoporous silica nanoparticles as a carrier platform for intracellular delivery of nucleic acids. *Biochemistry (Moscow)* **2017**, *82*, 655–662.

(42) Rashid, J. I. A.; Yusof, N. A. The strategies of DNA immobilization and hybridization detection mechanism in the construction of electrochemical DNA sensor: A review. *Sensing and bio-sensing research* **2017**, *16*, 19–31.

(43) Wagner, R.; Bag, S.; Trunzer, T.; Fraga-García, P.; Wenzel, W.; Berensmeier, S.; Franzreb, M. Adsorption of organic molecules on carbon surfaces: Experimental data and molecular dynamics simulation considering multiple protonation states. *J. Colloid Interface Sci.* **2021**, 589, 424–437.

(44) Sousa, F.; Cruz, C.; Queiroz, J. Amino acids–nucleotides biomolecular recognition: from biological occurrence to affinity chromatography. *J. Mol. Recognit.* **2010**, *23*, 505–518.

(45) Kushalkar, M. P.; Liu, B.; Liu, J. Promoting DNA Adsorption by Acids and Polyvalent Cations: Beyond Charge Screening. *Langmuir* **2020**, *36*, 11183–11195.

(46) Li, X.; Zhang, J.; Gu, H. Study on the adsorption mechanism of DNA with mesoporous silica nanoparticles in aqueous solution. *Langmuir* **2012**, *28*, 2827–2834.

(47) Romanowski, G.; Lorenz, M. G.; Wackernagel, W. Adsorption of plasmid DNA to mineral surfaces and protection against DNase I. *Appl. Environ. Microbiol.* **1991**, *57*, 1057–1061.

(48) Lorenz, M. G.; Wackernagel, W. Adsorption of DNA to sand and variable degradation rates of adsorbed DNA. *Appl. Environ. Microbiol.* **1987**, *53*, 2948–2952.

(49) Raspaud, E.; Pelta, J.; De Frutos, M.; Livolant, F. Solubility and charge inversion of complexes of DNA and basic proteins. *Phys. Rev. Lett.* **2006**, *97*, 068103.

4 Discussion

The focus of this work lies on the adsorption of biomolecules to bare silica. However, studying the interactions between silica and biomolecules raises an important question: What kind of interactions are possible on the silica surface leading to adsorption? To answer this question, the surface of silica must be studied first. As displayed in Figure 1.3, the silica surface consists of two surface-active sites: siloxane links and silanol groups. Siloxanes links have a hydrophobic character and can interact with non-polar or hydrophobic molecules. On the other hand, silanol groups are responsible for the hydrophilic character of silica, enabling interactions with polar groups or molecules by hydrogen bonds. Therefore, silica adsorbs water from the environment, and in the aqueous solution, silanol groups deprotonate depending on the pH, making silica a weak cation-exchanger. The negatively charged silanol surface groups can undergo electrostatic interactions. Therefore, the final question is: Which of these interactions are dominant and responsible for the adsorption of biomolecules to silica? This work focuses on proteins and DNA, whose surface interactions at the solid-liquid interface play an important role in various research fields. DNA is a polynucleotide consisting of a nucleobase, a sugar, and a phosphate group. Proteins are large polypeptides, which form from condensation between amino acids.

In order to design a suitable binding tag for silica and learn about biomolecule interactions on the silica surface, all 20 amino acids need to be investigated for their affinity towards the surface. Until now, no comparative experimental studies have covered all 20 amino acids. Most studies focus either on individual or selected amino acids. The most comprehensive studies are the works of Basiuk and Gromovoy, where they investigated 17 and 18 amino acids, respectively, using chromatographic retention in a neutral aqueous solution.^{101,102} Unfortunately, they did not cover arginine and lysine in their studies, which are expected to show interaction with silica and thus retention. All other amino acids showed no significant retention except proline, which also showed only weak adsorption towards silica. At the beginning of this work, a HPLC method to screen the amino acid interaction with silica had to be implemented. The goal was to ensure a stable method to investigate the interaction under different conditions. Different buffers, buffer concentrations, and amino acid concentrations were investigated because detection is another problem to face when working with amino acids. Except for aromatic amino acids, analyzing amino acids by HPLC usually involves pre-column derivatization with easy to detect substances such as o-phthalaldehyde, phenyl isothiocyanate, fluorescamine, or dansyl chloride.^{226,227} The problem with these substances is that the

derivatizing reagents react with the amino groups of amino acids, which were expected to be a vital part of the adsorption process.²²⁸ UV detection between 200 and 230 nm proved viable for low buffer concentrations of 10 to 50 mM to detect amino acid concentrations between 1 and 50 mM. Buffers were used mainly for two reasons. The first one is that the buffer is an important tool in biological systems to hold the pH at a stable point. Additionally, the silica surface charge quickly changes with pH. The second reason for using a buffer is to ensure mild eluting conditions for the zonal elution principle.¹⁹⁶ Otherwise, when using only water as the mobile phase, the interactions are too strong, and only binding or no binding can be detected instead of an affinity scale. Therefore, different buffers were investigated for background noise and binding influence.

The influence on the binding and the affinity scale are discussed in Section 3.1. As shown in Figure 1 of Section 3.1, the experimental and simulative results pointed out what would be expected. Most amino acids exhibit a Henry coefficient around 0 at neutral pH, and therefore, no retention and interactions. This simple observation can be explained by the zwitterionic state of most amino acids around neutral pH, as displayed in Figure 4.1. Additionally, the hydrated silica surface exhibits none to only a few siloxane links on the surface, rendering hydrophobic and non-polar interactions obsolete.¹³ Interestingly, the negatively charged glutamic and aspartic acid eluted even earlier than the non-binding tracer uracil. This effect is probably due to electrostatic repulsion between the opposing silica surface and the negatively charged amino acids, which was not reported before in literature. Due to the repulsion, the column volume for the negatively charged amino acids is reduced and thus results in faster runtimes through the column. Chromatography can make this effect visible due to the dynamic setup. In contrast, only binding or no binding can be observed in static setups.

While all three basic amino acids, histidine, lysine, and arginine, interact with silica, there is a significant difference in binding strength. Histidine exhibits only weak interactions and is in line with the findings of Vlasova and Golovkova.⁹⁵ Adsorption on silica starts around pH 5, and thus, the pH region of cationic histidine and dissociated silanol groups barely overlap. At pH > 7, histidine is mainly in its zwitterionic state, as displayed in Figure 4.1. Lysine and arginine are both in their cationic state and thus able to bind to silica. However, arginine binds more strongly to silica than lysine, presumably due to the side group properties. The guanidinium side group of arginine has three asymmetrical nitrogen atoms allowing for interactions in three possible directions. In contrast, the amino group of lysine only allows for

one direction of the interaction. Thus, arginine can form more electrostatic interactions with the silica surface resulting in a stronger interaction.^{229,230}

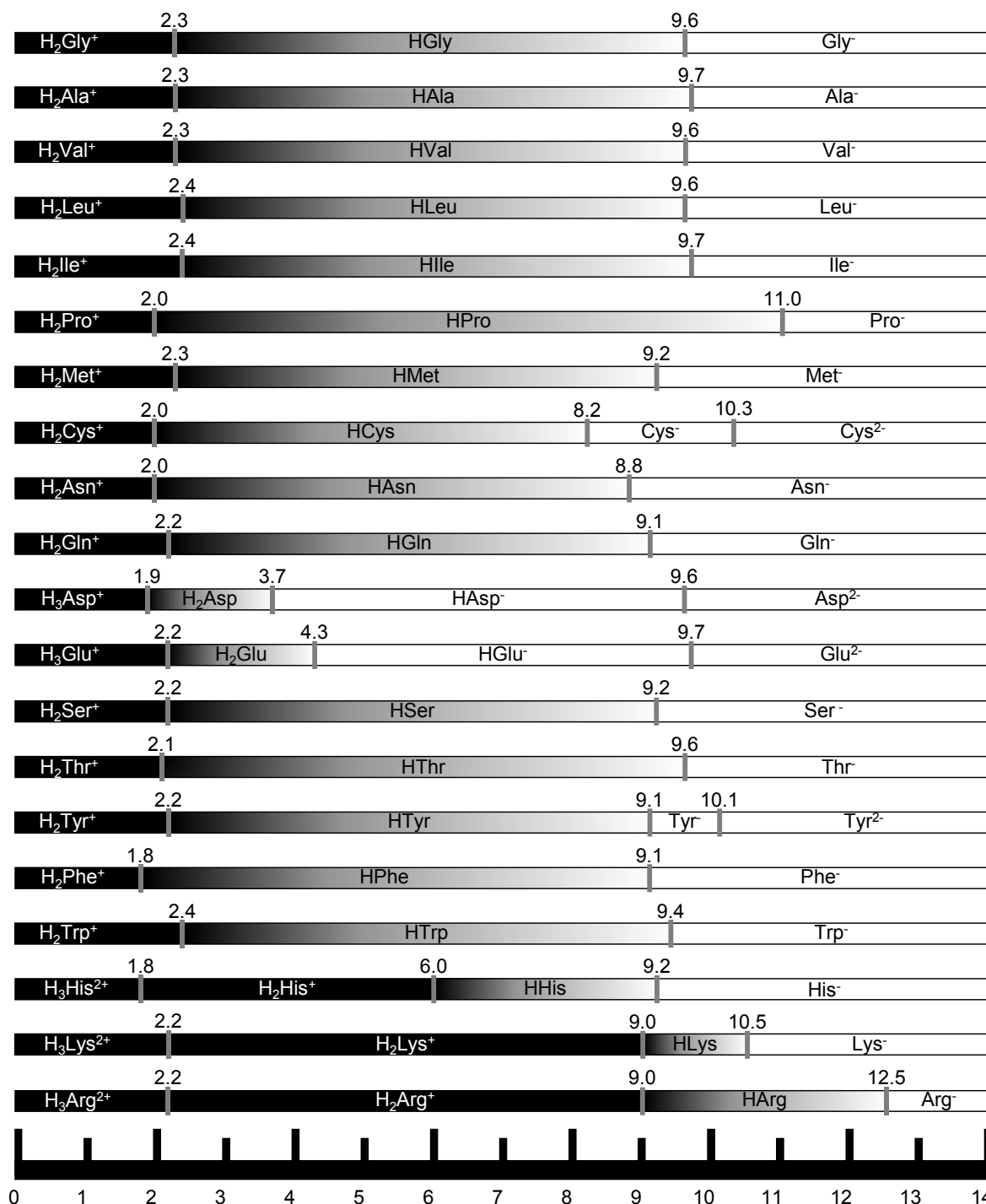


Figure 4.1: Acid–base characteristics of the 20 amino acids over the pH. Positively charged states are illustrated in black, while zwitterionic amino acids are displayed as gray (transition from black to white), and negatively charged states are illustrated in white.

Another possible explanation would be that arginine can penetrate the hydrate shell of silica more efficiently and thus make initial contact with the silica surface more easily than lysine.¹¹⁵ The results displayed in Section 3.1 point out the electrostatic interaction dominance. These

interactions are also described as ‘villains’ by RP-HPLC users, as the free silanol groups on the surface of the silica backbone influence the chromatographic separation leading to peak tailing and band broadening of basic compounds and biopolymers.²⁴

Therefore, the buffer effects due to the charge of the buffer molecules need to be considered.²³¹ In the case of TRIS, the buffer molecule can either have a positive charge or no charge with a $pK_a \sim 8.1$. MOPS buffer molecules have either a zwitterionic or negative net charge with a $pK_a \sim 7.2$. There are essentially two modes playing a critical role. As shown in Figure 2 of Section 3.1 either the positively charged TRIS moiety or the neutral MOPS can interact with silica, competing with the amino acids. Alternatively, the negatively charged MOPS interacts with the positively charged amino acid directly, which could negate the interaction with silica due to charge balancing. For the TRIS buffer, only the competing effect is critical. As a result, the interaction strength of lysine and arginine increases with increasing pH due to a higher negative charge density on the silica surface, as displayed in Figure 3 of Section 3.1. However, the situation is different for MOPS, as moderate attraction between the amino acids and the negatively charged MOPS molecules leads to cooperate adsorption (see Figure 4b of Section 3.1) of the complex filling up binding sites. Increasing pH increases the number of complexes, leading to reduced binding capacity up to the point where the negatively charged MOPS molecules outnumber the amino acids molecules. Afterward, the increasing surface charge density leads to higher capacity, resulting in the ‘wave’ form looking dependence of adsorption from the pH as displayed in Figure 5 of Section 3.1.

After identifying lysine and arginine as silica binders, the next step was to investigate the nature of the interaction. For that purpose, alanine, one of the simplest amino acids, and arginine, the strongest binder, were investigated in depth in Section 3.2. Both amino acids were capped according to Figure S2 and Figure S3 in Section 7.1.2 to achieve different charged derivatives. The work aimed to identify which functional groups of amino acids participate in the binding process. The implemented investigative setup of Section 3.1 was used again and extended by FMC measurements. The results in Section 3.2 regarding electrostatic interactions reflect the findings of Section 3.1. Zwitterionic variants of alanine and arginine do not interact with silica. The negatively charged alanine variant gets repulsed from the surface in the same matter as glutamic and aspartic acid. Positively charged alanine variants with blocked carboxyl groups can now interact with silica via the backbone amino group with the carboxyl group protruding (see histograms from MD simulation in Figure 2 of Section 3.2). In the case of arginine, the affinity scales with the net positive charge. However, there is a significant difference between

arginine, which exhibits the backbone charges and the guanidine charges, and the backbone capped arginine variant with only the guanidine group free. While both variants have a net charge of +1, the backbone capped arginine variant shows stronger interaction than the standard arginine (see Figure 3 of Section 3.2). As displayed in Figure 4 of Section 3.2, the guanidine side chain is always near the surface for all adsorbing arginine variants.⁹⁶ Concluding these findings, electrostatic interactions through positively charged groups in the amino acids dominated the adsorption, and additional positively charged groups in the side chain are needed for adsorption. The important role of the additional charge in the side chain of amino acids has also been described for other oxide materials such as MNPs.²³² However, the negatively charged carboxyl group has a crucial influence on these interactions. An essential result of the study comes from the FMC results, as they indicated that the electrostatic interaction is not accompanied by ion exchange on the surface as expected. The FMC heat exchange profiles indicated the nature of interaction being ion-pairing, which was theorized before but measured for the first time.^{44,94} Ion-pairing describes the association between a positive and negative ion through their electrostatic force of attraction.²³³ The ion-pairing occurs between the positively charged guanidine group of arginine and the negatively charged, deprotonated siloxide (SiO^-) group.

Until now, the purification processes with silica binding tags have been performed in equilibrated static systems and on some occasions with chromatographic-like elution. However, none of the processes was tested as classic chromatographic workflow. Additionally, the described peptide tags all derive from natural proteins and experimental optimization without rational design ideas. Studying the interactions of amino acids with silica is essential for designing or identifying a silica binding peptide tag. The information gained in Section 3.1 and 3.2 concluded that the tag needs to contain lysine or arginine, the amino backbone group increases the binding strength while the carboxy backbone group decreases the binding strength, and the affinity of arginine and lysine within a peptide chain is stronger than its free variant. From literature, it is also known that proline can substantially influence the affinity of a peptide.^{107,134} Furthermore, peptides only containing arginine residues exhibit weaker interaction than peptides containing spacer amino acids between positively charged residues.^{144,234} Due to the preliminary work of Schwaminger, Blank-Shim, and coworkers on biomolecule interaction with bare magnetic iron oxide nanoparticles (MNP),^{232,235–237} Berensmeier et al. developed a new binding tag for MNPs: the octapeptide (RH)4.^{238,239} The octapeptide with the sequence RHRHRHRH promised to be suitable as a silica binding tag. The peptide contains four arginine residues with histidine as a spacer in between. Furthermore, the

ability to bind to MNP and IMAC resin enables the tag to bind to multiple materials making it a multipurpose tag, which enables tandem affinity purification with one instead of two specific tags enabling the use of another tag as tandem tag.^{240,241}

After identifying the (RH)4-tag as a possible silica binder, the first goal was to demonstrate the binding of the tag in a chromatographic setup. However, the first step of a chromatographic process is selecting the stationary phase and the mobile phase buffer system. For sfGFP Davisil 643, small silica particles (35-70 μm) with medium-sized pores (15 nm), achieves high capacities and the same can be expected for eGFP.¹⁴⁹ For proteins with different sizes, other particles with smaller or bigger pores can be advantageous.²⁴² As buffer system, 50 mM TRIS pH 8.0 was chosen. 50 mM buffer salt is a common concentration for chromatographic processes involving electrostatic interactions.^{180,181} The pH value was chosen because more silanol groups will be deprotonated with higher pH, resulting in higher capacities, but not too high to start dissolving the silica or denature proteins. Furthermore, the pH must be higher than the respective IEP of the target protein. Otherwise, the protein will adsorb due to its positive surface charge.^{110,113,114,243}

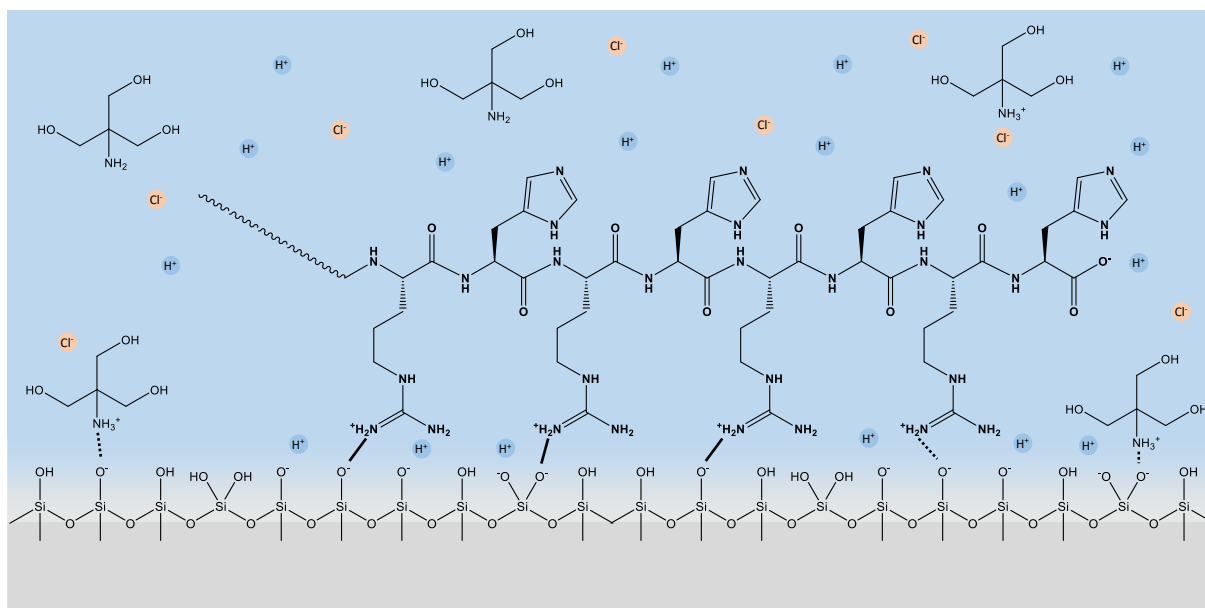


Figure 4.2: Illustration of the interaction of a C-terminal (RH)4-tag on silica in TRIS buffer. Positively charged TRIS molecules and the positively charged arginine groups interact with negatively charged siloxide groups on the surface of silica. Positively charged TRIS molecules are accompanied by chloride ions (Cl^- , orange circles), which are set free in solution upon adsorption. The wavy line symbolizes the host protein the tag is hunged on to. Full lines illustrate stronger interactions, dotted lines illustrate weaker interactions.

The adsorption of the (RH)4-tag is illustrated in Figure 4.2. The TRIS buffer is present as non-charged specie or positively charged specie, accompanied by a chloride ion. The positively charged TRIS species can interact with the negatively charged siloxide groups on the surface of silica, setting free the chloride ion upon adsorption. The (RH)4-tag can interact with the

negatively charged silica surface due to the positive charges of the arginine side groups via ion-pairing, displacing the TRIS buffer. The tag presumably rotates into a position, where all four arginine groups face towards the silica surface due to electrostatic attraction. The interaction of the last arginine in the tag facing the C-terminus presumably is a bit weaker than the interaction of the other arginine groups. This can be assumed based on the finding in Section 3.2. Therein, the mitigation of the interaction of arginine groups through the negatively charged carboxy group has been shown, which likely also has an effect in a tag system.

The model protein eGFP was used to investigate if the tag mediated the protein adsorption or unspecific binding leads to adsorption. Therefore, eGFP with and without (RH)4-tag was injected on the column, and the elution was monitored. Figure 2 of Section 3.3 shows that eGFP without the tag runs through the column without binding, while the tagged eGFP only elutes after adding lysine-containing elution buffer. The need for lysine buffer reflects the findings from Section 3.2, where ion-pairing was identified as the binding mechanism. Salts usually used in ion-exchange chromatography do not lead to elution of silica-tag bound proteins, and similar to affinity chromatography competitive reagents must be used to achieve elution.^{125,144,149} Lysine and arginine were identified as suitable reagents; they are non-toxic and can improve the stability of eluted proteins in solution.^{244–246} The purities and recovery achieved in Section 3.3 are comparable or higher to other silica-tag systems such as SB7 and Car9.^{125,144} The study also revealed that most unspecific binding of lysate proteins could be displaced by the (RH)4 fusion proteins. The reverse effect could be seen in the upscaling attempt where unspecific binding of lysate proteins decreased the purity of GFP-(RH)4 in the eluted fractions to around 80% due to most binding places on silica being free.

One of the most important performance parameters for chromatographic materials regarding productivity and usability is the dynamic binding capacity (DBC), calculated via Equation 1 of Section 3.3. The DBC describes the maximum load of target protein measured under realistic experimental conditions.^{180,181} The DBC was determined at 3 mg mL^{-1} , which is comparable to other fusion protein systems and corresponds to a load of around 10 mg g^{-1} .⁵ As a comparison, the equilibrium binding capacity (EBC) was determined at 450 mg g^{-1} . The DBC is connected to the EBC, but is influenced by the flow rate and dispersive factors such as mass transfer and thus usually lower.^{180,247} A higher residence times can result in a higher DBC value, but also leads to a prolonged process.¹⁸⁰ The DBC is one of the cost-determining factors in preparative chromatography. For low DBC, more material is needed for the purification step, and the material is usually the expensive part of the chromatographic setup. Higher DBCs can be

achieved for example by increasing the residence time through lowering the flow rate during the loading phase. However, this change must be viewed in the context of productivity, as longer runtimes can also lead to decreased productivity.²⁴⁸ Another method for increasing the DBC could be the screening of different buffer and silica systems. As shown in Section 3.1 the buffer can have a huge influence on the interaction and thus also on the capacity. The role of the silica particle and pore size was already discussed by other authors and can be a decisive factor regarding capacity.¹⁴⁹ And as already mentioned in Section 1.1 the manufacturing process can have an influence on the surface silanol groups. So, it would also make sense to screen different providers of silica particles. The selection of the right material gets crucial when working with other proteins that are significantly different in size to GFP. While increasing the capacity is one possibility to improve the productivity, process intensification is another. The silica columns could be used in a continuous mode such as simulated moving bed, which would also deal with the issue of overloading to achieve high purities. Lastly, silica as inexpensive material could be used as single-use technology, eliminating the need for time consuming cleaning protocols and validations and hence increase productivity by decreasing the total process time.

Silica affinity purification promises a low-cost, easy-to-use setup for purification of (RH)4-tagged proteins in one step. A 5 mL silica column requires 1.5 g Davisil 643, which costs roughly 0.60 €. In comparison, a ready-to-use IMAC column with 5 mL costs around 120 € (Macherey-Nagel Bioanalysis™ Protino™ Ni-NTA 5 mL FPLC™ Columns), which is 200x the costs of the silica material. However, in IMAC DBCs of up to 60 mg ml⁻¹ can be achieved at similar flow rate (1 ml min⁻¹) and residence time (2 min) compared to the silica approach in Section 3.3.²⁴⁹ This DBC is equivalent to 20x of the amount on the silica column, which still makes the silica column 10x more efficient than the IMAC regarding pure material costs. This calculation implies the IMAC column must be reused ten times at full capacity to match the material costs of the silica column, which can be replaced after each run. However, there are also other costs, which need to be considered for a thorough calculation. The most important parameter is productivity, the produced amount protein per time interval. Additionally, the individual process costs need to be determined properly because different buffers, especially for the elution, are used. As an orientation point, the elution reagent for silica is lysine, which costs around 85 € per 100 g (Carl Roth, 39665-12-8), and for IMAC, it is imidazole with costs around 57 € per 100 g (Sigma, 288-32-4). For a proper calculation and comparison of the process costs, some critical parameters are lacking, such as reusability count of the silica column and optimized DBC of the silica column. Furthermore, the comparable DBC on IMAC

for the same protein and such costs as stripping and reloading the IMAC material with metal ions must be determined. The (RH)₄-tag purification with bare silica is a promising technique due to the easy process parameters leading to high purities and recoveries, which led to the filing of a patent.²³⁹

After successfully implementing the simulation model in Section 3.1 and 3.2, Section 3.4 discusses the cooperative adsorption Langmuir model for DNA adsorption onto silica in the presence of different salts and amino acids. For DNA purification, solid-phase extraction is generally used, where high concentrations of salts mediate the binding of DNA to silica.¹⁶²⁻¹⁶⁵ In a recent study Vandeventer et al. demonstrated DNA binding to silica in amino acid buffers.¹⁷⁰ In the presence of positively charged amino acids DNA bound to silica. Also, in the presence of polar neutral and negatively charged amino acids, DNA was found on the surface of silica. However, as discussed in Section 3.4 and shown in Figure 4 of Section 3.4, DNA seems not to bind in the presence of negatively charged amino acids, and only around 30% of DNA can be found on the silica surface in the presence of glycine compared to arginine or potassium. Comparing the results with the study of Vandeventer the results found therein can be explained as follows. In the Vandeventer study each sample contained 400 mM of potassium ions, which already enabled DNA adsorption. In the presence of neutral polar amino acids, the interaction thus is mainly mediated by the potassium ions. In the case of negatively charged amino acids, the DNA and amino acid both compete to interact with the potassium ions on the silica surface, thus decreasing the amount of DNA able to bind to the silica surface. In the case of positively charged amino acids, the concentration of positive ions in solution is increased; thus, more DNA binds to silica. This effect is also shown in Figure 7 of Section 3.4. DNA only binds to the surface of silica in the presence of positively charged binding agents via a cation-bridge and depends on the concentration and valence of the cations.¹⁶²⁻¹⁶⁵ As displayed in Figure 5 of Section 3.4, with higher concentration and higher valency more DNA binds to the silica surface until a certain concentration (> 1.5 M) is reached, which caps the amount of bound DNA independent from the valency.^{165,169} Binding of DNA to silica in the presence of glycine presumably can be attributed to the charge state of the amino acid. As can be seen in Figure 4.1, at pH 5 the glycine (IEP 5.97) equilibrium is shifted towards the positive state, enabling glycine to act as cation-bridge. Due to the interaction mainly being driven by cations, methods using a silica surface functionalized with positively charged groups emerged for DNA purification.^{168,250} Taken the results from Section 3.1 into account, hydrogen bonding and hydrophobic interactions do not play a significant role for adsorption of amino acids at the silica surface in aqueous buffers. Therefore, adsorption of DNA to silica in aqueous solutions

presumably is also dominated by electrostatic interactions such as cation-bridges and less by hydrogen bonding or hydrophobic interactions. Hydrophobic interactions are also unlikely due to silica not exhibiting many siloxane links on the surface when being fully hydrated.^{13,18}

5 Conclusion and Outlook

Silica gel is the most common material used in liquid chromatography. The main advantages of silica regarding chromatographic processes are the high solvolytic and mechanical stability, the porous structure, and high surface area. In addition, the silica surface is easily modified via silanization, introducing different chemical groups to generate surfaces with desirable physicochemical properties. Bare silica and its derivatives, predominantly hydrophobic or hydrophilic functionalized, are usually used as an adsorbent in normal-phase (NPC), reversed-phase (RPC), and hydrophilic interaction liquid chromatography (HILIC), a variant of NPC. The main weakness of silica is the limited pH stability due to dissolution in alkaline solutions ($\text{pH} > 9$) and the silanol groups on the surface, which are considered ‘villains’ in RP-HPLC, especially for biomolecules and basic analytes due to interactions between positively charged groups with the negatively charged silica surface leading to peak broadening and thus inefficient separation. Understanding the interactions between the inorganic silica surface and biomolecules thus will help to turn enemies into friends.

Using different experimental and simulative approaches, we identified the amino acids interacting with the silica surface in neutral aqueous environments. For all 20 amino acids, the affinity for silica was measured and combined with MD simulation. Adsorption is dominated by the functional side group of the amino acids, and only additional positive charged groups in lysine and arginine lead to strong interactions with silica, with the latter exhibiting the stronger interaction. Zwitterionic and negatively charged amino acids cannot interact with silica mainly due to charge balancing between the backbone amino and carboxyl group or charge repulsion, respectively. The nature of the interaction is electrostatic interactions in the form of ion-pairing between positively charged amino and guanidine groups and negatively charged siloxide groups on the silica surface. Due to the electrostatic nature, the interaction is strongly influenced by the solution’s buffer and salt ions. Furthermore, experiments with capped amino acids revealed the mitigating effect of the backbone carboxyl group on the interaction strength. DNA adsorption on silica through positively charged binding agents such as salt ions and amino acids could be shown through the implemented cooperative Langmuir model.

Based on the amino acid interactions, the octapeptide (RH)₄ was identified as a suitable binding tag for silica, offering a low-cost and easy to handle purification process for recombinant proteins with high purities and recoveries. However, for a thorough cost breakdown some important parameters must still be determined after optimizing the process. Turning this old

enemy into a friend opens new perspectives in biotechnological downstream processing with the potential to replace some of the old methods still in use today.

Despite the remarkable advances, there are still unanswered questions regarding the biomolecule-silica interaction. In Section 3.1, the two buffers, TRIS and MOPS, showed different effects on the interaction of lysine and arginine to silica. It would be interesting in future works to investigate the effect of other buffers used in biotechnological systems such as the Good's buffers or phosphate. The bicarbonate buffer system as the main buffer component in the human blood would be worth investigating in a more medical context. It would also be interesting to see if these effects occur on other inorganic surfaces such as MNPs or an exclusive silica effect. In that sense, the flow microcalorimetry (FMC) studies of Section 3.2 could also be applied onto other inorganic surfaces or a wider variety of biomolecules such as proteins and nucleic acids to better understand biomolecule interactions with different surfaces. The final goal would be to generate various solid binding peptide (SBPs) for different surfaces.

An initial step towards a silica SBP was made with our proof-of-concept in Section 3.3. The goal here for the future would be to transfer this process to other proteins, especially enzymes and antibodies. When transferring the process to other proteins, the silica particles might need to be changed depending on the size of the respective proteins. Therefore, silicas with different particle and pore sizes need to be investigated regarding protein size to make the process as efficient as possible. Despite the already working process, there is still room for optimization. An investigation of different buffer systems on capacity and process control could further improve the process understanding. One of the most important tasks for the process is the increase in capacity, as capacity is strongly linked to productivity and thus the total cost of the process. Besides screening different buffer systems, there are also other ways to increase capacity such as the residence time of the protein on the column. Longer residence times can increase capacities but are often accompanied by lower productivity. Different flow rates must be tested with the respective capacities to ultimately find the best parameters for the highest productivity. With these optimized parameters, the cost comparison with other chromatographic methods is more realistic. However, for a realistic calculation, also the reusability of the silica column for multiple separations is a critical factor to be determined. As already discussed in Section 3.3, proteins bound to silica cannot be eluted with salt, enabling the combination with ion-exchange chromatography (IEX), especially anion exchange chromatography (AEX), for upscaling the process. AEX would complement the silica process because the same buffers can be used for both processes while different separation mechanisms

occur. In the silica column, the positively charged peptide tag is responsible for adsorption. In AEX, the negative charge of the protein will lead to adsorption. There are two ways to run these two columns. The eluate of the silica column with low salt concentration is loaded on the AEX and eluted from there with salt. Alternatively, the other way around, the salty eluate from the AEX is loaded on the silica column, where the salt does not lead to elution, followed by lysine elution. The silica column can thus be used as a capture or polishing step. Another possibility with this tag could be the design of a mixed mode stationary phase based on silica with functionalized groups enabling anion-exchange. With this combination, proteins would adsorb to silica through the (RH)₄-tag, and at the same time, the main body of the protein, which bears a negative net charge, adsorbs at the charged groups. Due to the high salt tolerance of the silica-tag system, a combination with hydrophobic interaction chromatography (HIC), which needs high salt concentration to work, could also be a promising attempt.

In Section 3.4, we shed light on DNA adsorption on silica in the presence of different salt and amino acids. Transferring these results onto RNA and plasmids would further help optimize the downstream process of nucleic acids, an essential resource in biotechnology and a promising tool in medicine in the near future. Furthermore, it would be interesting to see other positively charged molecules, as the commonly used salts, in DNA adsorption to silica. As shown in Section 3.4 arginine is a good alternative, though limited by solubility. An interesting comparison would be between magnesium and the capped, double positively charged arginine from Section 3.2. The question here would be if only valency plays a role, or also other parameters such as the size or the location of the charges plays a role, due to arginine having its charges on two different groups while magnesium is a single ion. In this context peptides would be interesting as binding agent. While being expensive to synthesize at the moment, with ongoing research peptide synthesis will get cheaper in the future. Regarding the binding mechanism it would be interesting and promising to apply FMC on these interactions. The FMC profiles could potentially give a deeper insight into the nature of the interaction between silica and DNA under different conditions. Consequently, the knowledge regarding the nature of interaction could be further improved and in the next step optimized and applied for techniques such as gene or drug delivery. Therefore, different buffer systems should be evaluated because interactions at the aqueous silica interface show interesting behaviors towards different buffer systems, as shown in Section 3.1.

6 References

- (1) La Rocha C. de, Conley D. J. *Silica Stories*; Springer International Publishing: Cham, 2017.
- (2) Lambert, J.-F. Adsorption and polymerization of amino acids on mineral surfaces: a review. *Orig. Life Evol. Biosph.* **2008**, *38*, 211–242.
- (3) Flörke, O. W., Graetsch, H. A., Brunk, F., Benda, L., Paschen, S., Bergna, H. E., Roberts, W. O., Welsh, W. A., Libanati, C., Ettlinger, M., Kerner, D., Maier, M., Meon, W., Schmoll, R., Gies, H., Schiffmann, D. Silica. In *Ullmann's Encyclopedia of Industrial Chemistry*; Wiley-VCH Verlag GmbH & Co. KGaA: Weinheim, Germany, 2000; Vols. 236, p. 22.
- (4) Rimola, A., Costa, D., Sodupe, M., Lambert, J.-F., Ugliengo, P. Silica surface features and their role in the adsorption of biomolecules: computational modeling and experiments. *Chem. Rev* **2013**, *113*, 4216–4313.
- (5) Lichty, J. J., Malecki, J. L., Agnew, H. D., Michelson-Horowitz, D. J., Tan, S. Comparison of affinity tags for protein purification. *Protein Expression Purif.* **2005**, *41*, 98–105.
- (6) Nawaz M., Kundu S. N., Sattar F. *Earth Crust*; InTech, 2019.
- (7) McDonough, W. F., Sun, S.-s. The composition of the Earth. *Chem. Geol.* **1995**, *120*, 223–253.
- (8) Clayton D. D. *Principles of stellar evolution and nucleosynthesis*; Univ. of Chicago Press: Chicago, 2007.
- (9) Zachariasen, W. H. The atomic arrangement in glass. *J. Am. Chem. Soc.* **1932**, *54*, 3841–3851.
- (10) Jin, R.-H. Understanding silica from the viewpoint of asymmetry. *Chemistry* **2019**, *25*, 6270–6283.
- (11) Bergna, H. E. Colloid Chemistry of Silica. In *The Colloid Chemistry of Silica*; Bergna, H. E., Ed.; American Chemical Society: Washington DC, 1994; Vols. 234, pp. 1–47.
- (12) Legrand A. P. *The Surface Properties of Silicas*, 1st ed.; Wiley, 1998.
- (13) Zhuravlev, L. T. The surface chemistry of amorphous silica. Zhuravlev model. *Colloids Surf., A* **2000**, *173*, 1–38.
- (14) Ikeda, T. Bacterial biosilicification: a new insight into the global silicon cycle. *Biosci. Biotechnol. Biochem.* **2021**, *85*, 1324–1331.
- (15) Curley, R., Holmes, J. D., Flynn, E. J. Can sustainable, monodisperse, spherical silica be produced from biomolecules? A review. *Appl Nanosci* **2021**, *11*, 1777–1804.
- (16) Kadapure, S. A. The biotechnology approach for sustainable concrete material – a review. *Mag. Concr. Res.* **2021**, *23*, 1–9.
- (17) Puppe, D. Review on protozoic silica and its role in silicon cycling. *Geoderma* **2020**, *365*, 114224.
- (18) Emami, F. S., Puddu, V., Berry, R. J., Varshney, V., Patwardhan, S. V., Perry, C. C., Heinz, H. Force field and a surface model database for silica to simulate interfacial properties in atomic resolution. *Chem. Mater.* **2014**, *26*, 2647–2658.
- (19) Taylor, E. W. Correlation of the Mohs's scale of hardness with the Vickers's hardness numbers. *Mineral. mag. j. Mineral. Soc.* **1949**, *28*, 718–721.
- (20) Hyde, E. D. E. R., Seyfaee, A., Neville, F., Moreno-Atanasio, R. Colloidal silica particle synthesis and future industrial manufacturing pathways: A review. *Ind. Eng. Chem. Res.* **2016**, *55*, 8891–8913.
- (21) Zhang, H., Guo, S., Wu, J., Wu, D., Wei, K., Ma, W. Effect of quartz crystal structure transformations on the removal of iron impurities. *Hydrometallurgy* **2021**, *204*, 105715.
- (22) Maher, S., Kumeria, T., Aw, M. S., Losic, D. Diatom silica for biomedical applications: Recent progress and advances. *Adv. Healthc. Mater.* **2018**, *7*, e1800552.

- (23) Nassif, N., Livage, J. From diatoms to silica-based biohybrids. *Chem. Soc. Rev.* **2011**, *40*, 849–859.
- (24) Buszewska-Forajta, M., Markuszewski, M. J., Kaliszan, R. Free silanols and ionic liquids as their suppressors in liquid chromatography. *J. Chromatogr. A* **2018**, *1559*, 17–43.
- (25) Boldridge, D. Morphological characterization of fumed silica aggregates. *Aerosol Sci Technol* **2010**, *44*, 182–186.
- (26) Belton, D. J., Deschaume, O., Perry, C. C. An overview of the fundamentals of the chemistry of silica with relevance to biosilicification and technological advances. *The FEBS journal* **2012**, *279*, 1710–1720.
- (27) Guerrero-Martínez, A., Pérez-Juste, J., Liz-Marzán, L. M. Recent progress on silica coating of nanoparticles and related nanomaterials. *Adv. Mater.* **2010**, *22*, 1182–1195.
- (28) Chang, C.-L., Fogler, H. S. Kinetics of silica particle formation in nonionic W/O microemulsions from TEOS. *AIChE J.* **1996**, *42*, 3153–3163.
- (29) Finnie, K. S., Bartlett, J. R., Barbé, C. J. A., Kong, L. Formation of silica nanoparticles in microemulsions. *Langmuir* **2007**, *23*, 3017–3024.
- (30) Chung, S.-H., Lee, D.-W., Kim, M.-S., Lee, K.-Y. The synthesis of silica and silica-ceria, core-shell nanoparticles in a water-in-oil (W/O) microemulsion composed of heptane and water with the binary surfactants AOT and NP-5. *J. Colloid Interface Sci.* **2011**, *355*, 70–75.
- (31) Grasset, F., Marchand, R., Marie, A.-M., Fauchadour, D., Fajardie, F. Synthesis of CeO₂@SiO₂ core-shell nanoparticles by water-in-oil microemulsion. Preparation of functional thin film. *J. Colloid Interface Sci.* **2006**, *299*, 726–732.
- (32) Zhang, J., Liu, Z., Han, B., Li, Z., Yang, G., Li, J., Chen, J. Preparation of silica and TiO₂-SiO₂ core-shell nanoparticles in water-in-oil microemulsion using compressed CO₂ as reactant and antisolvent. *J. Supercrit Fluids* **2006**, *36*, 194–201.
- (33) Drummond, C., McCann, R., Patwardhan, S. V. A feasibility study of the biologically inspired green manufacturing of precipitated silica. *Chem. Eng. J.* **2014**, *244*, 483–492.
- (34) Stöber, W., Fink, A., Bohn, E. Controlled growth of monodisperse silica spheres in the micron size range. *J. Colloid Interface Sci.* **1968**, *26*, 62–69.
- (35) Bourebrab, M. A., Oben, D. T., Durand, G. G., Taylor, P. G., Bruce, J. I., Bassindale, A. R., Taylor, A. Influence of the initial chemical conditions on the rational design of silica particles. *J. Solgel Sci Technol* **2018**, *88*, 430–441.
- (36) Ghimire, P. P., Jaroniec, M. Renaissance of Stöber method for synthesis of colloidal particles: New developments and opportunities. *J. Colloid Interface Sci.* **2021**, *584*, 838–865.
- (37) Bazuła, P. A., Arnal, P. M., Galeano, C., Zibrowius, B., Schmidt, W., Schüth, F. Highly microporous monodisperse silica spheres synthesized by the Stöber process. *Microporous Mesoporous Mater.* **2014**, *200*, 317–325.
- (38) Heiligt, F. J., Kränzlin, N., Süess, M. J., Niederberger, M. Anatase-silica composite aerogels: a nanoparticle-based approach. *J. Sol-Gel Sci Technol* **2014**, *70*, 300–306.
- (39) Kröger, N., Deutzmann, R., Sumper, M. Polycationic peptides from diatom biosilica that direct silica nanosphere formation. *Science* **1999**, *286*, 1129–1132.
- (40) Lechner, C. C., Becker, C. F. W. Silaffins in silica biomineralization and biomimetic silica precipitation. *Marine drugs* **2015**, *13*, 5297–5333.
- (41) Lutz, H., Jaeger, V., Berger, R., Bonn, M., Pfaendtner, J., Weidner, T. Biomimetic growth of ultrathin silica sheets using artificial amphiphilic peptides. *Adv. Mater. Interfaces* **2015**, *2*, 1500282.
- (42) Holmström, S. C., King, P. J. S., Ryadnov, M. G., Butler, M. F., Mann, S., Woolfson, D. N. Templating silica nanostructures on rationally designed self-assembled peptide fibers. *Langmuir* **2008**, *24*, 11778–11783.

- (43) Yu, J., Wang, Q., Zhang, X. Effects of external force fields on peptide self-assembly and biomimetic silica synthesis. *Appl. Surf. Sci.* **2014**, *311*, 799–807.
- (44) Patwardhan, S. V., Emami, F. S., Berry, R. J., Jones, S. E., Naik, R. R., Deschaume, O., Heinz, H., Perry, C. C. Chemistry of aqueous silica nanoparticle surfaces and the mechanism of selective peptide adsorption. *J. Am. Chem. Soc.* **2012**, *134*, 6244–6256.
- (45) Ostroverkhov, V., Waychunas, G. A., Shen, Y. R. New information on water interfacial structure revealed by phase-sensitive surface spectroscopy. *Phys. Rev. Lett.* **2005**, *94*, 46102.
- (46) Abendroth, R.P. Behavior of a pyrogenic silica in simple electrolytes. *J. Colloid Interface Sci.* **1970**, *34*, 591–596.
- (47) Bolt, G. H. Determination of the charge density of silica sols. *J. Phys. Chem.* **1957**, *61*, 1166–1169.
- (48) House, W. A., Orr, D. R. Investigation of the pH dependence of the kinetics of quartz dissolution at 25 °C. *J. Chem. Soc., Faraday Trans.* **1992**, *88*, 233–241.
- (49) Milonjić, S. K. Determination of surface ionization and complexation constants at colloidal silica/electrolyte interface. *Colloids Surf* **1987**, *23*, 301–312.
- (50) Sonnefeld. Determination of surface charge density constants for spherical silica particles using a linear transformation. *J. Colloid Interface Sci.* **1996**, *183*, 597–599.
- (51) Yates, D. E., Healy, T. W. The structure of the silica/electrolyte interface. *J. Colloid Interface Sci.* **1976**, *55*, 9–19.
- (52) Zerrouk, R., Foissy, A., Mercier, R., Chevallier, Y., Morawski, J.-C. Study of Ca²⁺-induced silica coagulation by small angle scattering. *J. Colloid Interface Sci.* **1990**, *139*, 20–29.
- (53) Pytlik, N., Brunner, E. Diatoms as potential “green” nanocomposite and nanoparticle synthesizers: challenges, prospects, and future materials applications. *MRS Commun* **2018**, *8*, 322–331.
- (54) Niculescu, V.-C. Mesoporous silica nanoparticles for bio-applications. *Front. Mater.* **2020**, *7*, 36.
- (55) Trewyn, B. G., Nieweg, J. A., Zhao, Y., Lin, V. S.-Y. Biocompatible mesoporous silica nanoparticles with different morphologies for animal cell membrane penetration. *Chem. Eng. J.* **2008**, *137*, 23–29.
- (56) Liberman, A., Mendez, N., Trogler, W. C., Kummel, A. C. Synthesis and surface functionalization of silica nanoparticles for nanomedicine. *Surf. Sci. Rep.* **2014**, *69*, 132–158.
- (57) Pajonk, G. M. Some applications of silica aerogels. *Colloid Polym. Sci.* **2003**, *281*, 637–651.
- (58) Akoum, R. A., Vaultot, C., Schwartz, D., Hirn, M.-P., Haidar, B. How silanization of silica particles affects the adsorption of PDMS chains on its surface. *J. Polym. Sci. B Polym. Phys.* **2010**, *48*, 2371–2378.
- (59) Kulkarni, S. A., Ogale, S. B., Vijayamohan, K. P. Tuning the hydrophobic properties of silica particles by surface silanization using mixed self-assembled monolayers. *J. Colloid Interface Sci.* **2008**, *318*, 372–379.
- (60) Borges, E. M. Silica, hybrid silica, hydride silica and non-silica stationary phases for liquid chromatography. *J. Chromatogr. Sci.* **2015**, *53*, 580–597.
- (61) Skoczylas, M., Krzemińska, K., Bocian, S., Buszewski, B. Silica Gel and its Derivatization for Liquid Chromatography. In *Encyclopedia of Analytical Chemistry*; Meyers, R. A., Ed.; John Wiley & Sons, Ltd: Chichester, UK, 2017; online, pp. 1–39.
- (62) Kirkland, J. J., Truszkowski, F. A., Dilks, C. H., Engel, G. S. Superficially porous silica microspheres for fast high-performance liquid chromatography of macromolecules. *J. Chromatogr. A* **2000**, *890*, 3–13.

- (63) Guillarme, D., Ruta, J., Rudaz, S., Veuthey, J.-L. New trends in fast and high-resolution liquid chromatography: a critical comparison of existing approaches. *Anal. Bioanal. Chem.* **2010**, *397*, 1069–1082.
- (64) Pesek, J. J., Matyska, M. T. Silica hydride surfaces: Versatile separation media for chromatographic and electrophoretic analyses. *J. Liq. Chromatogr. Relat. Technol.* **2006**, *29*, 1105–1124.
- (65) Pesek, J. J., Matyska, M. T., Hearn, M. T. W., Boysen, R. Temperature effects on solute retention for hydride-based stationary phases. *J. Sep. Sci.* **2007**, *30*, 1150–1157.
- (66) Pesek, J. J., Matyska, M. T., Larrabee, S. HPLC retention behavior on hydride-based stationary phases. *J. Sep. Sci.* **2007**, *30*, 637–647.
- (67) Yang, Y., Boysen, R. I., Kulsing, C., Matyska, M. T., Pesek, J. J., Hearn, M. T. W. Analysis of polar peptides using a silica hydride column and high aqueous content mobile phases. *J. Sep. Sci.* **2013**, *36*, 3019–3025.
- (68) Piccin, J. S., Cadaval, T. R. S.'A., Pinto, L. A. A. de, Dotto, G. L. Adsorption isotherms in liquid phase: experimental, modeling, and interpretations. In *Adsorption processes for water treatment and purification*; Bonilla-Petriciolet, A., Mendoza-Castillo, D. I., Reynel-Ávila, H. E., Eds.; Springer International Publishing: Cham, 2017; Vols. 69, pp. 19–51.
- (69) Al-Ghouti, M. A., Da'ana, D. A. Guidelines for the use and interpretation of adsorption isotherm models: A review. *J. Hazard. Mater.* **2020**, *393*, 122383.
- (70) Langmuir, I. The adsorption of gases on plane surfaces of glass, mica and platinum. *J. Am. Chem. Soc.* **1918**, *40*, 1361–1403.
- (71) Foo, K. Y., Hameed, B. H. Insights into the modeling of adsorption isotherm systems. *Chem. Eng. J.* **2010**, *156*, 2–10.
- (72) Swenson, H., Stadie, N. P. Langmuir's theory of adsorption: A centennial review. *Langmuir* **2019**, *35*, 5409–5426.
- (73) Brunauer, S., Emmett, P. H., Teller, E. Adsorption of gases in multimolecular layers. *J. Am. Chem. Soc.* **1938**, *60*, 309–319.
- (74) Wang, J., Guo, X. Adsorption isotherm models: Classification, physical meaning, application and solving method. *Chemosphere* **2020**, *258*, 127279.
- (75) Di Wu, Piszczek, G. Measuring the affinity of protein-protein interactions on a single-molecule level by mass photometry. *Anal. Biochem.* **2020**, *592*, 113575.
- (76) Nelson D. L., Cox M. M. *Lehninger principles of biochemistry*, 6th ed.; W.H. Freeman and Company: New York, 2013.
- (77) Costa, D., Savio, L., Pradier, C.-M. Adsorption of amino acids and peptides on metal and oxide surfaces in water environment: A synthetic and prospective review. *J. Phys. Chem. B* **2016**, *120*, 7039–7052.
- (78) Fenoglio, I., Fubini, B., Ghibaudi, E. M., Turci, F. Multiple aspects of the interaction of biomacromolecules with inorganic surfaces. *Adv. Drug Delivery Rev.* **2011**, *63*, 1186–1209.
- (79) Zaia, D. A. M. A review of adsorption of amino acids on minerals: was it important for origin of life? *Amino acids* **2004**, *27*, 113–118.
- (80) Stutz, H. Protein attachment onto silica surfaces--a survey of molecular fundamentals, resulting effects and novel preventive strategies in CE. *Electrophoresis* **2009**, *30*, 2032–2061.
- (81) Lopes, I., Piao, L., Stievano, L., Lambert, J.-F. Adsorption of amino acids on oxide supports: A solid-state NMR study of glycine adsorption on silica and alumina. *J. Phys. Chem. C* **2009**, *113*, 18163–18172.
- (82) Meng, M., Stievano, L., Lambert, J.-F. Adsorption and thermal condensation mechanisms of amino acids on oxide supports. 1. Glycine on silica. *Langmuir* **2004**, *20*, 914–923.

- (83) Rimola, A., Sodupe, M., Tosoni, S., Civalleri, B., Ugliengo, P. Interaction of glycine with isolated hydroxyl groups at the silica surface: first principles B3LYP periodic simulation. *Langmuir* **2006**, *22*, 6593–6604.
- (84) Rimola, A., Sodupe, M., Ugliengo, P. Affinity scale for the interaction of amino acids with silica surfaces. *J. Phys. Chem. C* **2009**, *113*, 5741–5750.
- (85) Amitay-Rosen, T., Kababya, S., Vega, S. A dynamic magic angle spinning NMR study of the local mobility of alanine in an aqueous environment at the inner surface of mesoporous materials. *J. Phys. Chem. B* **2009**, *113*, 6267–6282.
- (86) Ben Shir, I., Kababya, S., Amitay-Rosen, T., Balazs, Y. S., Schmidt, A. Molecular level characterization of the inorganic-bioorganic interface by solid state NMR: alanine on a silica surface, a case study. *J. Phys. Chem. B* **2010**, *114*, 5989–5996.
- (87) Ben Shir, I., Kababya, S., Schmidt, A. Binding specificity of amino acids to amorphous silica surfaces: Solid-state NMR of glycine on SBA-15. *J. Phys. Chem. C* **2012**, *116*, 9691–9702.
- (88) Ben Shir, I., Kababya, S., Schmidt, A. Molecular details of amorphous silica surfaces determine binding specificity to small amino acids. *J. Phys. Chem. C* **2014**, *118*, 7901–7909.
- (89) Nonella, M., Seeger, S. Investigating alanine-silica interaction by means of first-principles molecular-dynamics simulations. *ChemPhysChem* **2008**, *9*, 414–421.
- (90) Guo, C., Holland, G. P. Alanine adsorption and thermal condensation at the interface of fumed silica nanoparticles: A solid-state NMR investigation. *J. Phys. Chem. C* **2015**, *119*, 25663–25672.
- (91) Bouchoucha, M., Jaber, M., Onfroy, T., Lambert, J.-F., Xue, B. Glutamic acid adsorption and transformations on silica. *J. Phys. Chem. C* **2011**, *115*, 21813–21825.
- (92) O'Connor, A. J., Hokura, A., Kisler, J. M., Shimazu, S., Stevens, G. W., Komatsu, Y. Amino acid adsorption onto mesoporous silica molecular sieves. *Sep. Purif. Technol.* **2006**, *48*, 197–201.
- (93) Razvag, Y., Gutkin, V., Reches, M. Probing the interaction of individual amino acids with inorganic surfaces using atomic force spectroscopy. *Langmuir* **2013**, *29*, 10102–10109.
- (94) Stievano, L., Yu Piao, L., Lopes, I., Meng, M., Costa, D., Lambert, J.-F. Glycine and lysine adsorption and reactivity on the surface of amorphous silica. *Eur. J. Mineral.* **2007**, *19*, 321–331.
- (95) Vlasova, N. N., Golovkova, L. P. The adsorption of amino acids on the surface of highly dispersed silica. *Colloid J.* **2004**, *66*, 657–662.
- (96) Kitadai, N., Yokoyama, T., Nakashima, S. ATR-IR spectroscopic study of L-lysine adsorption on amorphous silica. *J. Colloid Interface Sci.* **2009**, *329*, 31–37.
- (97) Churchill, H., Teng, H., Hazen, R. M. Correlation of pH-dependent surface interaction forces to amino acid adsorption: Implications for the origin of life. *Am. Mineral.* **2004**, *89*, 1048–1055.
- (98) Gao, Q., Xu, W., Xu, Y., Wu, D., Sun, Y., Deng, F., Shen, W. Amino acid adsorption on mesoporous materials: influence of types of amino acids, modification of mesoporous materials, and solution conditions. *J. Phys. Chem. B* **2008**, *112*, 2261–2267.
- (99) Rimola, A., Civalleri, B., Ugliengo, P. Physisorption of aromatic organic contaminants at the surface of hydrophobic/hydrophilic silica geosorbents: a B3LYP-D modeling study. *Phys. Chem. Chem. Phys.* **2010**, *12*, 6357–6366.
- (100) Goscianska, J., Olejnik, A., Pietrzak, R. Adsorption of l-phenylalanine onto mesoporous silica. *Mater. Chem. Phys.* **2013**, *142*, 586–593.
- (101) Basiuk, V. A., Gromovoy, T. Y. Free energies of amino acid adsorption on silica in neutral aqueous medium as estimated from high-performance liquid-chromatographic retention data. *Amino acids* **1994**, *7*, 305–309.

- (102) Basiuk, V. A., Gromovoy, T. Y. Comparative study of amino acid adsorption on bare and octadecyl silica from water using high-performance liquid chromatography. *Colloids Surf., A* **1996**, *118*, 127–140.
- (103) Basiuk, V. A., Gromovoy, T. Y. Free energies of adsorption of amino acids, short linear peptides and 2,5-piperazinediones on silica from water as estimated from high-performance liquid-chromatographic retention data. *Adsorption* **1996**, *2*, 145–152.
- (104) Holinga, G. J., York, R. L., Onorato, R. M., Thompson, C. M., Webb, N. E., Yoon, A. P., Somorjai, G. A. An SFG study of interfacial amino acids at the hydrophilic SiO₂ and hydrophobic deuterated polystyrene surfaces. *J. Am. Chem. Soc.* **2011**, *133*, 6243–6253.
- (105) Guo, C., Holland, G. P. Investigating lysine adsorption on fumed silica nanoparticles. *J. Phys. Chem. C* **2014**, *118*, 25792–25801.
- (106) Emami, F. S., Puddu, V., Berry, R. J., Varshney, V., Patwardhan, S. V., Perry, C. C., Heinz, H. Prediction of specific biomolecule adsorption on silica surfaces as a function of pH and particle size. *Chem. Mater.* **2014**, *26*, 5725–5734.
- (107) Maity, S., Zanuy, D., Razvag, Y., Das, P., Alemán, C., Reches, M. Elucidating the mechanism of interaction between peptides and inorganic surfaces. *Phys. Chem. Chem. Phys.* **2015**, *17*, 15305–15315.
- (108) Lundqvist, M., Nygren, P., Jonsson, B.-H., Broo, K. Induction of structure and function in a designed peptide upon adsorption on a silica nanoparticle. *Angew. Chem., Int. Ed.* **2006**, *45*, 8169–8173.
- (109) Nygren, P., Lundqvist, M., Broo, K., Jonsson, B.-H. Fundamental design principles that guide induction of helix upon formation of stable peptide-nanoparticle complexes. *Nano letters* **2008**, *8*, 1844–1852.
- (110) Ghose, S., McNerney, T. M., Hubbard, B. Preparative protein purification on underivatized silica. *Biotechnol. Bioeng.* **2004**, *87*, 413–423.
- (111) Meissner, J., Prause, A., Bharti, B., Findenegg, G. H. Characterization of protein adsorption onto silica nanoparticles: influence of pH and ionic strength. *Colloid Polym. Sci.* **2015**, *293*, 3381–3391.
- (112) Parkes, M., Myant, C., Cann, P. M., Wong, J. S.S. The effect of buffer solution choice on protein adsorption and lubrication. *Tribol. Int.* **2014**, *72*, 108–117.
- (113) Turci, F., Ghibaudi, E., Colonna, M., Boscolo, B., Fenoglio, I., Fubini, B. An integrated approach to the study of the interaction between proteins and nanoparticles. *Langmuir* **2010**, *26*, 8336–8346.
- (114) van der Veen, M., Norde, W., Stuart, M. C. Electrostatic interactions in protein adsorption probed by comparing lysozyme and succinylated lysozyme. *Colloids Surf., B* **2004**, *35*, 33–40.
- (115) Mathé, C., Devineau, S., Aude, J.-C., Lagniel, G., Chédin, S., Legros, V., Mathon, M.-H., Renault, J.-P., Pin, S., Boulard, Y., Labarre, J. Structural determinants for protein adsorption/non-adsorption to silica surface. *PloS one* **2013**, *8*, e81346.
- (116) Graham, D.E., Phillips, M.C. Proteins at liquid interfaces. *J. Colloid Interface Sci.* **1979**, *70*, 403–414.
- (117) Wu, X., Narsimhan, G. Characterization of secondary and tertiary conformational changes of beta-lactoglobulin adsorbed on silica nanoparticle surfaces. *Langmuir* **2008**, *24*, 4989–4998.
- (118) Sethuraman, A., Vedantham, G., Imoto, T., Przybycien, T., Belfort, G. Protein unfolding at interfaces: slow dynamics of alpha-helix to beta-sheet transition. *Proteins* **2004**, *56*, 669–678.
- (119) Larsericsdotter, H., Oscarsson, S., Buijs, J. Thermodynamic analysis of proteins adsorbed on silica particles: Electrostatic effects. *J. Colloid Interface Sci.* **2001**, *237*, 98–103.

- (120) Lensun, L., Smith, T. A., Gee, M. L. Partial denaturation of silica-adsorbed bovine serum albumin determined by time-resolved evanescent wave-induced fluorescence spectroscopy. *Langmuir* **2002**, *18*, 9924–9931.
- (121) Moskovitz, Y., Srebnik, S. Conformational changes of globular proteins upon adsorption on a hydrophobic surface. *Phys. Chem. Chem. Phys.* **2014**, *16*, 11698–11707.
- (122) Donatan, S., Yazici, H., Bermek, H., Sarikaya, M., Tamerler, C., Urgen, M. Physical elution in phage display selection of inorganic-binding peptides. *Mater. Sci. Eng. C* **2009**, *29*, 14–19.
- (123) Eteshola, E., Brillson, L. J., Lee, S. C. Selection and characteristics of peptides that bind thermally grown silicon dioxide films. *Biomol. Eng.* **2005**, *22*, 201–204.
- (124) Naik, R. R., Brott, L. L., Clarson, S. J., Stone, M. O. Silica-precipitating peptides isolated from a combinatorial phage display peptide library. *J. Nanosci. Nanotechnol.* **2002**, *2*, 95–100.
- (125) Coyle, B. L., Baneyx, F. A cleavable silica-binding affinity tag for rapid and inexpensive protein purification. *Biotechnol. Bioeng.* **2014**, *111*, 2019–2026.
- (126) Wang, M., Qi, W., Xu, H., Yu, H., Zhang, S., Shen, Z. Affinity-binding immobilization of D-amino acid oxidase on mesoporous silica by a silica-specific peptide. *J. Ind. Microbiol. Biotechnol.* **2019**, *46*, 1461–1467.
- (127) Braun, K., Pochert, A., Lindén, M., Davoudi, M., Schmidtchen, A., Nordström, R., Malmsten, M. Membrane interactions of mesoporous silica nanoparticles as carriers of antimicrobial peptides. *J. Colloid Interface Sci.* **2016**, *475*, 161–170.
- (128) Han, W., Chilkoti, A., López, G. P. Self-assembled hybrid elastin-like polypeptide/silica nanoparticles enable triggered drug release. *Nanoscale* **2017**, *9*, 6178–6186.
- (129) Sprenger, K. G., Prakash, A., Drobny, G., Pfaendtner, J. Investigating the role of phosphorylation in the binding of silaffin peptide R5 to silica with molecular dynamics simulations. *Langmuir* **2018**, *34*, 1199–1207.
- (130) Yeo, K. B., Ki, M.-R., Park, K. S., Pack, S. P. Novel silica-forming peptides derived from *Ectocarpus siliculosus*. *Process Biochem.* **2017**, *58*, 193–198.
- (131) Abdelhamid, M. A. A., Motomura, K., Ikeda, T., Ishida, T., Hirota, R., Kuroda, A. Affinity purification of recombinant proteins using a novel silica-binding peptide as a fusion tag. *Appl. Microbiol. Biotechnol.* **2014**, *98*, 5677–5684.
- (132) Ikeda, T., Hata, Y., Ninomiya, K.-I., Ikura, Y., Takeguchi, K., Aoyagi, S., Hirota, R., Kuroda, A. Oriented immobilization of antibodies on a silicon wafer using Si-tagged protein A. *Anal. Biochem.* **2009**, *385*, 132–137.
- (133) Oren, E. E., Tamerler, C., Sahin, D., Hnilova, M., Seker, U. O. S., Sarikaya, M., Samudrala, R. A novel knowledge-based approach to design inorganic-binding peptides. *Bioinformatics* **2007**, *23*, 2816–2822.
- (134) Oren, E. E., Notman, R., Kim, I. W., Evans, J. S., Walsh, T. R., Samudrala, R., Tamerler, C., Sarikaya, M. Probing the molecular mechanisms of quartz-binding peptides. *Langmuir* **2010**, *26*, 11003–11009.
- (135) Phillips, D. C., York, R. L., Mermut, O., McCrea, K. R., Ward, R. S., Somorjai, G. A. Side chain, chain length, and sequence effects on amphiphilic peptide adsorption at hydrophobic and hydrophilic surfaces studied by sum-frequency generation vibrational spectroscopy and quartz crystal microbalance. *J. Phys. Chem. C* **2007**, *111*, 255–261.
- (136) Shi, B., Shin, Y. K., Hassanali, A. A., Singer, S. J. Biomolecules at the amorphous silica/water interface: Binding and fluorescence anisotropy of peptides. *Colloids Surf., B* **2017**, *157*, 83–92.
- (137) Sui, J., Tleugabulova, D., Brennan, J. D. Direct and indirect monitoring of peptide-silica interactions using time-resolved fluorescence anisotropy. *Langmuir* **2005**, *21*, 4996–5001.

- (138) York, R. L., Mermut, O., Phillips, D. C., McCrea, K. R., Ward, R. S., Somorjai, G. A. Influence of ionic strength on the adsorption of a model peptide on hydrophilic silica and hydrophobic polystyrene surfaces: Insight from SFG vibrational spectroscopy. *J. Phys. Chem. C* **2007**, *111*, 8866–8871.
- (139) Mermut, O., Phillips, D. C., York, R. L., McCrea, K. R., Ward, R. S., Somorjai, G. A. In situ adsorption studies of a 14-amino acid leucine-lysine peptide onto hydrophobic polystyrene and hydrophilic silica surfaces using quartz crystal microbalance, atomic force microscopy, and sum frequency generation vibrational spectroscopy. *J. Am. Chem. Soc.* **2006**, *128*, 3598–3607.
- (140) Taniguchi, K., Nomura, K., Hata, Y., Nishimura, T., Asami, Y., Kuroda, A. The Si-tag for immobilizing proteins on a silica surface. *Biotechnol. Bioeng.* **2007**, *96*, 1023–1029.
- (141) Ikeda, T., Ninomiya, K.-I., Hirota, R., Kuroda, A. Single-step affinity purification of recombinant proteins using the silica-binding Si-tag as a fusion partner. *Protein Expression Purif.* **2010**, *71*, 91–95.
- (142) Ikeda, T., Motomura, K., Agou, Y., Ishida, T., Hirota, R., Kuroda, A. The silica-binding Si-tag functions as an affinity tag even under denaturing conditions. *Protein Expression Purif.* **2011**, *77*, 173–177.
- (143) Ikeda, T., Kuroda, A. Why does the silica-binding protein "Si-tag" bind strongly to silica surfaces? Implications of conformational adaptation of the intrinsically disordered polypeptide to solid surfaces. *Colloids Surf., B* **2011**, *86*, 359–363.
- (144) Abdelhamid, M. A. A., Ikeda, T., Motomura, K., Tanaka, T., Ishida, T., Hirota, R., Kuroda, A. Application of volcanic ash particles for protein affinity purification with a minimized silica-binding tag. *J. Biosci. Bioeng.* **2016**, *122*, 633–638.
- (145) Abdelhamid, M. A. A., Yeo, K. B., Ki, M.-R., Pack, S. P. Self-encapsulation and controlled release of recombinant proteins using novel silica-forming peptides as fusion linkers. *Int. J. Biol. Macromol.* **2019**, *125*, 1175–1183.
- (146) Kim, J. K., Abdelhamid, M. A. A., Pack, S. P. Direct immobilization and recovery of recombinant proteins from cell lysates by using EctP1-peptide as a short fusion tag for silica and titania supports. *Int. J. Biol. Macromol.* **2019**, *135*, 969–977.
- (147) Abdelhamid, M. A. A., Meligy, A. M. A., Yeo, K. B., Lee, C.-S., Pack, S. P. Silaffin-3-derived pentalysine cluster as a new fusion tag for one-step immobilization and purification of recombinant *Bacillus subtilis* catalase on bare silica particles. *Int. J. Biol. Macromol.* **2020**, *159*, 1103–1112.
- (148) Yang, W., Hellner, B., Baneyx, F. Self-immobilization of Car9 fusion proteins within high surface area silica sol-gels and dynamic control of protein release. *Bioconjugate Chem.* **2016**, *27*, 2450–2459.
- (149) Soto-Rodríguez, J., Coyle, B. L., Samuelson, A., Aravagiri, K., Baneyx, F. Affinity purification of Car9-tagged proteins on silica matrices: Optimization of a rapid and inexpensive protein purification technology. *Protein Expression Purif.* **2017**, *135*, 70–77.
- (150) Xu, M., Bailey, M. J., Look, J., Baneyx, F. Affinity purification of Car9-tagged proteins on silica-derivatized spin columns and 96-well plates. *Protein Expression Purif.* **2020**, *170*, 105608.
- (151) Hellner, B., Alamdari, S., Pyles, H., Zhang, S., Prakash, A., Sprenger, K. G., Yoreo, J. J. de, Baker, D., Pfaendtner, J., Baneyx, F. Sequence-structure-binding relationships reveal adhesion behavior of the Car9 solid-binding peptide: An integrated experimental and simulation study. *J. Am. Chem. Soc.* **2020**, *142*, 2355–2363.
- (152) Hellner, B., Lee, S. B., Subramaniam, A., Subramanian, V. R., Baneyx, F. Modeling the cooperative adsorption of solid-binding proteins on silica: Molecular insights from surface plasmon resonance measurements. *Langmuir* **2019**, *35*, 5013–5020.
- (153) Kuroda A., Ikeda T., Funabashi H. *Purification method, purification kit, and silicon oxide-binding tag for use therein*(WO2016063926A1).

- (154) Baneyx F., Coyle B. L. *Affinity tags and processes for purifying and immobilizing proteins using same*(WO2015042464A1).
- (155) Ali, N., Rampazzo, R. d. C. P., Costa, A. D. T., Krieger, M. A. Current nucleic acid extraction methods and their implications to point-of-care diagnostics. *BioMed Res. Int.* **2017**, *2017*, 9306564.
- (156) Berensmeier, S. Magnetic particles for the separation and purification of nucleic acids. *Appl. Microbiol. Biotechnol.* **2006**, *73*, 495–504.
- (157) Price, C. W., Leslie, D. C., Landers, J. P. Nucleic acid extraction techniques and application to the microchip. *Lab Chip* **2009**, *9*, 2484–2494.
- (158) Vogelstein, B., Gillespie, D. Preparative and analytical purification of DNA from agarose. *PNAS* **1979**, *76*, 615–619.
- (159) Shin, J. H. Nucleic acid extraction techniques. In *Advanced Techniques in Diagnostic Microbiology*; Tang, Y.-W., Stratton, C. W., Eds.; Springer US: Boston, MA, 2013; Vols. 23, pp. 209–225.
- (160) Smerkova, K., Dostalova, S., Vaculovicova, M., Kynicky, J., Trnkova, L., Kralik, M., Adam, V., Hubalek, J., Provaznik, I., Kizek, R. Investigation of interaction between magnetic silica particles and lambda phage DNA fragment. *J. Pharm. Biomed* **2013**, *86*, 65–72.
- (161) Husakova, M., Kralik, P., Babak, V., Slana, I. Efficiency of DNA isolation methods based on silica columns and magnetic separation tested for the detection of *Mycobacterium avium* subsp. *Paratuberculosis* in milk and faeces. *Materials (Basel, Switzerland)* **2020**, *13*.
- (162) Kushalkar, M. P., Liu, B., Liu, J. Promoting DNA adsorption by acids and polyvalent cations: Beyond charge screening. *Langmuir* **2020**, *36*, 11183–11195.
- (163) Li, X., Zhang, J., Gu, H. Adsorption and desorption behaviors of DNA with magnetic mesoporous silica nanoparticles. *Langmuir* **2011**, *27*, 6099–6106.
- (164) Li, X., Zhang, J., Gu, H. Study on the adsorption mechanism of DNA with mesoporous silica nanoparticles in aqueous solution. *Langmuir* **2012**, *28*, 2827–2834.
- (165) Nguyen, T. H., Elimelech, M. Plasmid DNA adsorption on silica: kinetics and conformational changes in monovalent and divalent salts. *Biomacromolecules* **2007**, *8*, 24–32.
- (166) Geng, T., Bao, N., Gall, O. Z., Lu, C. Modulating DNA adsorption on silica beads using an electrical switch. *ChemComm* **2009**, 800–802.
- (167) Melzak, K. A., Sherwood, C. S., Turner, R. F.B., Haynes, C. A. Driving forces for DNA adsorption to silica in perchlorate solutions. *J. Colloid Interface Sci.* **1996**, *181*, 635–644.
- (168) Liu, L., Guo, Z., Huang, Z., Zhuang, J., Yang, W. Size-selective separation of DNA fragments by using lysine-functionalized silica particles. *Sci. Rep.* **2016**, *6*, 22029.
- (169) Vandeventer, P. E., Lin, J. S., Zwang, T. J., Nadim, A., Johal, M. S., Niemz, A. Multiphasic DNA adsorption to silica surfaces under varying buffer, pH, and ionic strength conditions. *J. Phys. Chem. B* **2012**, *116*, 5661–5670.
- (170) Vandeventer, P. E., Mejia, J., Nadim, A., Johal, M. S., Niemz, A. DNA adsorption to and elution from silica surfaces: influence of amino acid buffers. *J. Phys. Chem. B* **2013**, *117*, 10742–10749.
- (171) Isailovic, S., Li, H.-W., Yeung, E. S. Adsorption of single DNA molecules at the water/fused-silica interface. *J. Chromatogr. A* **2007**, *1150*, 259–266.
- (172) Scholes, C. A., Millar, D. P., Gee, M. L., Smith, T. A. Resonance energy-transfer studies of the conformational change on the adsorption of oligonucleotides to a silica interface. *J. Phys. Chem. B* **2011**, *115*, 6329–6339.

- (173) Ballardur, Theretz, Mandrand. Determination of the main forces driving DNA oligonucleotide adsorption onto aminated silica wafers. *J. Colloid Interface Sci.* **1997**, *194*, 408–418.
- (174) Cárdenas, M., Schillén, K., Pebalk, D., Nylander, T., Lindman, B. Interaction between DNA and charged colloids could be hydrophobically driven. *Biomacromolecules* **2005**, *6*, 832–837.
- (175) Shi, B., Shin, Y. K., Hassanali, A. A., Singer, S. J. DNA binding to the silica surface. *J. Phys. Chem. B* **2015**, *119*, 11030–11040.
- (176) Romanowski, G., Lorenz, M. G., Wackernagel, W. Adsorption of plasmid DNA to mineral surfaces and protection against DNase I. *Appl. Environ. Microbiol.* **1991**, *57*, 1057–1061.
- (177) Allemann, J. F., Bensimon, D., Jullien, L., Bensimon, A., Croquette, V. pH-dependent specific binding and combing of DNA. *Biophys. J.* **1997**, *73*, 2064–2070.
- (178) Nguyen, T. H., Chen, K. L., Elimelech, M. Adsorption kinetics and reversibility of linear plasmid DNA on silica surfaces: influence of alkaline earth and transition metal ions. *Biomacromolecules* **2010**, *11*, 1225–1230.
- (179) Poly, F., Chenu, C., Simonet, P., Rouiller, J., Jocteur Monrozier, L. Differences between linear chromosomal and supercoiled plasmid DNA in their mechanisms and extent of adsorption on clay minerals. *Langmuir* **2000**, *16*, 1233–1238.
- (180) Carta G., Jungbauer A. *Protein chromatography: Process development and scale-up*, 1st ed.; Wiley-VCH: Weinheim, op. 2010 (imp. 2011).
- (181) Schmidt-Traub H., Schulte M., Seidel-Morgenstern A., Eds. *Preparative chromatography*; Wiley-VCH: Weinheim, Germany, 2020.
- (182) Harrison R. G., Todd P., Rudge S. R., Petrides D. P. *Bioseparations science and engineering*, 2nd ed.; Oxford University Press: New York, NY, 2015.
- (183) Gritti, F., Guiochon, G. General HETP equation for the study of mass-transfer mechanisms in RPLC. *Anal. Chem.* **2006**, *78*, 5329–5347.
- (184) Gritti, F., Guiochon, G. Perspectives on the evolution of the column efficiency in liquid chromatography. *Anal. Chem.* **2013**, *85*, 3017–3035.
- (185) Hage, D. S. Chromatography. In *Principles and Applications of Clinical Mass Spectrometry*; Elsevier, 2018; Vols. 65, pp. 1–32.
- (186) Adamska, K., Voelkel, A., Sandomierski, M. Characterization of mesoporous aluminosilicate materials by means of inverse liquid chromatography. *J. Chromatogr. A* **2020**, *1610*, 460544.
- (187) Metzelder, F., Funck, M., Hüffer, T., Schmidt, T. C. Comparison of sorption to carbon-based materials and nanomaterials using inverse liquid chromatography. *Environ. Sci. Technol.* **2018**, *52*, 9731–9740.
- (188) Tao, P., Poddar, S., Sun, Z., Hage, D. S., Chen, J. Analysis of solute-protein interactions and solute-solute competition by zonal elution affinity chromatography. *Methods* **2018**, *146*, 3–11.
- (189) Iftekhhar, S., Ovbude, S. T., Hage, D. S. Kinetic analysis by affinity chromatography. *Front. Chem.* **2019**, *7*, 673.
- (190) Bednar, I., Tscheliessnig, R., Berger, E., Podgornik, A., Jungbauer, A. Surface energies of hydrophobic interaction chromatography media by inverse liquid chromatography. *J. Chromatogr. A* **2012**, *1220*, 115–121.
- (191) Buszewski, B., Bocian, S., Felinger, A. Excess isotherms as a new way for characterization of the columns for reversed-phase liquid chromatography. *J. Chromatogr. A* **2008**, *1191*, 72–77.
- (192) Ylä-Mäihäniemi, P. P., Williams, D. R. A comparison of frontal and nonfrontal methods for determining solid-liquid adsorption isotherms using inverse liquid chromatography. *Langmuir* **2007**, *23*, 4095–4101.

- (193) Bednar, I., Berger, E., Krajnc, N. L., Vidič, J., Podgornik, A., Jungbauer, A., Tscheliessnig, R. Surfaces energies of monoliths by inverse liquid chromatography and contact angles. *Langmuir* **2014**, *30*, 5435–5440.
- (194) Serroukh, S., Huber, P., Lallam, A. Adsorption behavior of optical brightening agent on microfibrillated cellulose studied through inverse liquid chromatography: The need to correct for axial dispersion effect. *J. Chromatogr. A* **2018**, *1533*, 17–29.
- (195) Mohammadi-Jam, S., Waters, K. E. Inverse gas chromatography applications: a review. *Adv. Colloid Interface Sci.* **2014**, *212*, 21–44.
- (196) Hage, D. S. High-performance affinity chromatography: a powerful tool for studying serum protein binding. *J. Chromatogr. B: Anal. Technol. Biomed. Life Sci.* **2002**, *768*, 3–30.
- (197) Li, Q., Wang, J., Zheng, Y. Y., Yang, L., Zhang, Y., Bian, L., Zheng, J., Li, Z., Zhao, X., Zhang, Y. Comparison of zonal elution and nonlinear chromatography in determination of the interaction between seven drugs and immobilised $\beta(2)$ -adrenoceptor. *J. Chromatogr. A* **2015**, *1401*, 75–83.
- (198) Da Silva, G. F. L., Plewka, J., Tscheliessnig, R., Lichtenegger, H., Jungbauer, A., Dias-Cabral, A. C. M. Antibody binding heterogeneity of protein A resins. *Biotechnol. J.* **2019**, *14*, e1800632.
- (199) Rosa, S. A.S.L., da Silva, C. L., Aires-Barros, M. R., Dias-Cabral, A. C., Azevedo, A. M. Thermodynamics of the adsorption of monoclonal antibodies in phenylboronate chromatography: Affinity versus multimodal interactions. *J. Chromatogr. A* **2018**, *1569*, 118–127.
- (200) Silva, G. L., Marques, F. S., Thrash, M. E., Dias-Cabral, A. C. Enthalpy contributions to adsorption of highly charged lysozyme onto a cation-exchanger under linear and overloaded conditions. *J. Chromatogr. A* **2014**, *1352*, 46–54.
- (201) Desch, R. J., Kim, J., Thiel, S. W. Interactions between biomolecules and an iron-silica surface. *Microporous Mesoporous Mater.* **2014**, *187*, 29–39.
- (202) Kim, J., Desch, R. J., Thiel, S. W., Gulianti, V. V., Pinto, N. G. Energetics of biomolecule adsorption on mesostructured cellular foam silica. *Microporous Mesoporous Mater.* **2013**, *170*, 95–104.
- (203) Korfhagen, J., Dias-Cabral, A. C., Thrash, M. E. Nonspecific effects of ion exchange and hydrophobic interaction adsorption processes. *Sep Sci Technol* **2010**, *45*, 2039–2050.
- (204) Katiyar, A., Thiel, S. W., Gulianti, V. V., Pinto, N. G. Investigation of the mechanism of protein adsorption on ordered mesoporous silica using flow microcalorimetry. *J. Chromatogr. A* **2010**, *1217*, 1583–1588.
- (205) Aguilar, P. A., Twarda, A., Sousa, F., Dias-Cabral, A. C. Thermodynamic study of the interaction between linear plasmid DNA and an anion exchange support under linear and overloaded conditions. *J. Chromatogr. A* **2014**, *1372C*, 166–173.
- (206) Kandori, K., Murata, K., Ishikawa, T. Microcalorimetric study of protein adsorption onto calcium hydroxyapatites. *Langmuir* **2007**, *23*, 2064–2070.
- (207) Thrash, M. E., Phillips, J. M., Pinto, N. G. An analysis of the interactions of BSA with an anion-exchange surface under linear and non-linear conditions. *Adsorption* **2005**, *10*, 299–307.
- (208) Burgess, R. R. A brief practical review of size exclusion chromatography: Rules of thumb, limitations, and troubleshooting. *Protein Expression Purif.* **2018**, *150*, 81–85.
- (209) To, B. C. S., Lenhoff, A. M. Hydrophobic interaction chromatography of proteins. IV. Protein adsorption capacity and transport in preparative mode. *J. Chromatogr. A* **2011**, *1218*, 427–440.
- (210) Jungbauer, A., Machold, C., Hahn, R. Hydrophobic interaction chromatography of proteins. III. Unfolding of proteins upon adsorption. *J. Chromatogr. A* **2005**, *1079*, 221–228.

- (211) Fekete, S., Beck, A., Veuthey, J.-L., Guillarme, D. Ion-exchange chromatography for the characterization of biopharmaceuticals. *J. Pharm. Biomed. Anal.* **2015**, *113*, 43–55.
- (212) Cummins, P. M., Rochfort, K. D., O'Connor, B. F. Ion-exchange chromatography: Basic principles and application. *Methods Mol. Biol.* **2017**, *1485*, 209–223.
- (213) Rodriguez, E. L., Poddar, S., Iftekhar, S., Suh, K., Woolfork, A. G., Ovbude, S., Pekarek, A., Walters, M., Lott, S., Hage, D. S. Affinity chromatography: A review of trends and developments over the past 50 years. *J. Chromatogr. B: Anal. Technol. Biomed. Life Sci.* **2020**, *1157*, 122332.
- (214) Ramos-de-la-Peña, A. M., González-Valdez, J., Aguilar, O. Protein A chromatography: Challenges and progress in the purification of monoclonal antibodies. *J. Sep. Sci.* **2019**, *42*, 1816–1827.
- (215) Mahmoodi, S., Pourhassan-Moghaddam, M., Wood, D. W., Majdi, H., Zarghami, N. Current affinity approaches for purification of recombinant proteins. *Cogent Biology* **2019**, *5*, 1665406.
- (216) Waugh, D. S. Making the most of affinity tags. *Trends Biotechnol.* **2005**, *23*, 316–320.
- (217) Zhao, X., Li, G., Liang, S. Several affinity tags commonly used in chromatographic purification. *J. Anal. Methods Chem.* **2013**, *2013*, 581093.
- (218) Mahmoudi Gomari, M., Saraygord-Afshari, N., Farsimadan, M., Rostami, N., Aghamiri, S., Farajollahi, M. M. Opportunities and challenges of the tag-assisted protein purification techniques: Applications in the pharmaceutical industry. *Biotechnol. Adv.* **2020**, *45*, 107653.
- (219) Orf, G. S., Redding, K. E. Expression and purification of affinity-tagged variants of the photochemical reaction center from *Halobacterium modesticaldum*. *Photosyn. Res.* **2019**, *142*, 335–348.
- (220) Kosobokova, E. N., Skrypnik, K. A., Kosorukov, V. S. Overview of fusion tags for recombinant proteins. *Biochemistry (Mosc)* **2016**, *81*, 187–200.
- (221) Kimple, M. E., Brill, A. L., Pasker, R. L. Overview of affinity tags for protein purification. *Curr. Protoc. Protein Sci.* **2013**, *73*, 9.9.1-9.9.23.
- (222) Terpe, K. Overview of tag protein fusions: from molecular and biochemical fundamentals to commercial systems. *Appl. Microbiol. Biotechnol.* **2003**, *60*, 523–533.
- (223) Barbosa, O., Ortiz, C., Berenguer-Murcia, Á., Torres, R., Rodrigues, R. C., Fernandez-Lafuente, R. Strategies for the one-step immobilization-purification of enzymes as industrial biocatalysts. *Biotechnol. Adv.* **2015**, *33*, 435–456.
- (224) Pacheco, B., Crombet, L., Loppnau, P., Cossar, D. A screening strategy for heterologous protein expression in *Escherichia coli* with the highest return of investment. *Protein Expression Purif.* **2012**, *81*, 33–41.
- (225) Freitas, A. I., Domingues, L., Aguiar, T. Q. Tag-mediated single-step purification and immobilization of recombinant proteins toward protein-engineered advanced materials. *J. Adv. Res.* **2021**, *17*, 1600554.
- (226) Gogami, Y., Okada, K., Oikawa, T. High-performance liquid chromatography analysis of naturally occurring D-amino acids in sake. *J. Chromatogr. B: Anal. Technol. Biomed. Life Sci.* **2011**, *879*, 3259–3267.
- (227) Khalil, N. Y., Darwish, I. A., Wani, T. A., Al-Majed, A.-R. A. Trace determination of lenalidomide in plasma by non-extractive HPLC procedures with fluorescence detection after pre-column derivatization with fluorescamine. *Chem. Cent. J.* **2013**, *7*, 52.
- (228) Dai, Z., Wu, Z., Wang, J., Wang, X., Jia, S., Bazer, F. W., Wu, G. Analysis of polyamines in biological samples by HPLC involving pre-column derivatization with o-phthalaldehyde and N-acetyl-L-cysteine. *Amino acids* **2014**, *46*, 1557–1564.
- (229) Li, L., Vorobyov, I., Allen, T. W. The different interactions of lysine and arginine side chains with lipid membranes. *J. Phys. Chem. B* **2013**, *117*, 11906–11920.

- (230) Sokalingam, S., Raghunathan, G., Soundrarajan, N., Lee, S.-G. A study on the effect of surface lysine to arginine mutagenesis on protein stability and structure using green fluorescent protein. *PloS one* **2012**, *7*, e40410.
- (231) Cugia, F., Sedda, S., Pitzalis, F., Parsons, D. F., Monduzzi, M., Salis, A. Are specific buffer effects the new frontier of Hofmeister phenomena? Insights from lysozyme adsorption on ordered mesoporous silica. *RSC Adv.* **2016**, *6*, 94617–94621.
- (232) Schwaminger, S. P., García, P. F., Merck, G. K., Bodensteiner, F. A., Heissler, S., Günther, S., Berensmeier, S. Nature of interactions of amino acids with bare magnetite nanoparticles. *J. Phys. Chem. C* **2015**, *119*, 23032–23041.
- (233) Marcus, Y., Hefter, G. Ion pairing. *Chem. Rev.* **2006**, *106*, 4585–4621.
- (234) Zhang, X., Chen, J., Li, E., Hu, C., Luo, S.-Z., He, C. Ultrahigh adhesion force between silica-binding peptide SB7 and glass substrate studied by single-molecule force spectroscopy and molecular dynamic simulation. *Front. Chem.* **2020**, *8*, 600918.
- (235) Blank-Shim, S. A., Schwaminger, S. P., Borkowska-Panek, M., Anand, P., Yamin, P., Fraga-García, P., Fink, K., Wenzel, W., Berensmeier, S. Binding patterns of homopeptides on bare magnetic nanoparticles: insights into environmental dependence. *Sci. Rep.* **2017**, *7*, 14047.
- (236) Schwaminger, S. P., Anand, P., Borkowska-Panek, M., Blank-Shim, S. A., Fraga-Garci A, P., Fink, K., Berensmeier, S., Wenzel, W. Rational design of iron oxide binding peptide tags. *Langmuir* **2019**, *35*, 8472–8481.
- (237) Schwaminger, S., Blank-Shim, S. A., Borkowska-Panek, M., Anand, P., Fraga-García, P., Fink, K., Wenzel, W., Berensmeier, S. Experimental characterization and simulation of amino acid and peptide interactions with inorganic materials. *Eng. Life Sci.* **2018**, *18*, 84–100.
- (238) Zanker, A. A., Ahmad, N., Son, T. H., Schwaminger, S. P., Berensmeier, S. Selective ene-reductase immobilization to magnetic nanoparticles through a novel affinity tag. *Biotechnol. J.* **2020**, e2000366.
- (239) S. Berensmeier, S. P. Schwaminger, S. A. Blank-Shim, P. Fraga García, Y. Kaveh-Baghbaderani, A. Zanker, S. Rauwolf, W. Wenzel. *Novel peptide tag*(EP20185909.7).
- (240) Xu, X., Song, Y., Li, Y., Chang, J., Zhang, H., An, L. The tandem affinity purification method: an efficient system for protein complex purification and protein interaction identification. *Protein Expression Purif.* **2010**, *72*, 149–156.
- (241) Li, Y. The tandem affinity purification technology: an overview. *Biotechnol. Lett.* **2011**, *33*, 1487–1499.
- (242) Zhu, M., Fuks, P., Carta, G. Protein adsorption in anion exchange resins - effects of polymer grafting, support structure porosity, and protein size. *J. Chem. Technol. Biotechnol* **2018**, *93*, 1948–1958.
- (243) Reifsnnyder, D. H., Olson, C. V., Etcheverry, T., Prashad, H., Builder, S. E. Purification of insulin-like growth factor-I and related proteins using underivatized silica. *J. Chromatogr. A* **1996**, *753*, 73–80.
- (244) Arakawa, T., Tsumoto, K., Kita, Y., Chang, B., Ejima, D. Biotechnology applications of amino acids in protein purification and formulations. *Amino acids* **2007**, *33*, 587–605.
- (245) Tsumoto, K., Umetsu, M., Kumagai, I., Ejima, D., Philo, J. S., Arakawa, T. Role of arginine in protein refolding, solubilization, and purification. *Biotechnol. Prog.* **2004**, *20*, 1301–1308.
- (246) Guo, J., Carta, G. Unfolding and aggregation of monoclonal antibodies on cation exchange columns: effects of resin type, load buffer, and protein stability. *J. Chromatogr. A* **2015**, *1388*, 184–194.
- (247) Carta, G. Predicting protein dynamic binding capacity from batch adsorption tests. *Biotechnol. J.* **2012**, *7*, 1216–1220.

-
- (248) Eslami, T., Jakob, L. A., Satzer, P., Ebner, G., Jungbauer, A., Lingg, N. Productivity for free: Residence time gradients during loading increase dynamic binding capacity and productivity. *Sep. Purif. Technol.* **2022**, *281*, 119985.
- (249) Rigüero, V., Clifford, R., Dawley, M., Dickson, M., Gastfriend, B., Thompson, C., Wang, S.-C., O'Connor, E. Immobilized metal affinity chromatography optimization for poly-histidine tagged proteins. *J. Chromatogr. A* **2020**, *1629*, 461505.
- (250) Sheng, W., Wei, W., Li, J., Qi, X., Zuo, G., Chen, Q., Pan, X., Dong, W. Amine-functionalized magnetic mesoporous silica nanoparticles for DNA separation. *Appl. Surf. Sci.* **2016**, *387*, 1116–1124.

7 Appendix

7.1 Supporting Information

7.1.1 Buffer influence on the amino acid silica interaction

The following pages contain the Supporting Information for Section 3.1.

ChemPhysChem

Supporting Information

Buffer Influence on the Amino Acid Silica Interaction

Saientan Bag⁺, Stefan Rauwolf⁺, Mikhail Suyetin, Sebastian P. Schwaminger,
Wolfgang Wenzel,^{*} and Sonja Berensmeier^{*}

Supporting Information

Table S1. Minima of the PMF profile and the binding affinity of all 20 amino acids with the silica calculated using umbrella sampling simulation.

Amino acid	Amino Acid 1 letter code	PMF Minima (kJoule/mol)	Binding Affinity [Kcal/C] (Arbitrary Unit)
Glycine	G	-8.3	3
Alanine	A	-9.2	5
Valine	V	-12.5	18
Leucine	L	-14.0	21
Isoleucine	I	-14.3	34
Proline	P	-11.5	10
Methionine	M	-14.2	24
Cysteine	C	-9.7	5
Asparagine	N	-11.8	11
Glutamine	Q	-13.6	20
Aspartic acid	D	-9.2	0.8
Glutamic acid	E	-5.7	1
Serine	S	-9.9	5
Threonine	T	-9.8	6
Tyrosine	Y	-15.4	46
Phenylalanine	F	-13.6	19
Tryptophan	W	-15.4	43
Histidine	H	-13.0	20
Lysine	K	-18.6	153
Arginine	R	-23.3	745

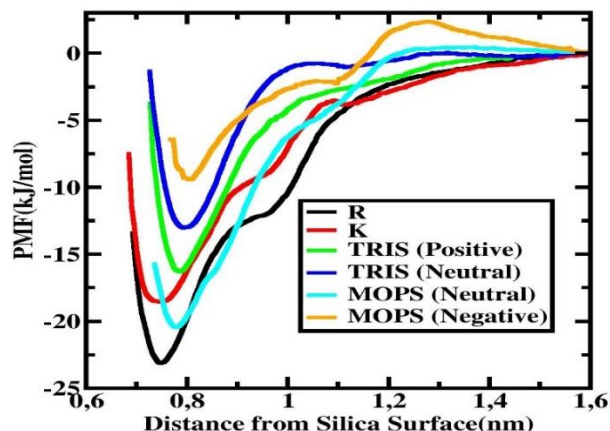


Figure S1. PMF profile of R and K and the buffer species.

Table S2. Minima of the PMF profile and the binding affinity of different buffer species. The numbers for R and K are also quoted for comparison.

Molecular Species	PMF minima (kJoule/mol)	Binding Affinity (K_{calc}/C) (Arbitrary Unit)
TRIS (neutral)	-13.0	16
TRIS (positive)	-16.4	49
MOPS (neutral)	-20.5	269
MOPS(Negative)	-9.5	4
K	-18.6	154
R	-23.3	745

Table S3. Interaction energy between two molecular species for R.

Species 1	Species 2	Interaction Energy (kJ/mol)*	Interaction Energy with respect to Arginine dimer (kJ/mol)*
Arginine	Arginine	-10	0
Arginine	MOPS(Negative)	-30	-20
Arginine	MOPS(Neutral)	-13	-3
Arginine	TRIS(Positive)	-7	3
Arginine	TRIS(Neutral)	-7	3
MOPS(Negative)	MOPS(Negative)	-10	0
MOPS(Neutral)	MOPS(Neutral)	-13	-3
TRIS(Positive)	TRIS(Positive)	1	11
TRIS(Neutral)	TRIS(Neutral)	-3	7

*interaction energies are reported at a separation of 8Å between the species

Table S4. Interaction energy between two molecular species for K.

Species 1	Species 2	Interaction Energy (kJ/mol)*	Interaction Energy with respect to Lysine dimer (kJ/mol)*
Lysine	Lysine	-8	0
Lysine	MOPS(Negative)	-20	-12
Lysine	MOPS(Neutral)	-12	-4
Lysine	TRIS(Positive)	-3	5
Lysine	TRIS(Neutral)	-5	5
MOPS(Negative)	MOPS(Negative)	-10	-2
MOPS(Neutral)	MOPS(Neutral)	-13	-5
TRIS(Positive)	TRIS(Positive)	1	9
TRIS(Neutral)	TRIS(Neutral)	-3	5

*interaction energies are reported at a separation of 8\AA between the species

Derivation of Cooperative Langmuir Model

Let's assume there are two different adsorbate species A and B. The species are assumed to be in the ideal gas phase unless these are adsorbed on the surface adsorption sites (shown as the black parabola in the schematic in Fig. S2) of the adsorbent. Each adsorption site can accommodate a maximum of two molecules where the adsorption phenomenon is governed by adsorbate-adsorbent interaction as well as adsorbate-adsorbate interaction.

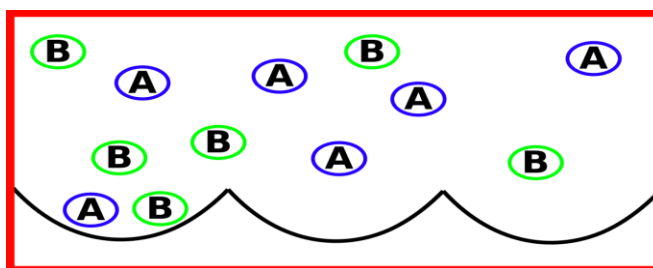


Figure S2. Schematic diagram representing a cooperative adsorption model of two different species A and B. The black semi circles are the adsorption sites, which can accommodate up to two molecules.

To formulate the statistical mechanics of this adsorption processes we first enumerate the different number of microstates for a single adsorption site (see the schematic in Fig.S3) as follows:

1. Adsorption site is empty.
2. Occupied by one A molecules and an empty spot.
3. Occupied by two A molecules.
4. Occupied by one B molecules and an empty spot.
5. Occupied by two B molecules.

6. Occupied by one A and one B molecules.

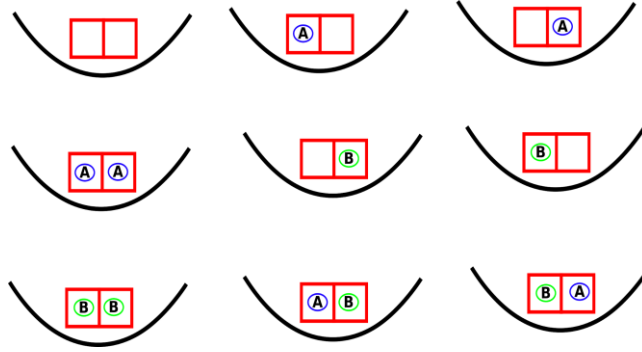


Figure S3. Different microstates for a single adsorption site (capable of holding two adsorbate molecules) in the presence of two adsorbates A and B.

U_A and U_B are the potential energy of the molecule A and B due to interaction with the adsorbent upon adsorption. U_{AA} is the interaction energy between two A molecules when both of these two are adsorbed on a single adsorption site. U_{BB} is the corresponding interaction energy for the B molecules and U_{AB} is the interaction energy between A and B in case the adsorption site is occupied by one A and one B molecule respectively.

The grand canonical partition function for the single adsorption site is then given by

$$\xi = 1 + 2\Lambda_A^{-3} V e^{-\beta U_A} e^{\beta \mu_A} + 2\Lambda_B^{-3} V e^{-\beta U_B} e^{\beta \mu_B} + \Lambda_A^{-6} V^2 e^{-\beta(2U_A+U_{AA})} e^{2\beta \mu_A} + \Lambda_B^{-6} V^2 e^{-\beta(2U_B+U_{BB})} e^{2\beta \mu_B} + 2\Lambda_A^{-3} V^2 \Lambda_B^{-3} V^2 e^{-\beta(U_A+U_B+U_{AB})} e^{\beta \mu_A} e^{\beta \mu_B} \quad (1)$$

Λ_A and Λ_B are the thermal de Broglie wavelength of the adsorbate molecule A and B respectively. V is the free volume offered by half of the adsorption site. Here, the terms $\Lambda_A^{-3} V$ and $\Lambda_B^{-3} V$ come from the configurational part of the partition function. μ_A and μ_B are the chemical potential of the molecular A and B respectively. Here, $\beta = 1/K_B T$. K_B is the Boltzmann constant and T is the temperature.

Now, if there are Γ independent adsorption sites, the total grand canonical partition function of the system is

$$\Xi = \xi^\Gamma \quad (2)$$

The expectation value of the number of adsorbed molecule A is then given by

$$\langle N_A \rangle = \left(\frac{\partial \log \Xi}{\partial (\beta \mu_A)} \right) \quad (3)$$

$$= \Gamma \frac{2\Lambda_A^{-3} V e^{-\beta U_A} e^{\beta \mu_A} + 2\Lambda_A^{-6} V^2 e^{-\beta(2U_A+U_{AA})} e^{2\beta \mu_A} + 2\Lambda_A^{-3} V^2 \Lambda_B^{-3} V^2 e^{-\beta(U_A+U_B+U_{AB})} e^{\beta \mu_A} e^{\beta \mu_B}}{1 + 2\Lambda_A^{-3} V e^{-\beta U_A} e^{\beta \mu_A} + 2\Lambda_B^{-3} V e^{-\beta U_B} e^{\beta \mu_B} + \Lambda_A^{-6} V^2 e^{-\beta(2U_A+U_{AA})} e^{2\beta \mu_A} + \Lambda_B^{-6} V^2 e^{-\beta(2U_B+U_{BB})} e^{2\beta \mu_B} + 2\Lambda_A^{-3} V^2 \Lambda_B^{-3} V^2 e^{-\beta(U_A+U_B+U_{AB})} e^{\beta \mu_A} e^{\beta \mu_B}}$$

Now, at equilibrium, the chemical potential of the molecular species A and B are related to their partial pressure according to following thermodynamic condition

$$\mu_A = \frac{1}{\beta} \log(\Lambda_A^3 \beta P_A); \quad \mu_B = \frac{1}{\beta} \log(\Lambda_B^3 \beta P_B) \quad (4)$$

And the Langmuir Binding Constant for the molecular species A and B defined as

$$K_A = \beta V e^{(-\beta U_A)}; K_B = \beta V e^{(-\beta U_B)} \quad (5)$$

Using equations (4) and (5), equation (3) can be rewritten in the following form

$$\langle N_A \rangle = \Gamma \frac{2P_A K_A + 2P_A^2 K_A^2 e^{-\beta U_{AA}} + 2P_A K_A P_B K_B e^{-\beta U_{AB}}}{1 + 2P_A K_A + P_A^2 K_A^2 e^{-\beta U_{AA}} + 2P_B K_B + P_B^2 K_B^2 e^{-\beta U_{BB}} + 2P_A K_A P_B K_B e^{-\beta U_{AB}}} \quad (6)$$

Similarly, we can write another equation for the expectation value of adsorbed molecule B. The equation (6) above is written in terms of the partial pressure of the adsorbates. Alternatively, it can be rewritten in terms of the equilibrium concentration of the adsorbates. If θ_A and θ_B are the concentration of the species A and B in equilibrium then,

$$P_A = C\theta_A \text{ and } P_B = C\theta_B \quad (7)$$

C is proportionality constant relating the pressure of an ideal gas with its concentration.

Now, let's define scaled Langmuir constant as,

$$K_A' = CK_A \text{ and } K_B' = CK_B \quad (8)$$

The equation (6) can therefore be alternatively written as,

$$\langle N_A \rangle / \Gamma = F_A = \frac{2K_A' \theta_A + 2\theta_A^2 K_A'^2 e^{-\beta U_{AA}} + 2\theta_A K_A' \theta_B K_B' e^{-\beta U_{AB}}}{1 + 2\theta_A K_A' + \theta_A^2 K_A'^2 e^{-\beta U_{AA}} + 2\theta_B K_B' + \theta_B^2 K_B'^2 e^{-\beta U_{BB}} + 2\theta_A K_A' \theta_B K_B' e^{-\beta U_{AB}}} \quad (9)$$

When there are no interactions between the molecules A and B, instead of invoking the cooperative adsorption model, we employ the non-cooperative Langmuir Adsorption model as shown schematically in Figure S4 below.

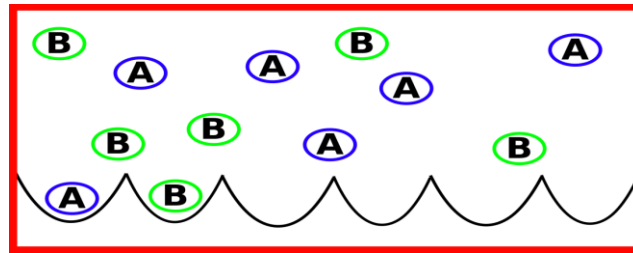


Figure S4. Schematic diagram representing non-cooperative competitive Langmuir adsorption model of two different species A and B. The black semi circles are the adsorption sites which can accommodate only one molecule.

In that case, the expectation value for the number of adsorbed A molecules is

$$\langle N_A \rangle / \Gamma = F_A = \frac{K_A' \theta_A}{1 + \theta_A K_A' + \theta_B K_B'} \quad (10)$$

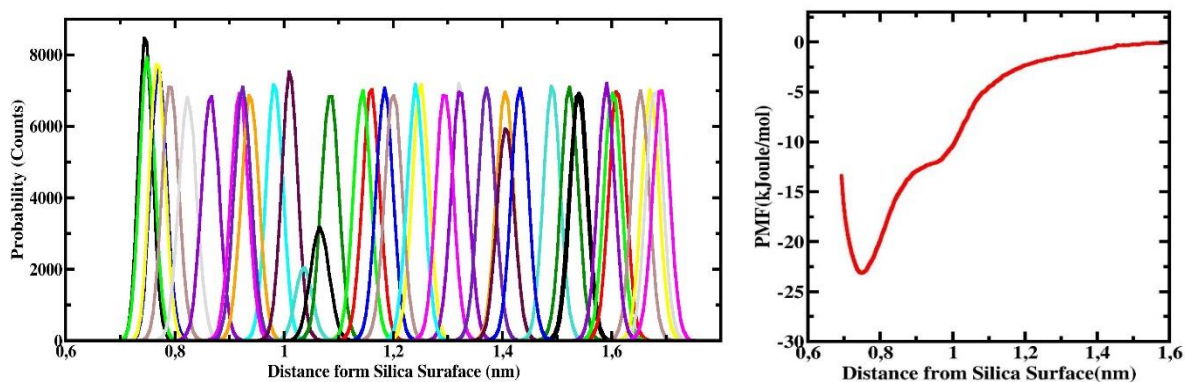


Figure S5. Histograms obtained from the US run with amino acid R and silica (left). The corresponding PMF profile (right).

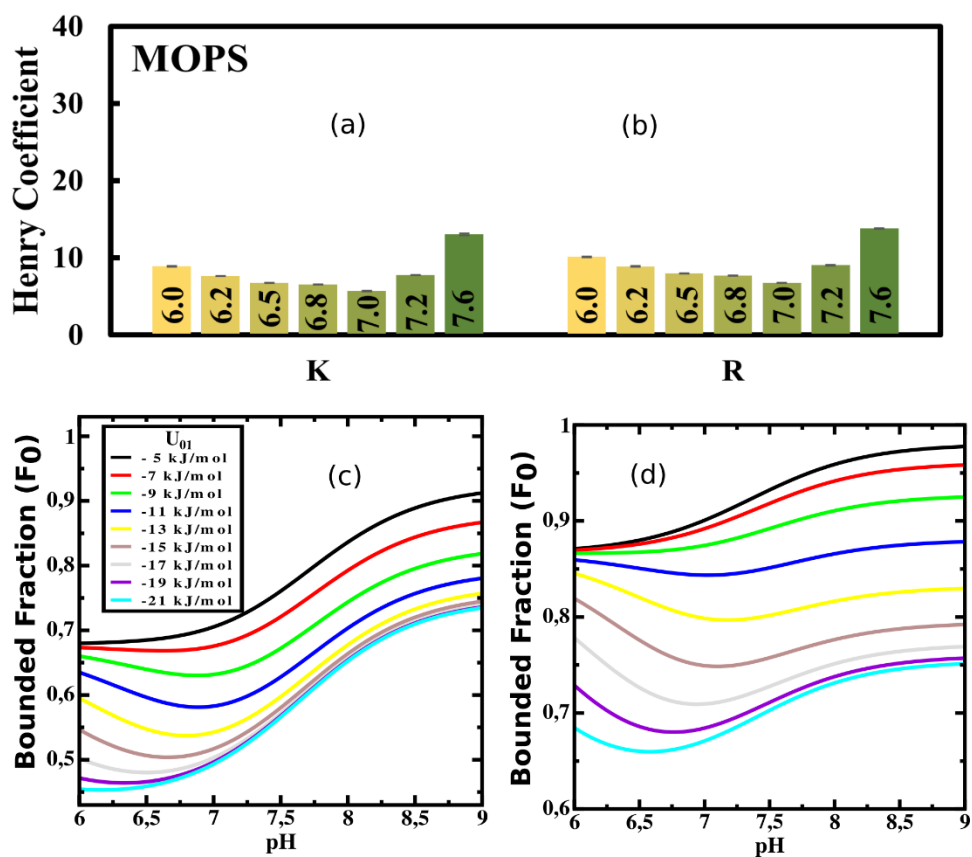


Figure S6: (a/b) Experimentally measured Henry coefficient of K/R as a function of pH in presence of MOPS buffer. (c/d) Fraction of K/R bound to silica for different values of the interaction energy (U_{01}) between K/R and MOPS (Negative) as a function of pH as calculated using multiscale modelling. The experimental Henry coefficient and calculated bounded fraction show qualitatively same behavior for $|U_{01}| > 7$ kJ/mol (or $|U_{01}| > 11$ kJ/mol) for K (or R).

Experimental setup

Table S5. Concentration of the amino acids as prepared for the chromatography experiment.

Amino acid	1-letter code	Concentration [mM]
Glycine	G	50
Alanine	A	50
Valine	V	50
Leucine	L	50
Isoleucine	I	50
Proline	P	25
Methionine	M	5
Cysteine	C	10
Asparagine	N	5
Glutamine	Q	10
Aspartic acid	D	15
Glutamic acid	E	25
Serine	S	50
Threonine	T	25
Tyrosine	Y	1
Phenylalanine	F	25
Tryptophan	W	1
Histidine	H	5
Lysine	K	50
Arginine	R	50

The chromatographic column was operated on an Agilent 1100 HPLC system with an UV/Vis detector. Amino acids (AAs) were measured at 210 nm, aromatic AAs additionally at 280 nm. The flow rate was ~ 12 cm min^{-1} for every run and the injection volume for every AA was 20 μL . The Henry coefficient H was determined with $H = k' / \phi$. Where k' is the retention factor of the AA and ϕ is the phase ratio of the column. The retention factor is calculated as $k' = (t_R - t_0)/t_0$. Here t_R stands for the retention time of the AA and t_0 for the retention time of a non-interacting tracer in this case 1 g L^{-1} uracil. The phase ratio of the column is calculated with $\phi = (1 - \epsilon^t) / \epsilon^t$. Here ϵ^t

is the total porosity of the column calculated with the flow rate $\dot{V} = 2 \text{ mL min}^{-1}$: $\varepsilon^t = (t_0 * \dot{V}) / V_{\text{column}}$. The volume of the column is 0.55 mL.

Table S6. Measured retention times and conversion in Henry coefficient for 18 amino acids in 10 mM TRIS pH 8 on silica gel 60. The total porosity was 0.52 and the phase ratio of the column 0.93. Retention times were measured at room temperature.

Analyte	Retention time [min]				Retention factor k' [-]		Henry coefficient H [-]	
					$\emptyset k'$	σ	H	σ
Uracil	0.28	0.28	0.29	0.29				
Glycine	0.29	0.29	0.29	0.29	0.00	0.00	0.01	0.00
Alanine	0.29	0.29	0.29	0.29	0.01	0.01	0.01	0.01
Valine	0.31	0.31	0.31	0.31	0.08	0.01	0.09	0.01
Leucine	0.32	0.32	0.32	0.32	0.11	0.00	0.12	0.00
Isoleucine	0.32	0.32	0.32	0.32	0.12	0.01	0.13	0.01
Methionine	0.31	0.31	0.31	0.31	0.08	0.00	0.09	0.00
Proline	0.37	0.37	0.37	0.37	0.29	0.01	0.31	0.01
Phenylalanine	0.31	0.31	0.31	0.31	0.09	0.00	0.10	0.00
Tryptophan	0.30	0.30	0.30	0.30	0.06	0.01	0.06	0.01
Threonine	0.28	0.28	0.28	0.28	0.01	0.00	0.01	0.00
Serine	0.28	0.28	0.28	0.28	0.03	0.00	0.03	0.00
Cysteine	0.26	0.26	0.26	0.26	0.08	0.01	0.09	0.01
Tyrosine	0.27	0.28	0.28	0.28	0.03	0.00	0.04	0.00
Asparagine	0.28	0.28	0.28	0.28	0.02	0.01	0.02	0.01
Glutamine	0.28	0.29	0.29	0.29	0.00	0.00	0.00	0.00
Aspartic acid	0.20	0.20	0.20	0.20	0.30	0.01	0.33	0.01
Glutamic acid	0.22	0.22	0.23	0.21	0.23	0.02	0.24	0.02
Histidine	0.41	0.42	0.42	0.43	0.48	0.01	0.51	0.02

Table S7. Measured retention times and conversion in Henry coefficient for arginine and lysine in 10 mM TRIS on silica gel 60 for different pH. The total porosity and the phase ration of the column for every buffer run are given in the line of buffer description. Retention times were measured at room temperature.

Analyte	Retention time [min]				Retention factor k' [-]		Henry coefficient H [-]	
					$\emptyset k'$	σ	H	σ
TRIS pH 7.2 ($\varepsilon_t = 0.58, \phi = 0.74$)								
Uracil	0.32	0.32	0.32					
Arginine	2.22	2.23	2.23	6.05	0.03	8.19	0.04	
Lysine	2.03	2.02	2.04	5.41	0.04	7.33	0.05	
TRIS pH 7.6 ($\varepsilon_t = 0.57, \phi = 0.77$)								
Uracil	0.31	0.31	0.31					
Arginine	3.23	3.24	3.24	9.41	0.02	12.24	0.03	

Lysine	2.82	2.83	2.83	8.09	0.03	10.52	0.03
TRIS pH 8.0 ($e_t = 0.56$, $\phi = 0.78$)							
Uracil	0.31	0.31	0.31				
Arginine	4.97	4.89	4.92	14.92	0.13	19.18	0.17
Lysine	4.38	4.33	4.33	13.05	0.09	16.77	0.11
TRIS pH 8.5 ($e_t = 0.54$, $\phi = 0.85$)							
Uracil	0.30	0.30	0.30				
Arginine	9.64	9.18	9.70	30.90	0.85	36.54	1.01
Lysine	8.84	9.07	8.86	28.94	0.28	34.22	0.33

Table S8. Measured retention times and conversion in Henry coefficient for arginine and lysine in 10 mM MOPS on silica gel 60 for different pH. The total porosity and the phase ration of the column for every buffer run are given in the line of buffer description. Retention times were measured at room temperature.

Analyte	Retention time [min]			Retention factor k' [-]		Henry coefficient H [-]	
				$\emptyset k'$	σ	H	σ
MOPS pH 6.0 ($e_t = 0.58$, $\phi = 0.72$)							
Uracil	0.32	0.32	0.32				
Arginine	2.67	2.63	2.64	7.25	0.06	10.11	0.09
Lysine	2.35	2.36	2.38	6.38	0.03	8.89	0.04
MOPS pH 6.2 ($e_t = 0.58$, $\phi = 0.71$)							
Uracil	0.32	0.32	0.32				
Arginine	2.37	2.35	2.34	6.32	0.04	8.88	0.05
Lysine	2.06	2.09	2.05	5.43	0.04	7.63	0.06
MOPS pH 6.5 ($e_t = 0.59$, $\phi = 0.70$)							
Uracil	0.33	0.32	0.32				
Arginine	2.13	2.12	2.12	5.54	0.01	7.96	0.02
Lysine	1.86	1.85	1.84	4.70	0.01	6.75	0.02
MOPS pH 6.8 ($e_t = 0.59$, $\phi = 0.69$)							
Uracil	0.33	0.33	0.33				
Arginine	2.04	2.05	2.06	5.31	0.03	7.67	0.04
Lysine	1.78	1.80	1.80	4.51	0.02	6.52	0.03
MOPS pH 7.0 ($e_t = 0.59$, $\phi = 0.70$)							
Uracil	0.33	0.32	0.32				
Arginine	1.84	1.85	1.86	4.72	0.04	6.74	0.06
Lysine	1.61	1.61	1.63	4.00	0.04	5.71	0.06
MOPS pH 7.2 ($e_t = 0.59$, $\phi = 0.70$)							
Uracil	0.32	0.32	0.32				

Arginine	2.36	2.37	2.38	6.34	0.04	9.02	0.05
Lysine	2.09	2.08	2.09	5.46	0.01	7.76	0.02
MOPS pH 7.6 ($\epsilon_t = 0.59$, $\varphi = 0.69$)							
Uracil	0.32	0.33	0.33				
Arginine	3.41	3.43	3.45	9.57	0.04	13.79	0.05
Lysine	3.28	3.23	3.29	9.05	0.08	13.04	0.12

7.1.2 Insights on alanine and arginine binding to silica with atomic resolution

The following pages contain the Supporting Information for Section 3.2.

Supplementary Information

Insights on Alanine and Arginine Binding to Silica with Atomic Resolution

*Stefan Rauwolf^{‡1}, Saientan Bag^{‡2}, Rodrigo Rouqueiro³, Sebastian P. Schwaminger¹, Ana Cristina Dias-Cabral³, Sonja Berensmeier^{*1} and Wolfgang Wenzel^{*2}*

¹Technical University of Munich, Department Mechanical Engineering, Bioseparation Engineering Group, Boltzmannstrasse 15, 85748 Garching, Germany; E-mail: s.berensmeier@tum.de

²Karlsruher Institute of Technology, Institute for Nanotechnology, Hermann-von-Helmholtz-Platz 1, 76344 Eggenstein-Leopoldshafen, Germany; E-mail: wolfgang.wenzel@kit.edu

³University Beira Interior, Department of Chemistry, CICS-UBI Health Science Research Center, Avenida Infante D. Henrique, 6200-506 Covilhã, Portugal

[‡]Authors contributed equally

^{*}Corresponding authors

Experimental Section

Materials:

The silica used for the experiments was Silica Gel 60 from AppliChem, Germany. The porous silica has a particle size of 40 to 60 μm . The pore diameter is 55 to 65 \AA and the pore volume 0.7 to 0.8 mL g^{-1} . The surface area is given as 450 to 550 $\text{m}^2 \text{g}^{-1}$. TRIS was purchased from VWR, Germany. pH of the TRIS buffer was adjusted to pH 7.4 with HCl. All amino acids (aa) were purchased as L-stereoisomer. L-Alanine was purchased from SERVA, Germany. L-Arginine (Cellpure $\geq 98\%$) was purchased from Carl Roth, Germany. L-alanine ethyl ester hydrochloride, L-alanine t-butyl ester hydrochloride, N-acetyl-L-alanine, N-a-acetyl-L-arginine dihydrate, L-arginine methyl ester dihydrochloride, and N-alpha-acetyl-L-arginine methyl ester hydrochloride were purchased from Carbosynth, UK. For the column, a column blank kit (Supelco[®]) with L x ID 25 cm x 4.6 mm was purchased from Sigma and shortened to a length of 3.5 cm resulting in a volume of 0.58 mL. The buffers were prepared in DI water. The aa were prepared in running buffer with concentrations of 50 mM for HPLC experiments. For the FMC experiments the aa were prepared in DI water with a concentration of 10 mM and adjusted to pH 7.4. All buffers were degassed and filtered through a 0.2 μm cellulose-acetate-filter from Labsolute, Germany. The aa were also filtered with 0.2 μm cellulose-acetate syringe filters from Macherey-Nagel, Germany.

FMC:

Thermodynamic studies were performed in a flow microcalorimeter (Microscal FMC 4 Vi, Microscal Limited, London, UK), operated in heat conduction mode (exothermic and endothermic signals are translated in the thermogram as a positive and negative peak, respectively). The 171 μL microcalorimeter cell is interfaced with two highly sensitive thermistors capable of detecting power changes with a magnitude of 10^{-7} W, resulting in an

energy resolution in the order of 10^{-9} J. The flowrate of 1.5 mL h^{-1} through the cell is controlled by precision syringe pumps (Harvard Apparatus, UK). A block heater is used to monitor and control the cell temperature. The FMC is also equipped with a multiport valve and an automated injection system, as with a conductivity monitor and a UV detector from Pharmacia (Uppsala, Sweden). Data acquisition, storage and processing were achieved using CALDOS 4 software (Microscal, Limited, UK). During the process, the thermistors detect a change in potential, convert it into power, and transmit it to the software which records the thermogram signal along the time span of the process. The calibration factor was obtained from the correlation between the areas of the peaks and the energy of heat pulses (3 mJ) resulting from electrical impulses of known power and duration. Peak de-convolution and peak area determination were performed with PeakFit 4.12 software (Seasolve Software Inc., San Jose, USA) using the Exponentially Modified Gaussian (EMG) model. The latter was employed due to its ability to model asymmetric signals. The exothermic and endothermic contributions to the overall heat of adsorption were calculated from the area of the respective deconvoluted peaks.

Retention factors:

The chromatographic column was operated on an Agilent 1100 HPLC system with an UV/Vis detector. aa were measured at 210, 220 and 230 nm. The injection volume for every aa was $20 \mu\text{L}$ and the flowrate was 2 mL min^{-1} for every run. The retention factor (Table S1 and S3) is calculated as $k' = (t_R - t_0)/t_0$. Here t_R stands for the retention time of the aa and t_0 for the retention time of a non-interacting tracer in this case 1 g L^{-1} uracil.

Amino Acid cappings:

The models for the uncapped arginine (Arg) and alanine (Ala) were generated using AmberTools. At physiological pH, Arg has a protonated amine group (NH_2^+) group in one end

and another zwitterionic group ($\text{NH}_3^+\text{-COO}^-$) on the other end, making it overall positively charged. The capping groups were built and attached with the uncapped aa using AVOGADRO. The capped aa are then parametrized in AmberTools. The partial charges are assigned according to AM1-BCC method which is also available in AmberTools.

In the case of Ala, the aa is overall neutral having a zwitterionic form ($\text{NH}_3^+\text{-COO}^-$) at physiological pH. The Ala was capped in two different ways (Figure S2). L-Alanine *tert*-butyl ester (A-tbutyl) and L-alanine ethyl ester (A-ethyl): Cap the COO^- part of the zwitterionic group keeping NH_3^+ part intact. Acetyl L-alanine (Ac-R, 4): Cap the NH_3^+ part of the zwitterionic group keeping COO^- part intact. Arg is capped in three different ways to generate its capped varieties (Figure S3): Acetyl-L-arginine (Ac-R): Cap the NH_3^+ part of the zwitterionic group keeping COO^- part intact. Acetyl-L-arginine methyl ester (Ac-ROMe): Cap both the NH_3^+ and the COO^- part of the zwitterionic group. L-Arginine methyl ester (R-OMe): Cap the COO^- part of the zwitterionic group keeping NH_3^+ part intact.

Molecular dynamic simulations:

As a first approximation of the silica surface, we used crystalline silica surface models taken from a database by Emani et al.¹ Among the different possibilities we chose Q3 silica surface model (see Figure S1 (a) and (b)) containing 4.7 silanol groups per nm^2 of the surface. Q3 is the notation (used in Si-NMR spectroscopy²) to represent Si with four oxygens attached and the number 3 denotes that there are 3 'Si' units attached through the oxygen to an individual silicon atom. The deprotonation of the surface silanol groups depend on the pH of the solution. We chose the silica surface model with 14% deprotonated silanol groups which corresponds to physiological pH (~ 7.4).¹ The chosen silica surface model had x, y, and z dimensions of ~ 33.6 , ~ 34.9 , and ~ 25.9 Å respectively containing 2184 number of atoms.

A simulation box with the silica in one end and aa in the middle was prepared. The system was then solvated in TIP3P water. Sufficient numbers of Na⁺ and Cl⁻ counter ions were added to achieve overall charge neutrality of the system.

The force field (FF) parameters for silica are taken from Emani et al.¹ All the remaining FF parameters are taken from AMBER99SB-ILDN FF. The snapshot of the initial system built for MD run is shown in Figure S1(c). The full system was first energy minimized using steepest descent and/or conjugate gradient method. With the minimized structure further MD simulation in NVT ensemble to equilibrate the system was performed. The silica surface is kept fixed during the simulation run and periodic boundary condition was imposed in all three directions. The x- and y-dimensions of the box were kept equal to the x- and y-dimensions of the silica surface, and the atoms located at the edge of the silica patch were connected through bonds via the periodic boundary condition to avoid boundary effects. A series of short NVT simulations with varying z dimensions of the box were performed thereafter to achieve the correct density of the water in the bulk. The partial water density for two different z dimensions of the simulation box is shown in Figure S1(d). For a z dimension of 8.6 nm very high (~1020 kg m⁻³) water density far away from the silica surface was found, while for 8.5 nm box dimension (z) the water density matches quite accurately (~1000 kg m⁻³) with the bulk density.

Nose-Hoover thermostat was used to maintain the system temperature at 300 K. The system with correct water density is further used for the subsequent MD runs. The aa was then pulled towards the silica surface. The system was equilibrated again when the aa was adsorbed to the silica. The simulation snapshots of the adsorbed structure of different uncapped and capped Arg are shown in Figure S9.

Umbrella Sampling

To generate the system for the umbrella sampling run, the aa is pulled away from the silica surface and system configurations saved at a regular distance (between the aa and the silica surface) interval of 0.1 Å. Therefore, the reaction coordinate for the umbrella sampling run is the distance between silica surface and the aa as shown in Figure S1(c). It is used a spring constant of 1000 kJ mol nm⁻² and the pull rate of 0.01 nm ps⁻¹ for the pulling simulations. The umbrella sampling simulations were performed with these configurations with the strength of the umbrella potential 1000 kJ mol nm⁻². Each umbrella sampling windows were first equilibrated for 4 ns and then from another 10 ns run and the histograms for PMF (potential of mean force) generation were saved. All the MD simulations were performed in GROMACS software package with 2 fs timestep. All the bonds involving hydrogen were constrained using the Lincs algorithm during the MD run. PMF curves were calculated using the Weighted Histogram Analysis Method (WHAM) also implemented in GROMACS. To quantify the relative binding affinity of the aa on silica surface the binding affinity constant by integrating the PMF profile weighted by Boltzmann probability was calculated as follows:

$$K_{calc} = C \int_0^{cutoff} \exp(-\beta W_{calc}(z)) dz \quad (S1)$$

Here $W_{calc}(z)$ is the calculated PMF profile as a function of the distance z between the silica surface and the center of mass of the aa. The cutoff is the distance up to which the aa is interacting with silica. $\beta=1/(K_b T)$, where K_b is Boltzmann constant and T is the temperature (taken as 300 K). The constant C depends on the details of the particular experimental setup, which cannot be determined very easily. However, irrespective of this constant, the relative binding affinity of the different aa can be well characterized by K_{calc}/C . In the present communication, this scaled binding affinity K_{calc}/C is reported everywhere.

Distance of amino-acid functional groups from silica surface

Here, we illustrate the distance (reported in Figure 2 and Figure 4 of the manuscript) calculation in the Figure S4 below. To calculate the distance of the center of mass of the different groups (e.g. NH_3^+) of the amino acid from the silica surface we selected all the silica surface atoms (shown in vdW representation in yellow). The z component (d_z) of the distance (d) between the center of mass (shown in orange) of these silica surface atoms and the center of mass of the respective groups of the amino acid (see Figure S4 below) are reported in the manuscript as the “distance”.

To understand the distances reported in Figure 4 and develop more clearer physical picture we have to note that COO^- group of L-arginine methyl ester (Figure 4(c)) and acetyl-L-arginine methyl ester (Figure 4(d)) are capped by methyl group ($-\text{CH}_3$) which takes part in binding too. Here we additionally perform calculations to generate a distance histogram for this CH_3 group too as shown in Figure S12 below. Now if we compare the distance appearing in Figures S12 (a), (c), and (d) we can easily see that the closest distances are not so different in three cases. The distance of these capped group ($\text{COO}-\text{CH}_3$) from silica surface is the average distance (from silica) of the coo (shown in blue) and CH_3 group (shown in violet) which is very similar to the distance of $\text{NH}_2-\text{NH}_2^+$ group as shown in Figure S2(c) and (d) below. Please note that if we also divide the $\text{NH}_2-\text{NH}_2^+$ group in two parts (NH_2 and NH_2^+) and calculate the distance separately for each group then one of the groups will come much closer to the silica.

Tables

Table S1: Measured retention times and conversion in retention factors for uncapped and capped A. The retention time of the tracer solution was 0.35 min. Retention times were measured at 25 °C.

Amino acid	Retention time [min]			Retention factor k' [-]	
				Ø k'	σ
Alanine	0.37	0.37	0.36	0.030	0.003
Ac-A	0.30	0.30	0.30	--	--
A-ethyl	2.83	3.02	3.14	7.4	0.448
A-tbutyl	2.91	2.98	2.92	7.3	0.097

Table S2: Exothermic and endothermic peak areas from deconvolution of FMC heat signals for alanine derivatives.

Amino acid	Exothermic event [mJ]		Endothermic event [mJ]	Net heat [mJ]	
	1	2		Ø	σ
Ac-A	-0.1986			-0.1986	
	-0.1274			-0.1274	-0.16
A-ethyl	-5.4873	-0.5970		-6.0840	
	-4.7681	-1.3724		-6.1405	-6.2
	-5.4494	-1.0259		-6.4753	0.2115
A-tbutyl	-8.6591	-0.6520		-9.3111	
	-8.3316	-0.5114		-8.8430	-8.9
	-7.5326	-1.1905		-8.7231	0.3107

Table S3: Exothermic and endothermic peak areas from deconvolution of FMC heat signals for arginine derivatives.

Amino acid	Exothermic event [mJ]		Endothermic event [mJ]	Net heat [mJ]	
	1	2		Ø	σ
Arginine	-2.9054			-2.9054	
	-2.7471			-2.7471	-2.81
	-2.7786			-2.7786	0.084
Ac-R	-4.8877		4.1674	-0.7230	
	-5.2169		4.5641	-0.6528	-0.74
R-OMe	-4.9423		4.1032	-0.8391	
	-10.9875			-10.9875	
	-10.6830			-10.6830	-10.3
Ac-R-OMe	-9.2730			-9.2730	0.915
	-6.3660			-6.3660	
	-5.7316			-5.7316	-5.9
			-5.7471	0.362	

Table S4: Measured retention times and conversion in retention factors for uncapped and capped R. The retention time of the tracer solution was 0.35 min. Retention times were measured at 25 °C.

Amino acid	Retention time [min]			Retention factor k' [-]	
				$\emptyset k'$	σ
Arginine	2.95	2.93	2.91	7.25	0.058
Ac-R	0.46	0.46	0.46	0.29	0.000
R-OMe	11.44	9.09	9.48	27	3.552
Ac-R-OMe	4.88	4.84	4.84	12.7	0.069

Figures

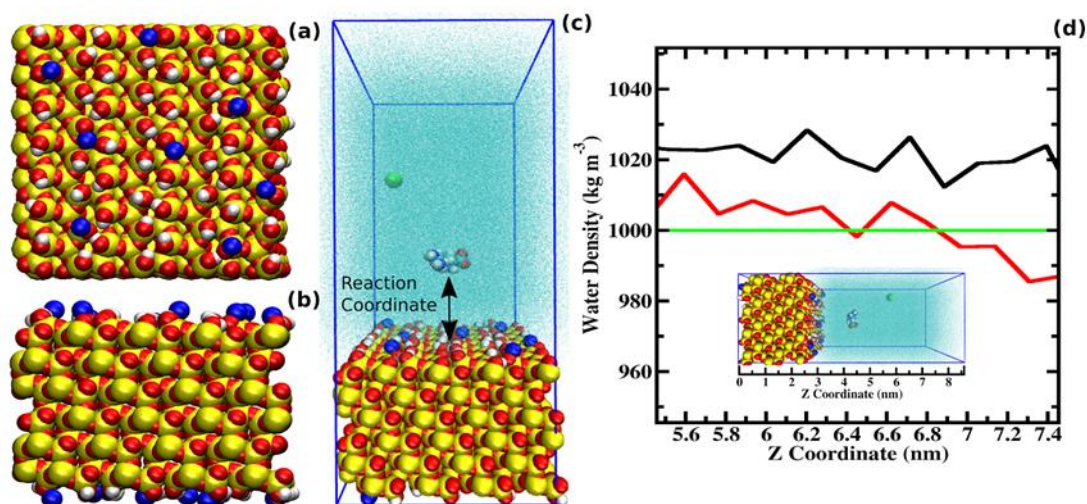


Figure S1: Atomistic model of the silica used in the MD simulation. (a) Top and (b) side view of the model. (c) Snapshot of the initial system prepared for simulation with silica in the end and the R in the middle of the simulation box. The surrounding water medium is not shown in full atomistic details but as collection of dots (“solvent” representation in VMD) for clarity. The silica atoms are shown in yellow, the carbon in cyan, oxygen in red hydrogens in white. The Na⁺ ions are shown in blue and Cl⁻ in green. The distance between the silica surface and the aa are used as the reaction coordinate for the umbrella sampling runs. (d) The partial density of water for two different z dimensions of the simulation box: 8.6 nm (in red) and 8.5 nm (in black).

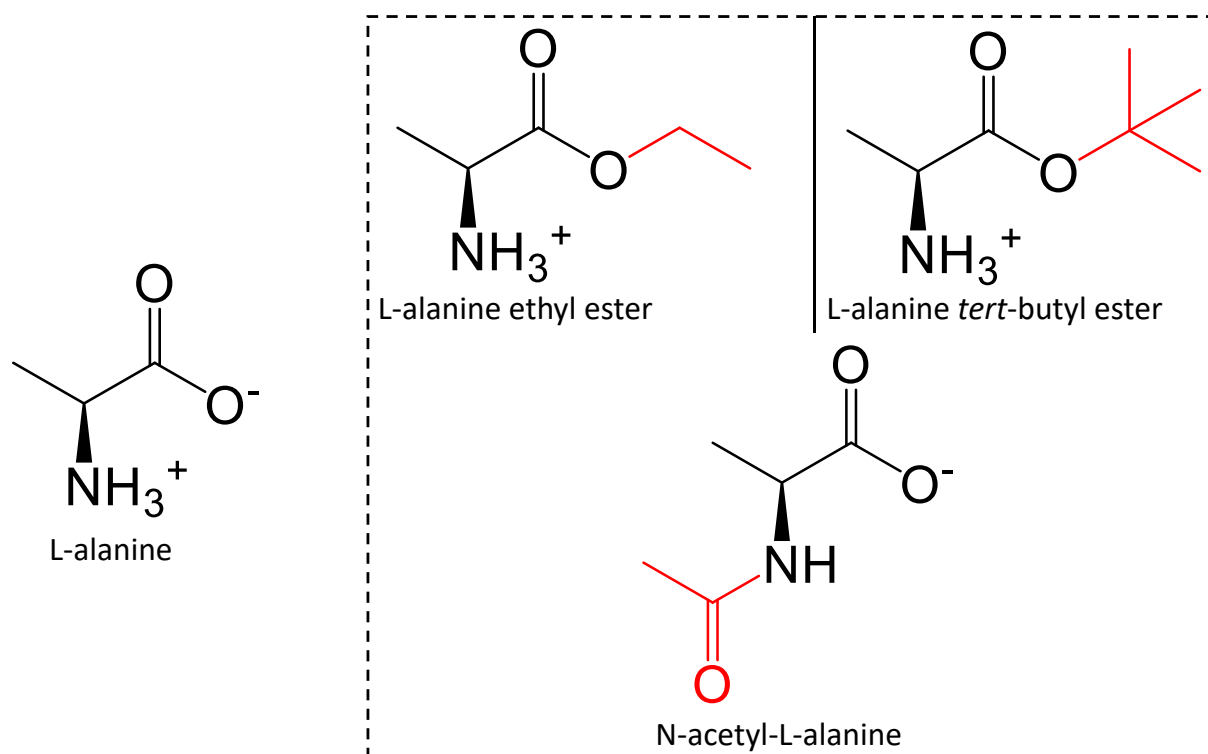


Figure S2: The molecular structure of uncapped and capped (red groups) alanine derivatives.

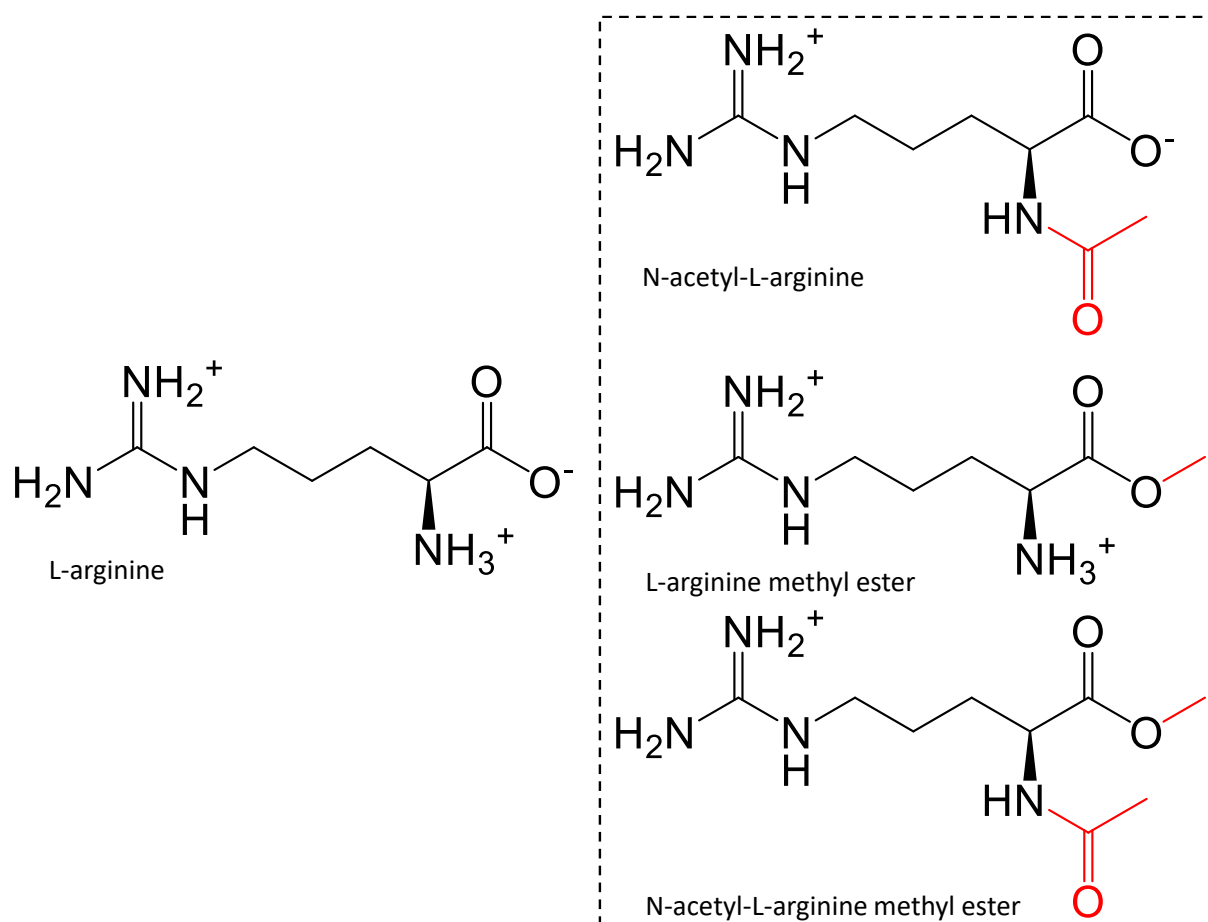


Figure S3: The molecular structure of uncapped and capped (red groups) arginine derivatives.

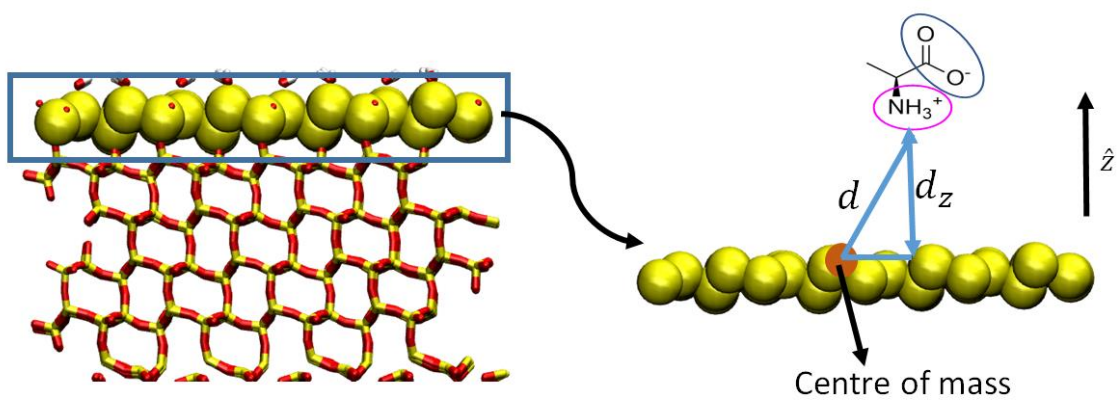


Figure S4: Schematic diagram showing the distance calculation from the silica surface to the amino acid groups.

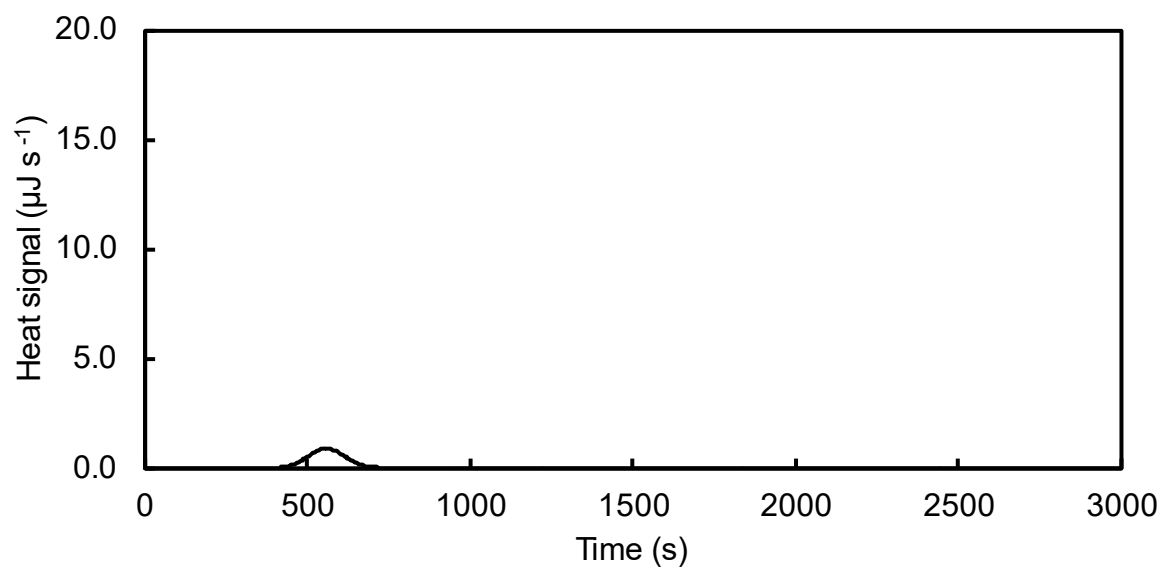


Figure S5: Heat exchange profile of 10 mM acetyl L-alanine in water pH 7.4. Injection volume: 30μL.

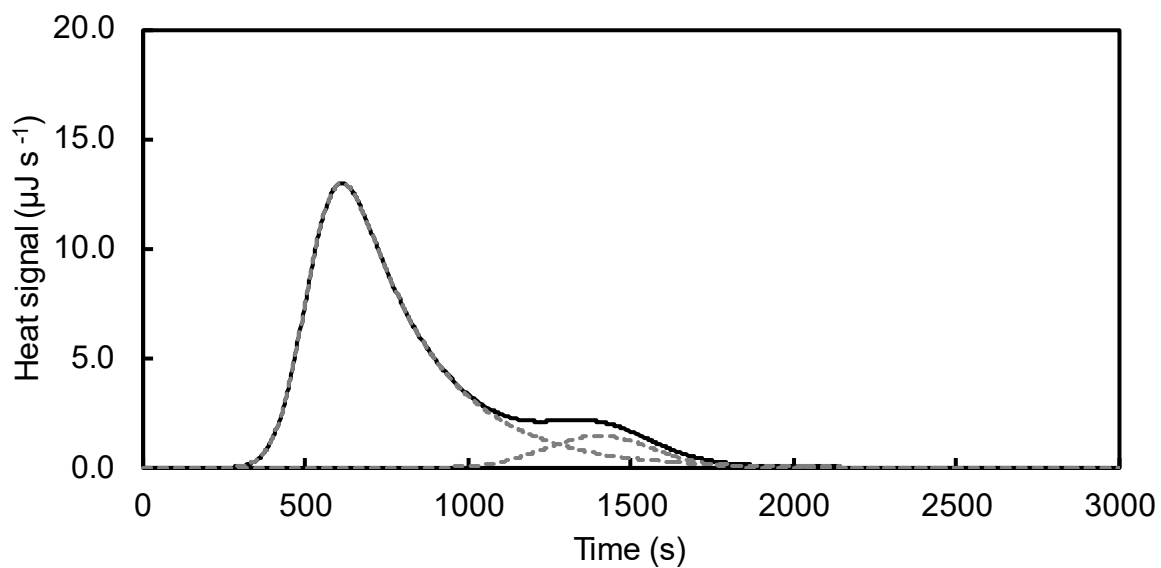


Figure S6: Heat exchange profile of 10 mM L-alanine ethyl ester in water pH 7.4. Injection volume: 30 μL . Curves presented are from total peak fit (black line) and peaks resulting from de-convolution (grey dotted lines).

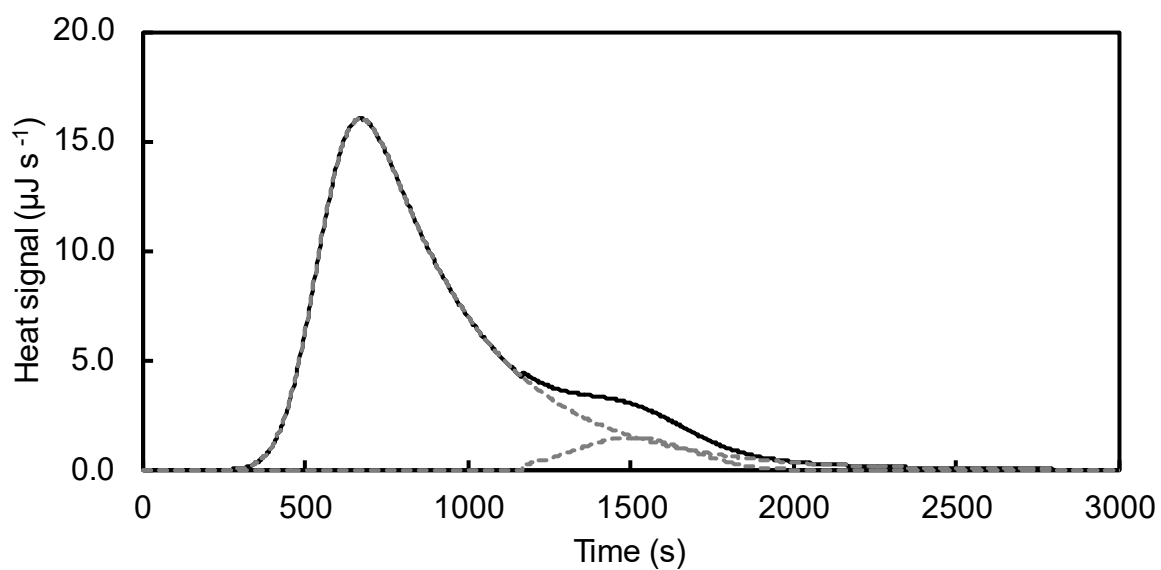


Figure S7: Heat exchange profile of 10 mM L-alanine *tert*-butyl ester in water pH 7.4. Injection volume: 30 μL . Curves presented are from total peak fit (black line) and peaks resulting from de-convolution (grey dotted lines).

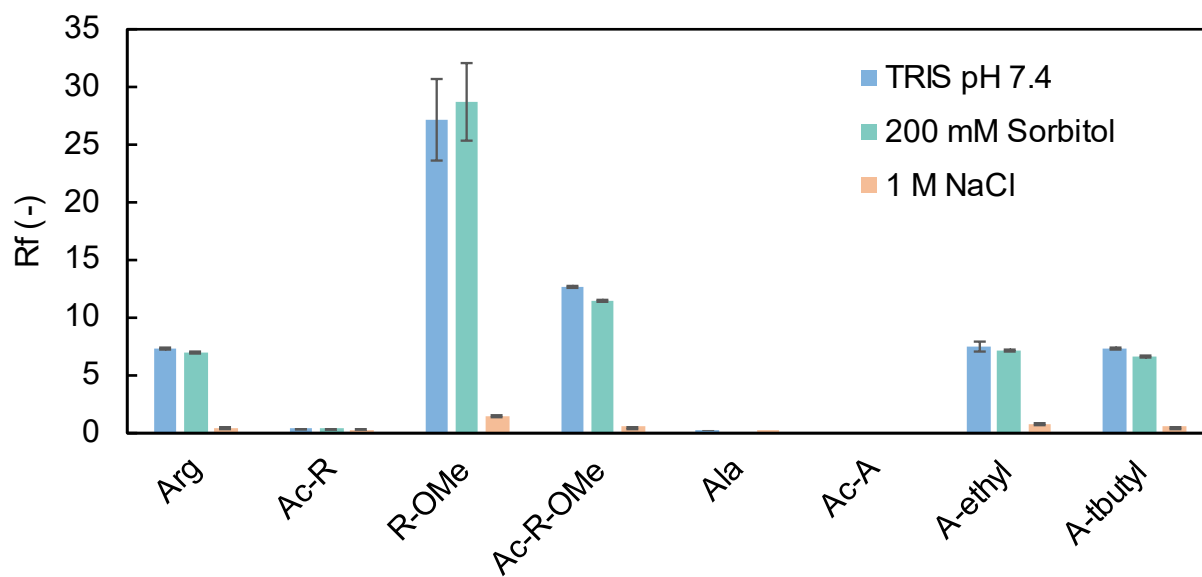


Figure S8: Zonal Elution experiments in 10 mM TRIS pH 7.4 (blue), supplemented with either 200 mM sorbitol (green) or 1 M NaCl (orange). Concentration of the amino acids were 50 mM each with 20 μ L injection. Retention factors were calculated using Uracil as tracer substance.

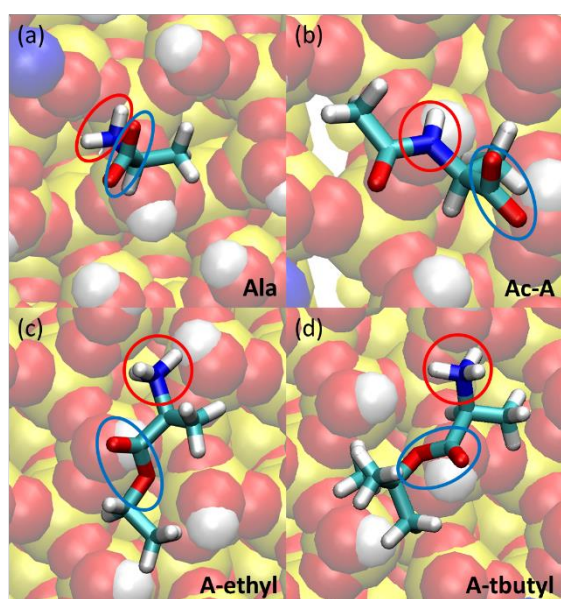


Figure S9: Equilibrated simulation snapshot of uncapped and capped alanine when it is adsorbed on silica. The silica surface under the aa was blurred for better clarity of the aa structures. The capped and uncapped NH_3^+ and the COO^- groups of the aa are highlighted by red and blue circles respectively.

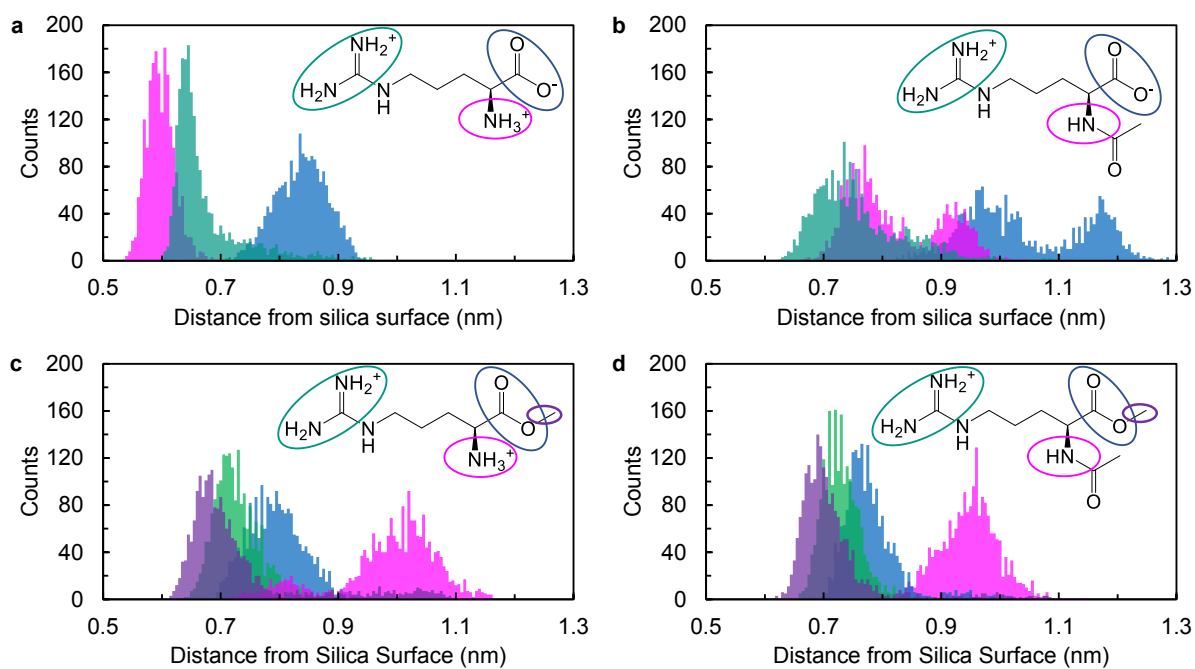


Figure S10: Histograms of the distances of the C- and N-terminus of L-arginine (a), acetyl-L-arginine (b), L-arginine methyl ester (c), and acetyl-L-arginine methyl ester (d) from the silica surface when the aa are adsorbed on silica as obtained from the MD simulation

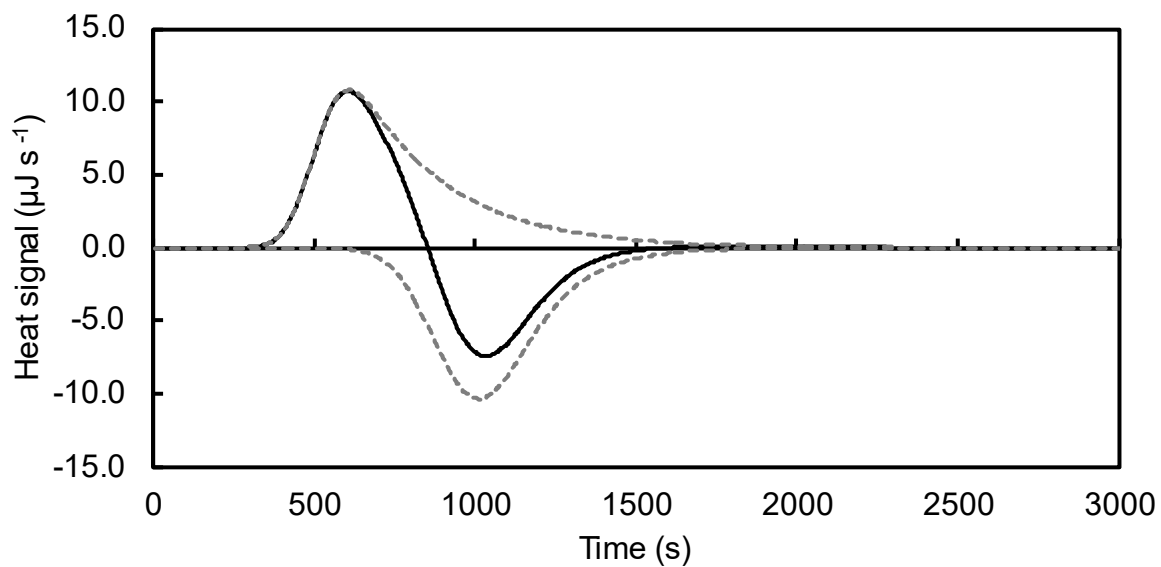


Figure S11: Heat exchange profile of 10 mM acetyl-L-arginine in water pH 7.4. Injection volume: 30 μL . Curves presented are from total peak fit (black line) and peaks resulting from de-convolution (grey dotted lines).

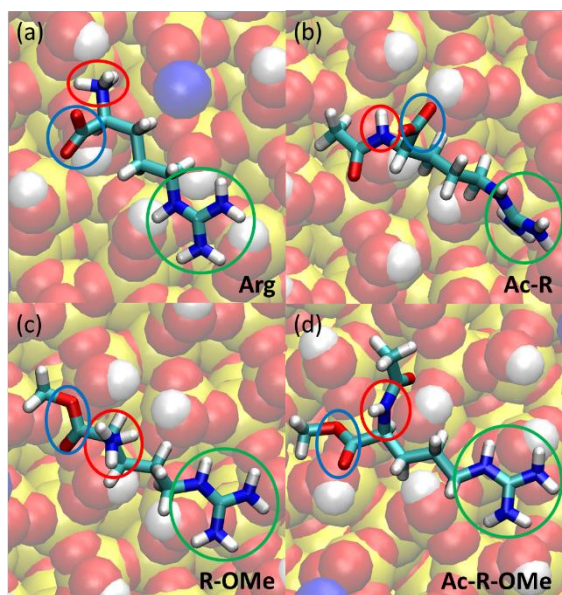


Figure S12: Equilibrated simulation snapshot of uncapped and capped arginine when it is adsorbed on silica. The silica surface under the aa was blurred for better clarity of the aa structures. The capped and uncapped NH_3^+ and the COO^- groups of the aa are highlighted by red and blue circles respectively. The positive $\text{C-NH}_2\text{-NH}_2^+$ groups are highlighted in green.

References

- (1) Emami, F. S., Puddu, V., Berry, R. J., Varshney, V., Patwardhan, S. V., Perry, C. C., Heinz, H. Force field and a surface model database for silica to simulate interfacial properties in atomic resolution. *Chem. Mater.* **2014**, *26*, 2647–2658.
- (2) Icopini, G. A., Brantley, S. L., Heaney, P. J. Kinetics of silica oligomerization and nanocolloid formation as a function of pH and ionic strength at 25°C. *Geochim. Cosmochim. Acta* **2005**, *69*, 293–303.

7.2 List of publications

Author(s)	Title	Reference/Datum	Category
Saientan Bag, Stefan Rauwolf, Mikhail Suyetin, Sebastian P. Schwaminger, Wolfgang Wenzel, Sonja Berensmeier	Buffer Influence on the Amino Acid Silica Interaction	ChemPhysChem, 21, 2347- 2356, 2020 DOI: 10.1002/cphc.202000572	Full Paper
Saientan Bag, Stefan Rauwolf, Sebastian P. Schwaminger, Wolfgang Wenzel, Sonja Berensmeier	DNA Binding to the Silica: Cooperative Adsorption in Action	Langmuir, 37 (19), 5902-5908, 2021. DOI: 10.1021/acs.langmuir.1c00381	Full Paper
Stefan Rauwolf, Tobias Steegmüller, Sebastian P Schwaminger, Sonja Berensmeier	Purification of a peptide tagged protein via an affinity chromatographic process with underivatized silica	Eng Life Sci, 2021 Jun 4;21(10):549-557 DOI: 10.1002/elsc.202100019	Full Paper
Sebastian P. Schwaminger, Stefan Fehn, Tobias Steegmüller, Stefan Rauwolf, Hannes Löwe, Katharina Pflüger-Grau, Sonja Berensmeier	Immobilization of PETase enzymes on magnetic iron oxide nanoparticles for the decomposition of microplastic PET	Nanoscale Adv., 2021, 3, 4395- 4399 DOI: 10.1039/D1NA00243K	Communication
Stefan Rauwolf, Saientan Bag, Rodrigo Rouqueiro, Sebastian P. Schwaminger, Ana Cristina Dias-Cabral, Sonja Berensmeier, Wolfgang Wenzel	Insights on alanine and arginine binding to silica with atomic resolution	J. Phys. Chem. Lett. 2021, 12, 38, 9384–9390 DOI: 10.1021/acs.jpcclett.1c02398	Communication
Sonja Berensmeier, Sebastian P. Schwaminger, Silvia A. Blank-Shim, Yasmin Kaveh- Baghbaderani, Alexander A. Zanker, Stefan Rauwolf, Wolfgang Wenzel	Novel Peptide Tag	WO 2022/013373 A1	Patent

7.3 Permissions

7.3.1 Buffer influence on the amino acid silica interaction

Open Access Article


This is an open access article distributed under the terms of the [Creative Commons CC BY](#) license, which permits unrestricted use, distribution, and reproduction in any medium, provided the original work is properly cited.

You are not required to obtain permission to reuse this article.


For an understanding of what is meant by the terms of the Creative Commons License, please refer to [Wiley's Open Access Terms and Conditions](#).

Permission is not required for this type of reuse.

7.3.2 Insights on alanine and arginine binding to silica with atomic resolution



[Home](#)
[Help](#)
[Live Chat](#)
[Sign in](#)
[Create Account](#)



DNA Binding to the Silica: Cooperative Adsorption in Action

Author: Saientan Bag, Stefan Rauwolf, Sebastian P. Schwaminger, et al

Publication: Langmuir

Publisher: American Chemical Society

Date: May 1, 2021

Copyright © 2021, American Chemical Society

PERMISSION/LICENSE IS GRANTED FOR YOUR ORDER AT NO CHARGE

This type of permission/license, instead of the standard Terms and Conditions, is sent to you because no fee is being charged for your order. Please note the following:

- Permission is granted for your request in both print and electronic formats, and translations.
- If figures and/or tables were requested, they may be adapted or used in part.
- Please print this page for your records and send a copy of it to your publisher/graduate school.
- Appropriate credit for the requested material should be given as follows: "Reprinted (adapted) with permission from {COMPLETE REFERENCE CITATION}. Copyright {YEAR} American Chemical Society." Insert appropriate information in place of the capitalized words.
- One-time permission is granted only for the use specified in your RightsLink request. No additional uses are granted (such as derivative works or other editions). For any uses, please submit a new request.

If credit is given to another source for the material you requested from RightsLink, permission must be obtained from that source.

BACK
CLOSE WINDOW

7.3.3 Purification of a peptide tagged protein via an affinity chromatographic process with underivatized silica

Open Access Article


This is an open access article distributed under the terms of the [Creative Commons CC BY](#) license, which permits unrestricted use, distribution, and reproduction in any medium, provided the original work is properly cited.

You are not required to obtain permission to reuse this article.


For an understanding of what is meant by the terms of the Creative Commons License, please refer to [Wiley's Open Access Terms and Conditions](#).

Permission is not required for this type of reuse.

7.3.4 DNA binding to the silica: Cooperative adsorption in action



[Home](#) | [Help](#) | [Live Chat](#) | [Sign in](#) | [Create Account](#)



DNA Binding to the Silica: Cooperative Adsorption in Action

Author: Saientan Bag, Stefan Rauwolf, Sebastian P. Schwaminger, et al

Publication: Langmuir

Publisher: American Chemical Society

Date: May 1, 2021

Copyright © 2021, American Chemical Society

PERMISSION/LICENSE IS GRANTED FOR YOUR ORDER AT NO CHARGE

This type of permission/license, instead of the standard Terms and Conditions, is sent to you because no fee is being charged for your order. Please note the following:

- Permission is granted for your request in both print and electronic formats, and translations.
- If figures and/or tables were requested, they may be adapted or used in part.
- Please print this page for your records and send a copy of it to your publisher/graduate school.
- Appropriate credit for the requested material should be given as follows: "Reprinted (adapted) with permission from {COMPLETE REFERENCE CITATION}. Copyright {YEAR} American Chemical Society." Insert appropriate information in place of the capitalized words.
- One-time permission is granted only for the use specified in your RightsLink request. No additional uses are granted (such as derivative works or other editions). For any uses, please submit a new request.

If credit is given to another source for the material you requested from RightsLink, permission must be obtained from that source.

BACK
CLOSE WINDOW